Gamma-Ray Bursts

Contents

1 Topics **177**

2 Participants **179**
2.1 ICRANet participants 179
2.2 Past collaborators 179
2.3 Ongoing collaborations 181
2.4 Students 182

3 Selected publications before 2005 **183**
3.1 Refereed journals 183
3.2 Conference proceedings 190

4 Publications (2005–2020) **195**
4.1 Refereed journals 195
4.2 Conference proceedings 237

1 Topics

- GRB classification in different families with different progenitor systems.
- "Genuine short" GRBs: Possible identifications and selection effects
- A modified spectral energy distribution for highly energetic GRBs
- The observed spectra of the P-GRBs
- GRB prompt emission spectra below 5 keV: challenges for future missions
- Interpretation of the ultra high energy emission from GRBs observed by Fermi, AGILE and MAGIC
- Analysis of different families of progenitors for GRBs with different energetics
- GRBs at redshift $z > 6$
- GRBs originating from a multiple collapse
- Prompt emission: the clumpiness of CBM
- Microphysical description of the interaction between the fireshell and the CBM
- Theoretical interpretation of the "plateau" phase in the X-ray afterglow
- Emission from newly born neutron stars, or "neo neutron stars".
- Induced Gravitational Collapse process for GRBs associated with supernovae.
- Redshift estimators for GRBs with no measured redshift.

- Binary Driven Hypernovae (BdHNe) as progenitor of GRBs via Induced Gravitational Collapse.
- GRB light curves as composed of different episodes.
- Different kinds of binary systems as GRB progenitors.
- "Cosmic Matrix" for GRBs.
- GRB X-Ray Flares and Gamma-Ray Flares.
- GRB afterglow theory consistent with the mildly relativistic velocities inferred from the observations.
- Gravitational wave emission associated to GRBs of different families.
- Extended thermal emission components in GRBs.
- GRBs from merging white dwarfs.
- "Inner engine" of GRB emission.
- Quantized emission in GRBs.

2 Participants

2.1 ICRANet participants

- David Arnett
- Carlo Luciano Bianco
- Massimo Della Valle
- Li Liang
- Rahim Moradi
- Jorge Armando Rueda Hernandez
- Remo Ruffini
- Narek Sahakyan
- Gregory Vereshchagin
- Yu Wang
- She-Sheng Xue

2.2 Past collaborators

- Andrey Baranov
- Maria Grazia Bernardini (OAB, Italy)
- Joao Braga (INPE, Brazil)
- Sabrina Casanova (MPIK, Germany)

- Letizia Caito
- Pascal Chardonnet (Université de Savoie, France)
- Guido Chincarini (Università di Milano "Bicocca", Italy)
- Demetrios Christodoulou (ETH Zurich, Switzerland)
- Alessandra Corsi (INAF-IASF Roma, Italy)
- Valeri Chechetkin
- Maria Giovanna Dainotti
- Thibault Damour (IHES, France)
- Maxime Enderli
- Walter Ferrara
- Federico Fraschetti (CEA Saclay, France)
- Roberto Guida
- Vahe Gurzadyan (Yerevan Physics Institute, Armenia)
- Wen-Biao Han
- Milos Kovacevic
- Massimiliano Lattanzi (Oxford Astrophysics, UK)
- Vincenzo Liccardo
- Hendrik Ludwig
- Marco Muccino
- Nino Panagia
- Barbara Patricelli (Pisa University, Italy)
- Elena Pian
- Giovanni Battista Pisani

- Giuliano Preparata (Università di Milano, Italy)
- Daria Primorac
- Jay D. Salmonson (Livermore Lab, USA)
- Vineeth Valsan
- Jim Wilson (Livermore Lab, USA)

2.3 Ongoing collaborations

- Alexey Aksenov (ITEP, Russia)
- Lorenzo Amati (INAF-IASF Bologna, Italy)
- Ulisses Barres de Almeida (CBPF, Brazil)
- Laura Marcela Becerra Bayona (Universidad Industrial de Santander, Colombia)
- Riccardo Belvedere (ICRANet-Rio, Brazil)
- Sandip Kumar Chakrabarti (S.N. Bose National Centre and Indian Centre for Space Physics, India)
- Christian Cherubini (Università Campus Biomedico, Italy)
- Alessandro Chieffi (INAF-IASF Roma, Italy)
- Stefano Covino (OAB, Italy)
- Gustavo de Barros (UFRJ, Brazil)
- Simonetta Filippi (Università Campus Biomedico, Italy)
- Filippo Frontera (Università di Ferrara, Italy)
- Chris Fryer (Los Alamos National Laboratories, USA).
- Dafne Guetta (OAR, Italy)
- Cristiano Guidorzi (OAB, Italy)

- Stanislav Kelner (MEPhI, Russia, and MPIK, Germany)
- Marco Limongi (OAR, Italy)
- Clovis Maia (University of Brasilia, Brazil)
- Vanessa Mangano (INAF-IASF Palermo, Italy)
- Grant Mathews (University of Notre Dame, USA)
- Ana Virginia Penacchioni (INPE, Brazil)
- Luis Juracy Rangel Lemos (Fundação Universidade Federal do Tocantins, Brazil)
- Soroush Shakeri (Isfahan University of Technology, Iran)
- Ivan Siutsou (ICRANet-Rio, Brazil)
- Susanna Vergani (Dunsink Observatory, Ireland)
- Francesco Vissani (INFN, Italy)
- Elena Zaninoni (ICRANet-Rio, Brazil)

2.4 Students

- Yerlan Aimuratov (IRAP PhD, Kazakhstan)
- Yen-Chen Chen (IRAP-PhD, China-Taiwan)
- Mile Karlika (IRAP PhD, Croatia)
- Ronaldo V. Lobato (IRAP-PhD, Brazil)
- J. David Melon Fuksman (IRAP PhD, Argentina)
- Jose Fernando Rodriguez Ruiz (IRAP PhD, Colombia)

3 Selected publications before 2005

3.1 Refereed journals

1. D. Christodoulou, R. Ruffini; "Reversible Transformations of a Charged Black Hole"; Physical Review D, 4, 3552 (1971).

   A formula is derived for the mass of a black hole as a function of its "irreducible mass", its angular momentum, and its charge. It is shown that 50% of the mass of an extreme charged black hole can be converted into energy as contrasted with 29% for an extreme rotating black hole.

2. T. Damour, R. Ruffini; "Quantum electrodynamical effects in Kerr-Newman geometries"; Physical Review Letters, 35, 463 (1975).

   Following the classical approach of Sauter, of Heisenberg and Euler and of Schwinger the process of vacuum polarization in the field of a "bare" Kerr-Newman geometry is studied. The value of the critical strength of the electromagnetic fields is given together with an analysis of the feedback of the discharge on the geometry. The relevance of this analysis for current astrophysical observations is mentioned.

3. G. Preparata, R. Ruffini, S.-S. Xue; "The dyadosphere of black holes and gamma-ray bursts"; Astronomy & Astrophysics, 338, L87 (1999).

   The "dyadosphere" has been defined as the region outside the horizon of a black hole endowed with an electromagnetic field (abbreviated to EMBH for "electromagnetic black hole") where the electromagnetic field exceeds the critical value, predicted by Heisenberg & Euler for $e^{\pm}$ pair production. In a very short time ($\sim O(\hbar/mc^2)$) a very large number of pairs is created there. We here give limits on the EMBH parameters leading to a Dyadosphere for $10M_{\odot}$ and $10^5 M_{\odot}$ EMBH's, and give as well the pair densities as functions of the radial coordinate. We here assume that the pairs reach thermodynamic equilibrium

with a photon gas and estimate the average energy per pair as a function of the EMBH mass. These data give the initial conditions for the analysis of an enormous pair-electromagnetic-pulse or "P.E.M. pulse" which naturally leads to relativistic expansion. Basic energy requirements for gamma ray bursts (GRB), including GRB971214 recently observed at z=3.4, can be accounted for by processes occurring in the dyadosphere. In this letter we do not address the problem of forming either the EMBH or the dyadosphere: we establish some inequalities which must be satisfied during their formation process.

4. R. Ruffini, J.D. Salmonson, J.R. Wilson, S.-S. Xue; "On the pair electromagnetic pulse of a black hole with electromagnetic structure"; Astronomy & Astrophysics, 350, 334 (1999).

   We study the relativistically expanding electron-positron pair plasma formed by the process of vacuum polarization around an electromagnetic black hole (EMBH). Such processes can occur for EMBH's with mass all the way up to $6 \times 10^5 M_\odot$. Beginning with a idealized model of a Reissner-Nordstrom EMBH with charge to mass ratio $\xi = 0.1$, numerical hydrodynamic calculations are made to model the expansion of the pair-electromagnetic pulse (PEM pulse) to the point that the system is transparent to photons. Three idealized special relativistic models have been compared and contrasted with the results of the numerically integrated general relativistic hydrodynamic equations. One of the three models has been validated: a PEM pulse of constant thickness in the laboratory frame is shown to be in excellent agreement with results of the general relativistic hydrodynamic code. It is remarkable that this precise model, starting from the fundamental parameters of the EMBH, leads uniquely to the explicit evaluation of the parameters of the PEM pulse, including the energy spectrum and the astrophysically unprecedented large Lorentz factors (up to 6×10^3 for a $10^3 M_\odot$ EMBH). The observed photon energy at the peak of the photon spectrum at the moment of photon decoupling is shown to range from 0.1 MeV to 4 MeV as a function of the EMBH mass. Correspondingly the total energy in photons is in the range of 10^{52} to 10^{54} ergs, consistent with observed gamma-ray bursts. In these computations we neglect the presence of baryonic matter which will be the subject of forthcoming publications.

5. R. Ruffini, J.D. Salmonson, J.R. Wilson, S.-S. Xue; "On the pair-electro magnetic pulse from an electromagnetic black hole surrounded by a baryonic remnant"; Astronomy & Astrophysics, 359, 855 (2000).

   The interaction of an expanding Pair-Electromagnetic pulse (PEM pulse) with

a shell of baryonic matter surrounding a Black Hole with electromagnetic structure (EMBH) is analyzed for selected values of the baryonic mass at selected distances well outside the dyadosphere of an EMBH. The dyadosphere, the region in which a super critical field exists for the creation of e+e- pairs, is here considered in the special case of a Reissner-Nordstrom geometry. The interaction of the PEM pulse with the baryonic matter is described using a simplified model of a slab of constant thickness in the laboratory frame (constant-thickness approximation) as well as performing the integration of the general relativistic hydrodynamical equations. Te validation of the constant-thickness approximation, already presented in a previous paper Ruffini et al. (1999) for a PEM pulse in vacuum, is here generalized to the presence of baryonic matter. It is found that for a baryonic shell of mass-energy less than 1% of the total energy of the dyadosphere, the constant-thickness approximation is in excellent agreement with full general relativistic computations. The approximation breaks down for larger values of the baryonic shell mass, however such cases are of less interest for observed Gamma Ray Bursts (GRBs). On the basis of numerical computations of the slab model for PEM pulses, we describe (i) the properties of relativistic evolution of a PEM pulse colliding with a baryonic shell; (ii) the details of the expected emission energy and observed temperature of the associated GRBs for a given value of the EMBH mass; $10^3 M_\odot$, and for baryonic mass-energies in the range 10^{-8} to 10^{-2} the total energy of the dyadosphere.

6. C.L. Bianco, R. Ruffini, S.-S. Xue; "The elementary spike produced by a pure e+e- pair-electromagnetic pulse from a Black Hole: The PEM Pulse"; Astronomy & Astrophysics, 368, 377 (2001).

   In the framework of the model that uses black holes endowed with electromagnetic structure (EMBH) as the energy source, we study how an elementary spike appears to the detectors. We consider the simplest possible case of a pulse produced by a pure e^+e^- pair-electro-magnetic plasma, the PEM pulse, in the absence of any baryonic matter. The resulting time profiles show a *Fast-Rise-Exponential-Decay* shape, followed by a power-law tail. This is obtained without any special fitting procedure, but only by fixing the energetics of the process taking place in a given EMBH of selected mass, varying in the range from 10 to 10^3 $M_\odot$ and considering the relativistic effects to be expected in an electron-positron plasma gradually reaching transparency. Special attention is given to the contributions from all regimes with Lorentz γ factor varying from $\gamma = 1$ to $\gamma = 10^4$ in a few hundreds of the PEM pulse travel time. Although the

main goal of this paper is to obtain the elementary spike intensity as a function of the arrival time, and its observed duration, some qualitative considerations are also presented regarding the expected spectrum and on its departure from the thermal one. The results of this paper will be comparable, when data will become available, with a subfamily of particularly short GRBs not followed by any afterglow. They can also be propedeutical to the study of longer bursts in presence of baryonic matter currently observed in GRBs.

7. R. Ruffini, C.L. Bianco, P. Chardonnet, F. Fraschetti, S.-S. Xue; "Relative spacetime transformations in Gamma-Ray Bursts"; The Astrophysical Journal, 555, L107 (2001).

   The GRB 991216 and its relevant data acquired from the BATSE experiment and RXTE and Chandra satellites are used as a prototypical case to test the theory linking the origin of gamma ray bursts (GRBs) to the process of vacuum polarization occurring during the formation phase of a black hole endowed with electromagnetic structure (EMBH). The relative space-time transformation paradigm (RSTT paradigm) is presented. It relates the observed signals of GRBs to their past light cones, defining the events on the worldline of the source essential for the interpretation of the data. Since GRBs present regimes with unprecedently large Lorentz γ factor, also sharply varying with time, particular attention is given to the constitutive equations relating the four time variables: the comoving time, the laboratory time, the arrival time at the detector, duly corrected by the cosmological effects. This paradigm is at the very foundation of any possible interpretation of the data of GRBs.

8. R. Ruffini, C.L. Bianco, P. Chardonnet, F. Fraschetti, S.-S. Xue; "On the interpretation of the burst structure of Gamma-Ray Bursts"; The Astrophysical Journal, 555, L113 (2001).

   Given the very accurate data from the BATSE experiment and RXTE and Chandra satellites, we use the GRB 991216 as a prototypical case to test the EMBH theory linking the origin of the energy of GRBs to the electromagnetic energy of black holes. The fit of the afterglow fixes the only two free parameters of the model and leads to a new paradigm for the interpretation of the burst structure, the IBS paradigm. It leads as well to a reconsideration of the relative roles of the afterglow and burst in GRBs by defining two new phases in this complex phenomenon: a) the injector phase, giving rise to the proper-GRB (P-GRB), and b) the beam-target phase, giving rise to the extended afterglow peak emission (E-APE) and to the afterglow. Such differentiation leads to a

natural possible explanation of the bimodal distribution of GRBs observed by BATSE. The agreement with the observational data in regions extending from the horizon of the EMBH all the way out to the distant observer confirms the uniqueness of the model.

9. R. Ruffini, C.L. Bianco, P. Chardonnet, F. Fraschetti, S.-S. Xue; "On a possible Gamma-Ray Burst-Supernova time sequence"; The Astrophysical Journal, 555, L117 (2001).

   The data from the Chandra satellite on the iron emission lines in the afterglow of GRB 991216 are used to give further support for the EMBH theory, which links the origin of the energy of GRBs to the extractable energy of electromagnetic black holes (EMBHs), leading to an interpretation of the GRB-supernova correlation. Following the relative space-time transformation (RSTT) paradigm and the interpretation of the burst structure (IBS) paradigm, we introduce a paradigm for the correlation between GRBs and supernovae. The following sequence of events is shown as kinematically possible and consistent with the available data: a) the GRB-progenitor star P_1 first collapses to an EMBH, b) the proper GRB (P-GRB) and the peak of the afterglow (E-APE) propagate in interstellar space until the impact on a supernova-progenitor star P_2 at a distance $\leq 2.69 \times 10^{17}$ cm, and they induce the supernova explosion, c) the accelerated baryonic matter (ABM) pulse, originating the afterglow, reaches the supernova remnants 18.5 hours after the supernova explosion and gives rise to the iron emission lines. Some considerations on the dynamical implementation of the paradigm are presented. The concept of induced supernova explosion introduced here specifically for the GRB-supernova correlation may have more general application in relativistic astrophysics.

10. R. Ruffini, C.L. Bianco, P. Chardonnet, F. Fraschetti, S.-S. Xue; "On the physical processes which lie at the bases of time variability of GRBs"; Il Nuovo Cimento B, 116, 99 (2001).

    The relative-space-time-transformation (RSTT) paradigm and the interpretation of the burst-structure (IBS) paradigm are applied to probe the origin of the time variability of GRBs. Again GRB 991216 is used as a prototypical case, thanks to the precise data from the CGRO, RXTE and Chandra satellites. It is found that with the exception of the relatively inconspicuous but scientifically very important signal originating from the initial "proper gamma ray burst" (P-GRB), all the other spikes and time variabilities can be explained by the interaction of the accelerated-baryonic-matter pulse with inhomogeneities in the

interstellar matter. This can be demonstrated by using the RSTT paradigm as well as the IBS paradigm, to trace a typical spike observed in arrival time back to the corresponding one in the laboratory time. Using these paradigms, the identification of the physical nature of the time variablity of the GRBs can be made most convincingly. It is made explicit the dependence of a) the intensities of the afterglow, b) the spikes amplitude and c) the actual time structure on the Lorentz gamma factor of the accelerated-baryonic-matter pulse. In principle it is possible to read off from the spike structure the detailed density contrast of the interstellar medium in the host galaxy, even at very high redshift.

11. R. Ruffini, C.L. Bianco, P. Chardonnet, F. Fraschetti, S.-S. Xue; "On the structures in the afterglow peak emission of gamma ray bursts"; The Astrophysical Journal, 581, L19 (2002).

    Using GRB 991216 as a prototype, it is shown that the intensity substructures observed in what is generally called the "prompt emission" in gamma ray bursts (GRBs) do originate in the collision between the accelerated baryonic matter (ABM) pulse with inhomogeneities in the interstellar medium (ISM). The initial phase of such process occurs at a Lorentz factor $\gamma \sim 310$. The crossing of ISM inhomogeneities of sizes $\Delta R \sim 10^{15}$ cm occurs in a detector arrival time interval of ~ 0.4 s implying an apparent superluminal behavior of $\sim 10^5 c$. The long lasting debate between the validity of the external shock model vs. the internal shock model for GRBs is solved in favor of the first.

12. R. Ruffini, C.L. Bianco, P. Chardonnet, F. Fraschetti, S.-S. Xue; "On the structure of the burst and afterglow of Gamma-Ray Bursts I: the radial approximation"; International Journal of Modern Physics D, 12, 173 (2003).

    We have recently proposed three paradigms for the theoretical interpretation of gamma-ray bursts (GRBs). (1) The relative space-time transformation (RSTT) paradigm emphasizes how the knowledge of the entire world-line of the source from the moment of gravitational collapse is a necessary condition in order to interpret GRB data. (2) The interpretation of the burst structure (IBS) paradigm differentiates in all GRBs between an injector phase and a beam-target phase. (3) The GRB-supernova time sequence (GSTS) paradigm introduces the concept of *induced supernova explosion* in the supernovae-GRB association. In the introduction the RSTT and IBS paradigms are enunciated and illustrated using our theory based on the vacuum polarization process occurring around an electromagnetic black hole (EMBH theory). The results are summarized

using figures, diagrams and a complete table with the space-time grid, the fundamental parameters and the corresponding values of the Lorentz gamma factor for GRB 991216 used as a prototype. In the following sections the detailed treatment of the EMBH theory needed to understand the results of the three above letters is presented. We start from the considerations on the dyadosphere formation. We then review the basic hydrodynamic and rate equations, the equations leading to the relative space-time transformations as well as the adopted numerical integration techniques. We then illustrate the five fundamental eras of the EMBH theory: the self acceleration of the e^+e^- pair-electromagnetic plasma (PEM pulse), its interaction with the baryonic remnant of the progenitor star, the further self acceleration of the e^+e^- pair-electroma-gnetic radiation and baryon plasma (PEMB pulse). We then study the approach of the PEMB pulse to transparency, the emission of the proper GRB (P-GRB) and its relation to the "short GRBs". Particular attention is given to the free parameters of the theory and to the values of the thermodynamical quantities at transparency. Finally the three different regimes of the afterglow are described within the fully radiative and radial approximations: the ultrarelativistic, the relativistic and the nonrelativistic regimes. The best fit of the theory leads to an unequivocal identification of the "long GRBs" as extended emission occurring at the afterglow peak (E-APE). The relative intensities, the time separation and the hardness ratio of the P-GRB and the E-APE are used as distinctive observational test of the EMBH theory and the excellent agreement between our theoretical predictions and the observations are documented. The afterglow power-law indexes in the EMBH theory are compared and contrasted with the ones in the literature, and no beaming process is found for GRB 991216. Finally, some preliminary results relating the observed time variability of the E-APE to the inhomogeneities in the interstellar medium are presented, as well as some general considerations on the EMBH formation. The issue of the GSTS paradigm will be the object of a forthcoming publication and the relevance of the iron-lines observed in GRB 991216 is shortly reviewed. The general conclusions are then presented based on the three fundamental parameters of the EMBH theory: the dyadosphere energy, the baryonic mass of the remnant, the interstellar medium density. An in depth discussion and comparison of the EMBH theory with alternative theories is presented as well as indications of further developments beyond the radial approximation, which will be the subject of paper II in this series. Future needs for specific GRB observations are outlined.

13. R. Ruffini, C.L. Bianco, P. Chardonnet, F. Fraschetti, V. Gurzadyan, S.-S. Xue; "On the instantaneous spectrum of gamma ray bursts"; International Journal of Modern Physics D, 13, 843 (2004).

    A theoretical attempt to identify the physical process responsible for the afterglow emission of Gamma-Ray Bursts (GRBs) is presented, leading to the occurrence of thermal emission in the comoving frame of the shock wave giving rise to the bursts. The determination of the luminosities and spectra involves integration over an infinite number of Planckian spectra, weighted by appropriate relativistic transformations, each one corresponding to a different viewing angle in the past light cone of the observer. The relativistic transformations have been computed using the equations of motion of GRBs within our theory, giving special attention to the determination of the equitemporal surfaces. The only free parameter of the present theory is the "effective emitting area" in the shock wave front. A self consistent model for the observed hard-to-soft transition in GRBs is also presented. When applied to GRB 991216 a precise fit $\left(\chi^2 \simeq 1.078\right)$ of the observed luminosity in the 2–10 keV band is obtained. Similarly, detailed estimates of the observed luminosity in the 50–300 keV and in the 10–50 keV bands are obtained.

3.2 Conference proceedings

1. R. Ruffini; "Beyond the critical mass: The dyadosphere of black holes"; in "Black Holes and High Energy Astrophysics", H. sato, N. Sugiyama, Editors; p. 167; Universal Academy Press (Tokyo, Japan, 1998).

    The "dyadosphere" (from the Greek word "duas-duados" for pairs) is here defined as the region outside the horizon of a black hole endowed with an electromagnetic field (abbreviated to EMBH for "electromagnetic black hole") where the electromagnetic field exceeds the critical value, predicted by Heisenberg and Euler for e^+e^- pair production. In a very short time ($\sim O(\hbar/mc^2)$), a very large number of pairs is created there. I give limits on the EMBH parameters leading to a Dyadosphere for $10M_\odot$ and $10^5M_\odot$ EMBH's, and give as well the pair densities as functions of the radial coordinate. These data give the initial conditions for the analysis of an enormous pair-electromagnetic-pulse or "PEM-pulse" which naturally leads to relativistic expansion. Basic energy requirements for gamma ray bursts (GRB), including GRB971214 recently observed at $z = 3.4$, can be accounted for by processes occurring in the dyado-

sphere.

2. R. Ruffini, C.L. Bianco, P. Chardonnet, F. Fraschetti, L. Vitagliano, S.-S. Xue; "New perspectives in physics and astrophysics from the theoretical understanding of Gamma-Ray Bursts"; in "COSMOLOGY AND GRAVITATION: Xth Brazilian School of Cosmology and Gravitation; 25th Anniversary (1977-2002)", Proceedings of the Xth Brazilian School on Cosmology and Gravitation, Mangaratiba, Rio de Janeiro (Brazil), July - August 2002, M. Novello, S.E. Perez Bergliaffa, Editors; AIP Conference Proceedings, 668, 16 (2003).

   If due attention is given in formulating the basic equations for the Gamma-Ray Burst (GRB) phenomenon and in performing the corresponding quantitative analysis, GRBs open a main avenue of inquiring on totally new physical and astrophysical regimes. This program is very likely one of the greatest computational efforts in physics and astrophysics and cannot be actuated using shortcuts. A systematic approach is needed which has been highlighted in three basic new paradigms: the relative space-time transformation (RSTT) paradigm, the interpretation of the burst structure (IBS) paradigm, the GRB-supernova time sequence (GSTS) paradigm. From the point of view of fundamental physics new regimes are explored: (1) the process of energy extraction from black holes; (2) the quantum and general relativistic effects of matter-antimatter creation near the black hole horizon; (3) the physics of ultrarelativisitc shock waves with Lorentz gamma factor $\gamma > 100$. From the point of view of astronomy and astrophysics also new regimes are explored: (i) the occurrence of gravitational collapse to a black hole from a critical mass core of mass $M \gtrsim 10 M_{\odot}$, which clearly differs from the values of the critical mass encountered in the study of stars "catalyzed at the endpoint of thermonuclear evolution" (white dwarfs and neutron stars); (ii) the extremely high efficiency of the spherical collapse to a black hole, where almost 99.99% of the core mass collapses leaving negligible remnant; (iii) the necessity of developing a fine tuning in the final phases of thermonuclear evolution of the stars, both for the star collapsing to the black hole and the surrounding ones, in order to explain the possible occurrence of the "induced gravitational collapse". New regimes are as well encountered from the point of view of nature of GRBs: (I) the basic structure of GRBs is uniquely composed by a proper-GRB (P-GRB) and the afterglow; (II) the long bursts are then simply explained as the peak of the afterglow (the E-APE) and their observed time variability is explained in terms of inhomogeneities in the interstellar medium (ISM); (III) the short bursts are

identified with the P-GRBs and the crucial information on general relativistic and vacuum polarization effects are encoded in their spectra and intensity time variability. A new class of space missions to acquire information on such extreme new regimes are urgently needed.

3. R. Ruffini, C.L. Bianco, P. Chardonnet, F. Fraschetti, S.-S. Xue; "The EMBH Model in GRB 991216 and GRB 980425"; in Proceedings of "Third Rome Workshop on Gamma-Ray Burst in the Afterglow Era", 17-20 September 2002; M. Feroci, F. Frontera, N. Masetti, L. Piro, Editors; ASP Conference Series, 312, 349 (2004).

   This is a summary of the two talks presented at the Rome GRB meeting by C.L. Bianco and R. Ruffini. It is shown that by respecting the Relative Space-Time Transformation (RSTT) paradigm and the Interpretation of the Burst Structure (IBS) paradigm, important inferences are possible: a) in the new physics occurring in the energy sources of GRBs, b) on the structure of the bursts and c) on the composition of the interstellar matter surrounding the source.

4. M.G. Bernardini, C.L. Bianco, P. Chardonnet, F. Fraschetti, R. Ruffini, S.-S. Xue; "A New Astrophysical 'Triptych': GRB030329/SN2003dh/ URCA-2"; in "GAMMA-RAY BURSTS: 30 YEARS OF DISCOVERY", Proceedings of the Los Alamos "Gamma Ray Burst Symposium", Santa Fe, New Mexico, 8 – 12 September 2003, E.E. Fenimore, M. Galassi, Editors; AIP Conference Proceedings, 727, 312 (2004).

   We analyze the data of the Gamma-Ray Burst/Supernova GRB030329/ SN2003dh system obtained by HETE-2, R-XTE, XMM and VLT within our theory for GRB030329. By fitting the only three free parameters of the EMBH theory, we obtain the luminosity in fixed energy bands for the prompt emission and the afterglow. Since the Gamma-Ray Burst (GRB) analysis is consistent with a spherically symmetric expansion, the energy of GRB030329 is $E = 2.1 \times 10^{52}$ erg, namely $\sim 2 \times 10^3$ times larger than the Supernova energy. We conclude that either the GRB is triggering an induced-supernova event or both the GRB and the Supernova are triggered by the same relativistic process. In no way the GRB can be originated from the supernova. We also evidence that the XMM observations, much like in the system GRB980425/SN1998bw, are not part of the GRB afterglow, as interpreted in the literature, but are associated to the Supernova phenomenon. A dedicated campaign of observations is needed to confirm the nature of this XMM source as a newly born neutron star cooling by generalized URCA processes.

5. F. Fraschetti, M.G. Bernardini, C.L. Bianco, P. Chardonnet, R. Ruffini, S.-S. Xue; "The GRB980425-SN1998bw Association in the EMBH Model"; in "GAMMA-RAY BURSTS: 30 YEARS OF DISCOVERY", Proceedings of the Los Alamos "Gamma Ray Burst Symposium", Santa Fe, New Mexico, 8 – 12 September 2003, E.E. Fenimore, M. Galassi, Editors; AIP Conference Proceedings, 727, 424 (2004).

   Our GRB theory, previously developed using GRB 991216 as a prototype, is here applied to GRB 980425. We fit the luminosity observed in the 40–700 keV, 2–26 keV and 2–10 keV bands by the BeppoSAX satellite. In addition the supernova SN1998bw is the outcome of an "induced gravitational collapse" triggered by GRB 980425, in agreement with the GRB-Supernova Time Sequence (GSTS) paradigm. A further outcome of this astrophysically exceptional sequence of events is the formation of a young neutron star generated by the SN1998bw event. A coordinated observational activity is recommended to further enlighten the underlying scenario of this most unique astrophysical system.

6. A. Corsi, M.G. Bernardini, C.L. Bianco, P. Chardonnet, F. Fraschetti, R. Ruffini, S.-S. Xue; "GRB 970228 Within the EMBH Model"; in "GAMMA-RAY BURSTS: 30 YEARS OF DISCOVERY", Proceedings of the Los Alamos "Gamma Ray Burst Symposium", Santa Fe, New Mexico, 8 – 12 September 2003, E.E. Fenimore, M. Galassi, Editors; AIP Conference Proceedings, 727, 428 (2004).

   We consider the gamma-ray burst of 1997 February 28 (GRB 970228) within the ElectroMagnetic Black Hole (EMBH) model. We first determine the value of the two free parameters that characterize energetically the GRB phenomenon in the EMBH model, that is to say the dyadosphere energy, $E_{dya} = 5.1 \times 10^{52}$ ergs, and the baryonic remnant mass M_B in units of E_{dya}, $B = M_B c^2 / E_{dya} = 3.0 \times 10^{-3}$. Having in this way estimated the energy emitted during the beam-target phase, we evaluate the role of the InterStellar Medium (ISM) number density (n_{ISM}) and of the ratio $\mathcal{R}$ between the effective emitting area and the total surface area of the GRB source, in reproducing the observed profiles of the GRB 970228 prompt emission and X-ray (2-10 keV energy band) afterglow. The importance of the ISM distribution three-dimensional treatment around the central black hole is also stressed in this analysis.

4 Publications (2005–2020)

4.1 Refereed journals

1. R. Ruffini, C.L. Bianco, P. Chardonnet, F. Fraschetti, V. Gurzadyan, S.-S. Xue; "Emergence of a filamentary structure in the fireball from GRB spectra"; International Journal of Modern Physics D, 14, 97 (2005).

   It is shown that the concept of a fireball with a definite filamentary structure naturally emerges from the analysis of the spectra of Gamma-Ray Bursts (GRBs). These results, made possible by the recently obtained analytic expressions of the equitemporal surfaces in the GRB afterglow, depend crucially on the single parameter R describing the effective area of the fireball emitting the X-ray and gamma-ray radiation. The X-ray and gamma-ray components of the afterglow radiation are shown to have a thermal spectrum in the comoving frame of the fireball and originate from a stable shock front described self-consistently by the Rankine-Hugoniot equations. Precise predictions are presented on a correlation between spectral changes and intensity variations in the prompt radiation verifiable, e.g., by the Swift and future missions. The highly variable optical and radio emission depends instead on the parameters of the surrounding medium. The GRB 991216 is used as a prototype for this model.

2. R. Ruffini, M.G. Bernardini, C.L. Bianco, P. Chardonnet, F. Fraschetti, V. Gurzadyan, M. Lattanzi, L. Vitagliano, S.-S. Xue; "Extracting energy from black holes: 'long' and 'short' GRBs and their astrophysical settings"; Il Nuovo Cimento C, 28, 589 (2005).

   The introduction of the three interpretational paradigms for Gamma-Ray Bursts (GRBs) and recent progress in understanding the X- and gamma-ray luminosity in the afterglow allow us to make assessments about the astrophysical settings of GRBs. In particular, we evidence the distinct possibility that some GRBs occur in a binary system. This subclass of GRBs manifests itself in a "tryptich": one component formed by the collapse of a massive star to a black

hole, which originates the GRB; a second component by a supernova and a third one by a young neutron star born in the supernova event. Similarly, the understanding of the physics of quantum relativistic processes during the gravitational collapse makes possible precise predictions about the structure of short GRBs.

3. M.G. Bernardini, C.L. Bianco, P. Chardonnet, F. Fraschetti, R. Ruffini, S.-S. Xue; "Theoretical interpretation of luminosity and spectral properties of GRB 031203"; The Astrophysical Journal, 634, L29 (2005).

   The X-ray and gamma-ray observations of the source GRB 031203 by INTEGRAL are interpreted within our theoretical model. In addition to a complete spacetime parameterization of the GRB, we specifically assume that the afterglow emission originates from a thermal spectrum in the comoving frame of the expanding baryonic matter shell. By determining the two free parameters of the model and estimating the density and filamentary structure of the ISM, we reproduce the observed luminosity in the 20-200 keV energy band. As in previous sources, the prompt radiation is shown to coincide with the peak of the afterglow, and the luminosity substructure is shown to originate in the filamentary structure of the ISM. We predict a clear hard-to-soft behavior in the instantaneous spectra. The time-integrated spectrum over 20 s observed by INTEGRAL is well fitted. Despite the fact that this source has been considered "unusual", it appears to us to be a normal low-energy GRB.

4. R. Ruffini, M.G. Bernardini, C.L. Bianco, P. Chardonnet, F. Fraschetti, S.-S. Xue; Evidence for isotropic emission in GRB991216; Advances in Space Research, 38, 1291 (2006).

   The issue of the possible presence or absence of jets in GRBs is here re-examined for GRB991216. We compare and contrast our theoretically predicted afterglow luminosity in the 2–10 keV band for spherically symmetric versus jetted emission. At these wavelengths the jetted emission can be excluded and data analysis confirms spherical symmetry. These theoretical fits are expected to be improved by the forthcoming data of the Swift mission.

5. R. Ruffini, M.G. Bernardini, C.L. Bianco, P. Chardonnet, F. Fraschetti, R. Guida, S.-S. Xue; "GRB 050315: A step toward understanding the uniqueness of the overall GRB structure"; The Astrophysical Journal, 645, L109 (2006).

Using the Swift data of GRB 050315, we are making progress toward understanding the uniqueness of our theoretically predicted gamma-ray burst (GRB) structure, which is composed of a proper GRB (P-GRB), emitted at the transparency of an electron-positron plasma with suitable baryon loading, and an afterglow comprising the so-called prompt emission due to external shocks. Thanks to the Swift observations, the P-GRB is identified, and for the first time we can theoretically fit detailed light curves for selected energy bands on a continuous timescale ranging over 106 s. The theoretically predicted instantaneous spectral distribution over the entire afterglow is presented, confirming a clear hard-to-soft behavior encompassing, continuously, the "prompt emission" all the way to the latest phases of the afterglow.

6. C.L. Bianco, L. Caito, R. Ruffini; "Theoretical interpretation of GRB 011121"; Il Nuovo Cimento B, 121, 1441 (2006).

   GRB011121 is analyzed as a prototype to understand the "flares" recently observed by Swift in the afterglow of many GRB sources. Detailed theoretical computation of the GRB011121 light curves in selected energy bands are presented and compared and contrasted with observational BeppoSAX data.

7. R. Ruffini, M.G. Bernardini, C.L. Bianco, P. Chardonnet, F. Fraschetti, R. Guida, S.-S. Xue; "GRB 050315: A step toward the uniqueness of the overall GRB structure"; Il Nuovo Cimento B, 121, 1367 (2006).

   Using the *Swift* data of GRB 050315, we progress on the uniqueness of our theoretically predicted Gamma-Ray Burst (GRB) structure as composed by a proper-GRB (P-GRB), emitted at the transparency of an electron-positron plasma with suitable baryon loading, and an afterglow comprising the so called "prompt emission" as due to external shocks. Thanks to the *Swift* observations, we can theoretically fit detailed light curves for selected energy bands on a continuous time scale ranging over 10^6 seconds. The theoretically predicted instantaneous spectral distribution over the entire afterglow confirms a clear hard-to-soft behavior encompassing, continuously, the "prompt emission" all the way to the latest phases of the afterglow. Consequences of the instrumental threshold on the definition of "short" and "long" GRBs are discussed.

8. M.G. Bernardini, C.L. Bianco, L. Caito, P. Chardonnet, A. Corsi, M.G. Dainotti, F. Fraschetti, R. Guida, R. Ruffini, S.-S. Xue; GRB970228 as a prototype for short GRBs with afterglow; Il Nuovo Cimento B, 121, 1439 (2006).

GRB970228 is analyzed as a prototype to understand the relative role of short GRBs and their associated afterglows, recently observed by Swift and HETE-II. Detailed theoretical computation of the GRB970228 light curves in selected energy bands are presented and compared with observational BeppoSAX data.

9. M.G. Dainotti, M.G. Bernardini, C.L. Bianco, L. Caito, R. Guida, R. Ruffini; "GRB060218 and GRBs associated with Supernovae Ib/c"; Astronomy & Astrophysics, 471, L29 (2007).

   Context: The *Swift* satellite has given continuous data in the range 0.3–150 keV from 0 s to 10^6 s for GRB060218 associated with SN2006aj. This Gamma-Ray Burst (GRB) which has an unusually long duration ($T_{90} \sim 2100$ s) fulfills the Amati relation. These data offer the opportunity to probe theoretical models for GRBs connected with Supernovae (SNe).
   Aims: We plan to fit the complete γ- and X-ray light curves of this long duration GRB, including the prompt emission, in order to clarify the nature of the progenitors and the astrophysical scenario of the class of GRBs associated with SNe Ib/c.
   Methods: We apply our "fireshell" model based on the formation of a black hole, giving the relevant references. It is characterized by the precise equations of motion and equitemporal surfaces and by the role of thermal emission.
   Results: The initial total energy of the electron-positron plasma $E^{tot}_{e^\pm} = 2.32 \times 10^{50}$ erg has a particularly low value, similar to the other GRBs associated with SNe. For the first time, we observe a baryon loading $B = 10^{-2}$ which coincides with the upper limit for the dynamical stability of the fireshell. The effective CircumBurst Medium (CBM) density shows a radial dependence $n_{cbm} \propto r^{-\alpha}$ with $1.0 \lesssim \alpha \lesssim 1.7$ and monotonically decreases from 1 to 10^{-6} particles/cm^3. This behavior is interpreted as being due to a fragmentation in the fireshell. Analogies with the fragmented density and filling factor characterizing Novae are outlined. The fit presented is particularly significant in view of the complete data set available for GRB060218 and of the fact that it fulfills the Amati relation.
   Conclusions: We fit GRB060218, usually considered as an X-Ray Flash (XRF), as a "canonical GRB" within our theoretical model. The smallest possible black hole, formed by the gravitational collapse of a neutron star in a binary system, is consistent with the especially low energetics of the class of GRBs associated with SNe Ib/c. We provide the first evidence for a fragmentation in the fireshell. This fragmentation is crucial in explaining both the unusually large T_{90} and the consequently inferred abnormally low value of the CBM effective

density.

10. M.G. Bernardini, C.L. Bianco, L. Caito, M.G. Dainotti, R. Guida, R. Ruffini; "GRB970228 and a class of GRBs with an initial spikelike emission"; Astronomy & Astrophysics, 474, L13 (2007).

    Context: The discovery by *Swift* and HETE-2 of an afterglow emission associated possibly with short GRBs opened the new problematic of their nature and classification. This issue has been further enhanced by the observation of GRB060614 and by a new analysis of the BATSE catalog which led to the identification of a new class of GRBs with "an occasional softer extended emission lasting tenths of seconds after an initial spikelike emission".
    Aims: We plan a twofold task: a) to fit this new class of "hybrid" sources within our "canonical GRB" scenario, where all GRBs are generated by a "common engine" (i.e. the gravitational collapse to a black hole); b) to propose GRB970228 as the prototype of the above mentioned class, since it shares the same morphology and observational features.
    Methods: We analyze *Beppo*SAX data on GRB970228 within the "fireshell" model and we determine the parameters describing the source and the CircumBurst Medium (CBM) needed to reproduce its light curves in the 40–700 keV and 2–26 keV energy bands.
    Results: We find that GRB970228 is a "canonical GRB", like e.g. GRB050315, with the main peculiarity of a particularly low average density of the CBM $\langle n_{cbm}\rangle \sim 10^{-3}$ particles/cm^3. We also simulate the light curve corresponding to a rescaled CBM density profile with $\langle n_{cbm}\rangle = 1$ particle/cm^3. From such a comparison it follows that the total time-integrated luminosity is a faithful indicator of the nature of GRBs, contrary to the peak luminosity which is merely a function of the CBM density.
    Conclusions: We call attention on discriminating the short GRBs between the "genuine" and the "fake" ones. The "genuine" ones are intrinsically short, with baryon loading $B \lesssim 10^{-5}$, as stated in our original classification. The "fake" ones, characterized by an initial spikelike emission followed by an extended emission lasting tenths of seconds, have a baryon loading $10^{-4} \lesssim B \leq 10^{-2}$. They are observed as such only due to an underdense CBM consistent with a galactic halo environment which deflates the afterglow intensity.

11. R. Guida, M.G. Bernardini, C.L. Bianco, L. Caito, M.G. Dainotti, R. Ruffini; "The Amati relation in the "fireshell" model"; Astronomy & Astrophysics, 487, L37 (2008).

Context: The cosmological origin of gamma-ray bursts (GRBs) has been firmly established, with redshifts up to $z = 6.29$. They are possible candidates for use as "distance indicators" for testing cosmological models in a redshift range hardly achievable by other cosmological probes. Asserting the validity of the empirical relations among GRB observables is now crucial for their calibration.
Aims: Motivated by the relation proposed by Amati and collaborators, we look within the "fireshell" model for a relation between the peak energy E_p of the νF_ν total time-integrated spectrum of the afterglow and the total energy of the afterglow E_{aft}, which in our model encompasses and extends the prompt emission.
Methods: The fit within the fireshell model, as for the "canonical" GRB050315, uses the complete arrival time coverage given by the Swift satellite. It is performed simultaneously, self-consistently, and recursively in the four BAT energy bands (15–25 keV, 25–50 keV, 50–100 keV, and 100-150 keV), as well as in the XRT one (0.2–10 keV). It uniquely determines the two free parameters characterizing the GRB source, the total energy $E_{tot}^{e^\pm}$ of the $e^\pm$ plasma and its baryon loading B, as well as the effective CircumBurst Medium (CBM) distribution. We can then build two sets of "gedanken" GRBs varying the total energy of the electron-positron plasma $E_{tot}^{e^\pm}$ and keeping the same baryon loading B of GRB050315. The first set assumes the one obtained in the fit of GRB050315 for the effective CBM density. The second set assumes instead a constant CBM density equal to the average value of the GRB050315 prompt phase.
Results: For the first set of "gedanken" GRBs we find a relation $E_p \propto (E_{aft})^a$, with $a = 0.45 \pm 0.01$, whose slope strictly agrees with the Amati one. Such a relation, in the limit $B \to 10^{-2}$, coincides with the Amati one. Instead, no correlation is found in the second set of "gedanken" GRBs.
Conclusions: Our analysis excludes the proper GRB (P-GRB) from the prompt emission, extends all the way to the latest afterglow phases, and is independent of the assumed cosmological model, since all "gedanken" GRBs are at the same redshift. The Amati relation, on the other hand, includes the P-GRB, focuses only on the prompt emission, being therefore influenced by the instrumental threshold that fixes the end of the prompt emission, and depends on the assumed cosmology. This might explain the intrinsic scatter observed in the Amati relation.

12. L. Caito, M.G. Bernardini, C.L. Bianco, M.G. Dainotti, R. Guida, R. Ruffini; "GRB060614: a "fake" short GRB from a merging binary system"; Astronomy & Astrophysics, 489, 501 (2009).

Context: GRB060614 observations by VLT and by Swift have infringed the traditionally accepted gamma-ray burst (GRB) collapsar scenario that purports the origin of all long duration GRBs from supernovae (SN). GRB060614 is the first nearby long duration GRB clearly not associated with a bright Ib/c SN. Moreover, its duration ($T_{90} \sim 100$ s) makes it hardly classifiable as a short GRB. It presents strong similarities with GRB970228, the prototype of a new class of "fake" short GRBs that appear to originate from the coalescence of binary neutron stars or white dwarfs spiraled out into the galactic halo. *Aims*: Within the "canonical" GRB scenario based on the "fireshell" model, we test if GRB060614 can be a "fake" or "disguised" short GRB. We model the traditionally termed "prompt emission" and discriminate the signal originating from the gravitational collapse leading to the GRB from the process occurring in the circumburst medium (CBM). *Methods*: We fit GRB060614 light curves in Swift's BAT ($15 - 150$ keV) and XRT ($0.2 - 10$ keV) energy bands. Within the fireshell model, light curves are formed by two well defined and different components: the proper-GRB (P-GRB), emitted when the fireshell becomes transparent, and the extended afterglow, due to the interaction between the leftover accelerated baryonic and leptonic shell and the CBM. *Results*: We determine the two free parameters describing the GRB source within the fireshell model: the total $e^{\pm}$ plasma energy ($E_{tot}^{e^{\pm}} = 2.94 \times 10^{51}$erg) and baryon loading ($B = 2.8 \times 10^{-3}$). A small average CBM density $\sim 10^{-3}$ particles/cm^3 is inferred, typical of galactic halos. The first spikelike emission is identified with the P-GRB and the following prolonged emission with the extended afterglow peak. We obtain very good agreement in the BAT ($15 - 150$ keV) energy band, in what is traditionally called "prompt emission", and in the XRT ($0.2 - 10$ keV) one. *Conclusions*: The *anomalous* GRB060614 finds a natural interpretation within our canonical GRB scenario: it is a "disguised" short GRB. The total time-integrated extended afterglow luminosity is greater than the P-GRB one, but its peak luminosity is smaller since it is deflated by the peculiarly low average CBM density of galactic halos. This result points to an old binary system, likely formed by a white dwarf and a neutron star, as the progenitor of GRB060614 and well justifies the absence of an associated SN Ib/c. Particularly important for further studies of the final merging process are the temporal structures in the P-GRB down to 0.1 s.

13. M.G. Bernardini, C.L. Bianco, L. Caito, M.G. Dainotti, R. Guida, R. Ruffini; "GRB970228 in the "canonical GRB" scenario"; Journal of the Korean Physical Society, 56, 1575 (2010).

Within the "fireshell" model, we define a "canonical GRB" light curve with two sharply different components: the proper-GRB (P-GRB), emitted when the optically thick fireshell of an electron-positron plasma originating from the phenomenon reaches transparency, and the afterglow, emitted due to the collision between the remaining optically thin fireshell and the circumburst medium (CBM). On the basis of the recent understanding of GRB970228 as the prototype for a new class of GRBs with "an occasional softer extended emission lasting tenths of seconds after an initial spikelike emission", we outline our "canonical GRB" scenario, originating from the gravitational collapse to a black hole, with special emphasis on the discrimination between "genuine" and "fake" short GRBs. Furthermore, we investigate how the GRB970228 analysis provides a theoretical explanation for the apparent absence of such a correlation for the GRBs belonging to this new class.

14. L. Caito, M.G. Bernardini, C.L. Bianco, M.G. Dainotti, R. Guida, R. Ruffini; "GRB060614: a preliminary result"; Journal of the Korean Physical Society, 56, 1579 (2010).

    The explosion of GRB 060614 produced a deep break in the GRB scenario and opened new horizons of investigation because it can't be traced back to any traditional scheme of classification. In fact, it manifests peculiarities both of long bursts and of short bursts, and above all, it is the first case of a long-duration near GRB without any bright Ib/c associated Supernova. We will show that, in our canonical GRB scenario, this "anomalous" situation finds a natural interpretation and allows us to discuss a possible variation in the traditional classification scheme, introducing a distinction between "genuine" and "fake" short bursts.

15. M.G. Dainotti, M.G. Bernardini, C.L. Bianco, L. Caito, R. Guida, R. Ruffini; "The astrophysical trypthic: GRB, SN and URCA can be extended to GRB060218?"; Journal of the Korean Physical Society, 56, 1588 (2010).

    The *Swift* satellite has given continuous data in the range 0.3–150 keV from 0 s to 10^6 s for GRB060218 associated with SN2006aj. This GRB is the fourth GRB spectroscopically associated with SNe after the cases of GRB980425-SN1998bw, GRB031203-SN2003lw, GRB 030329-SN2003dh. It has an unusually long duration ($T_{90} \sim 2100$ s). These data offer the opportunity to probe theoretical models for Gamma-Ray Bursts (GRBs) connected with Supernovae (SNe). We plan to fit the complete γ- and X-ray light curves of this long duration GRB,

including the prompt emission, in order to clarify the nature of the progenitors and the astrophysical scenario of the class of GRBs associated to SNe Ib/c. We apply our "fireshell" model based on the formation of a black hole, giving the relevant references. The initial total energy of the electron-positron plasma $E^{tot}_{e^\pm} = 2.32 \times 10^{50}$ erg has a particularly low value similarly to the other GRBs associated with SNe. For the first time we observe a baryon loading $B = 10^{-2}$ which coincides with the upper limit for the dynamical stability of the fireshell. The effective CircumBurst Medium (CBM) density shows a radial dependence $n_{cbm} \propto r^{-\alpha}$ with $1.0 \lesssim \alpha \lesssim 1.7$ and monotonically decreases from 1 to 10^{-6} particles/cm^3. Such a behavior is interpreted as due to a fragmentation in the fireshell. Such a fragmentation is crucial in explaining both the unusually large T_{90} and the consequently inferred abnormal low value of the CBM effective density. We fit GRB060218, usually considered as an X-Ray Flash (XRF), as a "canonical GRB" within our theoretical model. The smallest possible black hole, formed by the gravitational collapse of a neutron star in a binary system, is consistent with the especially low energetics of the class of GRBs associated with SNe Ib/c. We present the URCA process and the connection between the GRBs associated with SNe extended also to the case of GRB060218.

16. L. Izzo, M.G. Bernardini, C.L. Bianco, L. Caito, B. Patricelli, R. Ruffini; "GRB 090423 at Redshift 8.1: a Theoretical Interpretation"; Journal of the Korean Physical Society, 57, 551 (2010).

    GRB 090423 is the farthest gamma ray burst ever observed, with a redshift of about 8.1. We present within the fireshell scenario a complete analysis of this GRB. We model the prompt emission and the first rapid flux decay of the afterglow emission as being to the canonical emission of the interaction in the interval $0 \leq t \leq 440$ s by using accelerated baryonic matter with the circumburst medium. After the data reduction of the Swift data in the BAT (15 - 150 keV) and XRT (0.2 - 10 keV) energy bands, we interpret the light curves and the spectral distribution in the context of the fireshell scenario. We also confirm in this source the existence of a second component, a plateau phase, as being responsible for the late emission in the X-ray light curve. This extra component originates from the fact that the ejecta have a range of the bulk Lorentz Γ factor, which starts to interact each other ejecta at the start of the plateau phase.

17. L. Caito, L. Amati, M.G. Bernardini, C.L. Bianco, G. De Barros, L. Izzo, B. Patricelli, R. Ruffini; "GRB 071227: an additional case of a disguised

short burst"; Astronomy & Astrophysics, 521, A80 (2010).

Context: Observations of gamma-ray bursts (GRBs) have shown an hybridization between the two classes of long and short bursts. In the context of the fireshell model, the GRB light curves are formed by two different components: the *proper* GRB (P-GRB) and the extended afterglow. Their relative intensity is linked to the fireshell baryon loading B. The GRBs with P-GRB predominance are the short ones, the remainders are long. A new family of *disguised* short bursts has been identified: long bursts with a protracted low instantaneous luminosity due to a low density CircumBurst Medium (CBM). In the 15–150 keV energy band GRB 071227 exhibits a short duration (about 1.8s) spike-like emission followed by a very soft extended tail up to one hundred seconds after the trigger. It is a faint ($E_{iso} = 5.8 \times 10^{50}$) nearby GRB ($z = 0.383$) that does not have an associated type Ib/c bright supernova (SN). For these reasons, GRB 071227 has been classified as a short burst not fulfilling the Amati relation holding for long burst. *Aims:* We check the classification of GRB 071227 provided by the fireshell model. In particular, we test whether this burst is another example of a *disguised* short burst, after GRB 970228 and GRB 060614, and, for this reason, whether it fulfills the Amati relation. *Methods:* We simulate GRB 071227 light curves in the *Swift* BAT 15–50 keV bandpass and in the XRT (0.3–10 keV) energy band within the fireshell model. *Results:* We perform simulations of the tail in the 15–50 keV bandpass, as well as of the first part of the X-ray afterglow. This infers that: $E_{tot}^{e^\pm} = 5.04 \times 10^{51}$ erg, $B = 2.0 \times 10^{-4}$, $E_{P-GRB}/E_{aft} \sim 0.25$, and $\langle n_{cbm} \rangle = 3.33$ particles/cm^3. These values are consistent with those of "long duration" GRBs. We interpret the observed energy of the first hard emission by identifying it with the P-GRB emission. The remaining long soft tail indeed fulfills the Amati relation. *Conclusions:* Previously classified as a short burst, GRB 071227 on the basis of our analysis performed in the context of the fireshell scenario represents another example of a *disguised* short burst, after GRB 970228 and GRB 060614. Further confirmation of this result is that the soft tail of GRB 071227 fulfills the Amati relation.

18. M.G. Bernardini, C.L. Bianco, L. Caito, L. Izzo, B. Patricelli, R. Ruffini; "Analysis of GRB060607A within the fireshell model: prompt emission, X-ray flares and late afterglow phase"; Astronomy & Astrophysics, submitted to.

Context: GRB060607A is a very distant ($z = 3.082$) and energetic event ($E_{iso} \sim 10^{53}$ erg). Its main peculiarity is that the peak of the near-infrared (NIR) af-

terglow has been observed with the REM robotic telescope. This NIR peak has been interpreted as the afterglow onset within the fireball forward shock model, and the initial Lorentz gamma factor of the emitting system has been inferred. *Aims*: We analyze GRB060607A within the fireshell model. We emphasize the central role of the prompt emission in determining the initial Lorentz gamma factor of the extended afterglow and we interpret the X-ray flares as produced by the interaction of the optically thin fireshell with overdense CircumBurst Medium (CBM) clumps. *Methods*: We deal only with the Swift BAT and XRT observations, that are the basic contribution to the GRB emission and that are neglected in the treatment adopted in the current literature. The numerical modeling of the fireshell dynamics allows to calculate all its characteristic quantities, in particular the exact value of the Lorentz gamma factor at the transparency. *Results*: We show that the theoretically computed prompt emission light curves are in good agreement with the observations in all the *Swift* BAT energy bands as well as the spectra integrated over different time intervals. The flares observed in the decaying phase of the X-ray afterglow are also reproduced by the same mechanism, but in a region in which the typical dimensions of the clumps are smaller than the visible area of the fireshell and most energy lies in the X-ray band due to the hard-to-soft evolution. *Conclusions*: We show that it is possible to obtain flares with $\Delta t/t$ compatible with the observations when the three-dimensional structure of the CBM clumps is duly taken into account. We stop our analysis at the beginning of the X-ray plateau phase, since we suppose this originates from the instabilities developed in the collision between different subshells within a structured fireshell.

19. G. de Barros, M. G. Bernardini, C.L. Bianco, L. Caito, L. Izzo, B. Patricelli, R. Ruffini; "On the nature of GRB 050509b: a disguised short GRB"; Astronomy & Astrophyscs, 529, A130 (2011)

    Context: GRB 050509b, detected by the *Swift* satellite, is the first case where an X-ray afterglow has been observed associated with a short gamma-ray burst (GRB). Within the fireshell model, the canonical GRB light curve presents two different components: the proper-GRB (P-GRB) and the extended afterglow. Their relative intensity is a function of the fireshell baryon loading parameter B and of the CircumBurst Medium (CBM) density (n_{CBM}). In particular, the traditionally called short GRBs can be either "genuine" short GRBs (with $B \lesssim 10^{-5}$, where the P-GRB is energetically predominant) or "disguised" short GRBs (with $B \gtrsim 3.0 \times 10^{-4}$ and $n_{CBM} \ll 1$, where the extended afterglow is energetically predominant). *Aims*: We verify whether GRB 050509b can be clas-

sified as a "genuine" short or a "disguised" short GRB, in the fireshell model. *Methods*: We investigate two alternative scenarios. In the first, we start from the assumption that this GRB is a "genuine" short burst. In the second attempt, we assume that this GRB is a "disguised" burst. *Results*: If GRB 050509b were a genuine short GRB, there should initially be very hard emission which is ruled out by the observations. The analysis that assumes that this is a disguised short GRB is compatible with the observations. The theoretical model predicts a value of the extended afterglow energy peak that is consistent with the Amati relation. *Conclusions*: GRB 050509b cannot be classified as a "genuine" short GRB. The observational data are consistent with a "disguised" short GRB classification, i.e., a long burst with a weak extended afterglow "deflated" by the low density of the CBM. We expect that all short GRBs with measured redshifts are disguised short GRBs because of a selection effect: if there is enough energy in the afterglow to measure the redshift, then the proper GRB must be less energetic than the afterglow. The Amati relation is found to be fulfilled only by the extended afterglow excluding the P-GRB.

20. L. Caito, M.G. Bernardini, C.L. Bianco, L. Izzo, B. Patricelli, R. Ruffini; "GRB 071227: another disguised short burst"; International Journal of Modern Physics D, 20, 1931 (2011).

    Observations of Gamma-ray Bursts (GRBs) put forward in the recent years have revealed, with increasing evidence, that the historical classification between long and short bursts has to be revised. Within the Fireshell scenario, both short and long bursts are canonical bursts, consisting of two different phases. First, a Proper-GRB (P-GRB), that is the emission of photons at the transparency of the fireshell. Then, the Extended Afterglow, multiwavelength emission due to the interacion of the baryonic remnants of the fireshell with the CircumBurst Medium (CBM). We discriminate between long and short bursts by the amount of energy stored in the first phase with respect to the second one. Within the Fireshell scenario, we have introduced a third intermediate class: the disguised GRBs. They appear like short bursts, because their morphology is characterized by a first, short, hard episode and a following deflated tail, but this last part — coincident with the peak of the afterglow — is energetically predominant. The origin of this peculiar kind of sources is inferred to a very low average density of the environment (of the order of 10^{-3}). After GRB 970228 and GRB 060614, we find in GRB 071227 a third example of disguised burst.

21. L. Izzo, M.G. Bernardini, C.L. Bianco, L. Caito, B. Patricelli, L.J. Rangel Lemos, R. Ruffini; "GRB 080916C and the high-energy emission in the fireshell scenario"; International Journal of Modern Physics D, 20, 1949 (2011).

    In this paper we discuss a possible explanation for the high energy emission (up to $\sim$ GeV) seen in GRB 080916C. We propose that the GeV emission is originated by the collision between relativistic baryons in the fireshell after the transparency and the nucleons located in molecular clouds near the burst site. This collision should give rise pion production, whose immediate decay provides high energy photons, neutrinos and leptons. Using a public code (SYBILL) we simulate these relativistic collisions in their simple form, so that we can draw our preliminar results in this paper. We will present moreover our hypothesis that the delayed onset of this emission identifies in a complete way the P-GRB emission.

22. B. Patricelli, M.G. Bernardini, C.L. Bianco, L. Caito, L. Izzo, R. Ruffini, G. Vereshchagin; "A new spectral energy distribution of photons in the fireshell model of GRBs"; International Journal of Modern Physics D, 20, 1983 (2011).

    The analysis of various Gamma-Ray Bursts (GRBs) having a low energetics (an isotropic energy $E_{iso} \lesssim 10^{53}$ ergs) within the fireshell model has shown how the $N(E)$ spectrum of their prompt emission can be reproduced in a satisfactory way by a convolution of thermal spectra. Nevertheless, from the study of very energetic bursts ($E_{iso} \lesssim 10^{54}$ ergs) such as, for example, GRB 080319B, some discrepancies between the numerical simulations and the observational data have been observed. We investigate a different spectrum of photons in the comoving frame of the fireshell in order to better reproduce the spectral properties of GRB prompt emission within the fireshell model. We introduce a phenomenologically modified thermal spectrum: a thermal spectrum characterized by a different asymptotic power-law index in the low energy region. Such an index depends on a free parameter α, so that the pure thermal spectrum corresponds to the case $\alpha = 0$. We test this spectrum by comparing the numerical simulations with the observed prompt emission spectra of various GRBs. From this analysis it has emerged that the observational data can be correctly reproduced by assuming a modified thermal spectrum with $\alpha = -1.8$.

23. A.V. Penacchioni, R. Ruffini, L. Izzo, M. Muccino, C.L. Bianco, L. Caito, B. Patricelli, L. Amati; "Evidence for a proto-black hole and a double

astrophysical component in GRB 101023"; Astronomy & Astrophysics, 538, A58 (2012).

Context: It has been recently shown that GRB 090618, observed by AGILE, Coronas Photon, Fermi, Konus, Suzaku and Swift, is composed of two very different components: episode 1, lasting 50 s, shows a thermal plus power-law spectrum with a characteristic temperature evolving in time as a power law; episode 2 (the remaining 100 s) is a canonical long GRB. We have associated episode 1 to the progenitor of a collapsing bare core leading to the formation of a black hole: what was defined as a "proto black hole". *Aims*: In precise analogy with GRB 090618 we aim to analyze the 89s of the emission of GRB 101023, observed by Fermi, Gemini, Konus and Swift, to see if there are two different episodes: the first one presenting a characteristic black-body temperature evolving in time as a broken power law, and the second one consistent with a canonical GRB. *Methods*: To obtain information on the spectra, we analyzed the data provided by the GBM detector onboard the Fermi satellite, and we used the heasoft package XSPEC and RMFIT to obtain their spectral distribution. We also used the numerical code GRBsim to simulate the emission in the context of the fireshell scenario for episode 2. *Results*: We confirm that the first episode can be well fit by a black body plus power-law spectral model. The temperature changes with time following a broken power law, and the photon index of the power-law component presents a soft-to-hard evolution. We estimate that the radius of this source increases with time with a velocity of $1.5 \times 10^4 km/s$. The second episode appears to be a canonical GRB. By using the Amati and the Atteia relations, we determined the cosmological redshift, $z \sim 0.9 \pm 0.084(stat.) \pm 0.2(sys.)$. The results of GRB 090618 are compared and contrasted with the results of GRB 101023. Particularly striking is the scaling law of the soft X-ray component of the afterglow. *Conclusions*: We identify GRB 090618 and GRB 101023 with a new family of GRBs related to a single core collapse and presenting two astrophysical components: a first one related to the proto-black hole prior to the process of gravitational collapse (episode 1), and a second one, which is the canonical GRB (episode 2) emitted during the formation of the black hole. For the first time we are witnessing the process of a black hole formation from the instants preceding the gravitational collapse up to the GRB emission. This analysis indicates progress towards developing a GRB distance indicator based on understanding the P-GRB and the prompt emission, as well as the soft X-ray behavior of the late afterglow.

24. R. Negreiros, R. Ruffini, C. L. Bianco, J. A. Rueda; "Cooling of young

neutron stars in GRB associated to supernovae"; Astronomy & Astrophysics, 540, A12 (2012).

Context: The traditional study of neutron star cooling has been generally applied to quite old objects such as the Crab Pulsar (957 years) or the central compact object in Cassiopeia A (330 years) with an observed surface temperature $\sim 10^6$ K. However, recent observations of the late ($t = 10^8$–10^9 s) emission of the supernovae (SNe) associated to GRBs (GRB-SN) show a distinctive emission in the X-ray regime consistent with temperatures $\sim 10^7$–10^8 K. Similar features have been also observed in two Type Ic SNe SN 2002ap and SN 1994I that are not associated to GRBs. *Aims*: We advance the possibility that the late X-ray emission observed in GRB-SN and in isolated SN is associated to a hot neutron star just formed in the SN event, here defined as a neo-neutron star. *Methods*: We discuss the thermal evolution of neo-neutron stars in the age regime that spans from ~ 1 minute (just after the proto-neutron star phase) all the way up to ages < 10–100 yr. We examine critically the key factor governing the neo-neutron star cooling with special emphasis on the neutrino emission. We introduce a phenomenological heating source, as well as new boundary conditions, in order to mimic the high temperature of the atmosphere for young neutron stars. In this way we match the neo-neutron star luminosity to the observed late X-ray emission of the GRB-SN events: URCA-1 in GRB980425-SN1998bw, URCA-2 in GRB030329-SN2003dh, and URCA-3 in GRB031203-SN2003lw. *Results*: We identify the major role played by the neutrino emissivity in the thermal evolution of neo-neutron stars. By calibrating our additional heating source at early times to $\sim 10^{12}$–10^{15} erg/g/s, we find a striking agreement of the luminosity obtained from the cooling of a neo-neutron stars with the prolonged ($t = 10^8$–10^9 s) X-ray emission observed in GRB associated with SN. It is therefore appropriate a revision of the boundary conditions usually used in the thermal cooling theory of neutron stars, to match the proper conditions of the atmosphere at young ages. The traditional thermal processes taking place in the crust might be enhanced by the extreme high-temperature conditions of a neo-neutron star. Additional heating processes that are still not studied within this context, such as e^+e^- pair creation by overcritical fields, nuclear fusion, and fission energy release, might also take place under such conditions and deserve further analysis. *Conclusions*: Observation of GRB-SN has shown the possibility of witnessing the thermal evolution of neo-neutron stars. A new campaign of dedicated observations is recommended both of GRB-SN and of isolated Type Ic SN.

25. L. Izzo, R. Ruffini, A.V. Penacchioni, C.L. Bianco, L. Caito, S.K. Chakrabarti, J.A. Rueda, A. Nandi, B. Patricelli; "A double component in GRB 090618: a proto-black hole and a genuinely long gamma-ray burst"; Astronomy & Astrophysics, 543, A10 (2012).

Context: The joint X-ray and gamma-ray observations of GRB 090618 by very many satellites offer an unprecedented possibility of testing crucial aspects of theoretical models. In particular, they allow us to test (a) in the process of gravitational collapse, the formation of an optically thick e+e.-baryon plasma self-accelerating to Lorentz factors in the range $200 < \Gamma < 3000$; (b) its transparency condition with the emission of a component of 10^{53-54} baryons in the TeV region and (c) the collision of these baryons with the circumburst medium (CBM) clouds, characterized by dimensions of 10^{15-16} cm. In addition, these observations offer the possibility of testing a new understanding of the thermal and power-law components in the early phase of this GRB. *Aims*: We test the fireshell model of GRBs in one of the closest ($z = 0.54$) and most energetic ($E_{iso} = 2.90 \times 10^{53}$ erg) GRBs, namely GRB 090618. It was observed at ideal conditions by several satellites, namely *Fermi*, *Swift*, Konus-WIND, AGILE, RT-2, and Suzaku, as well as from on-ground optical observatories. *Methods*: We analyzed the emission from GRB 090618 using several spectral models, with special attention to the thermal and power-law components. We determined the fundamental parameters of a canonical GRB within the context of the fireshell model, including the identification of the total energy of the e^+e^- plasma, $E_{tot}^{e^+e^-}$, the proper GRB (P-GRB), the baryon load, the density and structure of the CBM. *Results*: We find evidence of the existence of two different episodes in GRB 090618. The first episode lasts 50 s and is characterized by a spectrum consisting of a thermal component, which evolves between $kT = 54$ keV and $kT = 12$ keV, and a power law with an average index $\gamma = 1.75 \pm 0.04$. The second episode, which lasts for ~ 100 s, behaves as a canonical long GRB with a Lorentz gamma factor at transparency of $\Gamma = 495$, a temperature at transparency of 29.22 keV and with a characteristic size of the surrounding clouds of $R_{cl} \sim 10^{15-16}$ cm and masses of $\sim 10^{22-24}$ g. *Conclusions*: We support the recently proposed two-component nature of GRB 090618, namely, episode 1 and episode 2, with a specific theoretical analysis.We furthermore illustrate that episode 1 cannot be considered to be either a GRB or a part of a GRB event, but it appears to be related to the progenitor of the collapsing bare core, leading to the formation of the black hole, which we call a "proto-black hole". Thus, for the first time, we are witnessing the process of formation of a black

hole from the phases just preceding the gravitational collapse all the way up to the GRB emission.

26. B. Patricelli, M.G. Bernardini, C.L. Bianco, L. Caito, G. De Barros, L. Izzo, R. Ruffini, G.V. Vereshchagin; "Analysis of GRB 080319B and GRB 050904 within the Fireshell Model: Evidence for a Broader Spectral Energy Distribution"; The Astrophysical Journal, 756, 16 (2012).

    The observation of GRB 080319B, with an isotropic energy $E_{iso} = 1.32 \times 10^{54}$ erg, and GRB 050904, with $E_{iso} = 1.04 \times 10^{54}$ erg, offers the possibility of studying the spectral properties of the prompt radiation of two of the most energetic Gamma Ray Bursts (GRBs). This allows us to probe the validity of the fireshell model for GRBs beyond 10^{54} erg, well outside the energy range where it has been successfully tested up to now (10^{49}–10^{53} erg). We find that in the low energy region, the prompt emission spectra observed by *Swift* BAT reveals more power than theoretically predicted. The opportunities offered by these observations to improve the fireshell model are outlined in this paper. One of the distinguishing features of the fireshell model is that it relates the observed GRB spectra to the spectrum in the comoving frame of the fireshell. Originally, a fully radiative condition and a comoving thermal spectrum were adopted. An additional power-law in the comoving thermal spectrum is required due to the discrepancy of the theoretical and observed light curves and spectra in the fireshell model for GRBs 080319B and 050904. A new phenomenological parameter α is correspondingly introduced in the model. We perform numerical simulations of the prompt emission in the *Swift* BAT bandpass by assuming different values of α within the fireshell model. We compare them with the GRB 080319B and GRB 050904 observed time-resolved spectra, as well as with their time-integrated spectra and light curves. Although GRB 080319B and GRB 050904 are at very different redshifts (z=0.937 and z=6.29 respectively), a value of $\alpha = -1.8$ leads for both of them to a good agreement between the numerical simulations and the observed BAT light curves, time-resolved and time-integrated spectra. Such a modified spectrum is also consistent with the observations of previously analyzed less energetic GRBs and reasons for this additional agreement are given. Perspectives for future low energy missions are outlined.

27. M. Muccino, R. Ruffini, C.L. Bianco, L. Izzo, A.V. Penacchioni; "GRB 090227B: The missing link between the genuine short and long GRBs"; The Astrophysical Journal, 763, 125 (2013).

The time-resolved spectral analysis of GRB 090227B, made possible by the *Fermi*-GBM data, allows to identify in this source the missing link between the genuine short and long GRBs. Within the Fireshell model of the Gamma-Ray Bursts (GRBs) we predict genuine short GRBs: bursts with the same inner engine of the long bursts but endowed with a severely low value of the Baryon load, $B \lesssim 5 \times 10^{-5}$. A first energetically predominant emission occurs at the transparency of the e^+e^- plasma, the Proper-GRB (P-GRB), followed by a softer emission, the extended afterglow. The typical separation between the two emissions is expected to be of the order of 10^{-3} – 10^{-2} s. We identify the P-GRB of GRB 090227B in the first 96 ms of emission, where a thermal component with the temperature $kT = (517 \pm 28)$ keV and a flux comparable with the non thermal part of the spectrum is observed. This non thermal component as well as the subsequent emission, where there is no evidence for a thermal spectrum, is identified with the extended afterglow. We deduce a theoretical cosmological redshift $z = 1.61 \pm 0.14$. We then derive the total energy $E^{tot}_{e^+e^-} = (2.83 \pm 0.15) \times 10^{53}$ ergs, the Baryon load $B = (4.13 \pm 0.05) \times 10^{-5}$, the Lorentz Γ factor at transparency $\Gamma_{tr} = (1.44 \pm 0.01) \times 10^4$, and the intrinsic duration $\Delta t' \sim 0.35$ s. We also determine the average density of the CircumBurst Medium (CBM), $\langle n_{CBM} \rangle = (1.90 \pm 0.20) \times 10^{-5}$ particles/cm^3. There is no evidence of beaming in the system. In view of the energetics and of the Baryon load of the source, as well as of the low interstellar medium and of the intrinsic time scale of the signal, we identify the GRB progenitor as a binary neutron star. From the recent progress in the theory of neutron stars, we obtain masses of the stars $m_1 = m_2 = 1.34 M_\odot$ and their corresponding radii $R_1 = R_2 = 12.24$ km and thickness of their crusts ~ 0.47 km, consistent with the above values of the Baryon load, of the energetics and of the time duration of the event.

28. A.V. Penacchioni, R. Ruffini, C.L. Bianco, L. Izzo, M. Muccino, G.B. Pisani, J.A. Rueda; "GRB 110709B in the induced gravitational collapse paradigm"; Astronomy & Astrophysics, 551, A133 (2013).

Context: GRB 110709B is the first source for which *Swift* BAT triggered twice, with a time separation of ~ 10 minutes. The first emission (called here Episode 1) goes from 40 s before the first trigger up to 60 s after it. The second emission (hereafter Episode 2) goes from 35 s before the second trigger to 100 s after it. These features reproduce the ones of GRB 090618, which has been recently interpreted within the Induced Gravitational Collapse paradigm (IGC). In line with this paradigm we assume the progenitor to be a close binary system composed of a core of an evolved star and a Neutron Star (NS). The evolved star

explodes as a Supernova (SN) and ejects material that is partially accreted by the NS. We identify this process with Episode 1. The accretion process brings the NS over its critical mass, thus gravitationally collapsing to a BH. This process leads to the GRB emission, Episode 2. The double trigger has given for the first time the possibility to have a coverage of the X-ray emission observed by XRT both prior to and during the prompt phase of GRB 110709B. *Aims*: We analyze the spectra and time variability of Episode 1 and 2 and compute the relevant parameters of the binary progenitor, as well as the astrophysical parameters both in the SN and the GRB phase in the IGC paradigm. *Methods*: We perform a time-resolved spectral analysis of Episode 1 by fitting the spectrum with a blackbody (BB) plus a power-law (PL) spectral model. From the BB fluxes and temperatures of Episode 1 and the luminosity distance d_L, we evaluate the evolution with time of the radius of the BB emitter, associated here to the evolution of the SN ejecta. We analyze Episode 2 within the Fireshell model, identifying the Proper-GRB (P-GRB) and simulating the light curve and spectrum. We establish the redshift to be $z = 0.75$, following the phenomenological methods by Amati, by Yonetoku and by Grupe, and our analysis of the late X-ray afterglow. It is most remarkable that the determination of the cosmological redshift on the ground of the scaling of the late X-ray afterglow, already verified in GRB 090618 and GRB 101023, is again verified by this analysis. *Results*: We find for Episode 1 a temperature of the BB component that evolves with time following a broken PL, with the slope of the PL at early times $\alpha = 0$ (constant function) and the slope of the PL at late times $\beta = -4 \pm 2$. The break occurs at $t = 41.21$ s. The total energy of Episode 1 is $E_{iso}^{(1)} = 1.42 \times 10^{53}$ erg. The total energy of Episode 2 is $E_{iso}^{(2)} = 2.43 \times 10^{52}$ erg. We find at transparency a Lorentz factor $\Gamma \sim 1.73 \times 10^2$, laboratory radius of 6.04×10^{13} cm, P-GRB observed temperature $kT_{P-GRB} = 12.36$ keV, baryon load $B = 5.7 \times 10^{-3}$ and P-GRB energy of $E_{P-GRB} = 3.44 \times 10^{50}$ erg. We find a remarkable coincidence of the cosmological redshift by the scaling of the XRT data and with three other phenomenological methods. *Conclusions*: We interpret GRB 110709B as a member of the IGC sources, together with GRB 970828, GRB 090618 and GRB 101023. The existence of the XRT data during the prompt phase of the emission of GRB 110709B (Episode 2) offers an unprecedented tool for improving the diagnostic of GRBs emission.

29. G.B. Pisani, L. Izzo, R. Ruffini, C.L. Bianco, M. Muccino, A.V. Penacchioni, J.A. Rueda, Y. Wang; "Novel distance indicator for gamma-ray bursts associated with supernovae"; Astronomy & Astrophysics, 552,

L5 (2013).

Context: In recent years it has been proposed that the temporal coincidence of a Gamma Ray Burst (GRB) and a type Ib/c supernova (SN) can be explained by the concept of Induced Gravitational Collapse (IGC) of a Neutron Star (NS) to a Black Hole (BH) by accretion of matter ejected by a SN Ib/c. This scenario reveals a possible common behavior in the late time X-ray emission of this subclass of GRBs. *Aims*: We want to test if such a common behavior can actually be present in the sources belonging to this GRB sub-class and if this may lead to a redshift estimator for these sources. *Methods*: We build a sample of GRBs belonging to this sub-class, and we rescale the X-ray light curves of all of them both in time and in flux to a common cosmological redshift. *Results*: We found that the X-ray light curves of all the GRBs of the sample with a measured redshift present a common late time behavior when rescaled to a common redshift $z = 1$. We then use this result to estimate the redshift of the GRBs of the sample with no measured redshift. *Conclusions*: The common behavior in the late decay of the X-ray light curves of the GRBs of the sample points to a common physical mechanism in this particular phase of the GRB emission, possibly related to the SN process. This scenario may represent an invaluable tool to estimate the redshift of GRBs belonging to this sub-class of events. More GRBs are therefore needed in order to enlarge the subclass and to make more stringent constraints on the redshift estimates performed with this method for GRBs pertaining to this class.

30. C.L. Bianco, M. G. Bernardini, L. Caito, G. De Barros, L. Izzo, M. Muccino, B. Patricelli, A.V. Penacchioni, G.B. Pisani, R. Ruffini; "The canonical GRB scenario"; Il Nuovo Cimento C, 36 s01, 21 (2013).

    The canonical GRB scenario implied by the fireshell model is briefly summarized.

31. A.V. Penacchioni, R. Ruffini, L. Izzo, M. Muccino, C.L. Bianco, L. Caito, B. Patricelli; "Evidences for a double component in the emission of GRB 101023"; Il Nuovo Cimento C, 36 s01, 117 (2013).

    In this work we present the results of the analysis of GRB 101023 in the fireshell scenario. Its redshift is not known, so we attempted to infer it from the Amati Relation, obtaining $z = 0.9$. Its light curve presents a double emission, which makes it very similar to the already studied GRB 090618. We called each part Episode 1 and Episode 2. We performed a time-resolved spectral

analysis with RMFIT using different spectral models, and fitted the light curve with a numerical code integrating the fireshell equations of motion. We used Fermi GBM data to build the light curve, in particular the second NaI detector, in the range (8.5–1000 keV). We considered different hypotheses regarding which part of the light curve could be the GRB and performed the analysis of all of them. We noticed a great variation of the temperature with time in the first episode, as well as almost no variation of the progenitor radius. We found that the first emission does not match the requirements for a GRB, while the second part perfectly agrees with being a canonical GRB, with a P-GRB lasting 4 s.

32. M. Muccino, R. Ruffini, C.L. Bianco, L. Izzo, A.V. Penacchioni, G.B. Pisani; "GRB 090510: A Disguised Short Gamma-Ray Burst with the Highest Lorentz Factor and Circumburst Medium"; The Astrophysical Journal, 772, 62 (2013).

GRB 090510, observed both by Fermi and AGILE satellites, is the first bright short-hard Gamma-Ray Burst (GRB) with an emission from the keV up to the GeV energy range. Within the Fireshell model, we interpret the faint precursor in the light curve as the emission at the transparency of the expanding e^+e^- plasma: the Proper-GRB (P-GRB). From the observed isotropic energy we assume a total plasma energy $E^{tot}_{e^+e^-} = (1.10 \pm 0.06) \times 10^{53}$erg and derive a Baryon load $B = (1.45 \pm 0.28) \times 10^{-3}$ and a Lorentz factor at transparency $\Gamma_{tr} = (6.7 \pm 1.6) \times 10^2$. The main emission $\sim$ 0.4s after the initial spike is interpreted as the extended afterglow, due to the interaction of the ultrarelativistic baryons with the CircumBurst Medium (CBM). Using the condition of fully radiative regime, we infer a CBM average spherically symmetric density of $\langle n_{CBM} \rangle = (1.85 \pm 0.14) \times 10^3$ particles/cm^3, one of the highest found in the Fireshell model. The value of the filling factor, $1.5 \times 10^{-10} \leq \mathcal{R} \leq 3.8 \times 10^{-8}$, leads to the estimate of filaments with densities $n_{fil} = n_{CBM}/\mathcal{R} \approx (10^6 - 10^{14})$ particles/cm^3. The sub-MeV and the MeV emissions are well reproduced. When compared to the canonical GRBs with $\langle n_{CBM} \rangle \approx 1$ particles/cm^3 and to the disguised short GRBs with $\langle n_{CBM} \rangle \approx 10^{-3}$ particles/cm^3, the case of GRB 090510 leads to the existence of a new family of bursts exploding in an over-dense galactic region with $\langle n_{CBM} \rangle \approx 10^3$ particles/cm^3. The joint effect of the high Γ_{tr} and the high density compresses in time and "inflates" in intensity the extended afterglow, making it appear as a short burst, which we here define as "disguised short GRB by excess". The determination of the above parameters values may represent an important step towards the explanation

of the GeV emission.

33. R. Ruffini, M. Muccino, C.L. Bianco, M. Enderli, L. Izzo, M. Kovacevic, A.V. Penacchioni, G.B. Pisani, J.A. Rueda, Y. Wang; "On Binary Driven Hypernovae and their nested late X-ray emission"; Astronomy & Astrophysics, 565, L10 (2014).

Context: The induced gravitational collapse (IGC) paradigm addresses the very energetic (10^{52}–10^{54} erg) long gamma-ray bursts (GRBs) associated to supernovae (SNe). Unlike the traditional "collapsar" model, an evolved FeCO core with a companion neutron star (NS) in a tight binary system is considered as the progenitor. This special class of sources, here named "binary driven hypernovae" (BdHNe), presents a composite sequence composed of four different episodes with precise spectral and luminosity features.
Aims: We first compare and contrast the steep decay, the plateau, and the power-law decay of the X-ray luminosities of three selected BdHNe (GRB 060729, GRB 061121, and GRB 130427A). Second, to explain the different sizes and Lorentz factors of the emitting regions of the four episodes, for definiteness, we use the most complete set of data of GRB 090618. Finally, we show the possible role of r-process, which originates in the binary system of the progenitor.
Methods: We compare and contrast the late X-ray luminosity of the above three BdHNe. We examine correlations between the time at the starting point of the constant late power-law decay t_a^*, the average prompt luminosity $\langle L_{iso} \rangle$, and the luminosity at the end of the plateau L_a. We analyze a thermal emission ($\sim$ 0.97–0.29 keV), observed during the X-ray steep decay phase of GRB 090618.
Results: The late X-ray luminosities of the three BdHNe, in the rest-frame energy band 0.3–10 keV, show a precisely constrained "nested" structure. In a space-time diagram, we illustrate the different sizes and Lorentz factors of the emitting regions of the three episodes. For GRB 090618, we infer an initial dimension of the thermal emitter of $\sim 7 \times 10^{12}$ cm, expanding at $\Gamma \approx 2$. We find tighter correlations than the Dainotti-Willingale ones.
Conclusions: We confirm a constant slope power-law behavior for the late X-ray luminosity in the source rest frame, which may lead to a new distance indicator for BdHNe. These results, as well as the emitter size and Lorentz factor, appear to be inconsistent with the traditional afterglow model based on synchrotron emission from an ultra-relativistic ($\Gamma \sim 10^2$–10^3) collimated jet outflow. We argue, instead, for the possible role of r-process, originating in the binary system, to power the mildly relativistic X-ray source.

34. R. Ruffini, L. Izzo, M. Muccino, G.B. Pisani, J.A. Rueda, Y. Wang, C. Barbarino, C.L. Bianco, M. Enderli, M. Kovacevic; "Induced gravitational collapse at extreme cosmological distances: the case of GRB 090423"; Astronomy & Astrophysics, 569, A39 (2014).

    Context: The induced gravitational collapse (IGC) scenario has been introduced in order to explain the most energetic gamma ray bursts (GRBs), $E_{iso} = 10^{52} - 10^{54}$ erg, associated with type Ib/c supernovae (SNe). It has led to the concept of binary-driven hypernovae (BdHNe) originating in a tight binary system composed by a FeCO core on the verge of a SN explosion and a companion neutron star (NS). Their evolution is characterized by a rapid sequence of events: 1) The SN explodes, giving birth to a new NS (νNS). The accretion of SN ejecta onto the companion NS increases its mass up to the critical value; 2) The consequent gravitational collapse is triggered, leading to the formation of a black hole (BH) with GRB emission; 3) A novel feature responsible for the emission in the GeV, X-ray, and optical energy range occurs and is characterized by specific power-law behavior in their luminosity evolution and total spectrum; 4) The optical observations of the SN then occurs.
    Aims: We investigate whether GRB 090423, one of the farthest observed GRB at $z = 8.2$, is a member of the BdHN family.
    Methods: We compare and contrast the spectra, the luminosity evolution, and the detectability in the observations by *Swift* of GRB 090423 with the corresponding ones of the best known BdHN case, GRB 090618.
    Results: Identification of constant slope power-law behavior in the late X-ray emission of GRB 090423 and its overlapping with the corresponding one in GRB 090618, measured in a common rest frame, represents the main result of this article. This result represents a very significant step on the way to using the scaling law properties, proven in Episode 3 of this BdHN family, as a cosmological standard candle.
    Conclusions: Having identified GRB 090423 as a member of the BdHN family, we can conclude that SN events, leading to NS formation, can already occur already at $z = 8.2$, namely at 650 Myr after the Big Bang. It is then possible that these BdHNe originate stem from 40-60 $M_\odot$ binaries. They are probing the Population II stars after the completion and possible disappearance of Population III stars.

35. M. Muccino, C.L. Bianco, L. Izzo, Y. Wang, M. Enderli, M. Kovacevic, G.B. Pisani, A.V. Penacchioni, R. Ruffini; "The Genuine Short GRB 090227B and the Disguised by Excess GRB 090510"; Gravitation and

Cosmology, 20, 197 (2014).

GRB 090227B and GRB 090510, traditionally classified as short gamma-ray Bursts (GRBs), indeed originate from different systems. For GRB 090227B we inferred a total energy of the e^+e^- plasma $E^{tot}_{e^+e^-} = (2.83 \pm 0.15) \times 10^{53}$ erg, a baryon load of $B = (4.1 \pm 0.05) \times 10^{-5}$, and a CircumBurst Medium (CBM) average density $\langle n_{CBM} \rangle = (1.90 \pm 0.20) \times 10^{-5}$ cm^{-3}. From these results we have assumed the progenitor of this burst to be a symmetric neutron stars (NSs) merger with masses $m = 1.34 M_\odot$, radii $R = 12.24$ km. GRB 090510, instead, has $E^{tot}_{e^+e^-} = (1.10 \pm 0.06) \times 10^{53}$ erg, $B = (1.45 \pm 0.28) \times 10^{-3}$, implying a Lorentz factor at transparency of $\Gamma = (6.7 \pm 1.7) \times 10^2$, which are characteristic of the long GRB class, and a very high CBM density, $\langle n_{CBM} \rangle = (1.85 \pm 0.14) \times 10^3$ cm^{-3}. The joint effect of the high values of Γ and of $\langle n_{CBM} \rangle$ compresses in time and "inflates" in intensity in an extended afterglow, making appear GRB 090510 as a short burst, which we here define as "disguised short GRB by excess" occurring an overdense region with 10^3 cm^{-3}.

36. M. Muccino, C.L. Bianco, L. Izzo, Y. Wang, M. Enderli, G.B. Pisani, A.V. Penacchioni, R. Ruffini; "Two short bursts originating from different astrophysical systems: The genuine short GRB 090227B and the disguised short GRB 090510 by excess"; Journal of the Korean Physical Society, 65, 865 (2014).

GRB 090227B and GRB 090510 are two gamma-ray bursts (GRBs) traditionally classified as short bursts. The major outcome of our analysis is that they indeed originate from different systems. In the case of GRB 090227B, from the inferred values of the total energy of the e^+e^- plasma, $E^{tot}_{e^+e^-} = (2.83 \pm 0.15) \times 10^{53}$ erg, the engulfed baryonic mass M_B, expressed as $B = M_B c^2 / E^{tot}_{e^+e^-} = (4.1 \pm 0.05) \times 10^{-5}$, and the circumburst medium (CBM) average density, $\langle n_{CBM} \rangle = (1.90 \pm 0.20) \times 10^{-5}$ cm^{-3}, we have assumed the progenitor of this burst to be a symmetric neutron star (NS) merger with masses $m = 1.34 M_\odot$, radii $R = 12.24$ km, and crustal thicknesses of ~ 0.47 km. In the case of GRB 090510, we have derived the total plasma energy, $E^{tot}_{e^+e^-} = (1.10 \pm 0.06) \times 10^{53}$ erg, the Baryon load, $B = (1.45 \pm 0.28) \times 10^{-3}$, and the Lorentz factor at transparency, $\Gamma = (6.7 \pm 1.7) \times 10^2$, which are characteristic of the long GRB class, as well as a very high CBM density, $\langle n_{CBM} \rangle = (1.85 \pm 0.14) \times 10^3$ cm^{-3}. The joint effect of the high values of Γ and $\langle n_{CBM} \rangle$ compresses in time and "inflates" in intensity the extended afterglow, making GRB 090510 appear to be a short burst, which we here define as a "disguised short GRB by excess", occurring

in an overdense region with 10^3 cm^{-3}.

37. R. Ruffini, Y. Wang, M. Kovacevic, C.L. Bianco, M. Enderli, M. Muccino, A.V. Penacchioni, G.B. Pisani, J. Rueda; "GRB 130427A and SN 2013cq: A Multi-wavelength Analysis of An Induced Gravitational Collapse Event"; The Astrophysical Journal, 798, 10 (2015).

    We have performed our data analysis of the observations by *Swift*, *NuStar* and *Fermi* satellites in order to probe the induced gravitational collapse (IGC) paradigm for GRBs associated with supernovae (SNe), in the "terra incognita" of GRB 130427A. We compare and contrast our data analysis with those in the literature. We have verified that the GRB 130427A conforms to the IGC paradigm by examining the power law behavior of the luminosity in the early 10^4 s of the XRT observations. This has led to the identification of the four different episodes of the "binary driven hypernovae" (BdHNe) and to the prediction, on May 2, 2013, of the occurrence of SN 2013cq, duly observed in the optical band on May 13, 2013. The exceptional quality of the data has allowed the identification of novel features in *Episode 3* including: a) the confirmation and the extension of the existence of the recently discovered "nested structure" in the late X-ray luminosity in GRB 130427A, as well as the identification of a spiky structure at 10^2 s in the cosmological rest-frame of the source; b) a power law emission of the GeV luminosity light curve and its onset at the end of *Episode 2*; c) different Lorentz Γ factors for the emitting regions of the X-ray and GeV emissions in this *Episode 3*. These results make it possible to test the details of the physical and astrophysical regimes at work in the BdHNe: 1) a newly born neutron star and the supernova ejecta, originating in *Episode 1*, 2) a newly formed black hole originating in *Episode 2*, and 3) the possible interaction among these components, observable in the standard features of *Episode 3*.

38. M. Muccino, R. Ruffini, C.L. Bianco, M. Enderli, M. Kovacevic, L. Izzo, A.V. Penacchioni, G.B. Pisani, J.A. Rueda, Y. Wang; "On binary driven hypernovae and their nested late X-ray emission"; Astronomy Reports, 59, 581 (2015).

    The induced gravitational collapse (IGC) paradigm addresses energetic (10^{52}–10^{54} erg), long gamma-ray bursts (GRBs) associated to supernovae (SNe) and proposes as their progenitors tight binary systems composed of an evolved FeCO core and a companion neutron star (NS). Their emission is characterized by four specific episodes: Episode 1, corresponding to the on-set of the FeCO

SN explosion and the accretion of the ejecta onto the companion NS; Episode 2, related the collapse of the companion NS to a black hole (BH) and to the emission of a long GRB; Episode 3, observed in X-rays and characterized by a steep decay, a plateau phase and a late power-law decay; Episode 4, corresponding to the optical SN emission due to the ^{56}Ni decay. We focus on Episode 3 and we show that, from the thermal component observed during the steep decay of the prototype GRB 090618, the emission region has a typical dimension of $\sim 10^{13}$ cm, which is inconsistent with the typical size of the emitting region of GRBs, e.g., $\sim 10^{16}$ cm. We propose, therefore, that the X-ray afterglow emission originates from a spherically symmetric SN ejecta expanding at $\Gamma \sim 2$ or, possibly, from the accretion onto the newly formed black hole, and we name these systems "binary driven hypernovae" (BdHNe). This interpretation is alternative to the traditional afterglow model based on the GRB synchrotron emission from a collimated jet outflow, expanding at ultra-relativistic Lorentz factor of $\Gamma \sim 10^2 - 10^3$ and originating from the collapse of a single object. We show then that the rest-frame energy band 0.3–10 keV X-ray luminosities of three selected BdHNe, GRB 060729, GRB 061121, and GRB 130427A, evidence a precisely constrained "nested" structure and satisfy precise scaling laws between the average prompt luminosity, $< L_{iso} >$, and the luminosity at the end of the plateau, L_a, as functions of the time at the end of the plateau. All these features extend the applicability of the "cosmic candle" nature of Episode 3. The relevance of r-process in fulfilling the demanding scaling laws and the nested structure are indicated.

39. R. Ruffini, J.A. Rueda, C. Barbarino, C. L. Bianco, H. Dereli, M. Enderli, L. Izzo, M. Muccino, A.V. Penacchioni, G.B. Pisani, Y. Wang; "Induced Gravitational Collapse in the BATSE era: the case of GRB 970828"; Astronomy Reports, 59, 626 (2015).

Following the recently established "Binary-driven HyperNova" (BdHN) paradigm, we here interpret GRB 970828 in terms of the four episodes typical of such a model. The "Episode 1", up to 40 s after the trigger time t_0, with a time varying thermal emission and a total energy of $E_{iso,1st} = 2.60 \times 10^{53}$ erg, is interpreted as due to the onset of an hyper-critical accretion process onto a companion neutron star, triggered by the companion star, an FeCO core approaching a SN explosion. The "Episode 2", observed up t_0+90 s, is interpreted as a canonical gamma ray burst, with an energy of $E_{tot}^{e^+e^-} = 1.60 \times 10^{53}$ erg, a baryon load of $B = 7 \times 10^{-3}$ and a bulk Lorentz factor at transparency of $\Gamma = 142.5$. From this Episode 2, we infer that the GRB exploded in an environment with a large av-

erage particle density $\langle n \rangle \approx 10^3$ particles/cm^3 and dense clouds characterized by typical dimensions of $(4 \div 8) \times 10^{14}$ cm and $\delta n/n \sim 10$. The "Episode 3" is identified from t_0+90 s all the way up to 10^{5-6} s: despite the paucity of the early X-ray data, typical in the BATSE, pre-Swift era, we find extremely significant data points in the late X-ray afterglow emission of GRB 970828, which corresponds to the ones observed in all BdHNe sources. The "Episode 4", related to the Supernova emission, does not appear to be observable in this source, due to the presence of darkening from the large density of the GRB environment, also inferred from the analysis of the Episode 2.

40. Y. Wang, R. Ruffini, M. Kovacevic, C.L. Bianco, M. Enderli, M. Muccino, A.V. Penacchioni, G.B. Pisani, J.A. Rueda; "Predicting supernova associated to gamma-ray burst 130427a"; Astronomy Reports, 59, 667 (2015).

    Binary systems constituted by a neutron star and a massive star are not rare in the universe. The Induced Gravitational Gamma-ray Burst (IGC) paradigm interprets Gamma-ray bursts as the outcome of a neutron star that collapses into a black hole due to the accretion of the ejecta coming from its companion massive star that underwent a supernova event. GRB 130427A is one of the most luminous GRBs ever observed, of which isotropic energy exceeds 10^{54} erg. And it is within one of the few GRBs obtained optical, X-ray and GeV spectra simultaneously for hundreds of seconds, which provides an unique opportunity so far to understand the multi-wavelength observation within the IGC paradigm, our data analysis found low Lorentz factor blackbody emission in the Episode 3 and its X-ray light curve overlaps typical IGC Golden Sample, which comply to the IGC mechanisms. We consider these findings as clues of GRB 130427A belonging to the IGC GRBs. We predicted on GCN the emergence of a supernova on May 2, 2013, which was later successfully detected on May 13, 2013.

41. R. Ruffini, M. Muccino, M. Kovacevic, F.G. Oliveira, J.A. Rueda, C.L. Bianco, M. Enderli, A.V. Penacchioni, G.B. Pisani, Y. Wang, E. Zaninoni; "GRB 140619B: a short GRB from a binary neutron star merger leading to black hole formation"; The Astrophysical Journal, 808, 190 (2015).

    We show the existence of two families of short GRBs, both originating from the merger of binary neutron stars (NSs): family-1 with $E_{iso} < 10^{52}$ erg, leading to a massive NS as the merged core, and family-2 with $E_{iso} > 10^{52}$ erg, leading to a black hole (BH). Following the identification of the prototype

GRB 090227B, we present the details of a new example of family-2 short burst: GRB 140619B. From the spectral analysis of the early ~ 0.2 s, we infer an observed temperature $kT = (324 \pm 33)$ keV of the e^+e^--plasma at transparency (P-GRB), a theoretically derived redshift $z = 2.67 \pm 0.37$, a total burst energy $E^{tot}_{e^+e^-} = (6.03 \pm 0.79) \times 10^{52}$ erg, a rest-frame peak energy $E_{p,i} = 4.7$ MeV, and a baryon load $B = (5.52 \pm 0.73) \times 10^{-5}$. We also estimate the corresponding emission of gravitational waves. Two additional examples of family-2 short bursts are identified: GRB 081024B and GRB 090510, remarkable for its well determined cosmological distance. We show that marked differences exist in the nature of the afterglows of these two families of short bursts: family-2 bursts, leading to BH formation, consistently exhibit high energy emission following the P-GRB emission; family-1 bursts, leading to the formation of a massive NS, should never exhibit high energy emission. We also show that both the families fulfill an $E_{p,i}$–E_{iso} relation with slope $\gamma = 0.59 \pm 0.07$ and a normalization constant incompatible with the one for long GRBs. The observed rate of such family-2 events is $\rho_0 = \left(2.1^{+2.8}_{-1.4}\right) \times 10^{-4}\mathrm{Gpc}^{-3}\mathrm{yr}^{-1}$.

42. R. Ruffini, Y. Aimuratov, C.L. Bianco, M. Enderli, M. Kovacevic, R. Moradi, M. Muccino, A.V. Penacchioni, G.B. Pisani, J.A. Rueda, Y. Wang; "Induced gravitational collapse in FeCO Core-Neutron star binaries and Neutron star-Neutron star binary mergers"; International Journal of Modern Physics A, 30, 1545023 (2015).

    We review the recent progress in understanding the nature of gamma-ray bursts (GRBs). The occurrence of GRB is explained by the Induced Gravitational Collapse (IGC) in FeCO Core-Neutron star binaries and Neutron star-Neutron star binary mergers, both processes occur within binary system progenitors. Making use of this most unexpected new paradigm, with the fundamental implications by the neutron star (NS) critical mass, we find that different initial configurations of binary systems lead to different GRB families with specific new physical predictions confirmed by observations.

43. R. Ruffini, M. Muccino, Y. Aimuratov, C.L. Bianco, C. Cherubini, M. Enderli, M. Kovacevic, R. Moradi, A.V. Penacchioni, G.B. Pisani, J.A. Rueda, Y. Wang; "GRB 090510: A genuine short-GRB from a binary neutron star coalescing into a Kerr-Newman black hole"; The Astrophysical Journal, 831, 178 (2016).

    In a new classification of merging binary neutron stars (NSs) we separate short gamma-ray bursts (GRBs) in two sub-classes. The ones with $E_{\mathrm{iso}} \lesssim 10^{52}$ erg

coalesce to form a massive NS and are indicated as short gamma-ray flashes (S-GRFs). The hardest, with $E_{\rm iso} \gtrsim 10^{52}$ erg, coalesce to form a black hole (BH) and are indicated as genuine short-GRBs (S-GRBs). Within the fireshell model, S-GRBs exhibit three different components: the P-GRB emission, observed at the transparency of a self-accelerating baryon-e^+e^- plasma; the prompt emission, originating from the interaction of the accelerated baryons with the circumburst medium; the high-energy (GeV) emission, observed after the P-GRB and indicating the formation of a BH. GRB 090510 gives the first evidence for the formation of a Kerr BH or, possibly, a Kerr-Newman BH. Its P-GRB spectrum can be fitted by a convolution of thermal spectra whose origin can be traced back to an axially symmetric dyadotorus. A large value of the angular momentum of the newborn BH is consistent with the large energetics of this S-GRB, which reach in the 1–10000 keV range $E_{\rm iso} = (3.95 \pm 0.21) \times 10^{52}$ erg and in the 0.1–100 GeV range $E_{\rm LAT} = (5.78 \pm 0.60) \times 10^{52}$ erg, the most energetic GeV emission ever observed in S-GRBs. The theoretical redshift $z_{\rm th} = 0.75 \pm 0.17$ that we derive from the fireshell theory is consistent with the spectroscopic measurement $z = 0.903 \pm 0.003$, showing the self-consistency of the theoretical approach. All S-GRBs exhibit GeV emission, when inside the *Fermi*-LAT field of view, unlike S-GRFs, which never evidence it. The GeV emission appears to be the discriminant for the formation of a BH in GRBs, confirmed by their observed overall energetics.

44. Ruffini, R.; Rueda, J. A.; Muccino, M.; Aimuratov, Y.; Becerra, L. M.; Bianco, C. L.; Kovacevic, M.; Moradi, R.; Oliveira, F. G.; Pisani, G. B.; Wang, Y.; On the classification of GRBs and their occurrence rates; The Astrophysical Journal, 832, 136 (2016).

There is mounting evidence for the binary nature of the progenitors of gamma-ray bursts (GRBs). For a long GRB, the induced gravitational collapse (IGC) paradigm proposes as progenitor, or "in-state", a tight binary system composed of a carbon-oxygen core ($\rm CO_{core}$) undergoing a supernova (SN) explosion which triggers hypercritical accretion onto a neutron star (NS) companion. For a short GRB, a NS-NS merger is traditionally adopted as the progenitor. We divide long and short GRBs into two sub-classes, depending on whether or not a black hole (BH) is formed in the merger or in the hypercritical accretion process exceeding the NS critical mass. For long bursts, when no BH is formed we have the sub-class of X-ray flashes (XRFs), with isotropic energy $E_{iso} \lesssim 10^{52}$ erg and rest-frame spectral peak energy $E_{p,i} \lesssim 200$ keV. When a BH is formed we have the sub-class of binary-driven hypernovae (BdHNe),

with $E_{iso} \gtrsim 10^{52}$ erg and $E_{p,i} \gtrsim 200$ keV. In analogy, short bursts are similarly divided into two sub-classes. When no BH is formed, short gamma-ray flashes (S-GRFs) occur, with $E_{iso} \lesssim 10^{52}$ erg and $E_{p,i} \lesssim 2$ MeV. When a BH is formed, the authentic short GRBs (S-GRBs) occur, with $E_{iso} \gtrsim 10^{52}$ erg and $E_{p,i} \gtrsim 2$ MeV. We give examples and observational signatures of these four sub-classes and their rate of occurrence. From their respective rates it is possible that "in-states" of S-GRFs and S-GRBs originate from the "out-states" of XRFs. We indicate two additional progenitor systems: white dwarf-NS and BH-NS. These systems have hybrid features between long and short bursts. In the case of S-GRBs and BdHNe evidence is given of the coincidence of the onset of the high energy GeV emission with the birth of a Kerr BH.

45. Becerra, L.; Bianco, C. L.; Fryer, C. L.; Rueda, J. A.; Ruffini, R.; On the induced gravitational collapse scenario of gamma-ray bursts associated with supernovae; The Astrophysical Journal, 833, 107 (2016).

    Following the induced gravitational collapse (IGC) paradigm of gamma-ray bursts (GRBs) associated with type Ib/c supernovae, we present numerical simulations of the explosion of a carbon-oxygen (CO) core in a binary system with a neutron-star (NS) companion. The supernova ejecta trigger a *hypercritical* accretion process onto the NS thanks to a copious neutrino emission and the trapping of photons within the accretion flow. We show that temperatures 1–10 MeV develop near the NS surface, hence electron-positron annihilation into neutrinos becomes the main cooling channel leading to accretion rates 10^{-9}–10^{-1} $M_\odot$ s^{-1} and neutrino luminosities 10^{43}–10^{52} erg s^{-1} (the shorter the orbital period the higher the accretion rate). We estimate the maximum orbital period, $P_{\rm max}$, as a function of the NS initial mass, up to which the NS companion can reach by hypercritical accretion the critical mass for gravitational collapse leading to black-hole (BH) formation. We then estimate the effects of the accreting and orbiting NS companion onto a novel geometry of the supernova ejecta density profile. We present the results of a 1.4×10^7 particle simulation which show that the NS induces accentuated asymmetries in the ejecta density around the orbital plane. We elaborate on the observables associated with the above features of the IGC process. We apply this framework to specific GRBs: we find that X-ray flashes (XRFs) and binary-driven hypernovae (BdHNe) are produced in binaries with $P > P_{\rm max}$ and $P < P_{\rm max}$, respectively. We analyze in detail the case of XRF 060218.

46. Pisani, G. B.; Ruffini, R.; Aimuratov, Y.; Bianco, C. L.; Kovacevic, M.;

Moradi, R.; Muccino, M.; Penacchioni, A. V.; Rueda, J. A.; Shakeri, S.; Wang, Y.; On the universal late X-ray emission of binary-driven hypernovae and its possible collimation; The Astrophysical Journal, 833, 159 (2016).

It has been previously discovered a universal power-law behaviour of the late X-ray emission (LXRE) of a "golden sample" (GS) of six long energetic GRBs, when observed in the rest-frame of the source. This remarkable feature, independent on the different isotropic energy (E_{iso}) of each GRB, has been used to estimate the cosmological redshift of some long GRBs. This analysis is here extended to a new class of 161 long GRBs, all with $E_{iso} > 10^{52}$ erg. These GRBs are indicated as binary-driven hypernovae (BdHNe) in view of their progenitors: a tight binary systems composed of a carbon-oxigen core (CO_{core}) and a neutron star (NS) undergoing an induced gravitational collapse (IGC) to a black hole (BH) triggered by the CO_{core} explosion as a supernova (SN). We confirm the universal behaviour of the LXRE for the "enlarged sample" (ES) of 161 BdHNe observed up to the end of 2015, assuming a double-cone emitting region. We obtain a distribution of half-opening angles peaking at $\theta = 17.62^{\circ}$, with mean value 30.05°, and a standard deviation 19.65°. This, in turn, leads to the possible establishment of a new cosmological candle. Within the IGC model, such universal LXRE behaviour is only indirectly related to the GRB and originates from the SN ejecta, of a standard constant mass, being shocked by the GRB emission. The fulfillment of the universal relation in the LXRE and its independence of the prompt emission, further confirmed in this article, establishes a crucial test for any viable GRB model.

47. Y. Aimuratov, R. Ruffini, M. Muccino, C.L. Bianco, A.V. Penacchioni, G.B. Pisani, D. Primorac, J.A. Rueda, Y. Wang; GRB 081024B and GRB 140402A: Two Additional Short GRBs from Binary Neutron Star Mergers; The Astrophysical Journal, 844, 83 (2017).

Theoretical and observational evidences have been recently gained for a two-fold classification of short bursts: 1) short gamma-ray flashes (S-GRFs), with isotropic energy $E_{iso} < 10^{52}$ erg and no BH formation, and 2) the authentic short gamma-ray bursts (S-GRBs), with isotropic energy $E_{iso} > 10^{52}$ erg evidencing a BH formation in the binary neutron star merging process. The signature for the BH formation consists in the on-set of the high energy (0.1–100 GeV) emission, coeval to the prompt emission, in all S-GRBs. No GeV emission is expected nor observed in the S-GRFs. In this paper we present

two additional S-GRBs, GRB 081024B and GRB 140402A, following the already identified S-GRBs, i.e., GRB 090227B, GRB 090510 and GRB 140619B. We also return on the absence of the GeV emission of the S-GRB 090227B, at an angle of 71^o from the *Fermi*-LAT boresight. All the correctly identified S-GRBs correlate to the high energy emission, implying no significant presence of beaming in the GeV emission. The existence of a common power-law behavior in the GeV luminosities, following the BH formation, when measured in the source rest-frame, points to a commonality in the mass and spin of the newly-formed BH in all S-GRBs.

48. J.A. Rueda, Y. Aimuratov, U. Barres de Almeida, L.M. Becerra, C.L. Bianco, C. Cherubini, S. Filippi, M. Karlica, M. Kovacevic, J.D. Melon Fuksman, R. Moradi, M. Muccino, A.V. Penacchioni, G.B. Pisani, D. Primorac, R. Ruffini, N. Sahakyan, S. Shakeri, Y. Wang; The binary systems associated with short and long gamma-ray bursts and their detectability; International Journal of Modern Physics D, 26, 1730016 (2017).

    Short and long-duration gamma-ray bursts (GRBs) have been recently subclassified into seven families according to the binary nature of their progenitors. For short GRBs, mergers of neutron star binaries (NS–NS) or neutron star-black hole binaries (NS-BH) are proposed. For long GRBs, the induced gravitational collapse (IGC) paradigm proposes a tight binary system composed of a carbon–oxygen core (COcore) and a NS companion. The explosion of the COcore as supernova (SN) triggers a hypercritical accretion process onto the NS companion which might reach the critical mass for the gravitational collapse to a BH. Thus, this process can lead either to a NS-BH or to NS–NS depending on whether or not the accretion is sufficient to induce the collapse of the NS into a BH. We shall discuss for the above compact object binaries: (1) the role of the NS structure and the equation-of-state on their final fate; (2) their occurrence rates as inferred from the X and gamma-ray observations; (3) the expected number of detections of their gravitational wave (GW) emission by the Advanced LIGO interferometer.

49. R. Ruffini, Y. Aimuratov, L.M. Becerra, C.L. Bianco, M. Karlica, M. Kovacevic, J.D. Melon Fuksman, R. Moradi, M. Muccino, A.V. Penacchioni, G.B. Pisani, D. Primorac, J.A. Rueda, S. Shakeri, G.V. Vereshchagin, Y. Wang, S.-S. Xue; The cosmic matrix in the 50th anniversary of relativistic astrophysics; International Journal of Modern Physics D, 26, 1730019 (2017).

Our concept of induced gravitational collapse (IGC paradigm) starting from a supernova occurring with a companion neutron star, has unlocked the understanding of seven different families of gamma ray bursts (GRBs), indicating a path for the formation of black holes in the universe. An authentic laboratory of relativistic astrophysics has been unveiled in which new paradigms have been introduced in order to advance knowledge of the most energetic, distant and complex systems in our universe. A novel cosmic matrix paradigm has been introduced at a relativistic cosmic level, which parallels the concept of an S-matrix introduced by Feynmann, Wheeler and Heisenberg in the quantum world of microphysics. Here the "in" states are represented by a neutron star and a supernova, while the "out" states, generated within less than a second, are a new neutron star and a black hole. This novel field of research needs very powerful technological observations in all wavelengths ranging from radio through optical, X-ray and gamma ray radiation all the way up to ultra-high-energy cosmic rays.

50. R. Ruffini, Y. Wang, Y. Aimuratov, U. Barres de Almeida, L.M. Becerra, C.L. Bianco, Y.C. Chen, M. Karlica, M. Kovacevic, L. Li, J.D. Melon Fuksman, R. Moradi, M. Muccino, A.V. Penacchioni, G.B. Pisani, D. Primorac, J.A. Rueda, S. Shakeri, G.V. Vereshchagin, S.-S. Xue; Early X-Ray Flares in GRBs; The Astrophysical Journal, 852, 53 (2018).

We analyze the early X-ray flares in the GRB "flare-plateau-afterglow" (FPA) phase observed by Swift-XRT. The FPA occurs only in one of the seven GRB subclasses: the binary-driven hypernovae (BdHNe). This subclass consists of long GRBs with a carbon-oxygen core and a neutron star (NS) binary companion as progenitors. The hypercritical accretion of the supernova (SN) ejecta onto the NS can lead to the gravitational collapse of the NS into a black hole. Consequently, one can observe a GRB emission with isotropic energy $E_{iso} \gtrsim 10^{52}$ erg, as well as the associated GeV emission and the FPA phase. Previous work had shown that gamma-ray spikes in the prompt emission occur at $\sim 10^{15}$–10^{17} cm with Lorentz gamma factor $\Gamma \sim 10^2$–10^3. Using a novel data analysis we show that the time of occurrence, duration, luminosity and total energy of the X-ray flares correlate with E_{iso}. A crucial feature is the observation of thermal emission in the X-ray flares that we show occurs at radii $\sim 10^{12}$ cm with $\Gamma \lesssim 4$. These model independent observations cannot be explained by the "fireball" model, which postulates synchrotron and inverse Compton radiation from a single ultra relativistic jetted emission extending from the prompt to the late afterglow and GeV emission phases. We show that

in BdHNe a collision between the GRB and the SN ejecta occurs at $\simeq 10^{10}$ cm reaching transparency at $\sim 10^{12}$ cm with $\Gamma \lesssim 4$. The agreement between the thermal emission observations and these theoretically derived values validates our model and opens the possibility of testing each BdHN episode with the corresponding Lorentz gamma factor.

51. R. Ruffini, J. Rodriguez, M. Muccino, J.A. Rueda, Y. Aimuratov, U. Barres de Almeida, L.M. Becerra, C.L. Bianco, C. Cherubini, S. Filippi, D. Gizzi, M. Kovacevic, R. Moradi, F.G. Oliveira, G.B. Pisani, Y. Wang; On the Rate and on the Gravitational Wave Emission of Short and Long GRBs; The Astrophysical Journal, 859, 30 (2018).

    On the ground of the large number of gamma-ray bursts (GRBs) detected with cosmological redshift, we classified GRBs in seven subclasses, all with binary progenitors which emit gravitational waves (GWs). Each binary is composed of combinations of carbon-oxygen cores (COcore), neutron stars (NSs), black holes (BHs), and white dwarfs (WDs). The long bursts, traditionally assumed to originate from a BH with an ultrarelativistic jetted emission, not emitting GWs, have been subclassified as (I) X-ray flashes (XRFs), (II) binary-driven hypernovae (BdHNe), and (III) BH-supernovae (BH-SNe). They are framed within the induced gravitational collapse paradigm with a progenitor COcore-NS/BH binary. The SN explosion of the COcore triggers an accretion process onto the NS/BH. If the accretion does not lead the NS to its critical mass, an XRF occurs, while when the BH is present or formed by accretion, a BdHN occurs. When the binaries are not disrupted, XRFs lead to NS-NS and BdHNe lead to NS-BH. The short bursts, originating in NS-NS, are subclassified as (IV) short gamma-ray flashes (S-GRFs) and (V) short GRBs (S-GRBs), the latter when a BH is formed. There are (VI) ultrashort GRBs (U-GRBs) and (VII) gamma-ray flashes (GRFs) formed in NS-BH and NS-WD, respectively. We use the occurrence rate and GW emission of these subclasses to assess their detectability by Advanced LIGO-Virgo, eLISA, and resonant bars. We discuss the consequences of our results in view of the announcement of the LIGO/Virgo Collaboration of the source GW 170817 as being originated by an NS-NS.

52. J.A. Rueda, R. Ruffini, Y. Wang, Y. Aimuratov, U. Barres de Almeida, C.L. Bianco, Y.-C. Chen, R.V. Lobato, C. Maia, D. Primorac, R. Moradi, J. Rodriguez; GRB 170817A-GW170817-AT 2017gfo and the observations of NS-NS, NS-WD and WD-WD mergers; Journal of Cosmology and Astroparticle Physics, 10, 006 (2018).

The LIGO-Virgo Collaboration has announced the detection of GW170817 and has associated it with GRB 170817A . These signals have been followed after 11 hours by the optical and infrared emission of AT 2017gfo. The origin of this complex phenomenon has been attributed to a neutron star-neutron star (NS-NS) merger. In order to probe this association we confront our current understanding of the gravitational waves and associated electromagnetic radiation with four observed GRBs originating in binaries composed of different combinations NSs and white dwarfs (WDs). We consider 1) GRB 090510 the prototype of NS-NS merger leading to a black hole (BH); 2) GRB 130603B the prototype of a NS-NS merger leading to massive NS (MNS) with an associated kilonova; 3) GRB 060614 the prototype of a NS-WD merger leading to a MNS with an associated kilonova candidate; 4) GRB 170817A the prototype of a WD-WD merger leading to massive WD with an associated AT 2017gfo-like emission. None of these systems support the above mentioned association. The clear association between GRB 170817A and AT 2017gfo has led to introduce a new model based on a new subfamily of GRBs originating from WD-WD mergers. We show how this novel model is in agreement with the exceptional observations in the optical, infrared, X- and gamma-rays of GRB 170817A-AT 2017gfo.

53. R. Ruffini, M. Karlica, N. Sahakyan, J.A. Rueda, Y. Wang, G.W. Mathews, C.L. Bianco, M. Muccino; A GRB Afterglow Model Consistent with Hypernova Observations; The Astrophysical Journal, 869, 101 (2018).

We describe the afterglows of the long gamma-ray-burst (GRB) 130427A within the context of a binary-driven hypernova. The afterglows originate from the interaction between a newly born neutron star (νNS), created by an Ic supernova (SN), and a mildly relativistic ejecta of a hypernova (HN). Such an HN in turn results from the impact of the GRB on the original SN Ic. The mildly relativistic expansion velocity of the afterglow ($\Gamma \sim 3$) is determined, using our model-independent approach, from the thermal emission between 196 and 461 s. The power law in the optical and X-ray bands of the afterglow is shown to arise from the synchrotron emission of relativistic electrons in the expanding magnetized HN ejecta. Two components contribute to the injected energy: the kinetic energy of the mildly relativistic expanding HN and the rotational energy of the fast-rotating highly magnetized ?NS. We reproduce the afterglow in all wavelengths from the optical (10^{14} Hz) to the X-ray band (10^{19} Hz) over times from 604 s to 5.18×10^6 s relative to the Fermi-GBM trigger. Initially, the emission is dominated by the loss of kinetic energy of the HN component.

After 10^5 s the emission is dominated by the loss of rotational energy of the νNS, for which we adopt an initial rotation period of 2 ms and a dipole plus quadrupole magnetic field of $\lesssim 7 \times 10^{12}$ G or $\sim 10^{14}$ G. This scenario with a progenitor composed of a COcore and an NS companion differs from the traditional ultra-relativistic-jetted treatments of the afterglows originating from a single black hole.

54. R. Ruffini, L.M. Becerra, C.L. Bianco, Y.-C. Chen, M. Karlica, M. Kovacevic, J.D. Melon Fuksman, R. Moradi, M. Muccino, G.B. Pisani, D. Primorac, J.A. Rueda, G.V. Vereshchagin, Y. Wang, S.-S. Xue; On the ultra-relativistic Prompt Emission (UPE), the Hard and Soft X-ray Flares, and the extended thermal emission (ETE) in GRB 151027A; The Astrophysical Journal, 869, 151 (2018).

    We analyze GRB 151027A within the binary-driven hypernova approach, with a progenitor of a carbon–oxygen core on the verge of a supernova (SN) explosion and a binary companion neutron star (NS). The hypercritical accretion of the SN ejecta onto the NS leads to its gravitational collapse into a black hole (BH), to the emission of the gamma-ray burst (GRB), and to a copious e+e- plasma. The impact of this e+e- plasma on the SN ejecta explains the early soft X-ray flare observed in long GRBs. Here, we apply this approach to the ultra-relativistic prompt emission (UPE) and to the hard X-ray flares. We use GRB 151027A as a prototype. From the time-integrated and the time-resolved analysis, we identify a double component in the UPE and confirm its ultra-relativistic nature. We confirm the mildly relativistic nature of the soft X-ray flare, of the hard X-ray flare, and of the extended thermal emission (ETE). We show that the ETE identifies the transition from an SN to a hypernova (HN). We then address the theoretical justification of these observations by integrating the hydrodynamical propagation equations of the e+e- into the SN ejecta, with the latter independently obtained from 3D smoothed particle hydrodynamics simulations. We conclude that the UPE, the hard X-ray flare, and the soft X-ray flare do not form a causally connected sequence. Within our model, they are the manifestation of the same physical process of the BH formation as seen through different viewing angles, implied by the morphology and the ~ 300 s rotation period of the HN ejecta.

55. R. Moradi, R. Ruffini, C.L. Bianco, Y.-C. Chen, M. Karlica, J.D. Melon Fuksman, D. Primorac, J.A. Rueda, S. Shakeri, Y. Wang, S.-S. Xue; Relativistic Behavior and Equitemporal Surfaces in Ultra-Relativistic Prompt

Emission Phase of Gamma-Ray Bursts; Astronomy Reports, 62, 905 (2018).

In this work we study a role of baryon load and interstellar medium density to explain the nature of peaks in the ultra-relativistic prompt emission (UPE) phase of Gamma-ray Bursts (GRBs). We study the behavior of their Γ Lorenz factor fromthe moment of transparency all the way up to interstellar medium. We finally study the characteristic of equitemporal surfaces in the UPE phase.

56. D. Primorac, M. Muccino, R. Moradi, Y. Wang, J.D. Melon Fuksman, R. Ruffini, C.L. Bianco, J.A. Rueda; Structure of the Prompt Emission of GRB 151027A Within the Fireshell Model; Astronomy Reports, 62, 933 (2018).

    Long gamma-ray burst GRB 151027A was observed by all three detectors onboard the Swift spacecraft, and many more, including MAXI, Konus-Wind and Fermi GBM/LAT instruments. This revealed a complex structure of the prompt and afterglow emission, consisting of a double-peak gammaray prompt with a quiescent period and a HRF/SXF within the X-ray afterglow, together with multiple BB components seen within the time-resolved spectral analysis. These features, within the fireshell model, are interpreted as the manifestation of the same physical process viewed at different angles with respect to the HN ejecta. Here we present the time-resolved and time-integrated spectral analysis used to determine the energy of the e-e+ plasma E_{tot} and the baryon load B. These quantities describe the dynamics of the fireshell up to the transparency point. We proceed with the light-curve simulation from which CBM density values and its inhomogeneities are deduced. We also investigate the properties of GRB 140206A, whose prompt emission exhibits a similar structure.

57. Y. Wang, J.A. Rueda, R. Ruffini, C.L. Bianco, L.M. Becerra, L. Li, M. Karlica; Two Predictions of Supernova: GRB 130427A/SN 2013cq and GRB 180728A/SN 2018fip; The Astrophysical Journal, 874, 39 (2019).

    On 2018 July 28, GRB 180728A triggered *Swift* satellites and, soon after the determination of the redshift, we identified this source as a type II binary-driven hypernova (BdHN II) in our model. Consequently, we predicted the appearance time of its associated supernova (SN), which was later confirmed as SN 2018fip. A BdHN II originates in a binary composed of a carbon-oxygen core (CO_{core}) undergoing SN, and the SN ejecta hypercritically accrete onto a companion neutron star (NS). From the time of the SN shock breakout to the time when the hypercritical accretion starts, we infer the binary separation

$\simeq 3 \times 10^{10}$ cm. The accretion explains the prompt emission of isotropic energy $\simeq 3 \times 10^{51}$ erg, lasting $\sim$ 10 s, and the accompanying observed blackbody emission from a thermal convective instability bubble. The new neutron star (νNS) originating from the SN powers the late afterglow from which a νNS initial spin of 2.5 ms is inferred. We compare GRB 180728A with GRB 130427A, a type I binary-driven hypernova (BdHN I) with isotropic energy $> 10^{54}$ erg. For GRB 130427A we have inferred an initially closer binary separation of $\simeq 10^{10}$ cm, implying a higher accretion rate leading to the collapse of the NS companion with consequent black hole formation, and a faster, 1 ms spinning νNS. In both cases, the optical spectra of the SNe are similar, and not correlated to the energy of the gamma-ray burst. We present three-dimensional smoothed-particle-hydrodynamic simulations and visualisations of the BdHNe I and II.

58. J.A. Rueda, R. Ruffini, Y. Wang, C.L. Bianco, J.M. Blanco-Iglesias, M. Karlica, P. Lorén-Aguilar, R. Moradi, N. Sahakyan; Electromagnetic emission of white dwarf binary mergers; Journal of Cosmology and Astroparticle Physics, 03, 044 (2019).

    It has been recently proposed that the ejected matter from white dwarf (WD) binary mergers can produce transient, optical and infrared emission similar to the "kilonovae" of neutron star (NS) binary mergers. To confirm this we calculate the electromagnetic emission from WD-WD mergers and compare with kilonova observations. We simulate WD-WD mergers leading to a massive, fast rotating, highly magnetized WD with an adapted version of the smoothed-particle-hydrodynamics (SPH) code Phantom. We thus obtain initial conditions for the ejecta such as escape velocity, mass and initial position and distribution. The subsequent thermal and dynamical evolution of the ejecta is obtained by integrating the energy-conservation equation accounting for expansion cooling and a heating source given by the fallback accretion onto the newly-formed WD and its magneto-dipole radiation. We show that magnetospheric processes in the merger can lead to a prompt, short gamma-ray emission of up to $\approx 10^{46}$ erg in a timescale of 0.1–1 s. The bulk of the ejecta initially expands non-relativistically with velocity 0.01 c and then it accelerates to 0.1 c due to the injection of fallback accretion energy. The ejecta become transparent at optical wavelengths around $\sim$ 7 days post-merger with a luminosity 10^{41}–10^{42} erg s^{-1}. The X-ray emission from the fallback accretion becomes visible around $\sim$ 150–200 day post-merger with a luminosity of 10^{39} erg s^{-1}. We also predict the post-merger time at which the central WD should appear as a pulsar depending on the value of the magnetic field and rotation period.

59. J.A. Rueda, R. Ruffini, Y. Wang; Induced Gravitational Collapse, Binary-Driven Hypernovae, Long Gramma-ray Bursts and Their Connection with Short Gamma-ray Bursts; Universe, 5, 110 (2019).

There is increasing observational evidence that short and long Gamma-ray bursts (GRBs) originate in different subclasses, each one with specific energy release, spectra, duration, etc, and all of them with binary progenitors. The binary components involve carbon-oxygen cores (CO_{core}), neutron stars (NSs), black holes (BHs), and white dwarfs (WDs). We review here the salient features of the specific class of binary-driven hypernovae (BdHNe) within the induced gravitational collapse (IGC) scenario for the explanation of the long GRBs. The progenitor is a CO_{core}-NS binary. The supernova (SN) explosion of the CO_{core}, producing at its center a new NS (νNS), triggers onto the NS companion a hypercritical, i.e., highly super-Eddington accretion process, accompanied by a copious emission of neutrinos. By accretion the NS can become either a more massive NS or reach the critical mass for gravitational collapse with consequent formation of a BH. We summarize the results on this topic from the first analytic estimates in 2012 all the way up to the most recent three-dimensional (3D) smoothed-particle-hydrodynamics (SPH) numerical simulations in 2018. Thanks to these results it is by now clear that long GRBs are richer and more complex systems than thought before. The SN explosion and its hypercritical accretion onto the NS explain the X-ray precursor. The feedback of the NS accretion, the NS collapse and the BH formation produce asymmetries in the SN ejecta, implying the necessity of a 3D analysis for GRBs. The newborn BH, the surrounding matter and the magnetic field inherited from the NS, comprises the *inner engine* from which the GRB electron-positron (e^+e^-) plasma and the high-energy emission are initiated. The impact of the e^+e^- on the asymmetric ejecta transforms the SN into a hypernova (HN). The dynamics of the plasma in the asymmetric ejecta leads to signatures depending on the viewing angle. This explains the ultrarelativistic prompt emission in the MeV domain and the mildly-relativistic flares in the early afterglow in the X-ray domain. The feedback of the νNS pulsar-like emission on the HN explains the X-ray late afterglow and its power-law regime. All of the above is in contrast with a simple GRB model attempting to explain the entire GRB with the kinetic energy of an ultrarelativistic jet extending through all of the above GRB phases, as traditionally proposed in the "collapsar-fireball" model. In addition, BdHNe in their different flavors lead to νNS-NS or νNS-BH binaries. The gravitational wave emission drives these binaries to merge

producing short GRBs. It is thus established a previously unthought interconnection between long and short GRBs and their occurrence rates. This needs to be accounted for in the cosmological evolution of binaries within population synthesis models for the formation of compact-object binaries.

60. R. Ruffini, J.D. Melon Fuksman, G.V. Vereshchagin; On the role of a cavity in the hypernova ejecta of GRB 190114C; The Astrophysical Journal, 883, 191 (2019).

    Within the binary-driven hypernova I (BdHN I) scenario, the gamma-ray burst GRB190114C originates in a binary system composed of a massive carbon-oxygen core (CO_{core}), and a binary neutron star (NS) companion. As the CO_{core} undergoes a supernova explosion with the creation of a new neutron star (νNS), hypercritical accretion occurs onto the companion binary neutron star until it exceeds the critical mass for gravitational collapse. The formation of a black hole (BH) captures 10^{57} baryons by enclosing them within its horizon, and thus a cavity of approximately 10^{11} cm is formed around it with initial density 10^{-7} g/cm^3. A further depletion of baryons in the cavity originates from the expansion of the electron-positron-photon ($e^+e^-\gamma$) plasma formed at the collapse, reaching a density of 10^{-14} g/cm^3 by the end of the interaction. It is demonstrated here using an analytical model complemented by a hydrodynamical numerical simulation that part of the $e^+e^-\gamma$ plasma is reflected off the walls of the cavity. The consequent outflow and its observed properties are shown to coincide with the featureless emission occurring in a time interval of duration t_{rf}, measured in the rest frame of the source, between 11 and 20 s of the GBM observation. Moreover, similar features of the GRB light curve were previously observed in GRB 090926A and GRB 130427A, all belonging to the BdHN I class. This interpretation supports the general conceptual framework presented in R. Ruffini et al. and guarantees that a low baryon density is reached in the cavity, a necessary condition for the operation of the "*inner engine*" of the GRB presented in an accompanying article.

61. R. Ruffini, R. Moradi, J.A. Rueda, L.M. Becerra, C.L. Bianco, C. Cherubini, S. Filippi, Y.C. Chen, M. Karlica, N. Sahakyan, Y. Wang, S.-S. Xue; On the GeV Emission of the Type I BdHN GRB 130427A; The Astrophysical Journal, 886, 82 (2019).

    We propose that the *inner engine* of a type I binary-driven hypernova (BdHN) is composed of a Kerr black hole (BH) in a non-stationary state, embedded in a uniform magnetic field B_0 aligned with the BH rotation axis, and surrounded

by an ionized plasma of extremely low density of 10^{-14} g cm^{-3}. Using GRB 130427A as a prototype we show that this *inner engine* acts in a sequence of *elementary impulses*. Electrons are accelerated to ultra-relativistic energy near the BH horizon and, propagating along the polar axis, $\theta = 0$, they can reach energies of $\sim 10^{18}$ eV, and partially contribute to ultra-high energy cosmic rays (UHECRs). When propagating with $\theta \neq 0$ through the magnetic field B_0 they give origin by synchrotron emission to GeV and TeV radiation. The mass of BH, $M = 2.3M_{\odot}$, its spin, $\alpha = 0.47$, and the value of magnetic field $B_0 = 3.48 \times 10^{10}$ G, are determined self-consistently in order to fulfill the energetic and the transparency requirement. The repetition time of each elementary impulse of energy $\mathcal{E} \sim 10^{37}$ erg, is $\sim 10^{-14}$ s at the beginning of the process, then slowly increasing with time evolution. In principle, this "*inner engine*" can operate in a GRB for thousands of years. By scaling the BH mass and the magnetic field the same "*inner engine*" can describe active galactic nuclei (AGN).

62. L. Li; Thermal Components in Gamma-ray Bursts. II. Constraining the Hybrid Jet Model; The Astrophysical Journal, 894, 100 (2020).

In explaining the physical origin of the jet composition of gamma-ray bursts (GRBs), a more general picture, i.e. the hybrid jet model (which introduced another magnetization parameter σ_0 on the basis of the traditional fireball model), has been well studied in Gao & Zhang. However, it still has not yet been applied to a large GRB sample. Here, we first employ the "top-down" approach of Gao & Zhang to diagnose the photosphere properties at the central engine to see how the hybrid model can account for the observed data as well, through applying a *Fermi* GRB sample (eight bursts) with the detected photosphere component, as presented in Li (our Paper I). We infer all physical parameters of a hybrid problem with three typical values of the radius of the jet base (r_0 = 10^7, 10^8, and 10^9 cm). We find that the dimensionless entropy for all the bursts shows $\eta \gg 1$ while the derived $(1+\sigma_0)$ for five bursts (GRB 081224, GRB 110721A, GRB 090719, GRB 100707, and GRB 100724) is larger than unity, indicating that in addition to a hot fireball component, another cold Poynting-flux component may also play an important role. Our analysis also shows that in a few time bins for all r_0 in GRB 081224 and GRB 110721A, the magnetization parameter at $\sim 10^{15}$cm $(1+\sigma_{r15})$ is greater than unity, which implies that internal-collision-induced magnetic reconnection and turbulence may be the mechanism to power the nonthermal emission, rather than internal shocks. We conclude that the majority of bursts (probably all) can be well explained by the hybrid jet problem.

63. J.A. Rueda, R. Ruffini, M. Karlica, R. Moradi, Y. Wang; Magnetic fields and afterglows of bdhne: inferences from grb 130427a, grb 160509a, grb 160625b, grb 180728a, and grb 190114c; The Astrophysical Journal, 893, 148 (2020).

    GRB 190114C is the first binary-driven hypernova (BdHN) fully observed from the initial supernova appearance to the final emergence of the optical SN signal. It offers an unprecedented testing ground for the BdHN theory and it is here determined and further extended to additional gamma-ray bursts (GRBs). BdHNe comprise two subclasses of long GRBs with progenitors a binary system composed of a carbon-oxygen star (CO_{core}) and a neutron star (NS) companion. The CO_{core} explodes as a SN leaving at its center a newborn NS (νNS). The SN ejecta hypercritically accretes both on the νNS and the NS companion. BdHNe I are the tightest binaries where the accretion leads the companion NS to gravitational collapse into a black hole (BH). In BdHN II the accretion onto the NS is lower, so there is no BH formation. We observe the same structure of the afterglow for GRB 190114C and other selected examples of BdHNe I (GRB 130427A, GRB 160509A, GRB 160625B) and for BdHN II (GRB 180728A). In all the cases the explanation of the afterglow is reached via the synchrotron emission powered by the νNS: their magnetic fields structures and their spin are determined. For BdHNe I, we discuss the properties of the magnetic field embedding the newborn BH, inherited from the collapsed NS and amplified during the gravitational collapse process, and surrounded by the SN ejecta.

64. J.A. Rueda, R. Ruffini; The blackholic quantum; European Physical Journal C, 80, 300 (2020).

    We show that the high-energy emission of GRBs originates in the *inner engine*: a Kerr black hole (BH) surrounded by matter and a magnetic field B_0. It radiates a sequence of discrete events of particle acceleration, each of energy $\mathcal{E} = \hbar\,\Omega_{\rm eff}$, the *blackholic quantum*, where $\Omega_{\rm eff} = 4(m_{\rm Pl}/m_n)^8(c\,a/G\,M)(B_0^2/\rho_{\rm Pl})\Omega_+$. Here M, $a = J/M$, $\Omega_+ = c^2\partial M/\partial J = (c^2/G)\,a/(2Mr_+)$ and r_+ are the BH mass, angular momentum per unit mass, angular velocity and horizon; m_n is the neutron mass, $m_{\rm Pl}$, $\lambda_{\rm Pl} = \hbar/(m_{\rm Pl}c)$ and $\rho_{\rm Pl} = m_{\rm Pl}c^2/\lambda_{\rm Pl}^3$, are the Planck mass, length and energy density. Here and in the following use CGS-Gaussian units. The timescale of each process is $\tau_{\rm el} \sim \Omega_+^{-1}$, along the rotation axis, while it is much shorter off-axis owing to energy losses such as synchrotron radiation. We show an analogy with the Zeeman and Stark effects, properly scaled from microphysics to macrophysics, that allows us to define the *BH magneton*,

$\mu_{\rm BH} = (m_{\rm Pl}/m_n)^4 (c\,a/G\,M) e\,\hbar/(Mc)$. We give quantitative estimates for GRB 130427A adopting $M = 2.3\ M_\odot$, $c\,a/(G\,M) = 0.47$ and $B_0 = 3.5 \times 10^{10}$ G. Each emitted *quantum*, $\mathcal{E} \sim 10^{37}$ erg, extracts only 10^{-16} times the BH rotational energy, guaranteeing that the process can be repeated for thousands of years. The *inner engine* can also work in AGN as we here exemplified for the supermassive BH at the center of M87.

4.2 Conference proceedings

1. R. Ruffini, M.G. Bernardini, C.L. Bianco, P. Chardonnet, F. Fraschetti, V. Gurzadyan, L. Vitagliano, S.-S. Xue; "The Blackholic energy: long and short Gamma-Ray Bursts (New perspectives in physics and astrophysics from the theoretical understanding of Gamma-Ray Bursts, II)"; in Proceedings of the XIth Brazilian School on Cosmology and Gravitation, Mangaratiba, Rio de Janeiro (Brazil), July – August 2004, M. Novello, S.E. Perez Bergliaffa, Editors; AIP Conference Proceedings, 782, 42 (2005).

   We outline the confluence of three novel theoretical fields in our modeling of Gamma-Ray Bursts (GRBs): 1) the ultrarelativistic regime of a shock front expanding with a Lorentz gamma factor ~ 300; 2) the quantum vacuum polarization process leading to an electron-positron plasma originating the shock front; and 3) the general relativistic process of energy extraction from a black hole originating the vacuum polarization process. There are two different classes of GRBs: the long GRBs and the short GRBs. We here address the issue of the long GRBs. The theoretical understanding of the long GRBs has led to the detailed description of their luminosities in fixed energy bands, of their spectral features and made also possible to probe the astrophysical scenario in which they originate. We are specially interested, in this report, to a subclass of long GRBs which appear to be accompanied by a supernova explosion. We are considering two specific examples: GRB980425/SN1998bw and GRB030329/SN2003dh. While these supernovae appear to have a standard energetics of 10^{49} ergs, the GRBs are highly variable and can have energetics 10^4 – 10^5 times larger than the ones of the supernovae. Moreover, many long GRBs occurs without the presence of a supernova. It is concluded that in no way a GRB can originate from a supernova. The precise theoretical understanding of the GRB luminosity we present evidence, in both these systems, the existence of an independent component in the X-ray emission, usually in-

terpreted in the current literature as part of the GRB afterglow. This component has been observed by Chandra and XMM to have a strong decay on scale of months. We have named here these two sources respectively URCA-1 and URCA-2, in honor of the work that George Gamow and Mario Shoenberg did in 1939 in this town of Urca identifying the basic mechanism, the Urca processes, leading to the process of gravitational collapse and the formation of a neutron star and a supernova. The further hypothesis is considered to relate this X-ray source to a neutron star, newly born in the Supernova. This hypothesis should be submitted to further theoretical and observational investigation. Some theoretical developments to clarify the astrophysical origin of this new scenario are outlined. We turn then to the theoretical developments in the short GRBs: we first report some progress in the understanding the dynamical phase of collapse, the mass-energy formula and the extraction of blackholic energy which have been motivated by the analysis of the short GRBs. In this context progress has also been accomplished on establishing an absolute lower limit to the irreducible mass of the black hole as well as on some critical considerations about the relations of general relativity and the second law of thermodynamics. We recall how this last issue has been one of the most debated in theoretical physics in the past thirty years due to the work of Bekenstein and Hawking. Following these conceptual progresses we analyze the vacuum polarization process around an overcritical collapsing shell. We evidence the existence of a separatrix and a dyadosphere trapping surface in the dynamics of the electron-positron plasma generated during the process of gravitational collapse. We then analyze, using recent progress in the solution of the Vlasov-Boltzmann-Maxwell system, the oscillation regime in the created electron-positron plasma and their rapid convergence to a thermalized spectrum. We conclude by making precise predictions for the spectra, the energy fluxes and characteristic time-scales of the radiation for short-bursts. If the precise luminosity variation and spectral hardening of the radiation we have predicted will be confirmed by observations of short-bursts, these systems will play a major role as standard candles in cosmology. These considerations will also be relevant for the analysis of the long-bursts when the baryonic matter contribution will be taken into account.

2. R. Ruffini, M.G. Bernardini, C.L. Bianco, P. Chardonnet, F. Fraschetti, V. Gurzadyan, L. Vitagliano, S.-S. Xue; “Black hole physics and astrophysics: The GRB-Supernova connection and URCA-1 – URCA-2”; in Proceedings of the Tenth Marcel Grossmann Meeting on General Rela-

tivity, Rio de Janeiro, Brazil, July 2003, M. Novello, S.E. Perez-Bergliaffa, Editors; p. 369; World Scientific, (Singapore, 2006).

We outline the confluence of three novel theoretical fields in our modeling of Gamma-Ray Bursts (GRBs): 1) the ultrarelativistic regime of a shock front expanding with a Lorentz gamma factor $\sim$ 300; 2) the quantum vacuum polarization process leading to an electron-positron plasma originating the shock front; and 3) the general relativistic process of energy extraction from a black hole originating the vacuum polarization process. There are two different classes of GRBs: the long GRBs and the short GRBs. We here address the issue of the long GRBs. The theoretical understanding of the long GRBs has led to the detailed description of their luminosities in fixed energy bands, of their spectral features and made also possible to probe the astrophysical scenario in which they originate. We are specially interested, in this report, to a subclass of long GRBs which appear to be accompanied by a supernova explosion. We are considering two specific examples: GRB980425/SN1998bw and GRB030329/SN2003dh. While these supernovae appear to have a standard energetics of 10^{49} ergs, the GRBs are highly variable and can have energetics 10^4 – 10^5 times larger than the ones of the supernovae. Moreover, many long GRBs occurs without the presence of a supernova. It is concluded that in no way a GRB can originate from a supernova. The precise theoretical understanding of the GRB luminosity we present evidence, in both these systems, the existence of an independent component in the X-ray emission, usually interpreted in the current literature as part of the GRB afterglow. This component has been observed by Chandra and XMM to have a strong decay on scale of months. We have named here these two sources respectively URCA-1 and URCA-2, in honor of the work that George Gamow and Mario Shoenberg did in 1939 in this town of Urca identifying the basic mechanism, the Urca processes, leading to the process of gravitational collapse and the formation of a neutron star and a supernova. The further hypothesis is considered to relate this X-ray source to a neutron star, newly born in the Supernova. This hypothesis should be submitted to further theoretical and observational investigation. Some theoretical developments to clarify the astrophysical origin of this new scenario are outlined.

3. M.G. Bernardini, C.L. Bianco, P. Chardonnet, F. Fraschetti, R. Ruffini, S.-S. Xue; "General features of GRB 030329 in the EMBH model"; in Proceedings of the Tenth Marcel Grossmann Meeting on General Relativity, Rio de Janeiro, Brazil, July 2003, M. Novello, S.E. Perez-Bergliaffa,

Editors; p. 2459; World Scientific, (Singapore, 2006).

GRB 030329 is considered within the EMBH model. We determine the three free parameters and deduce its luminosity in given energy bands comparing it with the observations. The observed substructures are compared with the predictions of the model: by applying the result that substructures observed in the extended afterglow peak emission (E-APE) do indeed originate in the collision of the accelerated baryonic matter (ABM) pulse with the inhomogeneities in the interstellar medium around the black-hole, masks of density inhomogeneities are considered in order to reproduce the observed temporal substructures. The induced supernova concept is applied to this system and the general consequences that we are witnessing are the formation of a cosmological thriptych of a black hole originating the GRB 030329, the supernova SN2003dh and a young neutron star. Analogies to the system GRB 980425–SN1998bw are outlined.

4. R. Ruffini, M.G. Bernardini, C.L. Bianco, P. Chardonnet, A. Corsi, F. Fraschetti, S.-S. Xue; "GRB 970228 and its associated Supernova in the EMBH model"; in Proceedings of the Tenth Marcel Grossmann Meeting on General Relativity, Rio de Janeiro, Brazil, July 2003, M. Novello, S.E. Perez-Bergliaffa, Editors; p. 2465; World Scientific, (Singapore, 2006).

   The γ-ray burst of 1997 February 28 is analyzed within the Electromagnetic Black Hole model. We first estimate the value of the total energy deposited in the dyadosphere, E_{dya}, and the amount of baryonic matter left over by the EMBH progenitor star, $B = M_B c^2 / E_{dya}$. We then consider the role of the interstellar medium number density n_{ISM} and of the ratio R between the effective emitting area and the total surface area of the γ-ray burst source, in reproducing the prompt emission and the X-ray afterglow of this burst. Some considerations are also done concerning the possibility of explaining, within the theory, the observed evidence for a supernova in the optical afterglow.

5. F. Fraschetti, M.G. Bernardini, C.L. Bianco, P. Chardonnet, R. Ruffini, S.-S. Xue; "Inferences on the ISM structure around GRB980425 and GRB980425-SN1998bw association in the EMBH Model"; in Proceedings of the Tenth Marcel Grossmann Meeting on General Relativity, Rio de Janeiro, Brazil, July 2003, M. Novello, S.E. Perez-Bergliaffa, Editors; p. 2451; World Scientific, (Singapore, 2006).

   We determine the four free parameters within the EMBH model for GRB 980425

and deduce its luminosity in given energy bands, its spectra and its time variability in the prompt radiation. We compute the basic kinematical parameters of GRB 980425. In the extended afterglow peak emission the Lorentz γ factor is lower than the critical value 150 which has been found in Ruffini et al. (2002) to be necessary in order to perform the tomography of the ISM surrounding the GRB as suggested by Dermer & Mitman (1999). The detailed structure of the density inhomogeneities as well as the effects of radial apparent superluminal effects are evaluated within the EMBH model. Under the assumption that the energy distribution of emitted radiation is thermal in the comoving frame, time integrated spectra of EMBH model for prompt emission are computed. The induced supernova concept is applied to this system and general consequences on the astrophysical and cosmological scenario are derived.

6. R. Ruffini, M.G. Bernardini, C.L. Bianco, P. Chardonnet, F. Fraschetti, R. Guida, S.-S. Xue; "GRB 050315: A step in the proof of the uniqueness of the overall GRB structure"; in "GAMMA-RAY BURSTS IN THE SWIFT ERA: Sixteenth Maryland Astrophysics Conference", Washington, DC, USA, November 29th – December 2nd 2005, Stephen S. Holt, Neil Gehrels, John A. Nousek, Editors; AIP Conference Proceedings, 836, 103 (2006).

   Using the Swift data of GRB 050315, we progress in proving the uniqueness of our theoretically predicted Gamma-Ray Burst (GRB) structure as composed by a proper-GRB, emitted at the transparency of an electron-positron plasma with suitable baryon loading, and an afterglow comprising the "prompt radiation" as due to external shocks. Detailed light curves for selected energy bands are theoretically fitted in the entire temporal region of the Swift observations ranging over 10^6 seconds.

7. R. Ruffini, M.G. Bernardini, C.L. Bianco, P. Chardonnet, F. Fraschetti, S.-S. Xue; "Theoretical Interpretation of GRB 031203 and URCA-3"; in "Relativistic Astrophysics and Cosmology - Einstein's Legacy", B. Aschenbach, V. Burwitz, G. Hasinger, B. Leibundgut, Editors; Springer-Verlag (2007).

8. R. Ruffini, M.G. Bernardini, C.L. Bianco, L. Caito, P. Chardonnet, M.G. Dainotti, F. Fraschetti, R. Guida, M. Rotondo, G. Vereshchagin, L. Vita-gliano, S.-S. Xue; "The Blackholic energy and the canonical Gamma-Ray Burst"; in Proceedings of the XIIth Brazilian School on Cosmology

and Gravitation, Mangaratiba, Rio de Janeiro (Brazil), September 2006, M. Novello, S.E. Perez Bergliaffa, Editors; AIP Conference Proceedings, 910, 55 (2007).

Gamma-Ray Bursts (GRBs) represent very likely "the" most extensive computational, theoretical and observational effort ever carried out successfully in physics and astrophysics. The extensive campaign of observation from space based X-ray and γ-ray observatory, such as the *Vela*, CGRO, BeppoSAX, HETE-II, INTEGRAL, *Swift*, R-XTE, *Chandra*, XMM satellites, have been matched by complementary observations in the radio wavelength (e.g. by the VLA) and in the optical band (e.g. by VLT, Keck, ROSAT). The net result is unprecedented accuracy in the received data allowing the determination of the energetics, the time variability and the spectral properties of these GRB sources. The very fortunate situation occurs that these data can be confronted with a mature theoretical development. Theoretical interpretation of the above data allows progress in three different frontiers of knowledge: **a)** the ultrarelativistic regimes of a macroscopic source moving at Lorentz gamma factors up to ~ 400; **b)** the occurrence of vacuum polarization process verifying some of the yet untested regimes of ultrarelativistic quantum field theories; and **c)** the first evidence for extracting, during the process of gravitational collapse leading to the formation of a black hole, amounts of energies up to 10^{55} ergs of blackholic energy — a new form of energy in physics and astrophysics. We outline how this progress leads to the confirmation of three interpretation paradigms for GRBs proposed in July 2001. Thanks mainly to the observations by *Swift* and the optical observations by VLT, the outcome of this analysis points to the existence of a "canonical" GRB, originating from a variety of different initial astrophysical scenarios. The communality of these GRBs appears to be that they all are emitted in the process of formation of a black hole with a negligible value of its angular momentum. The following sequence of events appears to be canonical: the vacuum polarization process in the dyadosphere with the creation of the optically thick self accelerating electron-positron plasma; the engulfment of baryonic mass during the plasma expansion; adiabatic expansion of the optically thick "fireshell" of electron-positron-baryon plasma up to the transparency; the interaction of the accelerated baryonic matter with the interstellar medium (ISM). This leads to the canonical GRB composed of a proper GRB (P-GRB), emitted at the moment of transparency, followed by an extended afterglow. The sole parameters in this scenario are the total energy of the dyadosphere E_{dya}, the fireshell baryon loading M_B defined by the di-

mensionless parameter $B \equiv M_B c^2 / E_{dya}$, and the ISM filamentary distribution around the source. In the limit $B \to 0$ the total energy is radiated in the P-GRB with a vanishing contribution in the afterglow. In this limit, the canonical GRBs explain as well the short GRBs. In these lecture notes we systematically outline the main results of our model comparing and contrasting them with the ones in the current literature. In both cases, we have limited ourselves to review already published results in refereed publications. We emphasize as well the role of GRBs in testing yet unexplored grounds in the foundations of general relativity and relativistic field theories.

9. R. Ruffini, M.G. Bernardini, C.L. Bianco, L. Caito, P. Chardonnet, M.G. Dainotti, F. Fraschetti, R. Guida, G. Vereshchagin, S.-S. Xue; "The role of GRB 031203 in clarifying the astrophysical GRB scenario"; in Proceedings of the 6^{th} Integral Workshop - The Obscured Universe, Moscow, (Russia), July 2006, S. Grebenev, R. Sunyaev, C. Winkler, A. Parmar, L. Ouwehand, Editors; ESA Special Publication, SP-622, 561 (2007).

   The luminosity and the spectral distribution of the afterglow of GRB 031203 have been presented within our theoretical framework, which envisages the GRB structure as composed by a proper-GRB, emitted at the transparency of an electron-positron plasma with suitable baryon loading, and an afterglow comprising the "prompt emission" as due to external shocks. In addition to the GRB emission, there appears to be a prolonged soft X-Ray emission lasting for 10^6–10^7 seconds followed by an exponential decay. This additional source has been called by us URCA-3. It is urgent to establish if this component is related to the GRB or to the Supernova (SN). In this second case, there are two possibilities: either the interaction of the SN ejecta with the interstellar medium or, possibly, the cooling of a young neutron star formed in the SN 2003lw process. The analogies and the differences between this triptych GRB 031203 / SN 2003lw / URCA-3 and the corresponding ones GRB 980425 / SN 1998bw / URCA-1 and GRB 030329 / SN 2003dh / URCA-2, as well as GRB 060218 / SN 2006aj are discussed.

10. M.G. Bernardini, C.L. Bianco, L. Caito, M.G. Dainotti, R. Guida, R. Ruffini; "GRB970228 and the class of GRBs with an initial spikelike emission: do they follow the Amati relation?"; in Relativistic Astrophysics – Proceedings of the 4^{th} Italian-Sino Workshop, Pescara (Italy), July 2007, C.L. Bianco, S.-S. Xue, Editors; AIP Conference Proceedings, 966, 7 (2008).

    On the basis of the recent understanding of GRB050315 and GRB060218, we

return to GRB970228, the first Gamma-Ray Burst (GRB) with detected afterglow. We proposed it as the prototype for a new class of GRBs with "an occasional softer extended emission lasting tenths of seconds after an initial spikelike emission". Detailed theoretical computation of the GRB970228 light curves in selected energy bands for the prompt emission are presented and compared with observational *Beppo*SAX data. From our analysis we conclude that GRB970228 and likely the ones of the above mentioned new class of GRBs are "canonical GRBs" have only one peculiarity: they exploded in a galactic environment, possibly the halo, with a very low value of CBM density. Here we investigate how GRB970228 unveils another peculiarity of this class of GRBs: they do not fulfill the "Amati relation". We provide a theoretical explanation within the fireshell model for the apparent absence of such correlation for the GRBs belonging to this new class.

11. C.L. Bianco, M.G. Bernardini, L. Caito, M.G. Dainotti, R. Guida, R. Ruffini; "The "Fireshell" Model and the "Canonical" GRB Scenario; in Relativistic Astrophysics – Proceedings of the 4^{th} Italian-Sino Workshop, Pescara (Italy), July 2007, C.L. Bianco, S.-S. Xue, Editors; AIP Conference Proceedings, 966, 12 (2008).

    In the "fireshell" model we define a "canonical GRB" light curve with two sharply different components: the Proper-GRB (P-GRB), emitted when the optically thick fireshell of electron-positron plasma originating the phenomenon reaches transparency, and the afterglow, emitted due to the collision between the remaining optically thin fireshell and the CircumBurst Medium (CBM). We outline our "canonical GRB" scenario, originating from the gravitational collapse to a black hole, with a special emphasis on the discrimination between "genuine" and "fake" short GRBs.

12. L. Caito, M.G. Bernardini, C.L. Bianco, M.G. Dainotti, R. Guida, R. Ruffini; "GRB 060614: A Progress Report"; in Relativistic Astrophysics – Proceedings of the 4^{th} Italian-Sino Workshop, Pescara (Italy), July 2007, C.L. Bianco, S.-S. Xue, Editors; AIP Conference Proceedings, 966, 16 (2008).

    The explosion of GRB 060614, detected by the Swift satellite, produced a deep break in the GRB scenario opening new horizons of investigation, because it can't be traced back to any traditional scheme of classification. In fact, it manifests peculiarities both of long bursts and of short bursts. Above all, it is the first case of long duration near GRB without any bright Ib/c associated Supernova. We will show that, in our canonical GRB scenario, this "anomalous"

situation finds a natural interpretation and allows us to discuss a possible variation to the traditional classification scheme, introducing the distinction between "genuine" and "fake" short bursts.

13. M.G. Dainotti, M.G. Bernardini, C.L. Bianco, L. Caito, R. Guida, R. Ruffini; "GRB 060218 and the Binaries as Progenitors of GRB-SN Systems"; in Relativistic Astrophysics – Proceedings of the 4^{th} Italian-Sino Workshop, Pescara (Italy), July 2007, C.L. Bianco, S.-S. Xue, Editors; AIP Conference Proceedings, 966, 25 (2008).

    We study the Gamma-Ray Burst (GRB) 060218: a particularly close source at $z = 0.033$ with an extremely long duration, namely $T_{90} \sim 2000$ s, related to SN 2006aj. This source appears to be a very soft burst, with a peak in the spectrum at 4.9 keV, therefore interpreted as an X-Ray Flash (XRF). It fullfills the Amati relation. I present the fitting procedure, which is time consuming. In order to show its sensitivity I also present two examples of fits with the same value of B and different value of $E^{tot}_{e^\pm}$. We fit the X- and γ-ray observations by *Swift* of GRB 060218 in the 0.1–150 keV energy band during the entire time of observations from 0 all the way to 10^6 s within a unified theoretical model. The free parameters of our theory are only three, namely the total energy $E^{tot}_{e^\pm}$ of the $e^\pm$ plasma, its baryon loading $B \equiv M_B c^2 / E^{tot}_{e^\pm}$, as well as the CircumBurst Medium (CBM) distribution. We justify the extremely long duration of this GRB by a total energy $E^{tot}_{e^\pm} = 2.32 \times 10^{50}$ erg, a very high value of the baryon loading $B = 1.0 \times 10^{-2}$ and the effective CircumBurst Medium (CBM) density which shows a radial dependence $n_{cbm} \propto r^{-\alpha}$ with $1.0 \leq \alpha \leq 1.7$ and monotonically decreases from 1 to 10^{-6} particles/cm^3. We recall that this value of the B parameter is the highest among the sources we have analyzed and it is very close to its absolute upper limit expected. By our fit we show that there is no basic differences between XRFs and more general GRBs. They all originate from the collapse process to a black hole and their difference is due to the variability of the three basic parameters within the range of full applicability of the theory. We also think that the smallest possible black hole, formed by the gravitational collapse of a neutron star in a binary system, is consistent with the especially low energetics of the class of GRBs associated with SNe Ib/c.

14. R. Guida, M.G. Bernardini, C.L. Bianco, L. Caito, M.G. Dainotti, R. Ruffini; "The Amati Relation within the Fireshell Model"; in Relativistic Astrophysics – Proceedings of the 4^{th} Italian-Sino Workshop, Pescara (Italy), July 2007, C.L. Bianco, S.-S. Xue, Editors; AIP Conference Proceedings,

966, 46 (2008).

In this work we show the existence of a spectral-energy correlation within our "fireshell" model for GRBs. The free parameters of the model are the total energy $E_{tot}^{e\pm}$ of the $e^{\pm}$ plasma and its baryon loading $B \equiv M_B\, c^2 / E_{tot}^{e\pm}$, characterizing the source, and the parameters describing the effective CircumBurst medium (CBM) distribution, namely its particle number density ρ and its effective emitting area R. We build a sample of pseudo-GRBs, i.e. a set of theoretically simulated light curves, varying the total energy of the electron-positron plasma $E_{tot}^{e\pm}$ and keeping the same baryon loading; the parametrization used to describe the distribution of the CircumBurst medium is the same as well for all the pseudo-GRBs. The values of these parameters (B, ρ and R) used in this work are equal to the ones assumed to fit GRB050315, a *Swift* burst representing a good example of what in the literature has been addressed as "canonical light curve". For each GRB of the sample we calculate the νF_ν spectrum integrating the theoretically computed light curve over the total time, namely from our T_0, the end of the Proper-GRB (P-GRB), up to the end of our afterglow phase, when the fireshell Lorentz gamma factor is close to unity; we exclude the P-GRB from this spectral computation because, following our "canonical" GRB scenario, this component of the GRB emission is physically different from the other component, that is our afterglow component, so one should take care in no mixing them. We find that the maximum of this spectrum, that is the observed peak energy $E_{p,tot}$, correlates with the initial electron-positron plasma energy $E_{tot}^{e\pm}$ in a way very similar to the Amati one: $E_{p,tot} \propto (E_{tot}^{e\pm})^{0.5}$.

15. R. Guida, M.G. Bernardini, C.L. Bianco, L. Caito, M.G. Dainotti, R. Ruffini; "Theoretical interpretation of the Amati relation within the fireshell model"; in GAMMA-RAY BURSTS 2007: Proceedings of the Santa Fe Conference, Santa Fe (NM, USA), November 2007, M. Galassi, D. Palmer, E. Fenimore, Editors; AIP Conference Proceedings, 1000, 60 (2008).

    We discuss within our theoretical "fireshell" model for Gamma-Ray Bursts (GRBs) the theoretical interpretation of the phenomenological correlation between the isotropic-equivalent radiated energy of the prompt emission E_{iso} and the cosmological rest-frame νF_ν spectrum peak energy E_p observed by Amati and collaborators. Possible reasons for some of the outliers of this relation are given.

16. L. Caito, M.G. Bernardini, C.L. Bianco, M.G. Dainotti, R. Guida, R. Ruffini; "GRB 060614: a Fake Short Gamma-Ray Burst"; in GAMMA-RAY BURSTS

2007: Proceedings of the Santa Fe Conference, Santa Fe (NM, USA), November 2007, M. Galassi, D. Palmer, E. Fenimore, Editors; AIP Conference Proceedings, 1000, 301 (2008).

The explosion of GRB 060614 produced a deep break in the GRB scenario and opened new horizons of investigation because it can't be traced back to any traditional scheme of classification. In fact, it manifests peculiarities both of long bursts and of short bursts and, above all, it is the first case of long duration near GRB without any bright Ib/c associated Supernova. We will show that, in our canonical GRB scenario, this "anomalous" situation finds a natural interpretation and allows us to discuss a possible variation to the traditional classification scheme, introducing the distinction between "genuine" and "fake" short bursts.

17. C.L. Bianco, M.G. Bernardini, L. Caito, M.G. Dainotti, R. Guida, R. Ruffini; "Short and canonical GRBs"; in GAMMA-RAY BURSTS 2007: Proceedings of the Santa Fe Conference, Santa Fe (NM, USA), November 2007, M. Galassi, D. Palmer, E. Fenimore, Editors; AIP Conference Proceedings, 1000, 305 (2008).

    Within the "fireshell" model for the Gamma-Ray Bursts (GRBs) we define a "canonical GRB" light curve with two sharply different components: the Proper-GRB (P-GRB), emitted when the optically thick fireshell of electron-positron plasma originating the phenomenon reaches transparency, and the afterglow, emitted due to the collision between the remaining optically thin fireshell and the CircumBurst Medium (CBM). We outline our "canonical GRB" scenario, with a special emphasis on the discrimination between "genuine" and "fake" short GRBs.

18. C.L. Bianco, M.G. Bernardini, L. Caito, M.G. Dainotti, R. Guida, R. Ruffini, G. Vereshchagin, S.-S. Xue; "The Equations of motion of the "fireshell""; in OBSERVATIONAL EVIDENCE FOR BLACK HOLES IN THE UNIVERSE: Proceedings of the 2^{nd} Kolkata Conference, Kolkata (India), February 2008, S.K. Chakrabarti, A.S. Majumdar, Editors; AIP Conference Proceedings, 1053, 259 (2008).

    The Fireshell originating a Gamma-Ray Burst (GRB) encompasses an optically thick regime followed by an optically thin one. In the first one the fireshell self-accelerates from a Lorentz gamma factor equal to 1 all the way to 200-300. The physics of this system is based on the continuous annihilation of electron-positron pairs in an optically thick e^+e^- plasma with a small baryon loading.

In the following regime, the optically thin fireshell, composed by the baryons left over after the transparency point, ballistically expands into the Circum-Burst Medium (CBM). The dynamics of the fireshell during both regimes will be analyzed. In particular we will re-examine the validity of the constant-index power-law relation between the fireshell Lorentz gamma factor and its radial coordinate, usually adopted in the current literature on the grounds of an "ultrarelativistic" approximation. Such expressions are found to be mathematically correct but only approximately valid in a very limited range of the physical and astrophysical parameters and in an asymptotic regime which is reached only for a very short time, if any.

19. M.G. Bernardini, C.L. Bianco, L. Caito, M.G. Dainotti, R. Guida, R. Ruffini; "The "Canonical" GRBs within the fireshell model"; in OBSERVATIONAL EVIDENCE FOR BLACK HOLES IN THE UNIVERSE: Proceedings of the 2^{nd} Kolkata Conference, Kolkata (India), February 2008, S.K. Chakrabarti, A.S. Majumdar, Editors; AIP Conference Proceedings, 1053, 267 (2008).

    Within the fireshell model we define a "canonical" GRB light curve with two sharply different components: the Proper-GRB (P-GRB), emitted when the optically thick fireshell of electron-positron plasma originating the phenomenon reaches transparency, and the afterglow, emitted due to the collision between the remaining optically thin fireshell and the CircumBurst Medium (CBM). On the basis of the recent understanding of GRB970228 as the prototype for a new class of GRBs with "an occasional softer extended emission lasting tenths of seconds after an initial spikelike emission" we outline our "canonical" GRB scenario, originating from the gravitational collapse to a black hole, with a special emphasis on the discrimination between short GRBs and the ones appearing as such due to their peculiar astrophysical setting.

20. M.G. Dainotti, M.G. Bernardini, C.L. Bianco, L. Caito, R. Guida, R. Ruffini; "GRB 060218: the density mask and its peculiarity compared to the other sources"; in OBSERVATIONAL EVIDENCE FOR BLACK HOLES IN THE UNIVERSE: Proceedings of the 2^{nd} Kolkata Conference, Kolkata (India), February 2008, S.K. Chakrabarti, A.S. Majumdar, Editors; AIP Conference Proceedings, 1053, 283 (2008).

    The Swift satellite has given continuous data in the range 0.3–150 keV from 0 s to 106 s for GRB060218 associated with SN2006aj. It has an unusually long duration ($T_{90} \sim 2100$ s). We plan to fit the complete γ- and X-ray light curves of this long duration GRB, including the prompt emission and we give peculiar

attention to the afterglow lightcurve in order to better constrain the density mask. We apply our "fireshell" model based on the formation of a black hole, giving the relevant references. The initial total energy of the electron-positron plasma $E_{e^\pm}^{tot} == 2.32 \times 10^{50}$ erg has a particularly low value similarly to the other GRBs associated with SNe. For the first time we observe a baryon loading $B = 10^{-2}$ which coincides with the upper limit for the dynamical stability of the fireshell. The effective CircumBurst Medium (CBM) density shows a radial dependence $n_{cbm} \propto r^{-a}$ with $1.0 \leq a \leq 1.7$ and monotonically decreases from 1 to 10^{-6} particles/cm^3. Such a behavior is interpreted as due to a fragmentation in the fireshell. Such a fragmentation is crucial in explaining both the unusually large T_{90} and the consequently inferred abnormal low value of the CBM effective density. We present the comparison between the density mask of this source and the ones of a normal GRB 050315 and a fake short, GRB 970228, making some assumptions on the CBM behaviour in the surrounding of the Black hole.

21. L. Caito, M.G. Bernardini, C.L. Bianco, M.G. Dainotti, R. Guida, R. Ruffini; "GRB 060614 in the canonical fireshell model"; in OBSERVATIONAL EVIDENCE FOR BLACK HOLES IN THE UNIVERSE: Proceedings of the 2nd Kolkata Conference, Kolkata (India), February 2008, S.K. Chakrabarti, A.S. Majumdar, Editors; AIP Conference Proceedings, 1053, 291 (2008).

    Gamma-Ray Burst (GRB) 060614 is the first nearby long duration GRB clearly not associated to any bright Ib/c Supernova. The explosion of this burst undermines one of the fundamental assumptions of the standard scenario and opens new horizons and hints of investigation. GRB 060614, hardly classifiable as a short GRB, is not either a "typical" long GRB since it occurs in a low star forming region. Moreover, it presents deep similarities with GRB 970228, which is the prototype of the "fake" short bursts, or better canonical GRBs disguised as short ones. Within the "fireshell" model, we test if this "anomalous" source can be a disguised short GRB.

22. L.J. Rangel Lemos, S. Casanova, R. Ruffini, S.S. Xue; "Fermi's approach to the study of pp interactions"; in OBSERVATIONAL EVIDENCE FOR BLACK HOLES IN THE UNIVERSE: Proceedings of the 2nd Kolkata Conference, Kolkata (India), February 2008, S.K. Chakrabarti, A.S. Majumdar, Editors; AIP Conference Proceedings, 1053, 275 (2008).

    The physics of hadronic interactions found much difficulties for explain the experimental data. In this work we study the approach of Fermi (1950) about

the multiplicity of pions emitted in pp interactions and in follow we compare with the modern approach

23. R. Ruffini, A.G. Aksenov, M.G. Bernardini, C.L. Bianco, L. Caito, M.G. Dainotti, G. De Barros, R. Guida, G.V. Vereshchagin, S.-S. Xue; "The canonical Gamma-Ray Bursts and their 'precursors"'; in 2008 NANJING GAMMA-RAY BURST CONFERENCE, Proceedings of the 2008 Nanjing Gamma-Ray Burst Conference, Nanjing (China), June 2008, Y.-F. Huang, Z.-G. Dai, B. Zhang, Editors; AIP Conference Proceedings, 1065, 219 (2008).

    The fireshell model for Gamma-Ray Bursts (GRBs) naturally leads to a canonical GRB composed of a proper-GRB (P-GRB) and an afterglow. P-GRBs, introduced by us in 2001, are sometimes considered "precursors" of the main GRB event in the current literature. We show in this paper how the fireshell model leads to the understanding of the structure of GRBs, with precise estimates of the time sequence and intensities of the P-GRB and the of the afterglow. It leads as well to a natural classification of the canonical GRBs which overcomes the traditional one in short and long GRBs.

24. M.G. Bernardini, C.L. Bianco, L. Caito, M.G. Dainotti, R. Guida, R. Ruffini; "Preliminary analysis of GRB060607A within the fireshell model"; in 2008 NANJING GAMMA-RAY BURST CONFERENCE; Proceedings of the 2008 Nanjing Gamma-Ray Burst Conference, Nanjing (China), June 2008, Y.-F. Huang, Z.-G. Dai, B. Zhang, Editors; AIP Conference Proceedings, 1065, 227 (2008).

    GRB060607A is a very distant ($z = 3.082$) and energetic event ($E_{iso} \sim 10^{53}$ erg). Its main peculiarity is that the peak of the near-infrared afterglow has been observed with the REM robotic telescope, allowing to infer the initial Lorentz gamma factor of the emitting system. We present a preliminary analysis of the spectra and light curves of GRB060607A prompt emission within the fireshell model. We show that the N(E) spectrum of the prompt emission, whose behavior is usually described as "simple power-law", can also be fitted in a satisfactory way by a convolution of thermal spectra as predicted by the model we applied. The theoretical time-integrated spectrum of the prompt emission as well as the light curves in the BAT and XRT energy band are in good agreement with the observations, enforcing the plausibility of our approach. Furthermore, the initial value of Lorentz gamma factor we predict is compatible with the one deduced from the REM observations.

25. C.L. Bianco, M.G. Bernardini, L. Caito, M.G. Dainotti, R. Guida, R. Ruffini; "The "fireshell" model and the "canonical GRB" scenario"; in 2008 NANJING GAMMA-RAY BURST CONFERENCE; Proceedings of the 2008 Nanjing Gamma-Ray Burst Conference, Nanjing (China), June 2008, Y.-F. Huang, Z.-G. Dai, B. Zhang, Editors; AIP Conference Proceedings, 1065, 223 (2008).

    The Swift observation of GRB 060614, as well as the catalog analysis by Norris & Bonnell (2006), opened the door "on a new Gamma-Ray Bursts (GRBs) classification scheme that straddles both long and short bursts" (Gehrels et al. 2006). Within the "fireshell" model for the Gamma-Ray Bursts (GRBs) we define a "canonical GRB" light curve with two sharply different components: the Proper-GRB (P-GRB), emitted when the optically thick fireshell of electron-positron plasma originating the phenomenon reaches transparency, and the afterglow, emitted due to the collision between the remaining optically thin fireshell and the CircumBurst Medium (CBM). We here outline our "canonical GRB" scenario, which implies three different GRB classes: the "genuine" short GRBs, the "fake" or "disguised" short GRBs and the other (so-called "long") GRBs. We also outline some implications for the theoretical interpretation of the Amati relation.

26. G. De Barros, M.G. Bernardini, C.L. Bianco, L. Caito, M.G. Dainotti, R. Guida, R. Ruffini; "Is GRB 050509b a "genuine" short GRB?"; in 2008 NANJING GAMMA-RAY BURST CONFERENCE; Proceedings of the 2008 Nanjing Gamma-Ray Burst Conference, Nanjing (China), June 2008, Y.-F. Huang, Z.-G. Dai, B. Zhang, Editors; AIP Conference Proceedings, 1065, 231 (2008).

    Within our "fireshell" model we introduced a "canonical" GRB scenario which differentiates physically the "proper GRB" (P-GRB) emission when photons decouple, and the afterglow emission due to interaction of the accelerated baryons with the CircumBurst Medium (CBM). The ratio between energetics of the two components is ruled by the baryon loading of the fireshell. We here analyse the possibility that GRB050509b is the first case of a "genuine" short GRB the ones with smaller baryon loading. In such a case, the GRB050509b "prompt emission" would be dominated by the "proper GRB" and, moreover, the P-GRB total energy would be greater than the afterglow one. Our fit of the afterglow data and of the P-GRB energetics indicates that this source present the smallest baryon loading we ever encountered so far, being on the order of

10^{-4}.

27. G. De Barros, A.G. Aksenov, C.L. Bianco, R. Ruffini, G.V. Vereshchagin; "Fireshell versus Fireball scenarios"; in 2008 NANJING GAMMA-RAY BURST CONFERENCE; Proceedings of the 2008 Nanjing Gamma-Ray Burst Conference, Nanjing (China), June 2008, Y.-F. Huang, Z.-G. Dai, B. Zhang, Editors; AIP Conference Proceedings, 1065, 234 (2008).

    We revisit Cavallo and Rees classification based on the analysis of initial conditions in electron-positron-photon plasma which appears suddenly around compact astrophysical objects and gives origin to GRBs. These initial conditions were recently studied in [1,2] by numerical integration of relativistic Boltzmann equations with collision integrals, including binary and triple interactions between particles. The main conclusion is that the pair plasma in GRB sources quickly reaches thermal equilibrium well before its expansion starts. In light of this work we comment on each of the four scenarios proposed by Cavallo and Rees and discuss their applicability to describe evolution of GRB sources.

28. M.G. Bernardini, C.L. Bianco, L. Caito, M.G. Dainotti, R. Guida, R. Ruffini; "GRB970228 as a prototype for the class of GRBs with an initial spikelike emission"; in Proceedings of the Eleventh Marcel Grossmann Meeting on General Relativity, Berlin, Germany, July 2006, H. Kleinert, R.T. Jantzen, Editors; World Scientific, (Singapore, 2008).

    We interpret GRB970228 prompt emission within our "canonical" GRB scenario, identifying the initial spikelike emission with the Proper-GRB (P-GRB) and the following bumps with the afterglow peak emission. Furthermore, we emphasize the necessity to consider the "canonical" GRB as a whole due to the highly non-linear nature of the model we applied.

29. M.G. Bernardini, C.L. Bianco, L. Caito, M.G. Dainotti, R. Guida, R. Ruffini; "GRB980425 and the puzzling URCA1 emission"; in Proceedings of the Eleventh Marcel Grossmann Meeting on General Relativity, Berlin, Germany, July 2006, H. Kleinert, R.T. Jantzen, Editors; World Scientific, (Singapore, 2008).

    We applied our "fireshell" model to GRB980425 observational data, reproducing very satisfactory its prompt emission. We use the results of our analysis to provide a possible interpretation for the X-ray emission of the source S1. The

effect on the GRB analysis of the lack of data in the pre-Swift observations is also outlined.

30. C.L. Bianco, M.G. Bernardini, L. Caito, P. Chardonnet, M.G. Dainotti, F. Fraschetti, R. Guida, R. Ruffini, S.-S. Xue; "Theoretical interpretation of 'long' and 'short' GRBs"; in Proceedings of the Eleventh Marcel Grossmann Meeting on General Relativity, Berlin, Germany, July 2006, H. Kleinert, R.T. Jantzen, Editors; World Scientific, (Singapore, 2008).

    Within the "fireshell" model we define a "canonical GRB" light curve with two sharply different components: the Proper-GRB (P-GRB), emitted when the optically thick fireshell of electron-positron plasma originating the phenomenon reaches transparency, and the afterglow, emitted due to the collision between the remaining optically thin fireshell and the CircumBurst Medium (CBM). We here present the consequences of such a scenario on the theoretical interpretation of the nature of "long" and "short" GRBs.

31. C.L. Bianco, M.G. Bernardini, P. Chardonnet, F. Fraschetti, R. Ruffini, S.-S. Xue; "Theoretical interpretation of luminosity and spectral properties of GRB 031203"; in Proceedings of the Eleventh Marcel Grossmann Meeting on General Relativity, Berlin, Germany, July 2006, H. Kleinert, R.T. Jantzen, Editors; World Scientific, (Singapore, 2008).

    We show how an emission endowed with an instantaneous thermal spectrum in the co-moving frame of the expanding fireshell can reproduce the time-integrated GRB observed non-thermal spectrum. An explicit example in the case of GRB 031203 is presented.

32. C.L. Bianco, R. Ruffini; "The 'Fireshell' model in the Swift era"; in Proceedings of the Eleventh Marcel Grossmann Meeting on General Relativity, Berlin, Germany, July 2006, H. Kleinert, R.T. Jantzen, Editors; World Scientific, (Singapore, 2008).

    We here re-examine the validity of the constant-index power-law relation between the fireshell Lorentz gamma factor and its radial coordinate, usually adopted in the current Gamma-Ray Burst (GRB) literature on the grounds of an "ultrarelativistic" approximation. Such expressions are found to be mathematically correct but only approximately valid in a very limited range of the physical and astrophysical parameters and in an asymptotic regime which is reached only for a very short time, if any.

33. L. Caito, M.G. Bernardini, C.L. Bianco, M.G. Dainotti, R. Guida, R. Ruffini; "Theoretical interpretation of GRB011121"; in Proceedings of the Eleventh Marcel Grossmann Meeting on General Relativity, Berlin, Germany, July 2006, H. Kleinert, R.T. Jantzen, Editors; World Scientific, (Singapore, 2008).

    GRB 011121, detected by the BeppoSAX satellite, is studied as a prototype to understand the presence of flares observed by Swift in the afterglow of many GRB sources. Detailed theoretical analysis of the GRB 011121 light curves in selected energy bands are presented and compared with observational data. An interpretation of the flare of this source is provided by the introduction of the three-dimensional structure of the CircumBurst Medium(CBM).

34. M.G. Dainotti, M.G. Bernardini, C.L. Bianco, L. Caito, R. Guida, R. Ruffini; "On GRB 060218 and the GRBs related to Supernovae Ib/c"; in Proceedings of the Eleventh Marcel Grossmann Meeting on General Relativity, Berlin, Germany, July 2006, H. Kleinert, R.T. Jantzen, Editors; World Scientific, (Singapore, 2008).

    We study the Gamma-Ray Burst (GRB) 060218: a particularly close source at $z = 0.033$ with an extremely long duration, namely $T_{90} \sim 2000$ s, related to SN 2006aj. This source appears to be a very soft burst, with a peak in the spectrum at 4.9 keV, therefore interpreted as an X-Ray Flash (XRF) and it obeys to the Amati relation. We fit the X- and γ-ray observations by Swift of GRB 060218 in the 0.1–150 keV energy band during the entire time of observations from 0 all the way to 106 s within a unified theoretical model. The details of our theoretical analysis have been recently published in a series of articles. The free parameters of the theory are only three, namely the total energy $E^{tot}_{e^\pm}$ of the $e^\pm$ plasma, its baryon loading $B = M_B c^2 / E^{tot}_{e^\pm}$, as well as the CircumBurst Medium (CBM) distribution. We fit the entire light curve, including the prompt emission as an essential part of the afterglow. We recall that this value of the B parameter is the highest among the sources we have analyzed and it is very close to its absolute upper limit expected. We successfully make definite predictions about the spectral distribution in the early part of the light curve, exactly we derive the instantaneous photon number spectrum N(E) and we show that although the spectrum in the co-moving frame of the expanding pulse is thermal, the shape of the final spectrum in the laboratory frame is clearly non thermal. In fact each single instantaneous spectrum is the result of an integration of thousands of thermal spectra over the corresponding EQuiTemporal Surfaces (EQTS). By

our fit we show that there is no basic differences between XRFs and more general GRBs. They all originate from the collapse process to a black hole and their difference is due to the variability of the three basic parameters within the range of full applicability of the theory.

35. R. Guida, M.G. Bernardini, C.L. Bianco, L. Caito, M.G. Dainotti, R. Ruffini; "Theoretical interpretation of GRB060124"; in Proceedings of the Eleventh Marcel Grossmann Meeting on General Relativity, Berlin, Germany, July 2006, H. Kleinert, R.T. Jantzen, Editors; World Scientific, (Singapore, 2008).

    We show the preliminary results of the application of our "fireshell" model to GRB060124. This source is very peculiar because it is the first event for which both the prompt and the afterglow emission were observed simultaneously by the three Swift instruments: BAT (15 - 350 keV), XRT (0,2 - 10 keV) and UVOT (170 - 650 nm), due to the presence of a precursor $\sim$ 570 s before the main burst. We analyze GRB060124 within our "canonical" GRB scenario, identifying the precursor with the P-GRB and the prompt emission with the afterglow peak emission. In this way we reproduce correctly the energetics of both these two components. We reproduce also the observed time delay between the precursor (P-GRB) and the main burst. The effect of such a time delay in our model will be discussed.

36. R. Ruffini, M.G. Bernardini, C.L. Bianco, L. Caito, P. Chardonnet, C. Cherubini, M.G. Dainotti, F. fraschetti, A. Geralico, R. Guida, B. Patricelli, M. Rotondo, J. Rueda Hernandez, G. Vereshchagin, S.-S. Xue; "Gamma-Ray Bursts"; in Proceedings of the Eleventh Marcel Grossmann Meeting on General Relativity, Berlin, Germany, July 2006, H. Kleinert, R.T. Jantzen, Editors; World Scientific, (Singapore, 2008).

    We show by example how the uncoding of Gamma-Ray Bursts (GRBs) offers unprecedented possibilities to foster new knowledge in fundamental physics and in astrophysics. After recalling some of the classic work on vacuum polarization in uniform electric fields by Klein, Sauter, Heisenberg, Euler and Schwinger, we summarize some of the efforts to observe these effects in heavy ions and high energy ion collisions. We then turn to the theory of vacuum polarization around a Kerr-Newman black hole, leading to the extraction of the blackholic energy, to the concept of dyadosphere and dyadotorus, and to the creation of an electron-positron-photon plasma. We then present a new theoretical approach encompassing the physics of neutron stars and heavy nuclei.

It is shown that configurations of nuclear matter in bulk with global charge neutrality can exist on macroscopic scales and with electric fields close to the critical value near their surfaces. These configurations may represent an initial condition for the process of gravitational collapse, leading to the creation of an electron-positron-photon plasma: the basic self-accelerating system explaining both the energetics and the high energy Lorentz factor observed in GRBs. We then turn to recall the two basic interpretational paradigms of our GRB model: 1) the Relative Space-Time Transformation (RSTT) paradigm and 2) the Interpretation of the Burst Structure (IBS) paradigm. These paradigms lead to a "canonical" GRB light curve formed from two different components: a Proper-GRB (P-GRB) and an extended afterglow comprising a raising part, a peak, and a decaying tail. When the P-GRB is energetically predominant we have a "genuine" short GRB, while when the afterglow is energetically predominant we have a so-called long GRB or a "fake" short GRB. We compare and contrast the description of the relativistic expansion of the electron-positron plasma within our approach and within the other ones in the current literature. We then turn to the special role of the baryon loading in discriminating between "genuine" short and long or "fake" short GRBs and to the special role of GRB 991216 to illustrate for the first time the "canonical" GRB bolometric light curve. We then propose a spectral analysis of GRBs, and proceed to some applications: GRB 031203, the first spectral analysis, GRB 050315, the first complete light curve fitting, GRB 060218, the first evidence for a critical value of the baryon loading, GRB 970228, the appearance of "fake" short GRBs. We finally turn to the GRB-Supernova Time Sequence (GSTS) paradigm: the concept of induced gravitational collapse. We illustrate this paradigm by the systems GRB 980425 / SN 1998bw, GRB 030329 / SN 2003dh, GRB 031203 / SN 2003lw, GRB 060218 / SN 2006aj, and we present the enigma of the URCA sources. We then present some general conclusions.

37. R. Ruffini, A.G. Aksenov, M.G. Bernardini, C.L. Bianco, L. Caito, M.G. Dainotti, G. De Barros, R. Guida, G. Vereshchagin, S.-S. Xue; "The canonical Gamma-Ray Bursts: long, 'fake'-'disguised' and 'genuine' short bursts; in PROBING STELLAR POPULATIONS OUT TO THE DISTANT UNIVERSE: CEFALU 2008, Proceedings of the International Conference; Cefalù (Italy), September 2008, G. Giobbi, A. Tornambe, G. Raimondo, M. Limongi, L. A. Antonelli, N. Menci, E. Brocato, Editors; AIP Conference Proceedings, 1111, 325 (2009).

    The Gamma-Ray Bursts (GRBs) offer the unprecedented opportunity to ob-

serve for the first time the blackholic energy extracted by the vacuum polarization during the process of gravitational collapse to a black hole leading to the formation of an electron-positron plasma. The uniqueness of the Kerr-Newman black hole implies that very different processes originating from the gravitational collapse a) of a single star in a binary system induced by the companion, or b) of two neutron stars, or c) of a neutron star and a white dwarf, do lead to the same structure for the observed GRB. The recent progress of the numerical integration of the relativistic Boltzmann equations with collision integrals including 2-body and 3-body interactions between the particles offer a powerful conceptual tool in order to differentiate the traditional "fireball" picture, an expanding hot cavity considered by Cavallo and Rees, as opposed to the "fireshell" model, composed of an internally cold shell of relativistically expanding electron-positron-baryon plasma. The analysis of the fireshell naturally leads to a canonical GRB composed of a proper-GRB and an extended afterglow. By recalling the three interpretational paradigms for GRBs we show how the fireshell model leads to an understanding of the GRB structure and to an alternative classification of short and long GRBs.

38. M.G. Bernardini, M.G. Dainotti, C.L. Bianco, L. Caito, R. Guida, R. Ruffini; "Prompt emission and X-ray flares: the case of GRB 060607 A"; in PROBING STELLAR POPULATIONS OUT TO THE DISTANT UNIVERSE: CEFALU 2008, Proceedings of the International Conference; Cefalù (Italy), September 2008, G. Giobbi, A. Tornambe, G. Raimondo, M. Limongi, L. A. Antonelli, N. Menci, E. Brocato, Editors; AIP Conference Proceedings, 1111, 383 (2009).

    GRB 060607A is a very distant and energetic event. Its main peculiarity is that the peak of the near-infrared (NIR) afterglow has been observed with the REM robotic telescope, allowing to estimate the initial Lorentz gamma factor within the fireball forward shock model. We analyze GRB 060607A within the fireshell model. The initial Lorentz gamma factor of the fireshell can be obtained adopting the exact solutions of its equations of motion, dealing only with the BAT and XRT observations, that are the basic contribution to the afterglow emission, up to a distance from the progenitor $r \sim 10^{18}$ cm. According to the "canonical GRB" scenario we interpret the whole prompt emission as the peak of the afterglow emission, and we show that the observed temporal variability of the prompt emission can be produced by the interaction of the fireshell with overdense CircumBurst Medium (CBM) clumps. This is indeed the case also of the X-ray flares which are present in the early phases of the

afterglow light curve.

39. C.L. Bianco, M.G. Bernardini, L. Caito, M.G. Dainotti, R. Guida, R. Ruffini; "The 'fireshell' model and the 'canonical GRB' scenario. Implications for the Amati relation"; in PROBING STELLAR POPULATIONS OUT TO THE DISTANT UNIVERSE: CEFALU 2008, Proceedings of the International Conference; Cefalù (Italy), September 2008, G. Giobbi, A. Tornambe, G. Raimondo, M. Limongi, L. A. Antonelli, N. Menci, E. Brocato, Editors; AIP Conference Proceedings, 1111, 587 (2009).

    Within the "fireshell" model for GRBs we define a "canonical GRB" light curve with two sharply different components: the Proper-GRB (P-GRB), emitted when the optically thick fireshell reaches transparency, and the extended afterglow, emitted due to the collision between the remaining optically thin fireshell and the CircumBurst Medium (CBM). We here outline our "canonical GRB" scenario, which implies three different GRB classes: the "genuine" short GRBs, the "fake" or "disguised" short GRBs and the other (so-called "long") GRBs. We will also outline the corresponding implications for the Amati relation, which are opening its use for cosmology.

40. R. Ruffini, A.G. Aksenov, M.G. Bernardini, C.L. Bianco, L. Caito, P. Chardonnet, M.G. Dainotti, G. De Barros, R. Guida, L. Izzo, B. Patricelli, L.J. Rangel Lemos, M. Rotondo, J.A. Rueda Hernandez, G. Vereshchagin, S.-S. Xue; "The Blackholic energy and the canonical Gamma-Ray Burst IV: the 'long', 'genuine short' and 'fake – disguised short' GRBs"; in Proceedings of the XIIIth Brazilian School on Cosmology and Gravitation, Mangaratiba, Rio de Janeiro (Brazil), July-August 2008, M. Novello, S.E. Perez Bergliaffa, Editors; AIP Conference Proceedings, 1132, 199 (2009).

    We report some recent developments in the understanding of GRBs based on the theoretical framework of the "fireshell" model, already presented in the last three editions of the "Brazilian School of Cosmology and Gravitation". After recalling the basic features of the "fireshell model", we emphasize the following novel results: 1) the interpretation of the X-ray flares in GRB afterglows as due to the interaction of the optically thin fireshell with isolated clouds in the CircumBurst Medium (CBM); 2) an interpretation as "fake - disguised" short GRBs of the GRBs belonging to the class identified by Norris & Bonnell; we present two prototypes, GRB 970228 and GRB 060614; both these cases are consistent with an origin from the final coalescence of a binary system in the

halo of their host galaxies with particularly low CBM density $n_{cbm} \sim 10^{-3}$ particles/cm^3; 3) the first attempt to study a genuine short GRB with the analysis of GRB 050509B, that reveals indeed still an open question; 4) the interpretation of the GRB-SN association in the case of GRB 060218 via the "induced gravitational collapse" process; 5) a first attempt to understand the nature of the "Amati relation", a phenomenological correlation between the isotropic-equivalent radiated energy of the prompt emission E_{iso} with the cosmological rest-frame νF_ν spectrum peak energy $E_{p,i}$. In addition, recent progress on the thermalization of the electron-positron plasma close to their formation phase, as well as the structure of the electrodynamics of Kerr-Newman Black Holes are presented. An outlook for possible explanation of high-energy phenomena in GRBs to be expected from the AGILE and the Fermi satellites are discussed. As an example of high energy process, the work by Enrico Fermi dealing with ultrarelativistic collisions is examined. It is clear that all the GRB physics points to the existence of overcritical electrodynamical fields. In this sense we present some progresses on a unified approach to heavy nuclei and neutron stars cores, which leads to the existence of overcritical fields under the neutron star crust.

41. A.G. Aksenov, M.G. Bernardini, C.L. Bianco, L. Caito, C. Cherubini, G. De Barros, A. Geralico, L. Izzo, F.A. Massucci, B. Patricelli, M. Rotondo, J.A. Rueda Hernandez, R. Ruffini, G. Vereshchagin, S.-S. Xue; "The fireshell model for Gamma-Ray Bursts"; in The Shocking Universe, Proceedings of the conference held in Venice (Italy), September 2009, G. Chincarini, P. D'Avanzo, R. Margutti, R. Salvaterra, Editors; SIF Conference Proceedings, 102, 451 (2010).

    The fireshell model for GRBs is briefly outlined, and the currently ongoing developments are summarized.

42. M.G. Bernardini, C.L. Bianco, L. Caito, L. Izzo, B. Patricelli, R. Ruffini; "The end of the prompt emission within the fireshell model"; in The Shocking Universe, Proceedings of the conference held in Venice (Italy), September 2009, G. Chincarini, P. D'Avanzo, R. Margutti, R. Salvaterra, Editors; SIF Conference Proceedings, 102, 489 (2010)

    The shallow decay emission, revealed by the Swift satellite in the X-ray afterglow of a good sample of bursts, is a puzzle. Within the fireshell model it has been recently proposed an alternative explanation: if we assume that after the prompt phase the system has a range of Lorentz factors, the plateau phase is

simply the product of the injection of slower material into the fireshell. This injection produces a modification both in the dynamics of the fireshell and in the spectrum of the emitted radiation. We postulate that this spread in the fireshell Lorentz factor occurs when the fireshell becomes transparent and do not depend on a prolonged activity of the central engine. The aim of this paper is to characterize dynamically the system in order to understand the nature of that material.

43. L. Izzo, M.G. Bernardini, C.L. Bianco, L. Caito, B. Patricelli, R. Ruffini; "GRB 090423 in the fireshell scenario"; in The Shocking Universe, Proceedings of the conference held in Venice (Italy), September 2009, G. Chincarini, P. D'Avanzo, R. Margutti, R. Salvaterra, Editors; SIF Conference Proceedings, 102, 537 (2010).

44. B. Patricelli, M.G. Bernardini, C.L. Bianco, L. Caito, L. Izzo, R. Ruffini, G. Vereshchagin; "A new spectral energy distribution of photons in the fireshell model of GRBs"; in The Shocking Universe, Proceedings of the conference held in Venice (Italy), September 2009, G. Chincarini, P. D'Avanzo, R. Margutti, R. Salvaterra, Editors; SIF Conference Proceedings, 102, 559 (2010).

    The fireshell model of Gamma Ray Bursts (GRBs) postulates that the emission process is thermal in the comoving frame of the fireshell, but this is just a first approximation. We investigate a different spectrum of photons in the comoving frame in order to better reproduce the observed spectral properties of GRB prompt emission. We introduce a modified thermal spectrum whose low energy slope depends on an index α, left as a free parameter. We test it by comparing the numerical simulations with observed BAT spectra integrated over different intervals of time. We find that the observational data can be correctly reproduced by assuming $\alpha = -1.8$.

45. C.L. Bianco, M.G. Bernardini, L. Caito, G. De Barros, L. Izzo, B. Patricelli, R. Ruffini; "Disguised Short Bursts and the Amati Relation"; in Deciphering the ancient universe with Gamma-Ray Bursts, Proceedings of the conference held in Kyoto (Japan), April 2010, N. Kawai, S. Nagataki, Editors; AIP Conference Proceedings, 1279, 299 (2010).

    The class of "Disguised short" GRBs implied by the fireshell scenario is presented, with special emphasis on the implications for the Amati relation.

46. L. Izzo, M.G. Bernardini, C.L. Bianco, L. Caito, B. Patricelli, L.J. Rangel Lemos, R. Ruffini; "On GRB 080916C and GRB 090902B observed by the Fermi satellite"; in Deciphering the ancient universe with Gamma-Ray Bursts, Proceedings of the conference held in Kyoto (Japan), April 2010, N. Kawai, S. Nagataki, Editors; AIP Conference Proceedings, 1279, 343 (2010).

    We propose a possible explanation, in the context of the Fireshell scenario, for the high-energy emission observed in GRB 080916C and GRB 090902B. The physical process underlying this emission consists mainly in the interaction of the baryon in the Fireshell with some high-density region around the burst site. Moreover we associate the observed delay of the onset of the high-energy emission as due to the P-GRB emission.

47. B. Patricelli, M.G. Bernardini, C.L. Bianco, L. Caito, G. De Barros, L. Izzo, R. Ruffini; "Black Holes in Gamma Ray Bursts"; in Deciphering the ancient universe with Gamma-Ray Bursts, Proceedings of the conference held in Kyoto (Japan), April 2010, N. Kawai, S. Nagataki, Editors; AIP Conference Proceedings, 1279, 406 (2010).

    Within the fireshell model, Gamma Ray Bursts (GRBs) originate from an optically thick $e^{\pm}$ plasma created by vacuum polarization process during the formation of a Black Hole (BH). Here we briefly recall the basic features of this model, then we show how it is possible to interpret GRB observational properties within it. In particular we present, as a specific example, the analysis of GRB 050904 observations of the prompt emission light curve and spectrum in the Swift BAT energy band (15-150 keV).

48. M.G. Bernardini, C.L. Bianco, L. Caito, M.G. Dainotti, R. Guida, R. Ruffini; "The GRB classification within the "fireshell" model: short, long and "fake" short GRBs"; in Proceedings of the 3rd Stueckelberg Workshop on Relativistic Field Theories, Pescara, Italy, July 2008, N. Carlevaro, R. Ruffini, G.V. Vereshchagin, Editors; Cambridge Scientific Publishers, (UK, 2011).

49. C.L. Bianco, M.G. Bernardini, L. Caito, M.G. Dainotti, R. Guida, R. Ruffini, G.V. Vereshchagin, S.-S. Xue; "Equations of motion of the "fireshell""; in Proceedings of the 3rd Stueckelberg Workshop on Relativistic Field Theories, Pescara, Italy, July 2008, N. Carlevaro, R. Ruffini, G.V. Vereshchagin, Editors; Cambridge Scientific Publishers, (UK, 2011).

50. L. Caito, M.G. Bernardini, C.L. Bianco, M.G. Dainotti, R. Guida, R. Ruffini; "GRB 060614: another example of "fake" short burst from a merging binary system"; in Proceedings of the 3rd Stueckelberg Workshop on Relativistic Field Theories, Pescara, Italy, July 2008, N. Carlevaro, R. Ruffini, G.V. Vereshchagin, Editors; Cambridge Scientific Publishers, (UK, 2011).

51. G. De Barros, M.G. Bernardini, C.L. Bianco, L. Caito, R. Guida, R. Ruffini; "Analysis of GRB 050509b"; in Proceedings of the 3rd Stueckelberg Workshop on Relativistic Field Theories, Pescara, Italy, July 2008, N. Carlevaro, R. Ruffini, G.V. Vereshchagin, Editors; Cambridge Scientific Publishers, (UK, 2011).

52. R. Ruffini, L. Izzo, A.V. Penacchioni, C.L. Bianco, L. Caito, S.K. Chakrabarti, A. Nandi; "GRB 090618: a possible case of multiple GRB?"; in Proceedings of the 25th Texas Symposium on Relativistic Astrophysics, held in Heidelberg (Germany), December 2010, F.M. Rieger, C. van Eldik, W. Hofmann, Editors; PoS(Texas2010), 101.

53. L.J. Rangel Lemos, C.L. Bianco, H.J. Mosquera Cuesta, J.A. Rueda, R. Ruffini; "Luminosity function of BATSE GRBs dominated by extended afterglow"; in Proceedings of the 25th Texas Symposium on Relativistic Astrophysics, held in Heidelberg (Germany), December 2010, F.M. Rieger, C. van Eldik, W. Hofmann, Editors; PoS(Texas2010), 204.

54. R. Ruffini, A.G. Aksenov, M.G. Bernardini, C.L. Bianco, L. Caito, P. Chardonnet, M.G. Dainotti, G. De Barros, R. Guida, L. Izzo, B. Patricelli, L.J. Rangel Lemos, M. Rotondo, J.A. Rueda Hernandez, G. Vereshchagin, She-Sheng Xue; "Black Holes Energetics and GRBs"; in The Sun, the Stars, the Universe and General Relativity: Proceedings of Sobral 2009; S.E. Perez Bergliaffa, M. Novello , R. Ruffini, Editors; Cambridge Scientific Publishers (UK, 2011).

55. C.L. Bianco, L. Amati, M.G. Bernardini, L. Caito, G. De Barros, L. Izzo, B. Patricelli, R. Ruffini; "The class of 'disguised' short GRBs and its implications for the Amati relation"; in GRBs as probes - from the progenitors environment to the high redshift Universe, Proceedings of the conference held in Como (Italy), May 2011, S. Campana, P. D'Avanzo, A. Melandri, Editors; Mem. S.A.It. Suppl., 21, 139 (2012).

56. A.V. Penacchioni, R. Ruffini, L. Izzo, M. Muccino, C.L. Bianco, L. Caito, B. Patricelli; "Evidences for a double component in the emission of GRB 101023"; in GRBs as probes - from the progenitors environment to the high redshift Universe, Proceedings of the conference held in Como (Italy), May 2011, S. Campana, P. D'Avanzo, A. Melandri, Editors; Mem. S.A.It. Suppl., 21, 230 (2012).

57. M.G. Bernardini, C.L. Bianco, L. Caito, L. Izzo, B. Patricelli, R. Ruffini; "The X-Ray Flares of GRB 060607A within the Fireshell Model"; in Proceedings of the Twelfth Marcel Grossmann Meeting on General Relativity, Paris, France, July 2009, T. Damour, R.T. Jantzen, R. Ruffini, Editors; World Scientific, (Singapore, 2012).

58. L. Izzo, M.G. Bernardini, C.L. Bianco, L. Caito, B. Patricelli, R. Ruffini; "GRB 090423 in the Fireshell Scenario: A Canonical GRB at Redshift 8.2"; in Proceedings of the Twelfth Marcel Grossmann Meeting on General Relativity, Paris, France, July 2009, T. Damour, R.T. Jantzen, R. Ruffini, Editors; World Scientific, (Singapore, 2012).

59. B. Patricelli, M.G. Bernardini, C.L. Bianco, L. Caito, L. Izzo, R. Ruffini, G.V. Vereshchagin; "A New Spectral Energy Distribution of Photons in the Fireshell Model of GRBs"; in Proceedings of the Twelfth Marcel Grossmann Meeting on General Relativity, Paris, France, July 2009, T. Damour, R.T. Jantzen, R. Ruffini, Editors; World Scientific, (Singapore, 2012).

60. C.L. Bianco, M.G. Bernardini, L. Caito, G. De Barros, L. Izzo, M. Muccino, B. Patricelli, A.V. Penacchioni, G.B. Pisani, R. Ruffini; "Needs for a new GRB classification following the fireshell model: "genuine short", "disguised short" and "long" GRBs"; in Proceedings of the Gamma-Ray Bursts 2012 Conference, held in Munich (Germany), May 2012, A. Rau, J. Greiner, Editors; PoS(GRB 2012), 043.

61. A.V. Penacchioni, G.B. Pisani, R. Ruffini, C.L. Bianco, L. Izzo, M. Muccino; "The proto-black hole concept in GRB 101023 and its possible extension to GRB 110709B"; in Proceedings of the Gamma-Ray Bursts 2012 Conference, held in Munich (Germany), May 2012, A. Rau, J. Greiner, Editors; PoS(GRB 2012), 042.

62. B. Patricelli, M.G. Bernardini, C.L. Bianco, L. Caito, L. Izzo, R. Ruffini; "GRB 050904: The study of a high redshift GRB within the Fireshell Model"; in Proceedings of the Twelfth Marcel Grossmann Meeting on General Relativity, Paris, France, July 2009, T. Damour, R.T. Jantzen, R. Ruffini, Editors; World Scientific, (Singapore, 2012).

63. L. Izzo, G.B. Pisani, M. Muccino, J.A. Rueda, Y.Wang, C.L. Bianco, A.V. Penacchioni, R. Ruffini; "A common behavior in the late X-ray afterglow of energetic GRB-SN systems"; EAS Publications Series, Volume 61, 595-597 (2013).

64. R. Ruffini; "Black Holes, Supernovae and Gamma Ray Bursts"; in Proceedings of the Thirteenth Marcel Grossmann Meeting on General Relativity, Stockholm, Sweden, July 2012, R.T. Jantzen, K. Rosquist, R. Ruffini, Editors; World Scientific, (Singapore, 2015).

65. M. Muccino, R. Ruffini, C.L. Bianco, L. Izzo, A.V. Penacchioni, G.B. Pisani; "GRB 090227B: The missing link between the genuine short and long GRBs"; in Proceedings of the Thirteenth Marcel Grossmann Meeting on General Relativity, Stockholm, Sweden, July 2012, R.T. Jantzen, K. Rosquist, R. Ruffini, Editors; World Scientific, (Singapore, 2015).

66. A.V. Penacchioni, R. Ruffini, C.L. Bianco, L. Izzo, M. Muccino, G.B. Pisani, J.A. Rueda; "The family of the Induced Gravitational Collapse scenario: The case of GRB 110709B"; in Proceedings of the Thirteenth Marcel Grossmann Meeting on General Relativity, Stockholm, Sweden, July 2012, R.T. Jantzen, K. Rosquist, R. Ruffini, Editors; World Scientific, (Singapore, 2015).

67. A.V. Penacchioni, R. Ruffini, C.L. Bianco, L. Izzo, M. Muccino, G.B. Pisani; "GRB 111228, analysis within the Induced Gravitational Collapse scenario and association with a supernova"; in Proceedings of the Thirteenth Marcel Grossmann Meeting on General Relativity, Stockholm, Sweden, July 2012, R.T. Jantzen, K. Rosquist, R. Ruffini, Editors; World Scientific, (Singapore, 2015).

68. G.B. Pisani, L. Izzo, R. Ruffini, C.L. Bianco, M. Muccino, A.V. Penacchioni, J.A. Rueda, Y. Wang; "On a novel distance indicator for Gamma-Ray Bursts associated with supernovae"; in Proceedings of the Thirteenth Marcel Grossmann Meeting on General Relativity, Stockholm,

Sweden, July 2012, R.T. Jantzen, K. Rosquist, R. Ruffini, Editors; World Scientific, (Singapore, 2015).

69. M. Muccino, R. Ruffini, C.L. Bianco, L. Izzo, A.V. Penacchioni, G.B. Pisani; "GRB 090510, explosion of a GRB in the highest circumburst medium even inferred: a disguised short GRB"; in Proceedings of the Thirteenth Marcel Grossmann Meeting on General Relativity, Stockholm, Sweden, July 2012, R.T. Jantzen, K. Rosquist, R. Ruffini, Editors; World Scientific, (Singapore, 2015).

70. L. Izzo, G.B. Pisani, M. Muccino, R. Ruffini, C.L. Bianco, M. Enderli, Y. Wang; "Hints for a physically based GRB distance indicator"; in Proceedings of the Thirteenth Marcel Grossmann Meeting on General Relativity, Stockholm, Sweden, July 2012, R.T. Jantzen, K. Rosquist, R. Ruffini, Editors; World Scientific, (Singapore, 2015).

71. R. Ruffini, Y. Aimuratov, V. Belinski, C.L. Bianco, M. Enderli, L. Izzo, M. Kovacevic, G.J. Mathews, R. Moradi, M. Muccino, A.V. Penacchioni, G.B. Pisani, J.A. Rueda, G.V. Vereshchagin, Y. Wang, S.-S. Xue; Cosmic matrix in the jubilee of relativistic astrophysics; in THE SECOND ICRANET CÉSAR LATTES MEETING: Supernovae, Neutron Stars and Black Holes, Proceedings of the conference held in Rio de Janeiro – Niterói – João Pessoa – Recife – Fortaleza (Brazil), 13-22 April 2015, U. Barres de Almeida, P. Chardonnet, R. Picanco Negreiros, J. Rueda, R. Ruffini, G. Vereshchagin, C. Zen Vasconcellos, Editors; AIP Conference Proceedings, 1693, 020001 (2015).

72. L. Becerra, C.L. Bianco, F. Cipolletta, M. Enderli, C.L. Fryer, L. Izzo, M. Kovacevic, R. Camargo Rodrigues de Lima, M. Muccino, F.G. de Oliveira, A.V. Penacchioni, G.B. Pisani, J.A. Rueda, R. Ruffini, Y. Wang, E. Zaninoni; Black holes, neutron stars and supernovae within the induced gravitational collapse paradigm for GRBs; in THE SECOND ICRANET CÉSAR LATTES MEETING: Supernovae, Neutron Stars and Black Holes, Proceedings of the conference held in Rio de Janeiro – Niterói – João Pessoa – Recife – Fortaleza (Brazil), 13-22 April 2015, U. Barres de Almeida, P. Chardonnet, R. Picanco Negreiros, J. Rueda, R. Ruffini, G. Vereshchagin, C. Zen Vasconcellos, Editors; AIP Conference Proceedings, 1693, 020002 (2015).

73. L.J. Rangel Lemos, C.L. Bianco, R. Ruffini; Applying the luminosity function statistics in the fireshell model; in THE SECOND ICRANET CÉSAR LATTES MEETING: Supernovae, Neutron Stars and Black Holes, Proceedings of the conference held in Rio de Janeiro – Niterói – João Pessoa – Recife – Fortaleza (Brazil), 13-22 April 2015, U. Barres de Almeida, P. Chardonnet, R. Picanco Negreiros, J. Rueda, R. Ruffini, G. Vereshchagin, C. Zen Vasconcellos, Editors; AIP Conference Proceedings, 1693, 070004 (2015).

74. J.A. Rueda, R. Ruffini, J.F. Rodriguez, M. Muccino, Y. Aimuratov, U. Barres de Almeida, L.M. Becerra, C.L. Bianco, C. Cherubini, S. Filippi, M. Kovacevic, R. Moradi, G.B. Pisani, Y. Wang; The binary progenitors of short and long GRBs and their gravitational-wave emission; EPJ Web of Conferences, 168, 01006 (2018).

75. M. Muccino, R. Ruffini, Y. Aimuratov, L.M. Becerra, C.L. Bianco, M. Karlika, M. Kovacevic, J.D. Melon Fuksman, R. Moradi, A.V. Penacchioni, G.B. Pisani, D. Primorac, J.A. Rueda, S. Shakeri, G.V. Vereshchagin, S.-S. Xue, Y. Wang; What can we learn from GRBs?; EPJ Web of Conferences, 168, 01015 (2018).

76. L.M. Becerra, C.L. Bianco, C. Fryer, J.A. Rueda, R. Ruffini; On the Induced Gravitational Collapse; EPJ Web of Conferences, 168, 02005 (2018).

77. G.B. Pisani, R. Ruffini, Y. Aimuratov, C.L. Bianco, M. Karlika, M. Kovacevic, R. Moradi, M. Muccino, A.V. Penacchioni, D. Primorac, J.A. Rueda, Y. Wang; The first ICRANet catalog of Binary-Driven Hypernovae; EPJ Web of Conferences, 168, 04002 (2018).

78. D. Primorac, R. Ruffini, G.B. Pisani, Y. Aimuratov, C.L. Bianco, M. Karlika, J.D. Melon Fuksman, R. Moradi, M. Muccino, A.V. Penacchioni, J.A. Rueda, Y. Wang; GRB 110731A within the IGC paradgm; EPJ Web of Conferences, 168, 04008 (2018).

79. J.D. Melon Fuksman, L.M. Becerra, C.L. Bianco, M. Karlika, M. Kovacevic, R. Moradi, M. Muccino, G.B. Pisani, D. Primorac, J.A. Rueda, R. Ruffini, G.V. Vereshchagin, Y. Wang; Evolution of an electron-positron plasma produced by induced gravitational collapse in binary-driven hypernovae; EPJ Web of Conferences, 168, 04009 (2018).

Draft version May 21, 2020
Typeset using LaTeX **preprint** style in AASTeX62

Thermal Components in Gamma-ray Bursts. II. Constraining the Hybrid Jet Model

Liang Li[1, 2, 3]

[1]*ICRANet, Piazza della Repubblica 10, I-65122 Pescara, Italy*
[2]*INAF – Osservatorio Astronomico d'Abruzzo, Via M. Maggini snc, I-64100, Teramo, Italy*
[3]*ICRA, Dipartimento di Fisica, Sapienza Universit di Roma, P.le Aldo Moro 5, I00185 Rome, Italy*

(Received August 6, 2019; Revised March 3, 2020; Accepted March 10, 2020; Published Mar 11, 2020)

ABSTRACT

In explaining the physical origin of the jet composition of gamma-ray bursts (GRBs), a more general picture, i.e. the hybrid jet model (which introduced another magnetization parameter σ_0 on the basis of the traditional fireball model), has been well studied in Gao & Zhang. However, it still has not yet been applied to a large GRB sample. Here, we first employ the "top-down" approach of Gao & Zhang to diagnose the photosphere properties at the central engine to see how the hybrid model can account for the observed data as well, through applying a *Fermi* GRB sample (eight bursts) with the detected photosphere component, as presented in Li (our Paper I). We infer all physical parameters of a hybrid problem with three typical values of the radius of the jet base ($r_0 = 10^7$, 10^8, and 10^9 cm). We find that the dimensionless entropy for all the bursts shows $\eta \gg 1$ while the derived $(1+\sigma_0)$ for five bursts (GRB 081224, GRB 110721A, GRB 090719, GRB 100707, and GRB 100724) is larger than unity, indicating that in addition to a hot fireball component, another cold Poynting-flux component may also play an important role. Our analysis also shows that in a few time bins for all r_0 in GRB 081224 and GRB 110721A, the magnetization parameter at $\sim 10^{15}$cm $(1+\sigma_{\rm r15})$ is greater than unity, which implies that internal-collision-induced magnetic reconnection and turbulence may be the mechanism to power the nonthermal emission, rather than internal shocks. We conclude that the majority of bursts (probably all) can be well explained by the hybrid jet problem.

Keywords: Gamma-ray Burst (629); Astronomy data analysis (1858); Relativistic jets (1390)

1. INTRODUCTION

One of the most fundamental, yet unsolved, questions in gamma-ray burst (GRB) physics is the nature of jet composition. A crucial debate focuses on the physical origin of jet compositions—

Corresponding author: Liang Li
liang.li@icranet.org

whether it is originated from a baryonic-dominated fireball (e.g., Pe'Er & Ryde 2017) or a Poynting-flux-dominated outflow (e.g., Zhang 2018).

An important scenario invokes a quasi-thermal component indicating a hot fireball origin, which is introduced by Paczynski (1986) and Goodman (1986) with a pure fireball picture (composed of positron-electron pair and hot photons) in the early time. Later, it is introduced by Shemi & Piran (1990) and Paczynski (1990) with a baryon-dominated fireball framework (baryons + positron-electron pair and hot photons) in order to be consistent with the observations. In this baryon-dominated fireball scenario, the two-component spectral scenario is expected to be found in the observed spectrum during the prompt emission: a quasi-thermal component originates from the fireball photosphere (Ruffini et al. 1999, 2000, 2013; Mészáros & Rees 2000; Rees & Mészáros 2005) when the optical depth goes to unity, and the emergent spectrum can be modified by the Planck-like function; a nonthermal component originates from the internal shocks (IS; Paczynski & Xu 1994; Rees & Meszaros 1994) in the optically thin region.

An alternative scenario invokes a nonthermal component from the synchrotron radiation of the Poynting-flux-dominated outflow (e.g., Zhang 2014). There are two possibilities to generate the prompt emission. One may originate from the matter-dominated emission region (Drenkhahn & Spruit 2002; Thompson 2006; Giannios 2008), while another may invoke the moderately Poynting-flux-dominated emission region via magnetic reconnection, such as an internal-collision-induced magnetic reconnection and turbulence (ICMART) event (Zhang & Yan 2011). The GRB emergent spectrum from such a scenario is likely to be in good agreement with the observations that the typical GRB spectrum is known with the Band-like form (Band et al. 1993), which is usually taken to represent a nonthermal emission component.

Observationally, a majority of GRBs present a nonthermal dominant Band-like spectrum. The Band function (Band et al. 1993) has two exponentially joined power laws, which are separated by typical peaks at $\sim$ hundreds keV, and the two power-law indices α (below the peak) and β (above the peak) are typically distributed at ~ -1.0 and ~ -2.2, respectively. Alternatively, the baryon-dominated fireball scenario has been also confirmed by the observations since a quasi-thermal spectral component was found in the time-integrated or the time-resolved spectral analysis for some GRBs (e.g., Ryde 2004; Ryde & Pe'er 2009; Ryde et al. 2010, 2019; Pe'Er et al. 2012; Iyyani et al. 2013, 2015; Acuner & Ryde 2018; Zhang et al. 2018; Acuner et al. 2019; Li 2019a,b; Liang et al. 2019; Ruffini et al. 2019a). These results were first discovered by the Burst And Transient Source Experiment (BATSE) on board the Compton Gamma Ray Observatory (CGRO), and later confirmed by the Gamma-ray Burst Monitor (GBM) on board the *Fermi* Gamma-ray Space Telescope. Meanwhile, the previous observations also revealed that thermal components exhibit diverse observational properties. They either can be detected during the entire duration of the prompt emission (e.g., GRB 100507; Ghirlanda et al. 2013) or may be only found at the beginning of the burst duration, and subsequently appear with a nonthermal component (e.g., Ryde 2004 for a BATSE sample and Li 2019b for a *Fermi* sample). On the other hand, thermal components can be grouped into two categories: the thermal-subdominant case and the thermal-dominant case. The former one invokes a thermal-subdominant component embedded into a nonthermal-dominant component (e.g., 110721A; Axelsson et al. 2012), while the later one invokes a thermal-dominant component accompanied by a nonthermal-subdominant component (e.g., 090902B; Ryde et al. 2010) or even a 'pure' blackbody (BB) emission (e.g., 930214, Ryde 2004). Noteworthy, the thermal-subdominant case can account

for a majority of the observations while the thermal-dominant cases are rarely observed. GRB 090902B is the most prominent one that the thermal-dominant component is observed either in the time-integrated spectral analysis (a dominant quasi-thermal component superposed on an underlying power-law component; Abdo et al. 2009) or the time-resolved spectral analysis (a multi-color BB component; Ryde et al. 2010).

A diverse spectral property found in the observations suggests that GRB ejecta may have a diverse jet composition. It may be neither fully matter-dominated ejecta nor fully magnetized outflows. More realistically, GRB outflows are likely to be a hybrid jet, which carries the two components simultaneously and launches at the central engine. In such a scenario, which component plays a leading role in the emission may be more important. Theoretically, the central engine models invoke either a hyper-accreting and fast-rotating black hole or a rapidly spinning and highly magnetized neutron star (magnetar). Therefore, a diverse jet composition is still expected: a hot component due to neutrino heating from the accretion disk or the proto neutron star, and a cold component associated with a Poynting flux launched from the black hole or the neutron star (e.g., Metzger et al. 2011; Lei et al. 2013; Gao & Zhang 2015).

The hybrid jet problem reported Gao & Zhang (2015) (see also Ryde 2004) introduces another magnetization parameter σ_0 on the basis of the traditional fireball model, which is defined as $\sigma_0 \equiv L_{\rm c}/L_{\rm b}$, where $L_{\rm b}$, $L_{\rm c}$, and $L_0 = L_{\rm b} + L_{\rm c}$ are the luminosities of hot (fireball) component, cold (Poynting-flux) component, and entire wind, respectively. The rapid evolution of the photosphere emission proprieties is therefore expected to be a result of the rapid evolution of (η, σ_0) pairs, where η is the dimensionless entropy of the outflow. The time-varying (η, σ_0) pair at the central engine could give rise to different observational characteristics. If $\eta \gg 1$ and $\sigma_0 \ll 1$, a hot fireball with a dominant photosphere emission component could be observed (e.g., GRB 090902B). Moreover, if η is smaller while σ_0 is larger, a subdominant photosphere emission component may be detected due to the thermal emission being suppressed (e.g., GRB 110721A). Finally, if η is close to unity and $\sigma_0 \gg 1$, we would only detect a nonthermal spectral component (e.g., GRB 080916C) since the outflow is fully dominated by a Poynting-flux component (highly magnetic outflow), and the photosphere component is completely suppressed. Therefore, the hybrid problem describes a more general picture, where the dimensionless entropy η (hot fireball component) and the magnetization parameter σ_0 (cold Poynting-flux component) are two key parameters at the central engine. In such a hybrid problem, the hot matter-dominated outflow described by the pure fireball model ($\eta \gg 1$ and $\sigma_0 \ll 1$) and the magnetized jet related to Poynting-flux-dominated outflow ($\eta \sim 1$ and $\sigma_0 \gg 1$) are two extreme cases, which have been fully studied. However, a general picture of a hybrid system was rarely investigated before Gao & Zhang (2015). Motivated by the introduction of the general formalism, which can cover all different possible cases, Gao & Zhang (2015) developed a theory of photosphere emission of a hybrid relativistic outflow. On the basis of an approximate dynamical evolution model of the hybrid system, two methods are proposed: the first one is the 'bottom-up' approach to predict the temperature ($T_{\rm obs}$) and luminosity ($L_{\rm BB}$) of the photosphere emission for a given pair of parameters (η, σ) at central engine; the second one is the 'top-down' approach to diagnose central engine parameters (η, σ) based on the observed quasi-thermal photosphere emission. They pointed out that adopting the 'bottom-up' approach, we could reproduce a variety of observed GRB prompt emission spectra by *Fermi* for the non-dissipative photosphere model if the (η, σ) pair

are allowed to vary in a wide range, and applying the 'top-down' approach to GRB 110721A, we can well explain the observational data.

Practically, it is more interesting to utilize the observational data to diagnose the properties at the central engine. Therefore, an attractive question is to know how the hybrid model can account for a large sample of *Fermi* bursts. Here, we address different questions based on the same *Fermi* GRB sample in a series of papers, focusing on the cases that the two-component spectral scenario (composited with a nonthermal component and a thermal component simultaneously) is clearly observed in their time-resolved spectral analysis. In the first paper of this series (Li 2019a, hereafter Paper I), we presented the study on how the thermal components affect the nonthermal spectral parameters. In this work, we continue our systematic study by applying the same GRB sample (listed in Table 1 of Paper I) as well as the 'top-down' approach of Gao & Zhang (2015) to diagnose the photosphere properties of a hybrid relativistic outflow. Meanwhile, we conduct a statistical analysis of the central engine properties of a large GRB sample. The goal in this task is to re-investigate the central engine properties by constraining the hybrid model with the observed data.

The paper is organized as follows: in Section 2, we present the methodology, which includes sample selection, data reduction, Bayesian inference, and Markov Chain Monte Carlo (MCMC) methods. In Section 3, we describe the fireball dynamical evolution of a hybrid relativistic outflow photosphere emission, and discuss some derived physical parameters. The results on constraining a hybrid jet system with our sample are presented in Section 4. The conclusions and discussions are illustrated in Section 5. Throughout the paper, the standard Λ-CDM cosmology with the parameters of $H_0 = 67.4$ kms^{-1} Mpc^{-1}, $\Omega_M = 0.315$, and $\Omega_\Lambda = 0.685$ is adopted (Planck Collaboration et al. 2018), and the convention $Q = 10^x Q_x$ is adopted in cgs units.

2. METHODOLOGY

2.1. *Sample Selection and Data Reduction*

We included in our analysis all the GRBs detected by the *Fermi*-GBM until 2019 March 31 and having a reported photospheric component in the spectrum. We focus on the *Fermi*-GBM observation since it covers a broad spectral window in energy (8 keV-40 MeV), and therefore the current GRB spectral models can be fully characterized. The GBM (Meegan et al. 2009) contains 12 sodium iodide (NaI; 8keV-1MeV) detectors (n0 to n9, na and nb) as well as 2 bismuth germanate (BGO; 200keV-40MeV) detectors (b0 and b1). The Time Tagged Event (TTE) and spectral response (rsp) files are used for the selected sets of detectors. We select at most three NaI detectors in order to obtain an angle of incidence less than 60° and one BGO detector with the lowest angle of incidence (Goldstein et al. 2012; Narayana Bhat et al. 2016) for the spectral analysis. A sample of 13 *Fermi*-GBM such bursts are available, and the detail spectral properties of these bursts have been reviewed in paper I. The sample is presented in Table 1 of paper I.

All temporal and spectral analysis in this work is implemented by adopting the Bayesian analysis package, i.e., the Multi-Mission Maximum Likelihood Framework (3ML, Vianello et al. 2015). Such a fully Bayesian approach was first applied in Li (2019b) for a *Fermi*-GBM bright GRB spectral catalog (see also Burgess et al. 2019; Li 2019a; Ryde et al. 2019; Yu et al. 2019). The background is fitted by selecting two typical off-source (pre- and post-source) intervals with an order 0-4 polynomial for the brightest NaI detector in photon counts, and the optimal order of the polynomial is determined by a likelihood ratio test. This optimal polynomial is then applied to fit each of the 128 energy channels

so as to estimate the background model for the rate in that channel. By integrating the optimal polynomial over source interval, we can obtain the background photon counts for each channel. We use the maximum likelihood-based statistics, the so-called Pgstat, given by a Poisson (observation, Cash 1979)-Gaussian (background) profile likelihood. Additionally, the error on the background can also be evaluated by assuming its distribution to be a Gauss. At least one background count per spectral bin is included to allow the Gaussian profile to be valid. In order to perform the time-resolved spectral analysis, we adopt the Bayesian Blocks (BBlocks; Scargle et al. 2013) method with false alarm probability p_0=0.01 to rebin the TTE lightcurve of the brightest NaI detector. Subsequently, all other used detectors are binned in matching time bins. If there is more than one triggered NaI detector, we select the brightest one that has the highest significance during the source interval. Then, we utilize it for the BBlocks and background fitting. On the other hand, in order to obtain a good fitting result, we adopt $S \geq 20$ (the definition of S see Vianello 2018) as the criterion to select the time bins that include enough source photons. This is because the spectral parameters obtained from the bins with lower S values (e.g., $S < 20$) typically have huge errors. To better infer physics from the spectral parameters, we selected the bursts with five $S \geq 20$ time bins (see also Li 2019b; Ryde et al. 2019). Then, the sample was reduced to eight bursts with this criterion. These bursts are GRB 081224, GRB 090719, GRB 090902B, GRB 100724B, GRB 110721A, GRB 160107A, and GRB 190114C. The time-resolved spectral fitting results for each selected burst have been reported in Tables 2-9 in paper I. Please note that we take the cut-off power-law (CPL) model as a proxy for the Band model to perform the spectral analysis throughout the paper. This is because thermal components are typically observed in the left shoulder of the Band spectrum (below $E_{\rm p}$); its presence does not affect the high-energy β index (above $E_{\rm p}$). The definition of each used model is presented in Appendix A1.

2.2. *Bayesian Inference and MCMC Methods*

The parameter estimation is the primary task when performing spectral fits. Practically, we can apply either a frequentist analysis approach or Bayesian analysis method to achieve this goal. To fit a model to data, the conventional wisdom in the frequentist approach can adopt χ^2 minimization or its variants, or more complex frequentist methods (e.g., Cstat, Pgstat) based on the Maximum Likelihood Estimation (MLE) technique. However, these traditional frequency methods are known to be problematic in some issues (e.g., Andrae et al. 2010; Greiner et al. 2016). In current years, the Bayesian analysis technique has gained in popularity, and fitting the Bayesian statistical models by adopting MCMC methods have become a standard tool for the parameter estimation in astronomy (e.g., Burgess et al. 2019; Li 2019a,b). In Bayesian inference, after the experimental data is obtained, Bayes's theorem is applied to infer and update the probability distribution of a specific set of model parameters. For instance, given an observed data set (D) and a profile model (M), the probability distribution $p(M \mid D)$, i.e., so-called *Posterior* probability, according to the Bayes's theorem, therefore is given by

$$p(M \mid D) = \frac{p(D \mid M)p(M)}{p(M)}, \tag{1}$$

where, $p(D \mid M)$ is the likelihood that combines the model and the observed data and expresses the probability to observe (or to generate) the data set D from given a model M with its parameters, $p(M)$ is prior on the model parameters, and $p(D)$ is called evidence, which is constant with the purpose of normalizing.

The informative priors are adopted by using the typical spectral parameters from the *Fermi*-GBM catalogue:

$$\begin{cases} \alpha_{\rm CPL} \sim \mathcal{N}(\mu=-1,\sigma=0.5) \\ E_{\rm CPL} \sim log\mathcal{N}(\mu=2,\sigma=1)\ \ {\rm keV} \\ A_{\rm CPL} \sim log\mathcal{N}(\mu=0,\sigma=2)\ \ {\rm cm^{-2}keV^{-1}s^{-1}} \\ kT_{\rm BB} \sim log\mathcal{N}(\mu=2,\sigma=1)\ \ {\rm keV} \\ A_{\rm BB} \sim log\mathcal{N}(\mu=-4,\sigma=2)\,{\rm cm^{-2}keV^{-1}s^{-1}} \end{cases} \tag{2}$$

The posterior distribution is obtained from the prior and sampling information, and the affection from prior distribution will be weaker with the increase of the sampling information. According to the Bayes's formalism, only the simplest posterior allows for an analytic solution when we utilize Bayesian posterior sampling. However, in most cases, a high-dimensional integration is required so that the posterior is generally impossible to compute. Therefore stochastic sampling techniques, such as MCMC (e.g., *emcee*; Goodman & Weare 2010) or nested (e.g., MULTINEST; Feroz et al. 2009, 2019) sampling methods, are necessary to be involved. In this paper, we employ the *emcee* to sample the posterior. For each sampling, we set the number of chains (=20), the number of learning samples (=2000) that we do not include in the final results, and the number of global samples (=10000). Since the Bayesian analysis provides the predictions described as probability distributions instead of point estimates, it provides the results that the uncertainty in the inferences could be quantified. Therefore, the parameters and error estimations can be straightforwardly obtained from the posterior distribution of any desired parameter. Probably, the posterior distribution deviates from any well-studied distributions (e.g. Gaussian or Poisson). Instead, it has a skewed and/or multi-modal form. Subsequently, the parameter estimation is obtained at A Maximum A Posteriori Probability from Bayesian posterior density distribution. The error range (or the credible level) is estimated from the Bayesian Highest Posterior Density (HPD) Interval, which covers a given percentage of the total probability density. Uncertainty therefore adopted the HPD interval at the 1σ (68%) Bayesian credible level, which is evaluated from the last 80% of the MCMC 10000 samples.

3. DERIVATION OF THE PHYSICAL PARAMETERS OF A HYBRID PROBLEM

GRB jets undergo different accelerate phases for different physical scenarios, as well as its acceleration laws. For the fireball model, the jet undergoes two phases: the acceleration phase and the coasting phase. In the acceleration phase, the bulk Lorentz factor Γ would initially abide by a simply linear law with radius r, $\Gamma \propto r$, until reaching the saturation radius $r_{\rm s}$, where Γ reaches to the maximum value defined by η, therefore, $\Gamma = r_{\rm s}/r_0 \equiv \eta$. Here, r_0 is the initial size of the flow, η is the initial internal energy per particle, which is defined as $\eta \equiv E/Mc^2$ or $\eta \equiv L_w/\dot{M}c^2$, $\dot{M}$ is the mass injection rate, c is the speed of light, and L_w is the isotropic equivalent burst luminosity. When the photosphere radius exceeds the saturation radius (coast phase), $\Gamma \equiv \eta$ (Meszaros & Rees 1993; Piran et al. 1993). Then, the flow will be in the coasting phase, and Γ stays the same at the maximum value until it gets to the IS radius. Finally, it enters into the deceleration phase.

For the Poynting-flux-dominated outflow, the magnetized jet may encounter three phases: the rapid acceleration phase, the slow acceleration phase, and the coasting phase. Two acceleration phases have different acceleration laws, which are separated by the 'Magneto-Sonic point' at $r_{\rm ra}$ (the radius of rapid acceleration). The acceleration law may be described with a power-law scaling, $\Gamma \propto r^{\lambda}$, with

power-law index ranging within $\frac{1}{2} < \lambda \leq 1$ (e.g., Komissarov et al. 2009; Granot et al. 2011) during the rapid acceleration phase ($r_0 < r < r_{\rm ra}$), while it may be written as a general scaling, $\Gamma \propto r^{\delta}$, with $0 < \delta \leq \frac{1}{3}$ (e.g., Mészáros & Rees 2011; Veres & Mészáros 2012) during the slow acceleration ($r_{\rm ra} < r < r_{\rm s}$), until reaching the coasting radius $r_{\rm c}$ where Γ reaches σ_0. Finally, the flow will be in the coasting phase ($r > r_{\rm s}$). In this phase, one has $\Gamma \equiv \Gamma_{\rm c}$.

For the hybrid jet system, the jet dynamic still undergoes three phases separated by $r_{\rm ra}$ and $r_{\rm s}$. Initially, it is the rapid acceleration phase dominated by the thermal acceleration ($r_0 < r < r_{\rm ra}$) until the rapid acceleration radius $r_{\rm ra}$, then the slow acceleration phase dominated by the magnetic acceleration ($r_{\rm ra} < r < r_{\rm s}$) until the saturation radius $r_{\rm s}$ (Mészáros & Rees 1997; Vlahakis & Königl 2003; Gao & Zhang 2015); finally, it is the coasting phase ($r > r_{\rm s}$), where $r_{\rm ra}$ it is defined by the larger one of the thermal coasting radius or the magneto-sonic point. Therefore, the acceleration law can approximately be written as $\Gamma \propto r$ for the rapid acceleration phase, $\Gamma \propto r^{\delta}$ during the slow acceleration phase, and $\Gamma \equiv \Gamma_{\rm c}$ when in the coasting phase.

In this paper, we focus on applying the observed data to diagnose the properties at the central engine for a hybrid problem. Such an interesting question was first worked out by Pe'er et al. (2007) for the pure fireball model. Three observed quantities can be obtained from the spectral fits: the observed BB temperature $kT_{\rm obs}$, the observed BB flux $F_{\rm BB}$, and the observed total flux $F_{\rm obs}$ (thermal+nonthermal). Once we know all of these three observed quantities ($kT_{\rm obs}$, $F_{\rm BB}$, and $F_{\rm obs}$), we can infer the values of the isotropic equivalent luminosity of the thermal component $L_{\rm BB}$, the Lorentz factor of the bulk motion of the flow at the photospheric radius η, and the physical size at the base of the flow r_0, through applying the method developed in Pe'er et al. (2007) for the case[1] of $r_{\rm ph} > r_{\rm c}$. In the pure fireball model, three unknowns ($L_{\rm BB}$, η, and r_0) can be solved by three known observed parameters ($kT_{\rm obs}$, $F_{\rm BB}$, and $F_{\rm obs}$).

In the hybrid problem, there are four unknown parameters at the central engine ($L_{\rm w}$, r_0, η, and σ_0) since another parameter σ_0 is introduced. Hence, it is unlikely to solve all of these four unknown parameters from the observed data. In this scenario, considering a realistic central engine, Gao & Zhang (2015) suggested that assuming a constant r_0 throughout a burst for analysis could be more reasonable. Following this concept, we can also derive all the relevant photosphere properties for a hybrid problem (e.g., η, $1+\sigma_0$, $r_{\rm ph}$, $\Gamma_{\rm ph}$, $1+\sigma_{\rm ph}$, $1+\sigma_{\rm r15}$), where $r_{\rm ph}$ is the photosphere radius, $\Gamma_{\rm ph}$ is the bulk Lorentz factor at $r_{\rm ph}$, $1+\sigma_{\rm ph}$ is the magnetization parameter at $r_{\rm ph}$, and $1+\sigma_{\rm r15}$ is the magnetization parameter at 10^{15} cm. Since the BB component is predicted only in the non-dissipative photosphere models, we pay special attention to such models. On the other hand, the magnetically dissipative photosphere models predict a much higher $E_{\rm p}$, which is disfavored by the observed spectrum (Bégué & Pe'er 2015). There are six different regimes for the photosphere properties in the hybrid system[2], which can be applied for outflows in the case of both sub-photospheric magnetic dissipation and non sub-photospheric magnetic dissipation. Regime I: $\eta > (1+\sigma)^{1/2}$ and $r_{\rm ph} < r_{\rm ra}$; Regime II: $\eta > (1+\sigma)^{1/2}$ and $r_{\rm ra} < r_{\rm ph} < r_{\rm c}$; Regime III: $\eta > (1+\sigma)^{1/2}$ and $r_{\rm ph} > r_{\rm c}$; Regime IV: $\eta < (1+\sigma)^{1/2}$ and $r_{\rm ph} < r_{\rm ra}$; Regime V: $\eta < (1+\sigma)^{1/2}$ and $r_{\rm ra} < r_{\rm ph} < r_{\rm c}$; Regime VI: $\eta < (1+\sigma)^{1/2}$ and $r_{\rm ph} > r_{\rm c}$. Similarly, the central engine parameters cannot be inferred in the case of $r_{\rm ph} < r_{\rm ra}$ due

[1] Note that the method cannot be applied for the cases of $r_{\rm ph} < r_{\rm c}$ since due to degeneracy.

[2] This is because the photosphere radius $r_{\rm ph}$ can be in three different regimes separated by $r_{\rm ra}$ and $r_{\rm c}$, and the Lorentz factor at $r_{\rm ra}$, $\Gamma_{\rm ra}$ has two different possible values for different central engine parameters: $\eta > (1+\sigma)^{1/2}$ and $\eta < (1+\sigma)^{1/2}$.

to the degeneracy for the hybrid problem (regimes I and IV). Therefore, our analysis will focus on the case of $r_{\rm ph} > r_{\rm ra}$ (regimes II, III, V, and VI).

4. RESULTS

We report the properties of the physical parameters of our sample for the hybrid problem in Table 1. For each burst, we present the results with three different r_0 values: r_0=10^7 cm, r_0=10^8 cm, and r_0=10^9 cm. For the bursts without redshift, we utilize a typical value ($z = 2$) instead. We will discuss further in §5 for why these values are adopted. By using the 'top-down' approach of Gao & Zhang (2015), we then derive all the relevant parameters of the hybrid problem at the central engine (η, $1+\sigma_0$, $r_{\rm ph}$, $\Gamma_{\rm ph}$, $1+\sigma_{\rm ph}$, $1+\sigma_{\rm r15}$). The inferred physical parameters depend on an assumed constant r_0 for the hybrid problem, which has been suggested in Gao & Zhang (2015). We present the temporal properties of these physical parameters as well as the two observed parameters (the ratio between the BB to total flux $F_{\rm BB}/F_{\rm obs}$ and the BB temperature $T_{\rm obs}$) for each burst in Figures 1-8.

We find that the temporal properties vary from burst to burst, even the same burst uses different values of r_0. To better express the temporal evolution properties of physical parameters, we denote different types (see Table 1 and below for detail definitions). Different temporal properties of the physical parameters may imply different central engine properties. For instance, $(1+\sigma_0)$ is expected to initially increase with time in some engine models (e.g., Metzger et al. 2011). The pure fireball model predicts $\Gamma_{\rm ph}$ initially rises with time, whereas both IS and ICMART scenarios expect $\Gamma_{\rm ph}$ decreases with time.

The analysis of characteristics on the temporal evolution of physical parameters has led up to identifying the following unique features of our sample:

- GRB 110721A. The time-resolved spectral analysis shows that 10 time bins that satisfy with our selection criteria (see §2). Through the regime judgment, we obtain 8, 8, and 6 time bins for r_0=10^7 cm, r_0=10^8 cm, and r_0=10^9 cm, respectively. We therefore use these time bins for physical inference. The redshift z=0.382 is reported in Berger (2011). Figure 1 presents the temporal evolution of physical parameters with different r_0 values for the hybrid problem. Throughout the burst duration, we find that for all r_0, the derived $\eta \gg 1$ for all time bins and the derived $(1+\sigma_0)$ is greater than unity for a majority of time bins. The results indicate that in addition to a hot fireball component, another cold Poynting-flux component may also play an important role at the central engine. Moreover, we find that η shows a monotonic *decreasing* (*d.*) trend while $(1+\sigma_0)$ exhibits a *decrease*-to-*increase* (*d.*-to-*i.*) trend, which is consistent with what is expected in some engine models (e.g., Metzger et al. 2011). On the other hand, $r_{\rm ph}$ presents an *increase-to-decrease* (*i.*-to-*d.*) trend and $\Gamma_{\rm ph}$ also shows a monotonic *decrease*. Interestingly, a good fraction of time bins for both $(1+\sigma_{\rm ph})$ and $(1+\sigma_{\rm r15})$ are above unity, which suggests that the radiation mechanism of nonthermal components for this burst may be an ICMRAT event rather than IS.

  The fitted parameters (e.g., $F_{\rm BB}$, $F_{\rm obs}$, and kT) obtained from different analysis (frequency or Bayesian) methods may differ. The inferred physical parameters by utilizing the fitted parameters obtained from Iyyani et al. (2013) are shown in Figure A1 (z=0.382) and A2 (z=3.512), while those from our Bayesian analysis are presented in Figure 1.

- GRB 081224. Burgess et al. (2014) reported the time-resolved spectral analysis. They suggested that the acceptable spectral fits required an additional BB component to the synchrotron

component. This result is confirmed by our Bayesian analysis. No redshift is reported for the burst, we therefore use a typical value (z=2). In total, we include five time bins for the analysis. The numbers of time bins of the regime judgment for each value of r_0 are listed in Table 1 (Column 4). We find that $\eta \gg 1$ for all time bins, and they show a monotonic *decreasing* behavior (Figure 2). While $(1+\sigma_0)$ rapidly *rise* from ~ 1 then *decay* later as a power law. When it reaches its maximum value, η reaches its minimum value correspondingly. The results suggest that the outflow for the burst could be dominated by a cold Poynting-flux component. On the other hand, both $r_{\rm ph}$ and $\Gamma_{\rm ph}$ present a *decrease-to-increase* trend. A few time bins for both $(1+\sigma_{\rm ph})$ and $(1+\sigma_{\rm r15})$ are above unity, which indicates that the ICMRAT event may be the preferred model than IS to explain the nonthermal component for the burst.

- GRB 090719. The burst was also revealed that the best model for the spectral fits require an additional BB component (Burgess et al. 2014), which is consistent with our Bayesian analysis. We obtain 12 time bins. Among these, 11, 10, and 7 bins satisfy with the regime judgment for r_0=10^7 cm, r_0=10^8 cm, and r_0=10^9 cm, respectively. Again, we apply a value of z=2 as a proxy for redshift. The temporal evolution of the physical parameters and the observational parameters are shown in Figure 3. Still, we find that $\eta \gg 1$ for all time bins with moderate-σ_0 for most time bins, i.e., $(1+\sigma_0)$>1. Except that, we also find that the derived $(1+\sigma_0)$ shows monotonic *increases* (*i.*) with time, which is consistent with the expectation in some central engine models (e.g., Metzger et al. 2011). On the other hand, $r_{\rm ph}$ and $\Gamma_{\rm ph}$ generally present a *flat-to-decrease* (*f.*-to-*d.*) trend. A few time bins for $(1+\sigma_{\rm ph})$ as well as $(1+\sigma_{\rm r15})$ are slightly greater than unity while the others are close to unity. One can tentatively draw the conclusion that a strongly cold Poynting-flux component is found in this burst. It is not clear that whether the ICMRAT event or IS is the radiation mechanism of nonthermal components for the burst, because it depends on which r_0 value is the true size at the central engine.

- GRB 100707. The burst was also analyzed in Burgess et al. (2014), and it was also suggested that an additional thermal component should be added to the spectral fitting in order to obtain an acceptable fitting. We include 11 time bins, and 11, 11, and 8 time bins satisfy with the regime judgment for r_0=10^7 cm, r_0=10^8 cm, and r_0=10^9 cm, respectively. Redshift is still adopted a typical value, namely, z=2. All time bins show $\eta \gg 1$, and present *flat-to-decrease* evolution, while $(1+\sigma_0)$ is initially close to unity and then *increases* (*f.*-to-*i.*) rapidly (Figure 4). Moreover, $r_{\rm ph}$ show an *increase-to-decrease* temporal trend while $\Gamma_{\rm ph}$ generally present a slow-to-fast *decrease*. We find that $(1+\sigma_{\rm ph})$ shows a very similar behavior in contrast to $(1+\sigma_0)$. Almost all of time bins for $(1+\sigma_{\rm r15})$ are close to unity (see Figure 4), implying that IS plays a more important role than ICMRAT to explain the nonthermal emission. The results suggest that a cold Poynting-flux component plays a prominent role at a later time since the derived $(1+\sigma_0)$ is larger than unity for all r_0. This is consistent with the observation that the thermal flux ratio ($F_{\rm BB}/F_{\rm obs}$) presents a strong temporal evolution (it decays rapidly with time) during the duration (Li 2019a).

- GRB 100724B. After conducting the detailed time-resolved spectral analysis, Guiriec et al. (2011) pointed out that the spectrum of GRB 100724B is dominated by the typical Band function, including a statistically significant thermal contribution. This burst is very bright, and many more time bins are available for the analysis. In total, we obtained 33 time bins.

There are 32, 31, and 30 time bins respectively conform to the regime judgment for r_0=10^7 cm, r_0=10^8 cm, and r_0=10^9 cm. There is no redshift observation, and we still utilize z= 2. Thermal flux ratio slightly *increases* while BB temperatures generally show a *flat* (*f.*) trend (Figure 5). We find that $\eta \gg 1$ for all time bins and shows a slightly monotonic-*increase* trend, while the derived $(1+\sigma_0)$ >1 for almost all of time bins and presents a monotonic *decrease* trend. On the other hand, $r_{\rm ph}$ and $\Gamma_{\rm ph}$ generally present a *flat* behavior. We also find that the derived $(1+\sigma_{\rm ph})$ and $(1+\sigma_{\rm r15})$ show a r_0-dependent behavior, i.e., nearly all time bins for a large r_0 (r_0=10^9cm) are beyond unity but for a smaller r_0 (r_0=10^7 cm) are close to unity. This implies that whether ICMRAT or IS is the mechanism to power the nonthermal emission depends on which r_0 is the true size at the central engine. A firm conclusion that can be drawn for this burst is that a prominent Poynting-flux component and a fireball component are both observed. Therefore, a hybrid jet problem should be considered.

- GRB 190114C. After performing the detail time-resolved spectral analysis and model comparisons, Wang et al. (2019) recently reported that during the first spike of the burst, adding a BB greatly improves the fitting over the CPL model—around 2.7 to $\sim$ 5.5 s. This burst is a very bright, and we include 18 time bins from 2.7 to 5.5 s. Through regime judgment, 17, 17, and 9 time bins are obtained for r_0=10^7 cm, r_0=10^8 cm, and r_0=10^9 cm, respectively. Redshift is adopted z= 0.424 reported by Selsing et al. (2019). The thermal flux ratio is very high (Figure 6) and without significant evolution, with an average $\sim$ 30% for all time bins, which is much higher than the typical observations. BB temperature generally shows a monotonic *decreasing* behavior. All time bins show $\eta \gg 1$ while for a majority of time bins the derived $(1+\sigma_0)$ is $\sim$ unity for a small r_0 (10^7cm) but above unity for a large r_0 (10^9 cm) (r_0-dependent). Also, we find that $r_{\rm ph}$ shows *increases* while $\Gamma_{\rm ph}$ generally present a *flat*-to-*decrease* temporal trend. Interestingly, no time bins for all r_0 the derived $(1+\sigma_{\rm r15})$ are above unity (r_0-independent), while $(1+\sigma_{\rm ph})$ show a r_0-dependent behavior.

- GRB 090902B. The burst shows the thermal dominate form (Ryde et al. 2010), both in the time-integrated or time-resolved spectral analysis. Moreover, GRB 090902B is a very bright burst, and 48 time bins are obtained. The redshift of z=1.822 was measured by Cucchiara et al. (2009). Three radii (r_0=10^7 cm, r_0=10^8 cm, and r_0=10^9 cm) correspond to 47, 47, 33 bins, satisfying with the regime judgments. In Figure 7, we present temporal evolutions of all physical parameters, ratios, and BB temperature. The thermal flux ratios reach a very high value at early times, with an average value $\sim$ 70%, then decrease to $\sim$ 20 % at later times. We find that all time bins show $\eta \gg 1$ and show dramatic *flat*-to-*decrease* properties. Both $(1+\sigma_0)$ and $(1+\sigma_{r15})$ exhibit a r_0-dependent behavior, while there is no time bin for all r_0 the derived $(1+\sigma_{\rm r15})$ is greater than unity, indicating that IS is the mechanism to power the nonthermal emission. Interestingly, $r_{\rm ph}$ shows a *flat-to-increase* behavior whereas $\Gamma_{\rm ph}$ presents a *flat-to-decrease* behavior.

- GRB 160107A. The burst is another case which reveals the thermal-dominant form, and Kawakubo et al. (2018) suggests the best spectral model is PL+BB. No redshift is reported and z =2 is still adopted. All nine time bins still show $\eta \gg 1$ and showing a *flat* behavior (Figure 8). Furthermore, we find that both $(1+\sigma_0)$ and $(1+\sigma_{\rm ph})$, as well as $r_{\rm ph}$ and $\Gamma_{\rm ph}$, also present a *flat* temporal trend throughout the duration. r_0-dependent behavior is significantly found in

both $(1+\sigma_0)$ and $(1+\sigma_{\rm ph})$. We do not find any time bin where $(1+\sigma_{\rm r15})$ is greater than unity, implying that IS is the dominant mechanism to power the nonthermal emission.

In order to have a global view on the statistical properties of the physical parameters for the hybrid problem, we present the distributions of each relevant physical parameter, comparing them with three typical values of r_0 (Figure 9). For a small r_0, we find η tends to be large while $(1+\sigma_0)$ tends to be small. The peaks of η are distributed at ~ 150 for r_0=10^9 cm and at $\sim 4\times10^3$ for r_0=10^7 cm, while the peaks of $(1+\sigma_0)$ are close to unity for r_0=10^7 cm and ~ 10 for r_0=10^9 cm. We find that $(1+\sigma_0)$ typically ranges within $(1 \sim 100)$ for all selected r_0 values. On the other hand, both $r_{\rm ph}$ and $\Gamma_{\rm ph}$ generally share the same peak between different values of r_0 (except for r_0=10^9 cm), in which the peaks are around 10^{12} cm for $r_{\rm ph}$ and ~ 500 for $\Gamma_{\rm ph}$. We do not find a clear trend for $(1+\sigma_{15})$ and $(1+\sigma_{\rm r15})$ due to a small sample size.

In Figure 10, we display some key correlation analysis for the hybrid parameters. We find that the η-$(F_{\rm BB}/F_{\rm obs})$ plot shows a clear monotonous-positive relation, whereas both the $(1+\sigma_0)$-$(F_{\rm BB}/F_{\rm obs})$ and η-$(1+\sigma_0)$ plots present a strong monotonous-negative relation. The results are consistent with the predicted expectation in the hybrid model—a high thermal flux ratio tends to be a high η and small $(1+\sigma_0)$. The thermal flux ratio and η track each other since both denote the strength of the thermal component. Therefore, both of them have an opposite relation with $(1+\sigma_0)$. For $r_{\rm ph}$-$\Gamma_{\rm ph}$, we also find a positive relation. For η-kT and $(1+\sigma_0)$-kT relations, we do not find a clear trend.

5. CONCLUSION AND DISCUSSION

GRB jets are more likely to originate from a hybrid system, which consists of a quasi-thermal (hot fireball) component as well as a nonthermal (cold Poynting-flux) component at the central engine concomitantly. The hybrid model has been discussed in detail in Gao & Zhang (2015). However, it has not yet been applied to a large sample of *Fermi* GRBs. In this paper, we first applied the top-down approach of Gao & Zhang (2015) to diagnose a large sample of *Fermi* GRBs with the detected photosphere component, and then carried out a statistical analysis of the central engine properties. In total, we included eight such GRBs for our analysis (see our Paper I for details). In order to obtain the observational parameters, we first employed a Bayesian analysis and MCMC method to fit our sample. Three observed quantities are obtained, including: BB temperature kT, BB flux $F_{\rm BB}$, and thermal flux ratio $F_{\rm BB}/F_{\rm obs}$. After the regime judgment, we inferred all the relevant physical parameters for the hybrid problem from the corresponding formula of each regime (see Appendix A2), including η, $(1+\sigma_0)$, $r_{\rm ph}$, $\Gamma_{\rm ph}$, $(1+\sigma_{\rm ph})$, and $(1+\sigma_{\rm r15})$. Our analysis is based on the assumption that r_0 is a constant. Considering several realistic scenarios for a central engine, we adopted three typical values of r_0: r_0=10^7cm, r_0=10^8cm, and r_0=10^9cm. For the busts without redshift observation, we use a typical value ($z = 2$) instead. After analyzing the evolutionary properties of the physical parameters in our sample, we found $\eta \gg 1$ in all time bins of all bursts, indicating a hot fireball component. We also found that in some time bins in five bursts (GRB 081224, GRB 110721A, GRB 090719, GRB 100707, and GRB 100724) the derived $(1+\sigma_0)$ is greater than unity for all selected r_0 values, implying that a cold Poynting-flux component may also play an important role for these GRBs, and therefore the hybrid jet problem must be involved. The other three bursts (GRB 190114C, GRB 090902B, and GRB 160107A) show r_0-dependent behavior, which means whether this is possible or not depends on which r_0 is the true size at the central engine. If r_0 is small (=10^7cm), one has $(1+\sigma_0) \sim 1$, this in agreement with the case of $\eta \gg 1$ and $\sigma_0 \ll 1$ in the hybrid problem; if r_0

is large (=10^9cm), we have $(1+\sigma_0) > 1$, this still can be explained by the hybrid problem, where η is smaller and σ_0 is larger. Interestingly, we found that $(1+\sigma_{\rm r15})>1$ for some time bins for all r_0 in GRB 081224 and GRB 110721A. This indicates that the ICMART event rather than IS is the mechanism to power the nonthermal emission. Other GRBs, either exhibit r_0-dependent behavior (GRB 090719, GRB 100707, GRB 100724B, and GRB 160107A), or have no time bin (GRB 190114C and GRB 090902B) satisfying $(1+\sigma_{\rm r15})$ >1. Temporal properties of the physical parameter show that basically, the thermal flux ratio is directly proportional to η, but inversely proportional to $(1+\sigma_0)$, which is the natural expectation predicted by the hybrid problem. Since a high thermal flux ratio indicates a strong thermal component and a weak cold Poynting-flux component, η should be large and $(1+\sigma_0)$ should be small. Moreover, the global parameter relations show that the η-$(F_{\rm BB}/F_{\rm obs})$ plot presents a monotonic-positive relation, whereas the $(1+\sigma_0)$-$(F_{\rm BB}/F_{\rm obs})$ plot shows a monotonic-negative relation. In conclusion, in a more general hybrid jet model, which introduces another magnetization parameter σ_0 on the basis of the traditional fireball model, at least a majority of *Fermi* bursts (probably all) can be well interpreted.

Finally, in our analysis, several caveats are worth mentioning. The first one is the problem of the selection value of r_0. In the hybrid problem, our analysis is based on the assumption of a constant r_0. We adopted the values of three r_0 (r_0=10^7cm, r_0=10^8cm, and r_0=10^9cm), which span two orders of magnitude. However, our results significantly vary with different r_0 values. Since it is impossible to give an accurately true value of r_0, this leads us to make some not very confident explanations in some cases. For instance, in GRB 09092B, the burst has the highest thermal flux ratio. When r_0=10^7cm, all time bins have $(1+\sigma_0)\sim$ 1. However, when r_0=10^8cm, only a part of time bins show $(1+\sigma_0)\sim$ 1. Moreover, when r_0=10^9cm, no time bin has $(1+\sigma_0)\sim$ 1; rather, all time bins have $(1+\sigma_0)>1$. Such r_0-dependent behavior is evidenced from another burst, GRB 190114C, which also has a very high thermal flux ratio. Gao & Zhang (2015) studied a case (GRB 110721A) but applied different r_0 values: r_0= 10^8 cm, r_0= 10^9 cm, and r_0= 10^{10} cm. Using r_0=10^{10} cm for the analysis may be a little big, since the size of a naked engine (a hyper-accreting black hole or a millisecond magnetar) is $r_0 \sim 10^7$ cm, or for a 're-born' fireball (considering an extended envelope of a collapsar progenitor), $r_0 \sim R_*\theta_j \sim 10^9 R_{*,10}\theta_{j,-1}$ cm (where R_* is the size of the progenitor star, and θ_j is the jet opening angle). On the other hand, only a very small number of time bins of $r_0 = 10^{10}$ cm can go through the regime judgment (one for GRB 100707A, two for GRB 110721A, three for GRB 090902B, and no time bin for other five bursts).

The second one is the redshift problem. In our sample, the redshift of more than half of the GRBs is unknown. However, in reality, the derivation of some physical parameters require a redshift measurement. In order to test the effect of various redshift values on the results, we compare the temporal properties of the physical parameters with five different z values for GRB 110721A (Figure A3): $z = 0.382$, $z = 1$, $z = 2$, $z = 3.512$, and $z = 8$. For simplicity, our test is only based on a typical radius, $r_0 = 10^8$ cm. 0.382 and 3.512 are two candidates of observed values of redshift for GRB 110721A, as reported in Berger (2011), and the former is preferred. We find that the effect of redshift is moderate, which has an impact on the results within one order of magnitude. Therefore, our calculations are adopted a typical value ($z = 2$) for the bursts, whose redshift is unknown. More interestingly, we find that η, $r_{\rm ph}$, and $\Gamma_{\rm ph}$ are more sensitive than $(1+\sigma_0)$, $(1+\sigma_{\rm ph})$, and $(1+\sigma_{\rm r15})$ replying on the selection of redshift. However, for those GRBs without redshift measurement, we still need to be cautious in explaining the physical parameters.

Last, our current work is based on the assumption that GRBs have a jet structure. There are some other models (e.g., Induced Gravitational Collapse model) may also well account for the observations. For example, in recent months there has been the identification of the GRB "inner engine" in GRB 130427A (Ruffini et al. 2019b). This inner engine, applied also to GRB 190114C, GRB 160509A and GRB 160625B (Liang et al. 2019) evidenced that the MeV radiation observed by *Fermi*-GBM occurs close to the Black Hole, is not collimated and has a self-similar temporal structure. Quantized GeV emission, observed by *Fermi* Large Area Telescope, originates very close to the Black Hole horizon and represents the GRB jetted emission (Rueda & Ruffini 2020).

I appreciate the valuable comments from the anonymous referee. I would like to thank Dr. Yu Wang, Prof. Felix Ryde, Prof. He Gao, Dr. Rahim Moradi, Prof. She Sheng Xue, Prof. Gregory Vereshchagin, Prof. Jorge Rueda, and Prof. Carlo Luciano Bianco for useful discussions, and the support from Prof. Remo Ruffini. I particularly thank to Prof. Bing Zhang for giving an initial idea on the subject and much useful discussions. This research made use of the High Energy Astrophysics Science Archive Research Center (HEASARC) Online Service at the NASA/Goddard Space Flight Center (GSFC).

Facilities: *Fermi*/GBM

Software: 3ML (Vianello et al. 2015), MULTINEST (Feroz & Hobson 2008; Feroz et al. 2009, 2019), emcee (Foreman-Mackey et al. 2013), and Matplotlib (Hunter 2007)

REFERENCES

Abdo, A. A., Ackermann, M., Ajello, M., et al. 2009, ApJL, 706, L138, doi: 10.1088/0004-637X/706/1/L138

Acuner, Z., & Ryde, F. 2018, MNRAS, 475, 1708, doi: 10.1093/mnras/stx3106

Acuner, Z., Ryde, F., & Yu, H.-F. 2019, MNRAS, 487, 5508, doi: 10.1093/mnras/stz1356

Andrae, R., Schulze-Hartung, T., & Melchior, P. 2010, arXiv e-prints. https://arxiv.org/abs/1012.3754

Axelsson, M., Baldini, L., Barbiellini, G., et al. 2012, ApJL, 757, L31, doi: 10.1088/2041-8205/757/2/L31

Band, D., Matteson, J., Ford, L., et al. 1993, ApJ, 413, 281, doi: 10.1086/172995

Bégué, D., & Pe'er, A. 2015, ApJ, 802, 134, doi: 10.1088/0004-637X/802/2/134

Berger, E. 2011, GRB Coordinates Network, 12193, 1

Burgess, J. M., Greiner, J., Bégué, D., & Berlato, F. 2019, MNRAS, 490, 927, doi: 10.1093/mnras/stz2589

Burgess, J. M., Preece, R. D., Connaughton, V., et al. 2014, ApJ, 784, 17, doi: 10.1088/0004-637X/784/1/17

Cash, W. 1979, ApJ, 228, 939, doi: 10.1086/156922

Cucchiara, A., Fox, D. B., Tanvir, N., & Berger, E. 2009, GRB Coordinates Network, 9873, 1

Drenkhahn, G., & Spruit, H. C. 2002, A&A, 391, 1141, doi: 10.1051/0004-6361:20020839

Feroz, F., & Hobson, M. P. 2008, MNRAS, 384, 449, doi: 10.1111/j.1365-2966.2007.12353.x

Feroz, F., Hobson, M. P., & Bridges, M. 2009, MNRAS, 398, 1601, doi: 10.1111/j.1365-2966.2009.14548.x

Feroz, F., Hobson, M. P., Cameron, E., & Pettitt, A. N. 2019, The Open Journal of Astrophysics, 2, 10, doi: 10.21105/astro.1306.2144

Foreman-Mackey, D., Hogg, D. W., Lang, D., & Goodman, J. 2013, PASP, 125, 306, doi: 10.1086/670067

Gao, H., & Zhang, B. 2015, ApJ, 801, 103, doi: 10.1088/0004-637X/801/2/103

Ghirlanda, G., Pescalli, A., & Ghisellini, G. 2013, MNRAS, 432, 3237, doi: 10.1093/mnras/stt681
Giannios, D. 2008, A&A, 480, 305, doi: 10.1051/0004-6361:20079085
Goldstein, A., Burgess, J. M., Preece, R. D., et al. 2012, ApJS, 199, 19, doi: 10.1088/0067-0049/199/1/19
Goodman, J. 1986, ApJL, 308, L47, doi: 10.1086/184741
Goodman, J., & Weare, J. 2010, Communications in Applied Mathematics and Computational Science, 5, 65, doi: 10.2140/camcos.2010.5.65
Granot, J., Komissarov, S. S., & Spitkovsky, A. 2011, MNRAS, 411, 1323, doi: 10.1111/j.1365-2966.2010.17770.x
Greiner, J., Burgess, J. M., Savchenko, V., & Yu, H.-F. 2016, ApJL, 827, L38, doi: 10.3847/2041-8205/827/2/L38
Guiriec, S., Connaughton, V., Briggs, M. S., et al. 2011, ApJL, 727, L33, doi: 10.1088/2041-8205/727/2/L33
Hunter, J. D. 2007, Computing in Science and Engineering, 9, 90, doi: 10.1109/MCSE.2007.55
Iyyani, S., Ryde, F., Axelsson, M., et al. 2013, MNRAS, 433, 2739, doi: 10.1093/mnras/stt863
Iyyani, S., Ryde, F., Ahlgren, B., et al. 2015, MNRAS, 450, 1651, doi: 10.1093/mnras/stv636
Kawakubo, Y., Sakamoto, T., Nakahira, S., et al. 2018, PASJ, 70, 6, doi: 10.1093/pasj/psx152
Komissarov, S. S., Vlahakis, N., Königl, A., & Barkov, M. V. 2009, MNRAS, 394, 1182, doi: 10.1111/j.1365-2966.2009.14410.x
Lei, W.-H., Zhang, B., & Liang, E.-W. 2013, ApJ, 765, 125, doi: 10.1088/0004-637X/765/2/125
Li, L. 2019a, ApJS, 245, 7, doi: 10.3847/1538-4365/ab42de(Paper I)
—. 2019b, ApJS, 242, 16, doi: 10.3847/1538-4365/ab1b78
Liang, L., Ruffini, R., Rueda, J. A., et al. 2019, arXiv e-prints, arXiv:1910.12615. https://arxiv.org/abs/1910.12615
Meegan, C., Lichti, G., Bhat, P. N., et al. 2009, ApJ, 702, 791, doi: 10.1088/0004-637X/702/1/791
Meszaros, P., & Rees, M. J. 1993, ApJ, 405, 278, doi: 10.1086/172360
Mészáros, P., & Rees, M. J. 1997, ApJL, 482, L29, doi: 10.1086/310692
—. 2000, ApJ, 530, 292, doi: 10.1086/308371
—. 2011, ApJL, 733, L40, doi: 10.1088/2041-8205/733/2/L40
Metzger, B. D., Giannios, D., Thompson, T. A., Bucciantini, N., & Quataert, E. 2011, MNRAS, 413, 2031, doi: 10.1111/j.1365-2966.2011.18280.x
Narayana Bhat, P., Meegan, C. A., von Kienlin, A., et al. 2016, ApJS, 223, 28, doi: 10.3847/0067-0049/223/2/28
Paczynski, B. 1986, ApJL, 308, L43, doi: 10.1086/184740
—. 1990, ApJ, 363, 218, doi: 10.1086/169332
Paczynski, B., & Xu, G. 1994, ApJ, 427, 708, doi: 10.1086/174178
Pe'Er, A., & Ryde, F. 2017, International Journal of Modern Physics D, 26, 1730018, doi: 10.1142/S021827181730018X
Pe'er, A., Ryde, F., Wijers, R. A. M. J., Mészáros, P., & Rees, M. J. 2007, ApJL, 664, L1, doi: 10.1086/520534
Pe'Er, A., Zhang, B.-B., Ryde, F., et al. 2012, MNRAS, 420, 468, doi: 10.1111/j.1365-2966.2011.20052.x
Piran, T., Shemi, A., & Narayan, R. 1993, MNRAS, 263, 861, doi: 10.1093/mnras/263.4.861
Planck Collaboration, Aghanim, N., Akrami, Y., et al. 2018, arXiv e-prints, arXiv:1807.06209. https://arxiv.org/abs/1807.06209
Rees, M. J., & Meszaros, P. 1994, ApJL, 430, L93, doi: 10.1086/187446
Rees, M. J., & Mészáros, P. 2005, ApJ, 628, 847, doi: 10.1086/430818
Rueda, J. A., & Ruffini, R. 2020, European Physical Journal C, 80, 300, doi: 10.1140/epjc/s10052-020-7868-z
Ruffini, R., Salmonson, J. D., Wilson, J. R., & Xue, S.-S. 1999, A&A, 350, 334
—. 2000, A&A, 359, 855
Ruffini, R., Siutsou, I. A., & Vereshchagin, G. V. 2013, ApJ, 772, 11, doi: 10.1088/0004-637X/772/1/11
Ruffini, R., Li, L., Moradi, R., et al. 2019a, arXiv e-prints, arXiv:1904.04162. https://arxiv.org/abs/1904.04162
Ruffini, R., Moradi, R., Rueda, J. A., et al. 2019b, ApJ, 886, 82, doi: 10.3847/1538-4357/ab4ce6
Ryde, F. 2004, ApJ, 614, 827, doi: 10.1086/423782
Ryde, F., & Pe'er, A. 2009, ApJ, 702, 1211, doi: 10.1088/0004-637X/702/2/1211

Ryde, F., Yu, H.-F., Dereli-Bégué, H., et al. 2019, MNRAS, 484, 1912, doi: 10.1093/mnras/stz083

Ryde, F., Axelsson, M., Zhang, B. B., et al. 2010, ApJL, 709, L172, doi: 10.1088/2041-8205/709/2/L172

Scargle, J. D., Norris, J. P., Jackson, B., & Chiang, J. 2013, ApJ, 764, 167, doi: 10.1088/0004-637X/764/2/167

Selsing, J., Fynbo, J. P. U., Heintz, K. E., & Watson, D. 2019, GRB Coordinates Network, 23695, 1

Shemi, A., & Piran, T. 1990, ApJL, 365, L55, doi: 10.1086/185887

Thompson, C. 2006, ApJ, 651, 333, doi: 10.1086/505290

Veres, P., & Mészáros, P. 2012, ApJ, 755, 12, doi: 10.1088/0004-637X/755/1/12

Vianello, G. 2018, ApJS, 236, 17, doi: 10.3847/1538-4365/aab780

Vianello, G., Lauer, R. J., Younk, P., et al. 2015, arXiv e-prints. https://arxiv.org/abs/1507.08343

Vlahakis, N., & Königl, A. 2003, ApJ, 596, 1104, doi: 10.1086/378227

Wang, Y., Li, L., Moradi, R., & Ruffini, R. 2019, arXiv e-prints. https://arxiv.org/abs/1901.07505

Yu, H.-F., Dereli-Bégué, H., & Ryde, F. 2019, ApJ, 886, 20, doi: 10.3847/1538-4357/ab488a

Zhang, B. 2014, International Journal of Modern Physics D, 23, 1430002, doi: 10.1142/S021827181430002X

—. 2018, The Physics of Gamma-Ray Bursts, doi: 10.1017/9781139226530

Zhang, B., & Yan, H. 2011, ApJ, 726, 90, doi: 10.1088/0004-637X/726/2/90

Zhang, B.-B., Zhang, B., Castro-Tirado, A. J., et al. 2018, Nature Astronomy, 2, 69, doi: 10.1038/s41550-017-0309-8

Table 1. Photosphere Properties of the Hybrid Jet Problem of Our Sample.

GRB	z	r_0	Spectrum[a] (Overall)	η	$(1+\sigma_0)$	$r_{\rm ph}$	$\Gamma_{\rm ph}$	$(1+\sigma_{\rm ph})$	$(1+\sigma_{\rm r15})$
	(Used Value)	(cm)	(Number)	(Evolution)	(Evolution,>1)	(Evolution)	(Evolution)	(>1)	(>1)
(1)	(2)	(3)	(4)	(5)	(6)	(7)	(8)	(9)	(10)
081224	2	10^7	5(5)	*d.*	*i.*-to-*d.*, (4)	*d.*-to-*i.*	*d.*-to-*i.*	4	3
		10^8	2(5)	*d.*	*i.*, (2)	*d.*	*d.*	1	1
		10^9	0(5)	...	...	...	...	...	...
090719	2	10^7	11(12)	*d.*	*i.*, (7)	*f.*-to-*d.*	*f.*-to-*d.*	3	0
		10^8	10(12)	*d.*	*i.*, (10)	*f.*-to-*d.*	*f.*-to-*d.*	6	2
		10^9	7(12)	*d.*	*i.*, (7)	*f.*	*f.*	7	4
100707	2	10^7	11(11)	*f.*-to-*d.*	*f.*-to-*i.*, (4)	*d.*	*i.*	2	0
		10^8	11(11)	*f.*-to-*d.*	*d.*-to-*i.*, (9)	*i.*-to-*d.*	*f.*-to-*d.*	4	2
		10^9	8(11)	*d.*	*d.*-to-*i.*, (8)	*i.*-to-*d.*	*f.*-to-*d.*	7	1
100724B	2	10^7	32(33)	*i.*	*d.*, (22)	*f.*	*f.*	2	0
		10^8	31(33)	*f.*	*d.*, (31)	*f.*	*f.*	19	1
		10^9	30(33)	*f.*	*d.*, (30)	*f.*	*f.*	30	23
110721A	0.382	10^7	8(10)	*d.*	*d.*-to-*i.*, (7)	*i.*-to-*d.*	*d.*	1	0
		10^8	8(10)	*d.*	*d.*-to-*i.*, (8)	*i.*-to-*d.*	*d.*	6	1
		10^9	6(10)	*d.*	*d.*-to-*i.*, (6)	*i.*-to-*d.*	*d.*	6	4
190114C	0.424	10^7	17(18)	*d.*	*d.*, (0)	*i.*	*d.*	0	0
		10^8	17(18)	*f.*	*d.*, (12)	*i.*	*f.*-to-*d.*	3	0
		10^9	9(18)	*f.*	*f.*, (9)	*i.*	*f.*-to-d.	8	0
090902B	1.882	10^7	47(48)	*f.*-to-*d.*	*f.*, (0)	*f.*-to-*d.*	*f.*-to-*d.*	0	0
		10^8	47(48)	*f.*-to-*d.*	*f.*, (29)	*f.*-to-*d.*	*f.*-to-*d.*	0	0
		10^9	33(48)	*f.*-to-*d.*	*f.*, (33)	*f.*-to-*i.*	*f.*-to-*d.*	31	0
160107A	2	10^7	9(9)	*f.*	*f.*, (2)	*f.*	*f.*	0	0
		10^8	9(9)	*f.*	*f.*, (9)	*f.*	*f.*	1	0
		10^9	9(9)	*f.*	*f.*, (9)	*f.*	*f.*	9	2

Note.The parameters we list include: GRB name (Column 1), used value of redshift (Column 2), used value of r_0 (Column 3), time bin of passed regime judgements and total (Column 4), temporal properties of $\eta \gg 1$ (Column 5), time bin of $(1+\sigma_0)>1$ (Column 6), temporal properties of $r_{\rm ph}$ (Column 7) and $\Gamma_{\rm ph}$ (Column 8), time bin of $(1+\sigma_{\rm ph})>1$ (Column 9), and time bin of $(1+\sigma_{\rm r15})>1$ (Column 10).

[a] The inferred physical parameters are based on different regimes defined for the hybrid problem, which requires regime judgment, see Table 2 of Gao & Zhang (2015). To ensure that our methods are correct, we first adopt the same spectral data (obtained from Iyyani et al. 2013) and values of r_0 (r_0=10^8 cm, r_0=10^9 cm, and r_0=10^{10}) for a test case (GRB 110721A) as also used in Gao & Zhang (2015). We find our results are the same as that of Gao & Zhang (2015), indicating our approaches are correct.

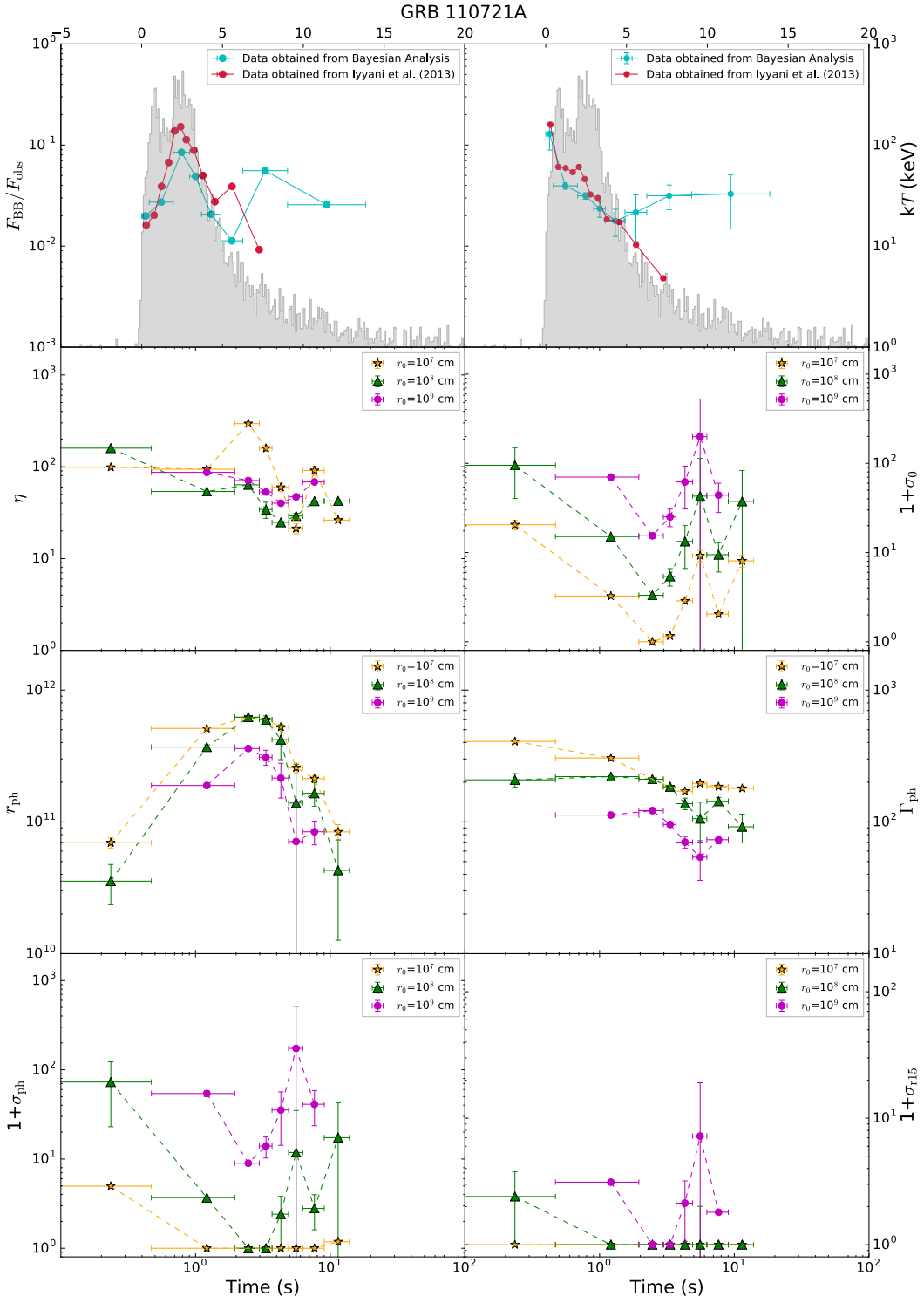

Figure 1. Temporal evolution of thermal flux ratio, BB temperature, and all physical parameters (η, $1+\sigma_0$, $r_{\rm ph}$, $\Gamma_{\rm ph}$, $1+\sigma_{\rm ph}$, $1+\sigma_{\rm r15}$) of the hybrid problem for GRB 110721A. The fitted parameters are obtained from the best fitting of the CPL+BB model by using Bayesian analysis + MCMC method. The physical parameters are calculated by using top-down approach of Gao & Zhang (2015), and considering the case in a non-dissipative photosphere. Regime judgment is used from Table 2 of Gao & Zhang (2015). The redshift of z=0.382 is adopted. Three values of r_0 are used and different colors represent different values of r_0: r_0=10^7 cm (orange), r_0=10^8 cm (green), and r_0=10^9 cm (purple). Note that the two observed parameters (top panels) share the same time scale in the linear-log plots while the physical parameters (all the other panels) share the same time scale in the log-log plots.

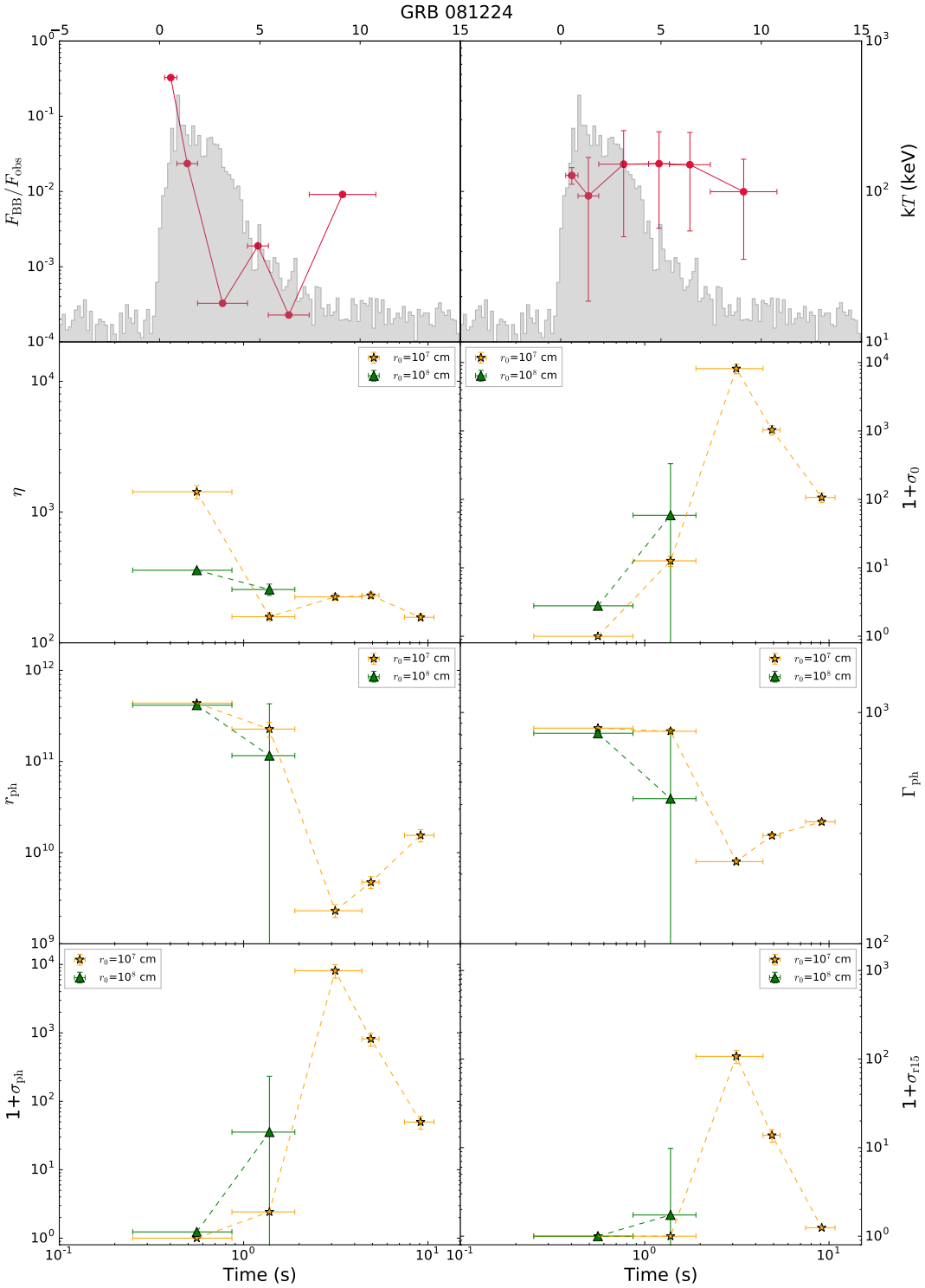

Figure 2. Same as Figure 1, but for GRB 081224.

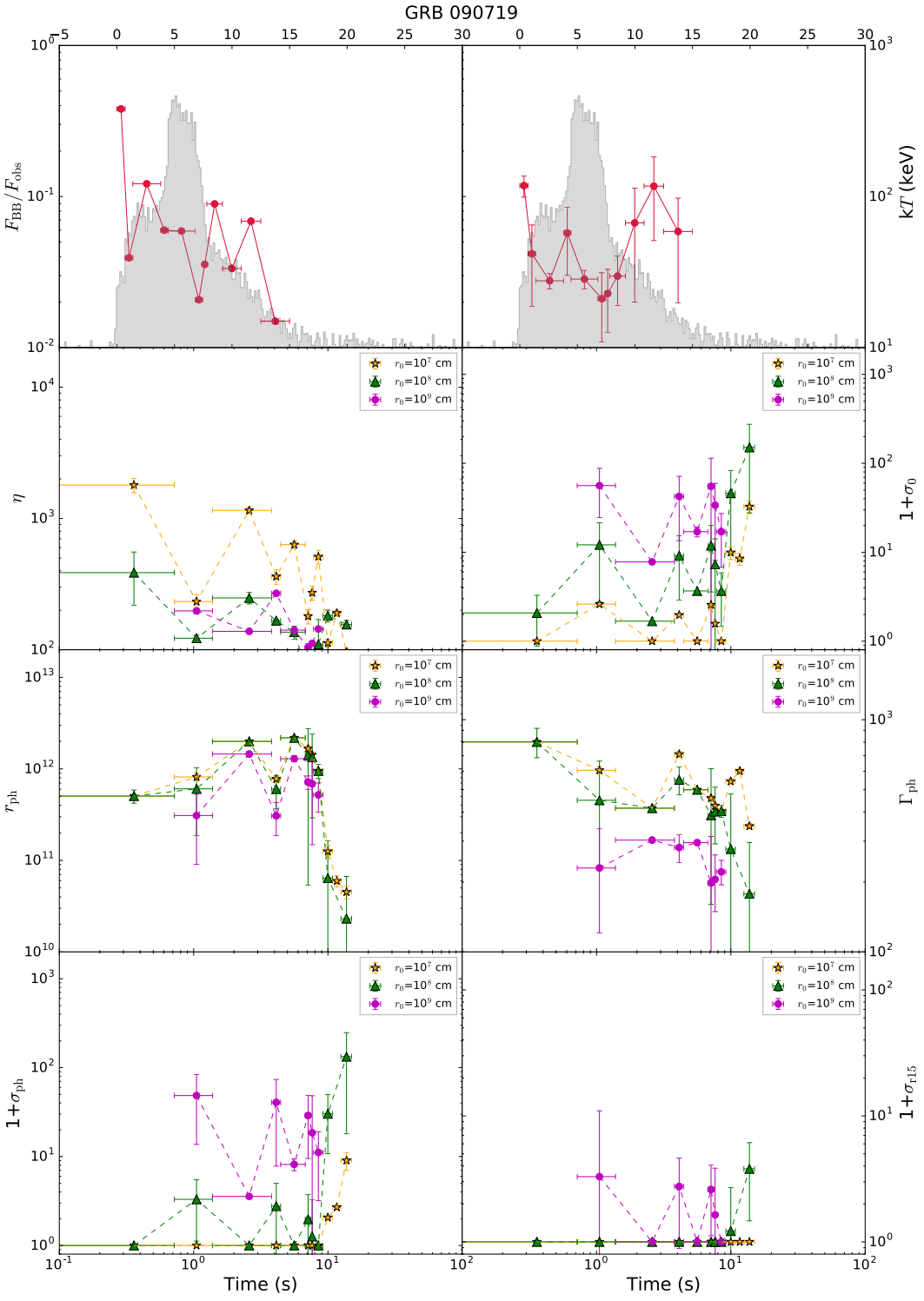

Figure 3. Same as Figure 1, but for GRB 090719.

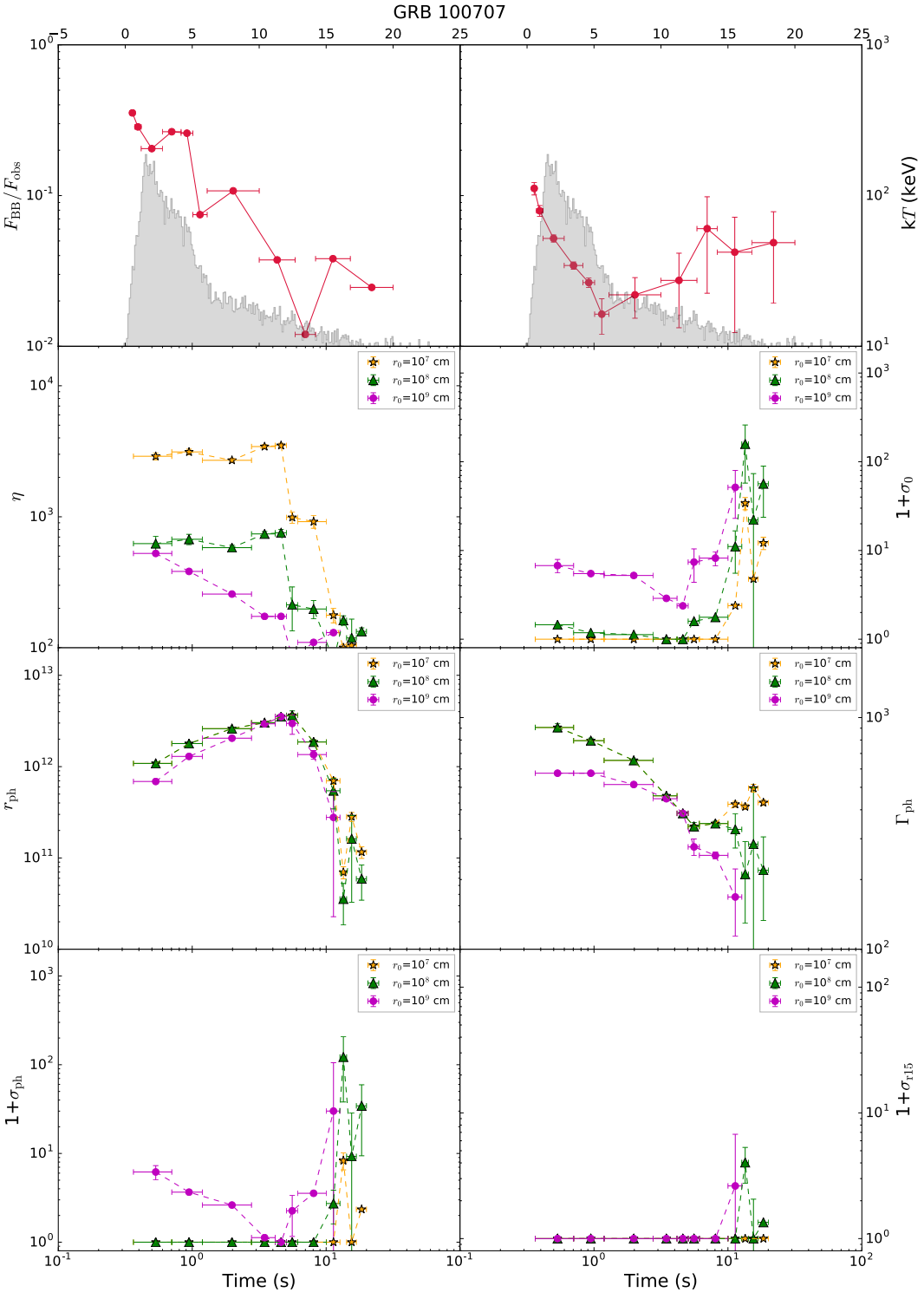

Figure 4. Same as Figure 1, but for GRB 100707.

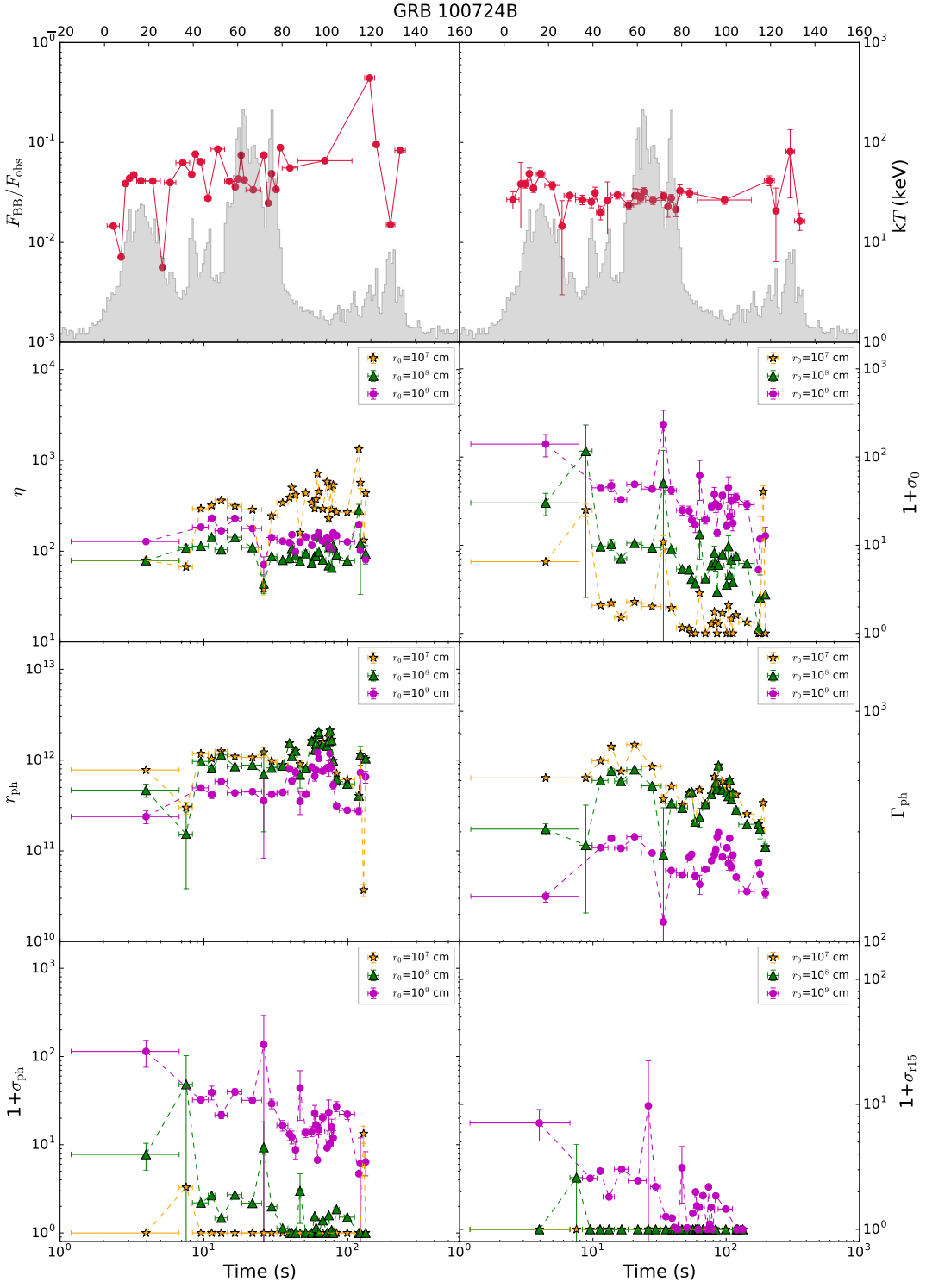

Figure 5. Same as Figure 1, but for GRB 100724B.

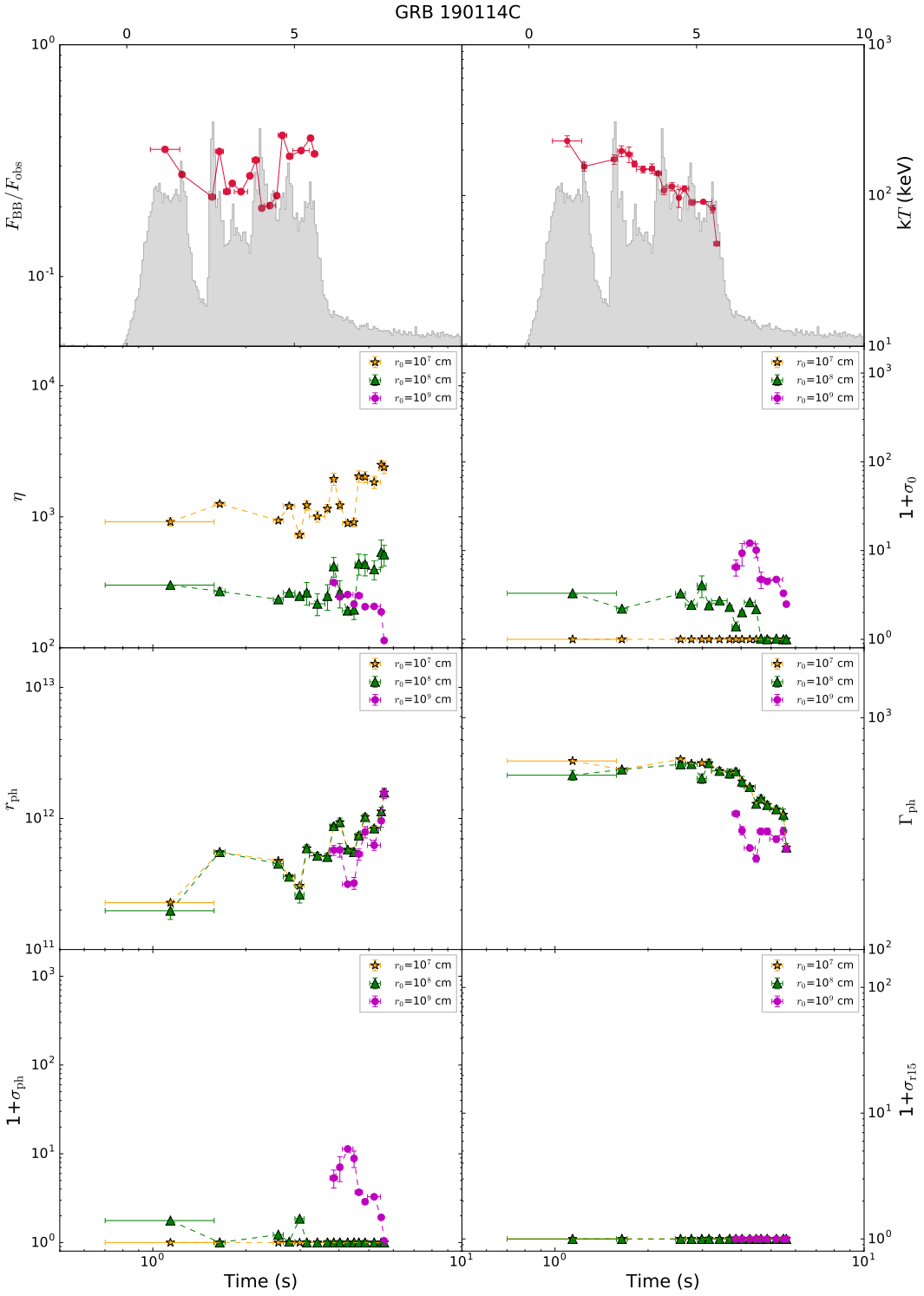

Figure 6. Same as Figure 1, but for GRB 190114C.

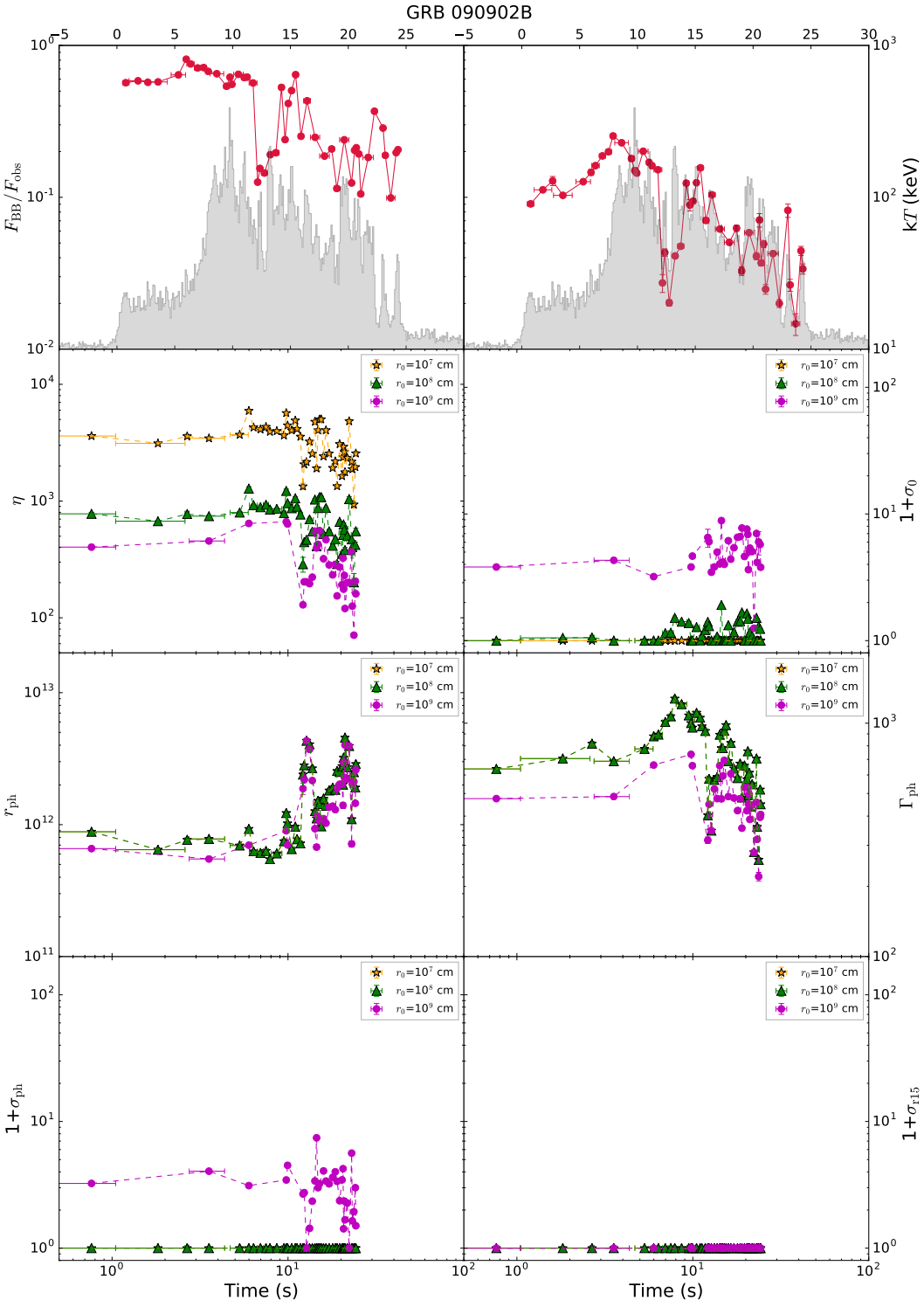

Figure 7. Same as Figure 1, but for GRB 090902B.

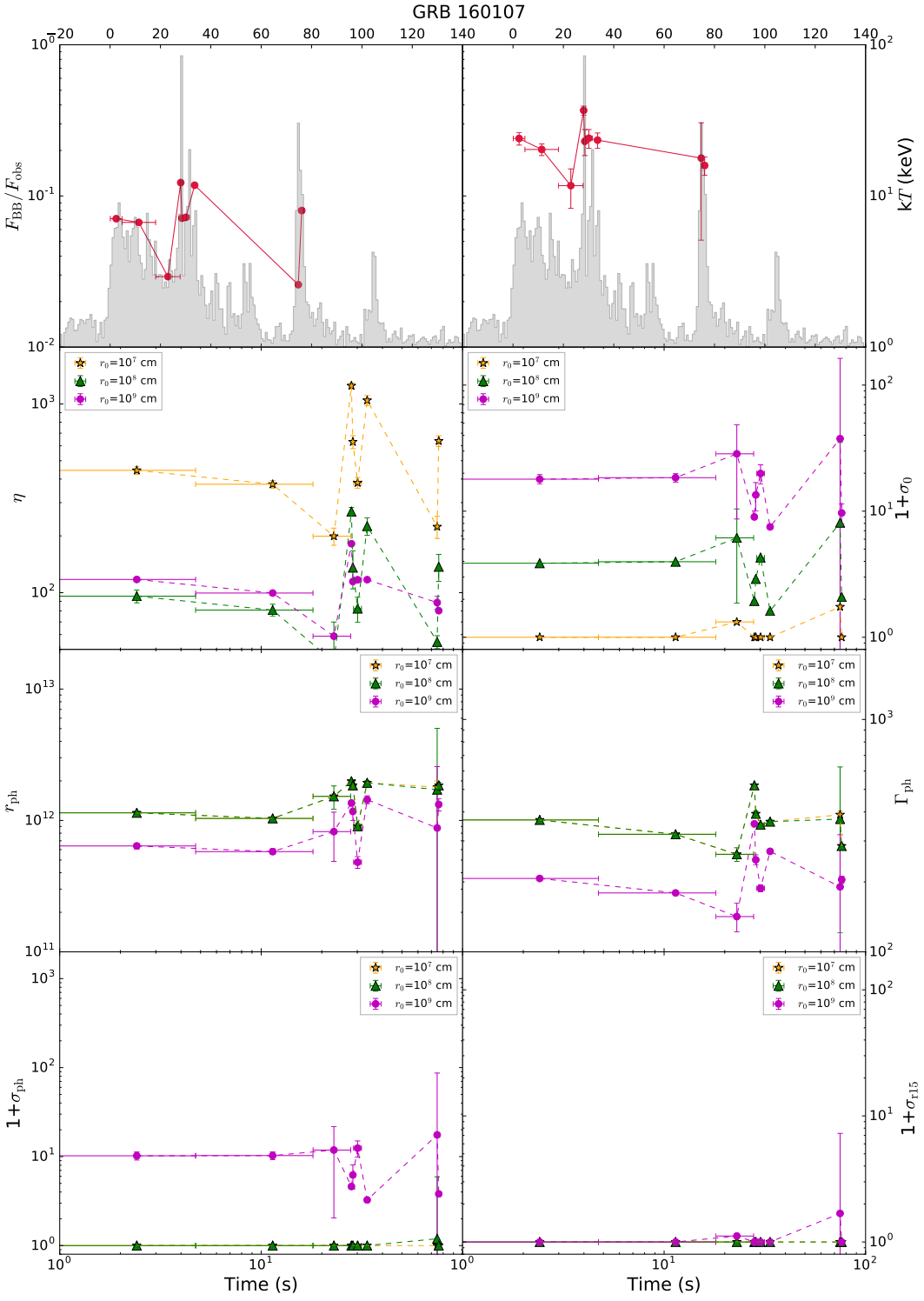

Figure 8. Same as Figure 1, but for GRB 160107A.

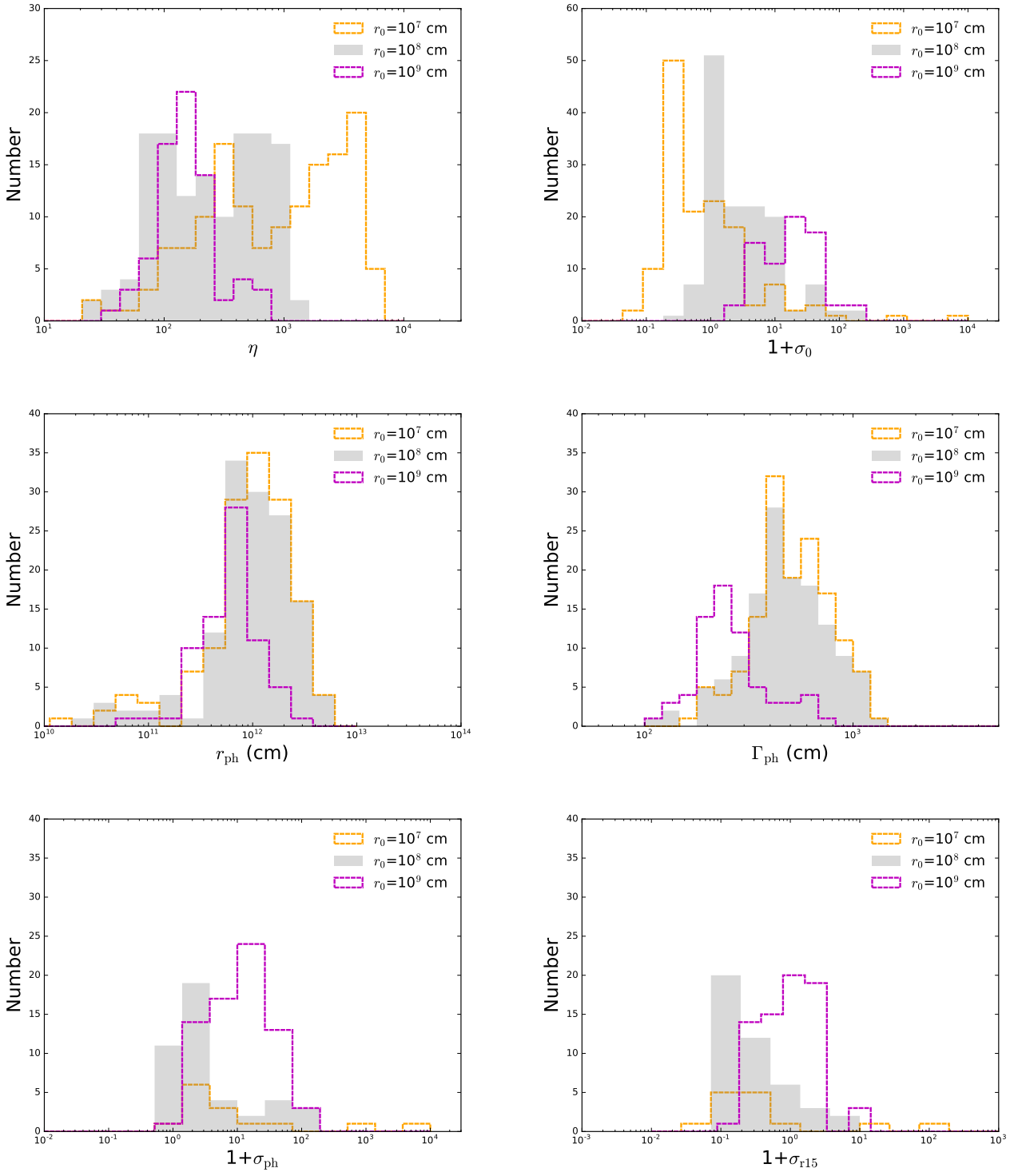

Figure 9. Distributions of characteristic parameters of the hybrid problem, which is based on the assumptions of constant values of r_0: r_0=10^7 cm (orange), r_0=10^8 cm (grey), and r_0=10^9 cm (purple). Upper-left panel: for η-distribution; upper-right panel: for $(1+\sigma_0)$-distribution; middle-left panel: for $r_{\rm ph}$-distribution; middle-right panel: for $\Gamma_{\rm ph}$-distribution; bottom-left panel: for $(1+\sigma_{\rm ph})$-distribution; bottom-right panel: for $(1+\sigma_{\rm r15})$-distribution.

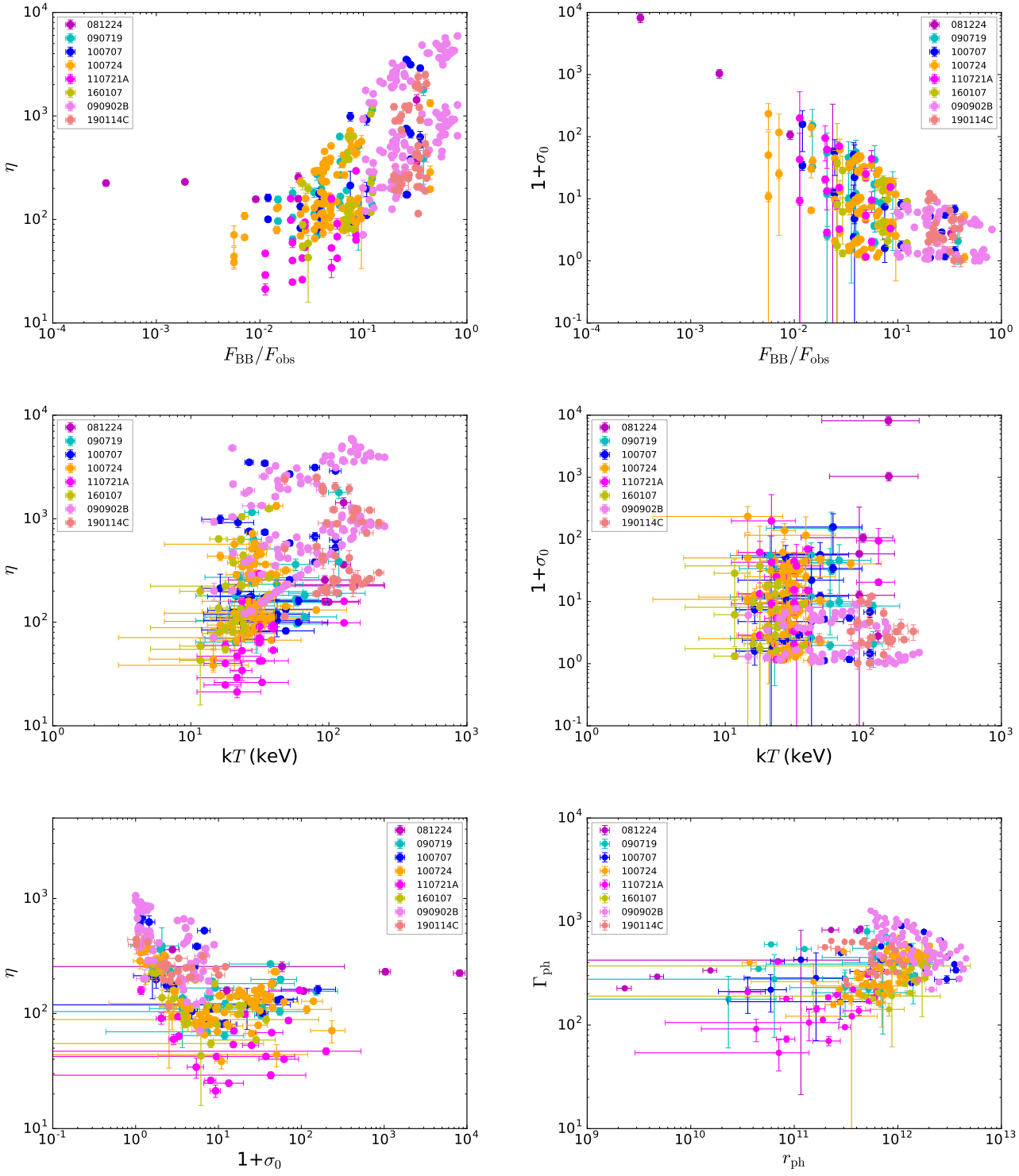

Figure 10. Scatter plots of several characteristic parameters of the hybrid problem (based on all r_0): the η-($F_{\rm BB}/F_{\rm obs}$) plot (upper-left panel), the $(1+\sigma_0)$-($F_{\rm BB}/F_{\rm obs}$) plot (upper-right panel), the η-kT plot (middle-left panel); the $(1+\sigma_0)$-kT plot (middle-right panel), the η-$(1+\sigma_0)$ plot (bottom-left panel), and the $\Gamma_{\rm ph}$-$r_{\rm ph}$ plot (bottom-right panel).

APPENDIX

In this appendix, we present the definition of used models (Appendix A1); the expressions of the regimes II, III, VI and V of 'top-down' approach (Appendix A2); and provide additional figures to show the temporal evolution of the physical parameters of the hybrid problem for GRB 110721A but based on the fitted parameters obtained from Iyyani et al. (2013) with different redshift (Appendix A3).

A1. DEFINITION OF MODELS

The Band function (Band et al. 1993) in the photon number spectrum is defined as

$$f_{\rm BAND}(E) = A \begin{cases} (\frac{E}{E_{\rm piv}})^{\alpha} \exp(-\frac{E}{E_0}), & E \leq (\alpha-\beta)E_0 \\ [\frac{(\alpha-\beta)E_0}{E_{\rm piv}}]^{(\alpha-\beta)} \exp(\beta-\alpha)(\frac{E}{E_{\rm piv}})^{\beta}, & E \geq (\alpha-\beta)E_0 \end{cases} \tag{A1}$$

where

$$E_{\rm p} = (2+\alpha)E_0, \tag{A2}$$

where A is the normalization factor at 100 keV in units of ph cm^{-2}keV^{-1}s^{-1}, $E_{\rm piv}$ is the pivot energy fixed at 100 keV, α and β are the low-energy and high-energy power-law photon spectral indices, respectively. The two spectral regimes are separated by the break energy E_0 in units of keV, and $E_{\rm p}$ is the peak energy in the νF_ν space in units of keV.

The cutoff power law, or the so-called Comptonized model (COMP), which is written as

$$f_{\rm COMP}(E) = A \left(\frac{E}{E_{\rm piv}}\right)^{\alpha} \exp(-\frac{E}{E_0}) \tag{A3}$$

The single power law is defined as

$$f_{\rm PL}(E) = A \left(\frac{E}{E_{\rm piv}}\right)^{\Gamma} \tag{A4}$$

where A is the normalization and Γ is the spectral index.

The BB emission can be modified by Planck spectrum, which is given by the photon flux

$$f_{\rm BB}(E,t) = A(t) \frac{E^2}{\exp[\frac{E}{kT(t)}] - 1}, \tag{A5}$$

where E is the photon energy, k is the Boltzmann constant. The BB emission depends on two free parameters only: temperature, $T(t)$, and the normalization, $A(t)$.

A2. FORMALISM OF 'TOP-DOWN' APPROACH

For regime II (see also Eq.(37) in Gao & Zhang 2015), we have:

$$
\begin{aligned}
1+\sigma_0 &= 25.5(1+z)^{4/3}\left(\frac{kT_{\rm obs}}{50{\rm keV}}\right)^{4/3}\times\left(\frac{F_{\rm BB}}{10^{-8}{\rm ergs^{-1}cm^{-2}}}\right)^{-1/3} r_{0,9}^{2/3} f_{\rm th,-1}^{-1} f_\gamma^{-1} d_{L,28}^{-2/3},\\
\eta &= 74.8(1+z)^{11/12}\left(\frac{kT_{\rm obs}}{50{\rm keV}}\right)^{11/12}\times\left(\frac{F_{\rm BB}}{10^{-8}{\rm ergs^{-1}cm^{-2}}}\right)^{1/48} r_{0,9}^{5/24} d_{L,28}^{1/24},\\
r_{\rm ph} &= 1.78\times10^{10}{\rm cm}(1+z)^{-25/12}\left(\frac{kT_{\rm obs}}{50{\rm keV}}\right)^{-25/12}\times\left(\frac{F_{\rm BB}}{10^{-8}{\rm ergs^{-1}cm^{-2}}}\right)^{37/48} r_{0,9}^{-7/24} d_{L,28}^{37/24},\\
\Gamma_{\rm ph} &= 46.4(1+z)^{-1/12}\left(\frac{kT_{\rm obs}}{50{\rm keV}}\right)^{-1/12}\times\left(\frac{F_{\rm BB}}{10^{-8}{\rm ergs^{-1}cm^{-2}}}\right)^{13/48} r_{0,9}^{-7/24} d_{L,28}^{13/24},\\
1+\sigma_{\rm ph} &= 41.2(1+z)^{7/3}\left(\frac{kT_{\rm obs}}{50{\rm keV}}\right)^{-7/12}\times\left(\frac{F_{\rm BB}}{10^{-8}{\rm ergs^{-1}cm^{-2}}}\right)^{-7/12} r_{0,9}^{7/6} f_{\rm th,-1}^{-1} f_\gamma^{-1} d_{L,28}^{-7/6},\\
1+\sigma_{r15} &= 1.08(1+z)^{59/36}\left(\frac{kT_{\rm obs}}{50{\rm keV}}\right)^{59/36}\times\left(\frac{F_{\rm BB}}{10^{-8}{\rm ergs^{-1}cm^{-2}}}\right)^{-47/144} r_{0,9}^{77/72} f_{\rm th,-1}^{-1} f_\gamma^{-1} d_{L,28}^{-47/72},
\end{aligned}
\tag{A6}
$$

For regime III and regime VI (see also Eq.(38) in Gao & Zhang 2015), we have:

$$
\begin{aligned}
1+\sigma_0 &= 5.99(1+z)^{4/3}\left(\frac{kT_{\rm obs}}{50{\rm keV}}\right)^{4/3}\times\left(\frac{F_{\rm BB}}{10^{-8}{\rm ergs^{-1}cm^{-2}}}\right)^{-1/3} r_{0,9}^{2/3} f_{\rm th,-1}^{-1} f_\gamma^{-1} d_{L,28}^{-2/3},\\
\eta &= 20.3(1+z)^{-5/6}\left(\frac{kT_{\rm obs}}{50{\rm keV}}\right)^{11/12}\times\left(\frac{F_{\rm BB}}{10^{-8}{\rm ergs^{-1}cm^{-2}}}\right)^{11/24} r_{0,9}^{-2/3} f_{\rm th,-1}^{-3/4} f_\gamma^{-3/4} d_{L,28}^{11/12},\\
r_{\rm ph} &= 4.09\times10^{11}{\rm cm}(1+z)^{-3/2}\left(\frac{kT_{\rm obs}}{50{\rm keV}}\right)^{-5/8}\times\left(\frac{F_{\rm BB}}{10^{-8}{\rm ergs^{-1}cm^{-2}}}\right)^{5/8} f_{\rm th,-1}^{-1/4} f_\gamma^{-1/4} d_{L,28}^{5/4},\\
\Gamma_{\rm ph} &= 121.3(1+z)^{1/2}\left(\frac{kT_{\rm obs}}{50{\rm keV}}\right)^{1/2}\times\left(\frac{F_{\rm BB}}{10^{-8}{\rm ergs^{-1}cm^{-2}}}\right)^{1/8} f_{\rm th,-1}^{-1/4} f_\gamma^{-1/4} d_{L,28}^{1/4},
\end{aligned}
\tag{A7}
$$

For regime V (see also Eq.(39) in Gao & Zhang 2015), we have:

$$
\begin{aligned}
1+\sigma_0 &= 6.43(1+z)^{4/3}\left(\frac{kT_{\rm obs}}{50{\rm keV}}\right)^{4/3}\times\left(\frac{F_{\rm BB}}{10^{-8}{\rm ergs^{-1}cm^{-2}}}\right)^{-1/3} r_{0,9}^{2/3} f_{\rm th,-1}^{-1} f_\gamma^{-1} d_{L,28}^{-2/3},\\
\eta &= 105.0(1+z)^{7/6}\left(\frac{kT_{\rm obs}}{50{\rm keV}}\right)^{7/6}\times\left(\frac{F_{\rm BB}}{10^{-8}{\rm ergs^{-1}cm^{-2}}}\right)^{5/24} r_{0,9}^{1/12} f_{\rm th,-1}^{1/2} f_\gamma^{1/2} d_{L,28}^{5/12},\\
r_{\rm ph} &= 4.62\times10^{10}{\rm cm}(1+z)^{-13/6}\left(\frac{kT_{\rm obs}}{50{\rm keV}}\right)^{-13/6}\times\left(\frac{F_{\rm BB}}{10^{-8}{\rm ergs^{-1}cm^{-2}}}\right)^{17/24} r_{0,9}^{-1/4} f_{\rm th,-1}^{-1/6} f_\gamma^{-1/6} d_{L,28}^{17/12},\\
\Gamma_{\rm ph} &= 15.3(1+z)^{-1/6}\left(\frac{kT_{\rm obs}}{50{\rm keV}}\right)^{-1/6}\times\left(\frac{F_{\rm BB}}{10^{-8}{\rm ergs^{-1}cm^{-2}}}\right)^{-5/24} r_{0,9}^{-1/4} f_{\rm th,-1}^{-1/6} f_\gamma^{-1/6} d_{L,28}^{5/24},\\
1+\sigma_{\rm ph} &= 44.2(1+z)^{8/3}\left(\frac{kT_{\rm obs}}{50{\rm keV}}\right)^{8/3}\times\left(\frac{F_{\rm BB}}{10^{-8}{\rm ergs^{-1}cm^{-2}}}\right)^{-1/3} r_{0,9} f_{\rm th,-1}^{-1/3} f_\gamma^{-1/3} d_{L,28}^{-2/3},\\
1+\sigma_{r15} &= 1.59(1+z)^{35/18}\left(\frac{kT_{\rm obs}}{50{\rm keV}}\right)^{35/18}\times\left(\frac{F_{\rm BB}}{10^{-8}{\rm ergs^{-1}cm^{-2}}}\right)^{-7/72} r_{0,9}^{11/12} f_{\rm th,-1}^{-7/18} f_\gamma^{-7/18} d_{L,28}^{-7/36}.
\end{aligned}
\tag{A8}
$$

Here note that regime VI has the identical scalings as regime III. f_γ is given by $f_\gamma{=}L_\gamma/L_{\rm w}$, which connects the total flux $F_{\rm obs}$ to the wind luminosity $L_{\rm w}$; and $f_{\rm th}{=}F_{\rm BB}/F_{\rm obs}$, is the thermal flux ratio, which can be directly measured from the data. f_γ and r_0 are taken as constants and can be estimated to a typical values (e.g., $f_\gamma{=}0.5$ and $r_0{=}10^8$ cm.)

A3. ADDITIONAL FIGURES

Here we show the additional Figure A1-A3. For comparison, Figure A1 and A2 show the same analysis for a studied case (GRB 110721A) but the fitted parameters are obtained from Iyyani et al. (2013), which are baed on two candidates of observed values of redshift: $z{=}0.382$ (Figure A1) and $z{=}3.512$ (Figure A2). Figure A3 displays the results of the different redshift, which is based on a typical r_0 value (10^8 cm).

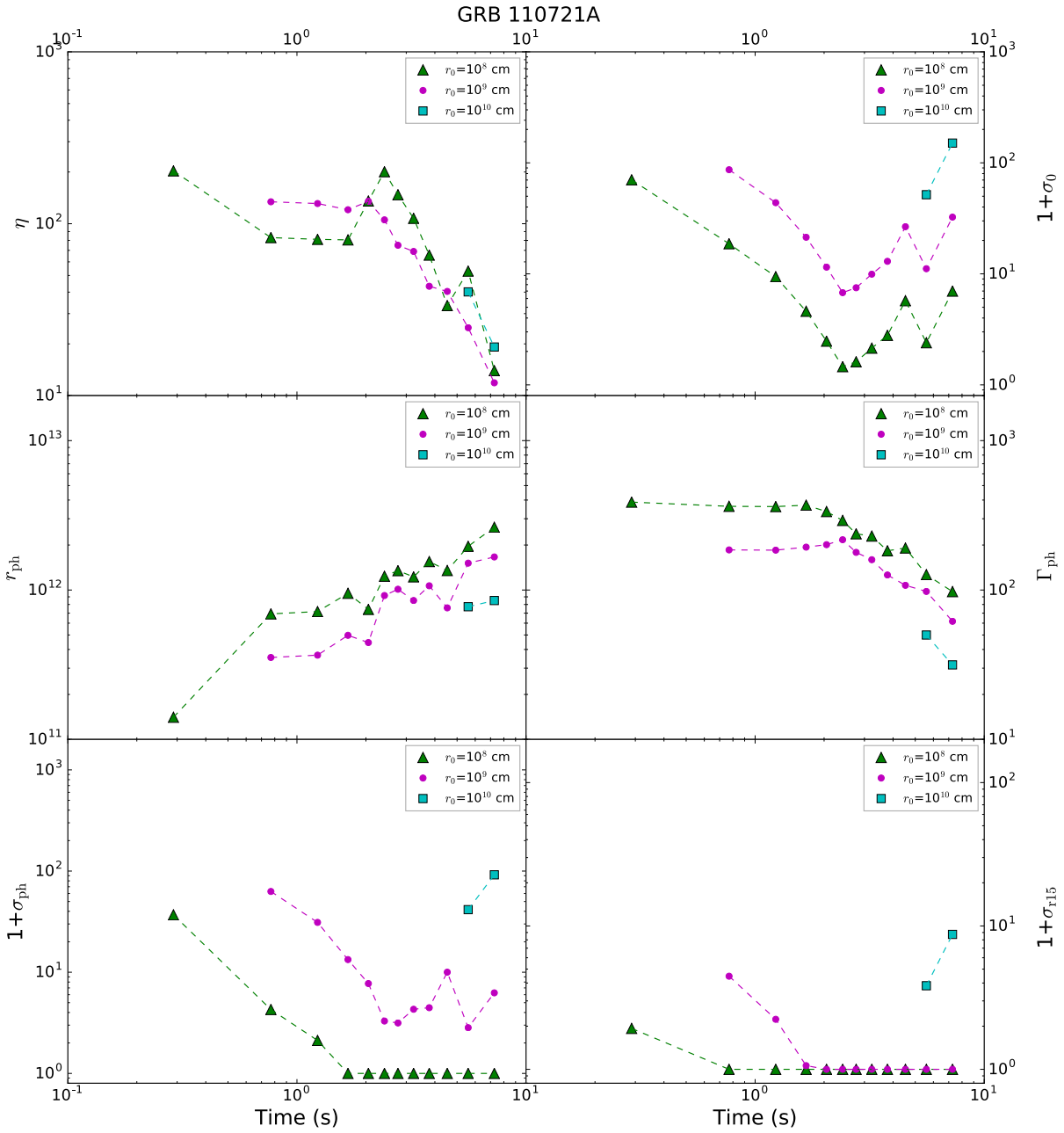

Figure A1. Same as Figure 1, but the fitted parameters are adopted from Iyyani et al. (2013). Here we notice that η is less that $\Gamma_{\rm ph}$ in some time bins, which is impossible. The reason is that the jet is still in the acceleration phase; however, we use the coasting phase to derive physical parameters.

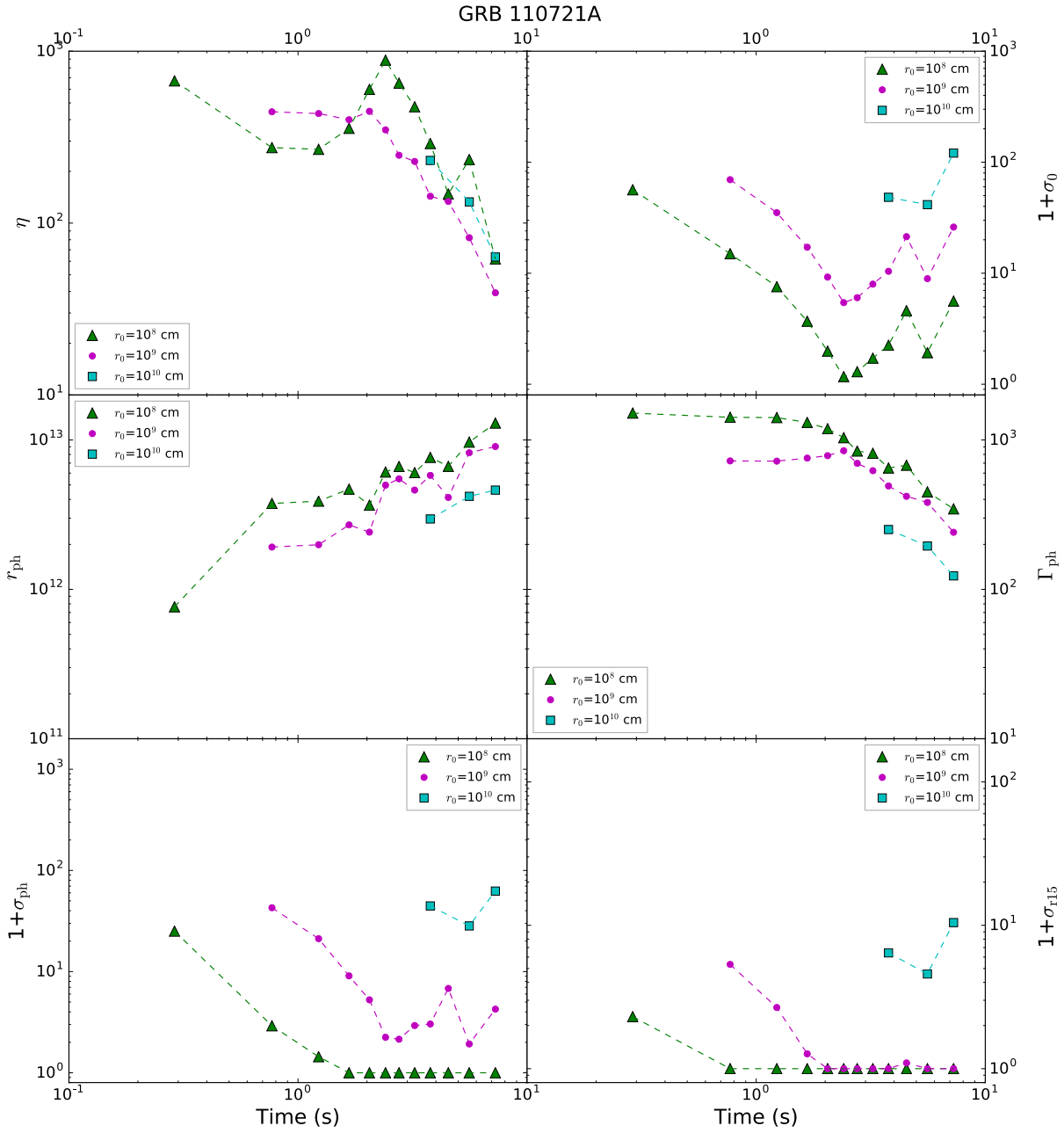

Figure A2. Same as Figure A1, but redshift is adopted z=3.512.

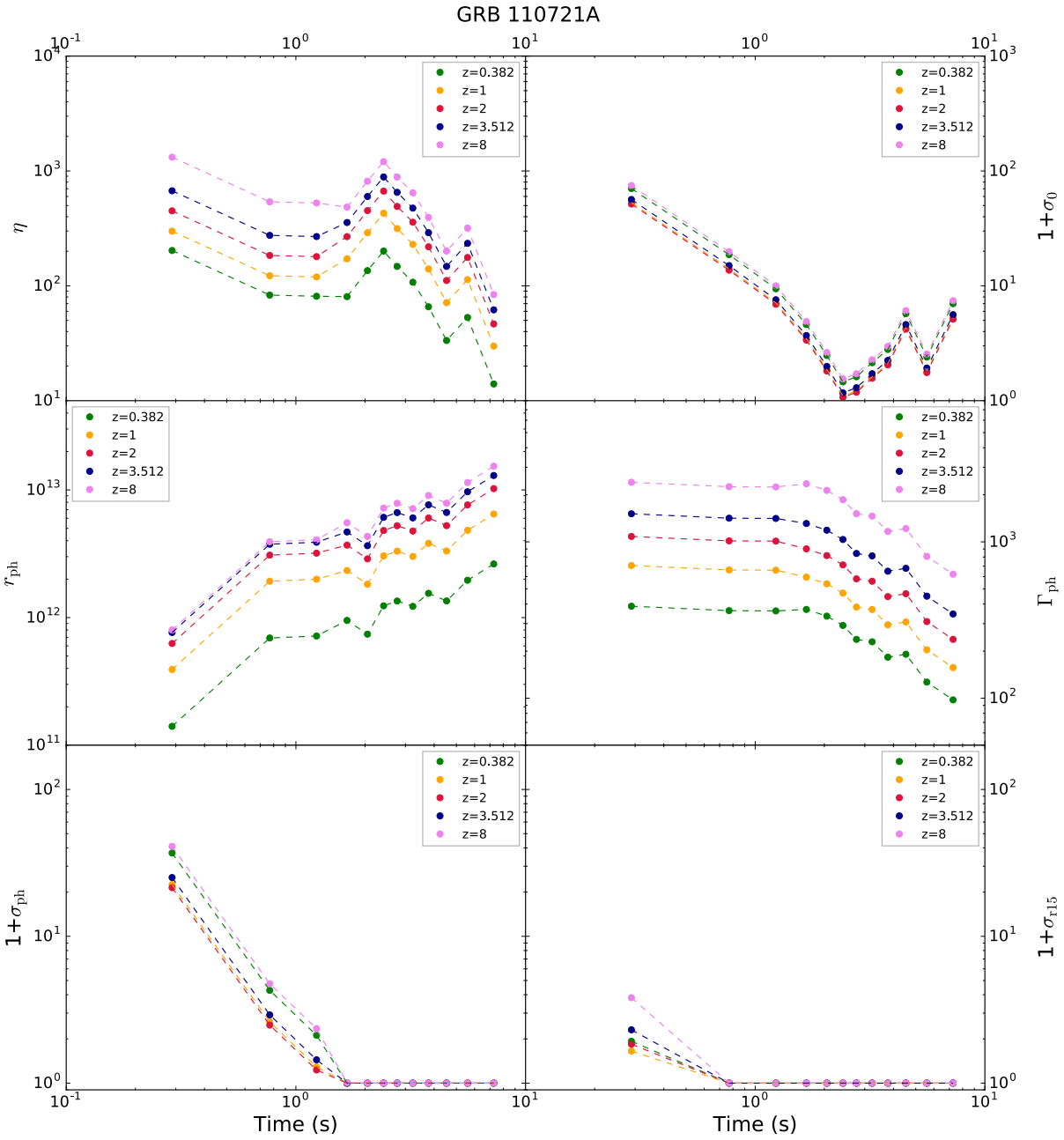

Figure A3. Comparison of the evolutional properties of the physical parameters for the hybrid jet problem with different redshifts, which is based on a typical value of r_0 ($=10^8$cm). Different colors indicate different redshift values. The fitted parameters are obtained from Iyyani et al. (2013).

Draft version March 17, 2020
Typeset using LaTeX **twocolumn** style in AASTeX62

Magnetic Fields and Afterglows of BdHNe: Inferences from GRB 130427A, GRB 160509A, GRB 160625B, GRB 180728A and GRB 190114C

J. A. Rueda,[1,2,3,4,5,6] Remo Ruffini,[1,2,3,7,8] Mile Karlica,[1,2,7] Rahim Moradi,[1,2,9] and Yu Wang[1,2,9]

[1] *ICRA, Dipartimento di Fisica, Sapienza Università di Roma, P.le Aldo Moro 5, 00185 Rome, Italy.*
[2] *ICRANet, P.zza della Repubblica 10, 65122 Pescara, Italy. yu.wang@icranet.org*
[3] *ICRANet-Rio, Centro Brasileiro de Pesquisas Físicas, Rua Dr. Xavier Sigaud 150, 22290–180 Rio de Janeiro, Brazil.*
[4] *ICRANet-Ferrara, Dipartimento di Fisica e Scienze della Terra, Università degli Studi di Ferrara, Via Saragat 1, I–44122 Ferrara, Italy*
[5] *Dipartimento di Fisica e Scienze della Terra, Università degli Studi di Ferrara, Via Saragat 1, I–44122 Ferrara, Italy*
[6] *INAF, Istituto di Astrofisica e Planetologia Spaziali, Via Fosso del Cavaliere 100, 00133 Rome, Italy.*
[7] *Université de Nice Sophia Antipolis, CEDEX 2, Grand Château Parc Valrose, Nice, France.*
[8] *INAF, Viale del Parco Mellini 84, 00136 Rome, Italy.*
[9] *INAF – Osservatorio Astronomico d'Abruzzo,Via M. Maggini snc, I-64100, Teramo, Italy. rahim.moradi@inaf.it*

ABSTRACT

GRB 190114C is the first binary-driven hypernova (BdHN) fully observed from the initial supernova appearance to the final emergence of the optical SN signal. It offers an unprecedented testing ground for the BdHN theory and it is here determined and further extended to additional gamma-ray bursts (GRBs). BdHNe comprise two subclasses of long GRBs with progenitors a binary system composed of a carbon-oxygen star (CO_{core}) and a neutron star (NS) companion. The CO_{core} explodes as a SN leaving at its center a newborn NS (νNS). The SN ejecta hypercritically accretes both on the νNS and the NS companion. BdHNe I are the tightest binaries where the accretion leads the companion NS to gravitational collapse into a black hole (BH). In BdHN II the accretion onto the NS is lower, so there is no BH formation. We observe the same structure of the afterglow for GRB 190114C and other selected examples of BdHNe I (GRB 130427A, GRB 160509A, GRB 160625B) and for BdHN II (GRB 180728A). In all the cases the explanation of the afterglow is reached via the synchrotron emission powered by the νNS: their magnetic fields structures and their spin are determined. For BdHNe I, we discuss the properties of the magnetic field embedding the newborn BH, inherited from the collapsed NS and amplified during the gravitational collapse process, and surrounded by the SN ejecta.

Keywords: gamma-ray bursts: general — binaries: general — stars: neutron — supernovae: general — black hole physics

1. INTRODUCTION

We first shortly review the traditional afterglow models and the possible alternatives. This task has been facilitated by the appearance of the comprehensive book by Zhang (2018). We focus on the additional results introduced since by the understanding: of the X-ray flare (Ruffini et al. 2018b), of the afterglow of GRB 130427A (Ruffini et al. 2018a), and of GRB 190114C (Ruffini et al. 2019a,b).

We first recall the well known discoveries by the Beppo-SAX satellite:

a) the discovery of the first afterglow in GRB 970228, Costa et al. 1997);

b) the consequent identification of the cosmological redshift of GRBs (GRB 970508, Metzger et al. 1997) which proved the cosmological nature of GRBs and their outstanding energetics;

c) the first clear coincidence of a long GRB with the onset of a supernova (GRB 980425/SN 1998bw, Galama et al. 1998).

Even before these discoveries, three contributions, based on first principles, formulated models for long GRBs assuming their cosmological nature and originating from a BH formation. At the time, these works expressed the point of view of a small minority. A parallel successful move was done by Paczynski and collaborators for short GRBs (Paczynski 1991, 1992; Narayan et al. 1992). The aforementioned three contributions are the following:

a) Damour & Ruffini (1975) predicted that vacuum polarization process occurring around an overcritical Kerr-Newman black hole (BH) leads toward GRB energetics of up to 10^{54} erg, linking their activities as well to the emergence of ultra-high energy cosmic rays (UHECRs);

b) the works of Rees & Meszaros (1992); Mészáros & Rees (1997) also proposed a BH as the origin of GRBs but there, an ultra-relativistic blastwave, whose expansion follows the Blandford-McKee self-similar solution, was used to explain the prompt emission phase (Blandford & McKee 1976);

c) the work of Woosley (1993) linked the GRB origin to a Kerr BH emitting an ultra-relativistic jet originating from the accretion of toroidal material onto the BH. There, it was presented the idea that for long GRBs the BH would be likely produced from the direct collapse of a massive star, a "failed" SN leading to a large BH of approximately $5M_\odot$, possibly as high as $10M_\odot$, a "collapsar".

1.1. *Traditional afterglow model originating from BH*

The paper by Damour & Ruffini (1975) has started only recently to attract attention in binary-driven hypernovae (BdHNe) in the context of the exact solution of the Einstein-Maxwell equations by Wald (1974), see section 2 for further details. The papers by Rees & Meszaros (1992); Mészáros & Rees (1997) and by Woosley (1993), on the contrary, have lead to the *traditional* GRB model. There, the afterglow is explained by assuming the synchrotron/synchrotron self-Compton (SSC) emission from accelerated electrons in the slowing down process of an ultra-relativistic blastwave of $\Gamma \sim 1000$ by the circumburst medium (Waxman & Piran 1994; Wijers et al. 1997; Sari & Piran 1995; Sari 1997; Sari et al. 1998). This has become known as the *ultra-relativistic shockwave model*. As pointed out by Zhang (2018), this ultra-relativistic blastwave model has been traditionally adopted in order to explain a vast number of observations:

(i) the X-ray afterglow including the steep and the shallow decay phases all the way to the X-ray flares (see section 2.2.2 in Zhang 2018);

(ii) the optical and the radio afterglow (see sections 2.2.3 and 2.2.4 in Zhang 2018);

(iii) the high-energy afterglow in the GeV emission (see sections 2.2.5 in Zhang 2018).

Related to the above traditional approach were the papers by Ruffini & Wilson (1975) and Blandford & Znajek (1977), which addressed the gravitational accretion of magnetized plasma of infinite conductivity into a Kerr BH. Such a gravitation-dominated accretion theory implies the need of a large magnetic field ($\sim 10^{15}$ G) and high density ($\sim 10^{12}$–10^{13} g cm^{-3}) near the last stable orbit around a $\sim 3\ M_\odot$ BH. This gravitation-dominated accretion has been commonly adopted as an input for the above-mentioned ultra-relativistic jetted emission from an accretion (at a rate $\sim 1\ M_\odot$ s^{-1}) onto Kerr BH to power a GRB of luminosity $\sim 10^{52}$ erg s^{-1}.

Since 2018, it has become clear that the three above processes do not share a common origin, and they are not related to an ultra-relativistic blastwave.

An electrodynamical accretion process of ionized plasma alternative to the gravitational-dominated accretion theory, has been announced (see companion paper Ruffini et al. 2019a), operating at density of $\sim 10^{-14}$ g cm^{-3} (see section 8).

1.2. *Role of magnetars and spinning neutron stars*

In parallel, a variety of models have been developed adopting, instead of a BH, an energy injection from various combinations of NSs and "magnetars". Dai & Lu (1998a,b); Zhang & Mészáros (2001) adopted an energy injection from a long-lasting spinning-down millisecond pulsar or a magnetar (magnetic dipole strength $\sim 10^{15}$ G). Within this approach, the shallow decay or the plateau observed at times $\sim 10^2$–10^4 s it is attributed to the energy injection by the magnetic dipole radiation (see e.g. Fan & Xu 2006; de Pasquale et al. 2007; Fan et al. 2013). The magnetar model is consistent with the so-called "internal plateaus", namely the ones which end with a very steep decay slope, which cannot be explained solely by the external shock waves. The steep drop is thus explained by the sudden decrease of the energy injection by the pulsar/magnetar engine at the characteristic life-time of magneto-dipole emission (Troja et al. 2007; Lü & Zhang 2014; Rowlinson et al. 2010, 2013; Lü et al. 2015; Li et al. 2018b). All these alternative models converge finally to the *ultra-relativistic shockwave model*. We show below how from 2018 the observations sharply constrain this model.

As we will show below, in the binary driven hypernova (BdHN) scenario, the GRB afterglow originates from mildly-relativistic expanding SN ejecta with energy injection from the newly-born NS (hereafter νNS) at its center, and from the νNS pulsar emission itself.

1.3. *The role of binary progenitors in GRBs*

Alternatively to the above models, addressing the GRB within a single progenitor scenario, fundamen-

tal papers presented a vast number of possible binary progenitors for GRBs (Fryer et al. 1999; Heger et al. 2003). Following this seminal paper, we have developed the concept of BdHN, which is recalled in Sec. 2. This model includes three different components: 1) a CO_{core} undergoing a SN explosion in presence of a binary NS companion; 2) an additional NS, indicated as a νNS, the newborn NS originating at the center of the SN, accreting the SN ejecta and giving origin to the afterglow; 3) the formation of the BH by the hypercritical accretion of the SN ejecta onto the preexisting NS companion, giving rise to the GeV emission.

Since the beginning of 2018, there have been considerable advances in the time-resolved spectral analysis of GRBs by the state-of-the-art algorithms and tools (Skilling 2004; Vianello et al. 2017). Thanks to this methodology, conceptually different from the Band function approach (see e.g. Ruffini et al. 2019b), together with an improved feedback from three-dimensional smoothed-particle-hydrodynamics (SPH) simulations (Becerra et al. 2019), three new results have followed from the BdHN analysis which question the traditional approach.

1) The explanation of the X-ray flares in the "flare-plateau-afterglow" (FPA) phase (Ruffini et al. 2018b) as originating from a BdHN observed in the orbital plane of the binary progenitor system. In particular, the observational data of soft X-ray flares in the early ($t \sim 100$ s rest-frame) FPA phase indicate that the emission arises from a mildly-relativistic system with Lorentz factor $\Gamma \sim 2$–5 (Ruffini et al. 2018b).

2) We investigated the FPA phase of GRB 130427A using the time-resolved spectral analysis on the early X-ray data (Ruffini et al. 2015, 2019c; Wang et al. 2019b). There, from the thermal emission in the FPA phase (see Fig. 7 in Ruffini et al. 2015), it was established an upper limit of ~ 0.9 c to the expansion velocity. Such a mildly-relativistic expansion of the FPA phase emitter was further confirmed in GRB 151027A (Ruffini et al. 2018c) by the soft and hard X-ray observations, and in GRB 171205A by the optical emission lines (Izzo et al. 2019). It motivated the first detailed model, applied to GRB 130427A, of the plateau-afterglow emission of the FPA phase (Ruffini et al. 2018a; Wang et al. 2019b), as arising from the synchrotron radiation by relativistic electrons within the mildly-relativistic expanding SN ejecta magnetized by the νNS.

3) One of the newest results on GRB 1901114C infers the GeV emission, originating in the traditional model at distances 10^{12}–10^{16} cm, to originate instead from electrodynamical process of BH rotational energy extraction very close to the BH horizon (Ruffini et al. 2019c). This electrodynamical process occurs in a very low-density environment of $\sim 10^{-14}$ g cm^{-3}, and leads to an energy per particle up to 10^{18} eV. This is confirmed by the simulations in the accompanying cavity generated by the BH accretion (Ruffini et al. 2019a).

All the above shows the different role in a BdHN I of three main components: the SN, the νNS and the newborn BH. In this article, we aim to further clarify, confirm and extend the explanation of the plateau-afterglow emission of the FPA phase, as powered by the SN and the νNS interaction within the BdHN scenario, following the treatment presented in Ruffini et al. (2018a); Wang et al. (2019b). We analyze the cases of GRB 130427A, GRB 180728A, GRB 160509A, GRB 160625B and GRB 190114C.

The article is organized as follows. In Sec. 2, we recall the physical and astrophysical properties of the BdHN model. In Sec. 3, we recall the observational properties of the GRBs analyzed in this work. In Sec. 4, we simulate the X-ray afterglow of the above-mentioned sources by the mild-relativistic synchrotron model and infer the magnetic field of the νNS based on the framework presented in Wang et al. (2019b). The nature of the obtained magnetic field of the νNS is discussed in Sec. 6. In Sec. 7, we discuss the possible nature of the magnetic field around the newborn BH in a BdHN. Finally, in Sec. 8 we outline our conclusions.

2. THE BINARY-DRIVEN HYPERNOVA (BDHN) SCENARIO

The BdHN model has been introduced for the explanation of long-duration gamma-ray bursts (GRBs) and it is based on the induced gravitational collapse (IGC) paradigm (Rueda & Ruffini 2012), occurring in a specific binary system which follows from a specific evolutionary path (see Fig. 1 and Fryer et al. 2014; Becerra et al. 2015; Fryer et al. 2015; Rueda et al. 2019, for details).

As Fig. 1 shows, the system starts with a binary composed of two main-sequence stars, say of 15 and 12 solar masses, respectively. At a given time, at the end of its thermonuclear evolution, the more massive star undergoes the core-collapse supernova (SN) and forms a neutron star (NS). The system then enters the X-ray binary phase. After possibly multiple common-envelope phases and binary interactions (see Fryer et al. 2014, 2015, and references therein), the hydrogen and helium envelope of the other main-sequence star are stripped, leaving exposed its core that is rich in carbon and oxygen. For short, we refer to it as carbon-oxygen core (CO_{core}) following the literature on the subject (see e.g. Nomoto et al. 1994; Filippenko et al. 1995; Iwamoto et al. 2000; Pian et al. 2006; Yoshida & Umeda 2011). The sys-

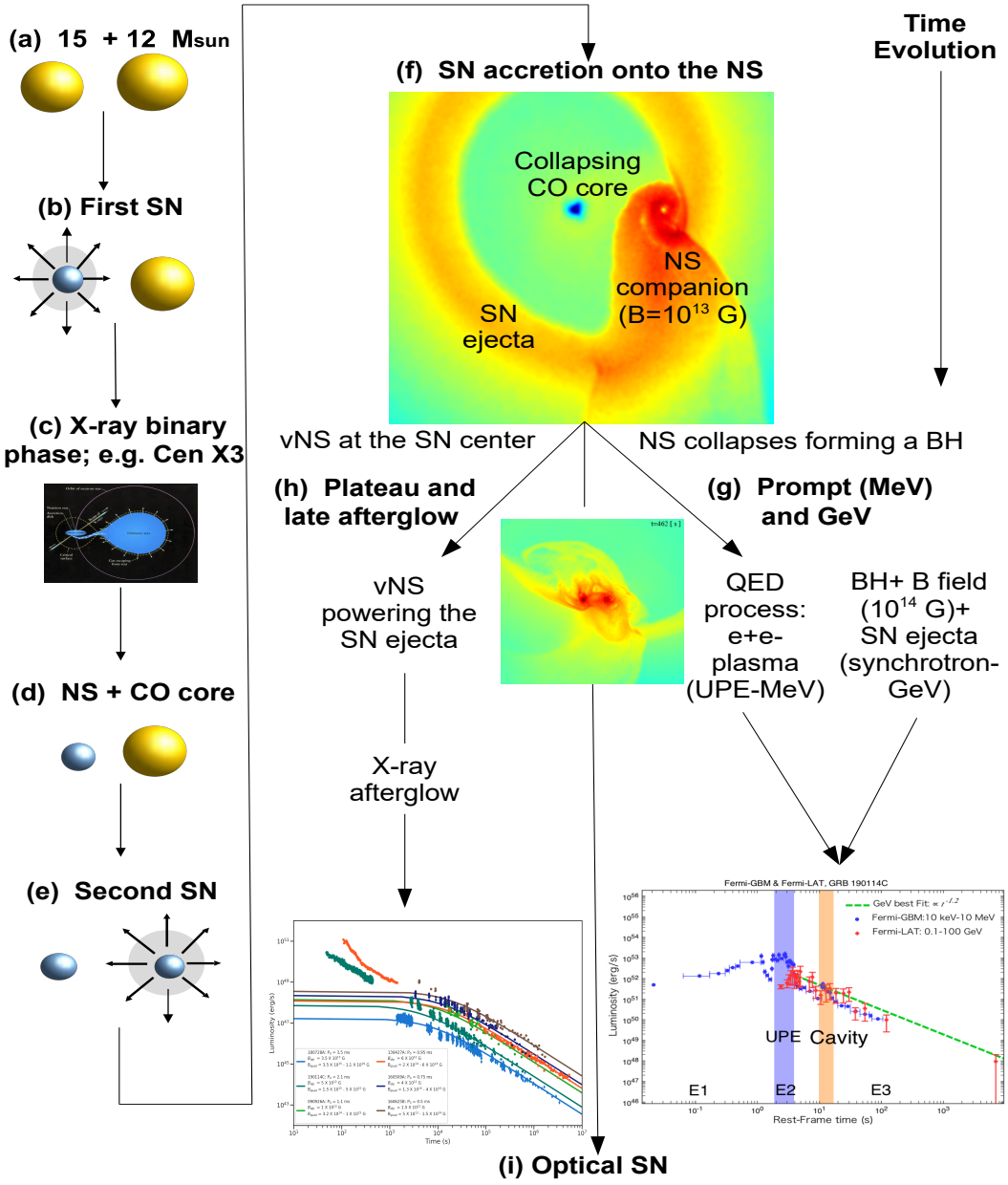

Figure 1. Schematic evolutionary path of a massive binary up to the emission of a BdHN. (a) Binary system composed of two main-sequence stars of 15 and 12 solar masses, respectively. (b) At a given time, the more massive star undergoes the core-collapse SN and forms a NS (which might have a magnetic field $B \sim 10^{13}$ G). (c) The system enters the X-ray binary phase. (d) The core of the remaining evolved star, rich in carbon and oxygen, for short CO_{core}, is left exposed since the hydrogen and helium envelope have been striped by binary interactions and possibly multiple common-envelope phases (not shown in this diagram). The system is, at this stage, a CO_{core}-NS binary, which is taken as the initial configuration of the BdHN model (Fryer et al. 2014; Becerra et al. 2015, 2016, 2019). (e) The CO_{core} explodes as SN when the binary period is of the order of few minutes, the SN ejecta of a few solar masses start to expand and a fast rotating, newborn NS, for short νNS, is left in the center. (f) The SN ejecta accrete onto the NS companion, forming a massive NS (BdHN II) or a BH (BdHN I; this example), depending on the initial NS mass and the binary separation. Conservation of magnetic flux and possibly additional MHD processes amplify the magnetic field from the NS value to $B \sim 10^{14}$ G around the newborn BH. At this stage the system is a νNS-BH binary surrounded by ionized matter of the expanding ejecta. (g) The accretion, the formation and the activities of the BH contribute to the GRB prompt gamma-ray emission and GeV emission (not the topic of this work)

.

tem at this stage is a CO_{core}-NS binary in tight orbit (period of the order of few minutes), which is taken as the initial configuration of the BdHN scenario in which the IGC phenomenon occurs (Fryer et al. 2014; Becerra et al. 2015, 2016, 2019).

We now proceed to describe the BdHN scenario. At the end of its thermonuclear evolution the CO_{core} undergoes a core-collapse SN (of type Ic in view of the hydrogen and helium absence). Matter is ejected but also a the center of the SN, a newborn NS is formed, for short referred to as νNS, to differentiate it from the accreting NS binary companion. As we shall see, this differentiation is necessary in view of the physical phenomena and corresponding observables in a BdHN associated with each of them. Owing to the short orbital period, the SN ejecta produce a hypercritical (i.e. highly super-Eddington) accretion process onto the NS companion. The material hits the NS surface developing and outward shock which creates an accretion "atmosphere" of very high density and temperature on top the NS. These conditions turn to be appropriate for the thermal production of positron-electron (e^+e^-) pairs which, when annihilating, leads to a copious production of neutrino-antineutrino ($\nu\bar{\nu}$) which turn to be the most important carriers of the gravitational energy gain of the accreting matter, allowing the rapid and massive accretion to continue. We refer to Fryer et al. (2014); Becerra et al. (2016, 2018) for details on the hypercritical accretion and the involved neutrino physics.

Depending on the specific system parameters, i.e. mass of the binary components, orbital period, SN explosion energy, etc, two possible fates for the NS are possible (see Becerra et al. (2015, 2016, 2019) for details on the relative influence of each parameter in the system). For short binary periods, i.e. $\sim$ 5 min, the NS reaches the critical mass for gravitational collapse and forms a BH (see e.g. Fryer et al. 2015; Becerra et al. 2015, 2016, 2019). We have called this kind of system a BdHN type I (Wang et al. 2019b). A BdHN I emits an isotropic energy $E_{\rm iso} \gtrsim 10^{52}$ erg and gives origin to a new binary composed by the NS formed at the center of the SN, hereafter νNS, and the BH formed by the collapse of the NS. For longer binary periods, the hypercritical accretion onto the NS is not sufficient to bring it to the critical mass and a more massive NS (MNS) is formed. We have called these systems BdHN of type II (Wang et al. 2019b) and they emit energies $E_{\rm iso} \lesssim 10^{52}$ erg. A BdHN II gives origin to a new binary composed by the νNS and the MNS.

The BdHNe I represent, in our binary classification of GRBs, the totality of long GRBs with energy larger than 10^{52} erg while, the BdHN II with their energy smaller than 10^{52} erg, are far from unique and there is a variety of long GRBs in addition to them which can have similar energetics; e.g. double white dwarf (WD-WD) mergers and NS-WD mergers (see Ruffini et al. 2016, 2018d; Wang et al. 2019b, for details).

Three-dimensional, numerical SPH simulations of BdHNe have been recently presented in Becerra et al. (2019). These simulations improve and extends the previous ones by Becerra et al. (2016). A fundamental contribution of these simulations has been to provide a visualisation of the morphology of the SN ejecta which is modified from the initial spherical symmetry. A low-density cavity is carved by the NS companion and, once its collapses, further by the BH formation process (see also Ruffini et al. 2019b). Such an asymmetric density distribution leads to a dependence of the GRB description as a function of the observer viewing angle: in the orbital/equatorial plane or in the plane orthogonal to it (Becerra et al. 2016; Ruffini et al. 2018b,c; Becerra et al. 2019) and as a function of the orbital period of the binary, in the simulation of Fig. 2 about 300 s (Ruffini et al. 2018c).

The SN transforms into a hypernova (HN) as a result of the energy and momentum transfer of the e^+e^- plasma (Ruffini et al. 2018c; Becerra et al. 2019). The SN shock breakout and the hypercritical accretion can be observed as X-ray precursors (Becerra et al. 2016; Wang et al. 2019b). The e^+e^- feedback also produces gamma- and X-ray flares observed in the early afterglow (Ruffini et al. 2018b). There is then the most interesting emission episode which is related to the νNS originated from the SN explosion. Namely, the synchrotron emission by relativistic electrons, injected from the νNS pulsar emission into the HN ejecta in presence of the νNS magnetic field, explain the X-ray afterglow and its power-law luminosity (Ruffini et al. 2018a; Wang et al. 2019b). Finally, the HN is observed in the optical bands few days after the GRB trigger, powered by the energy release of the nickel decay.

Figure 1 and Table 1 summarize the above correspondence between the BdHN physical process and each GRB observable, emphasizing the role of each component of the binary system. We also refer the reader to Rueda et al. (2019), and references therein, for a recent review on the physical processes at work and related observables in BdHNe I and II.

3. GRBS (BDHNE I) OF THE PRESENT WORK

GRB 130427A is one of the best observed GRBs, it locates at redshift $z \sim 0.34$ (Levan et al. 2013), more than 50 observatories participated the observation. It hits the record of the brightness in the gamma-ray emission, so

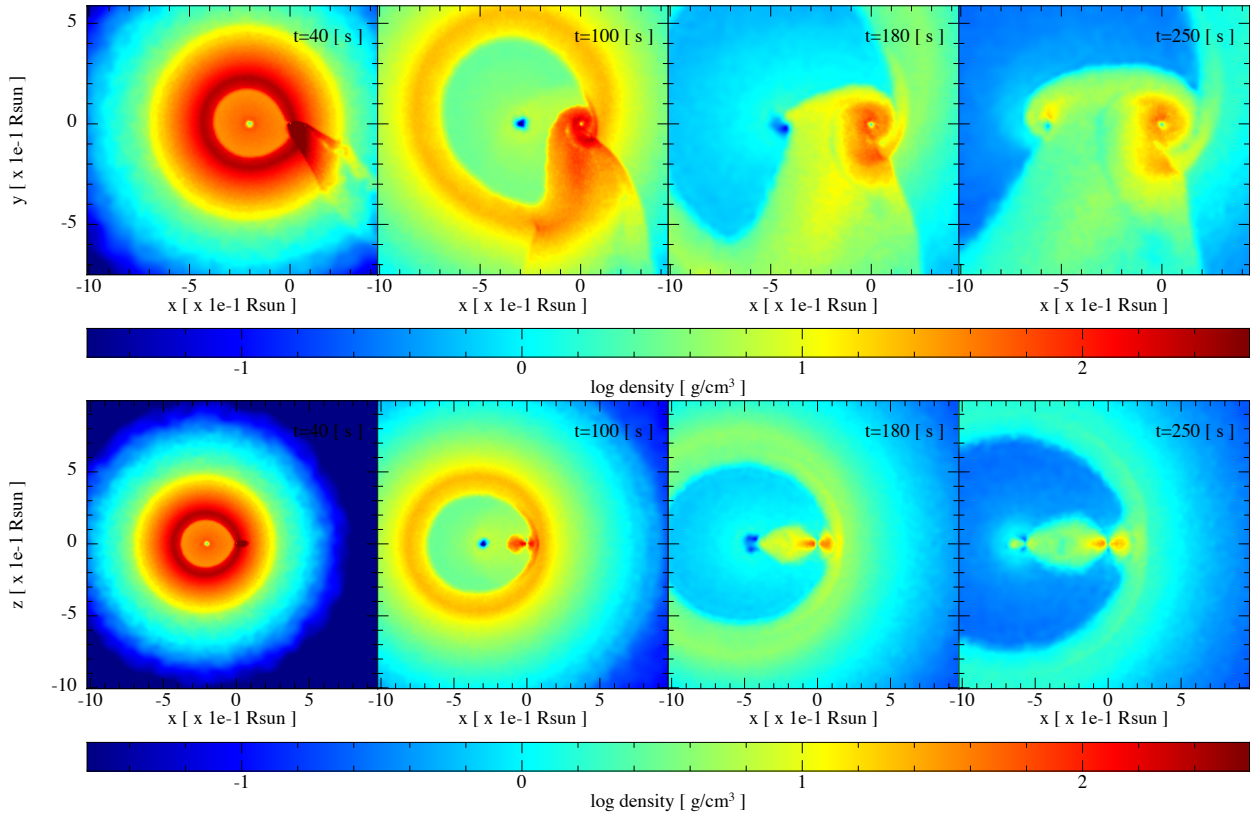

Figure 2. SPH simulation of a BdHN I: model '25M1p1e' of Table 2 in Becerra et al. (2019). The binary progenitor is composed of a CO_{core} of $\approx 7\ M_\odot$ produced by a zero-age main-sequence star (ZAMS) star of $25\ M_\odot$ (see Table 1 in Becerra et al. 2019), and a $2\ M_\odot$ NS companion. The orbital period is ≈ 5 min. Each frame, from left to right, corresponds to selected increasing times being $t = 0$ s the instant of the SN shock breakout. The upper panel shows the mass density on the equatorial plane and the lower panel the plane orthogonal to the equatorial one. The reference system is rotated and translated to align the x-axis with the line joining the binary components. The origin of the reference system is located at the NS companion position. The first frame corresponds to $t = 40$ s and it shows that the particles entered into the NS capture region forms a tail behind it. These particles then circularize around the NS forming a thick disk which is already visible in the second frame at $t = 100$ s. Part of the SN ejecta is also attracted by the νNS accreting onto it; this is appreciable in the third frame at $t = 180$ s. At $t = 250$ s (about one orbital period), a disk structure has been formed around the νNS and the NS companion. To guide the eye, the νNS is at the x-coordinate: -2.02, -2.92, -3.73 and -5.64 for $t = 40$ s, 100 s, 180 s and 250 s, respectively. This figure has been produced with the *SNsplash* visualization program (Price 2011). The figure has been taken from Becerra et al. (2019) with the permission of the authors.

that Fermi-GBM was saturated. It also hits the record of GeV observation with more that 500 photons above 100 MeV received, and the GeV emission observed till $\sim 10^4$ s (Ackermann et al. 2014).

The shape of its prompt emission consists a ~ 3 s precursor, followed by a multipeaked pulse lasting ~ 10 s. At time ~ 120 s, an additional flare appears, then it enters the afterglow (Maselli et al. 2014). The X-ray afterglow is observed by Swift and NuStar. Swift covers discretely from ~ 150 s to $\sim 10^7$ s (Li et al. 2015), and NuStar observes three epochs, starting approximately 1.2, 4.8 and 5.4 days, for observational duration 30.5, 21.2, and 12.3 ks (Kouveliotou et al. 2013). The power-law decay index of the late time afterglow after ~ 2000 s gives ~ -1.32 (Ruffini et al. 2015).

The optical spectrum reveals that 16.7 days after the GRB trigger, a typical of SNe Ic emerges (Xu et al. 2013; Li et al. 2018a), as predicted by Ruffini et al. (2013).

GRB 160509A, at redshift $z \sim 1.17$ (Tanvir et al. 2016), is a strong source of GeV emission, including a 52 GeV photon arriving at 77 s, and a 29 GeV photon arriving ~ 70 ks (Laskar et al. 2016).

GRB 160509A consists of two emission periods, $0-40$ s and $280 - 420$s (Tam et al. 2017). The first period exhibits a single pulse structure for sub-MeV emission, and a double pulses structure for ~ 100 MeV emission. The second period is in the sub-MeV energy range with double pulses structure. Swift-XRT started the observation ~ 7000 s after the burst, with a shallow power-law decay

Table 1. Summary of the GRB observables associated with each BdHN I component and physical phenomena.

BdHN component/phenomena	GRB observable				
	X-ray precursor	Prompt (MeV)	GeV-TeV emission	X-ray flares early afterglow	X-ray plateau and late afterglow
SN breakout[a]	⊗				
Hypercritical accretion onto the NS[b]	⊗				
e^+e^- from BH formation: transparency in low baryon load region[c]		⊗			
Inner engine: newborn BH + B-field+SN ejecta[d]			⊗		
e^+e^- from BH formation: transparency in high baryon load region (SN ejecta)[e]				⊗	
Synchrotron emission by νNS injected particles on SN ejecta[f]					⊗
νNS pulsar-like emission[f]					⊗

References—[a]Wang et al. (2019b),[b]Fryer et al. (2014); Becerra et al. (2016); Rueda et al. (2019),[c]Bianco et al. (2001),[d]Ruffini et al. (2018e, 2019c,b,a), [e]Ruffini et al. (2018b), [f]Ruffini et al. (2018a); Wang et al. (2019b) and this work.

of index ~ -0.6, followed by a normal decay of power-law index ~ -1.45 after 5×10^4 s (Tam et al. 2017; Li et al. 2018b).

There is no supernova association reported, the optical signal of supernova can hardly be confirmed for GRBs with redshift > 1, since the absorption is intense (Woosley & Bloom 2006).

GRB 160625B, at redshift 1.406 (Xu et al. 2016), is a bright GRB with the speciality that the polarisation has been detected. Fermi-LAT has detected more than 300 photons with energy > 100 MeV (Lü et al. 2017).

The gamma-ray light curve has three distinct pulses (Li 2019; Zhang et al. 2018). The first short pulse is totally thermal, it lasts ~ 2 s; the second bright pulse starts from ~ 180 s and ends at ~ 240 s; the last weak pulse emerges from ~ 330 s and lasts ~ 300 s. The total isotropic energy reaches $\sim 3 \times 10^{54}$ erg (Alexander et al. 2017; Lü et al. 2017).

Swift-XRT starts the observation at late time ($> 10^4$ s), a power-law behaviour with decaying index ~ -1.25.

There is no supernova confirmation, possibly it is due to the redshift > 1 (Woosley & Bloom 2006).

GRB 190114C, at redshift $z \sim 0.42$ (Selsing et al. 2019), is the first GRB with TeV photon detection by MAGIC (Mirzoyan et al. 2019; MAGIC Collaboration et al. 2019). It has twin features as GRB 130427A (Wang et al. 2019a), and it caught great attention as well.

The prompt emission of GRB 190114C starts by a multipeaked pulse, its initial ~ 1.5 s is non-thermal, then followed by a possible thermal emission till ~ 1.8 s. The confident thermal emission exists during the peak of the pulse, from $2.7 - 5.5$ s. The GeV emission starts from 2.7 s, initiated with a spiky structure, then follows a power-law decay with index ~ -1.2 (Ruffini et al. 2019b). The GeV emission is very luminous, more than 200 photons with energy > 100 MeV are received. The X-ray afterglow observed by Swift-XRT shows a persistent power-law decay behaviour, with decaying index ~ 1.35 (Wang et al. 2019a).

An continuous observational campaign lasting ~ 50 days unveiled the SN emergence at ~ 15 days after the GRB (Melandri et al. 2019), which is consistent with the prediction of 18.8 ± 3.7 days after the GRB by Ruffini et al. (2019d).

4. X-RAY AFTERGLOW OF GRB AND MAGNETIC FIELD OF νNS

The newborn NS at the center of the SN, i.e the νNS, ejects high-energy particles as in traditional pulsar models. This means that these particles escape from the νNS magnetosphere through the so-called "open" magnetic field lines, namely the field lines which cannot close within the light cylinder radius that determines the size of the co-rotating magnetosphere. Those particles interact with the SN ejecta, which by expanding in the νNS magnetic field, produce synchrotron radiation which we discuss below. Hence, the acceleration mechanism is similar to the one occurring in traditional SN remnants but with two main differences in our case: 1) we have a ~ 1 ms νNS pulsar powering the SN ejecta and 2) the SN ejecta are at a radius $\sim 10^{12}$ cm at the beginning of the afterglow, at rest-frame time $t \sim 100$ s, since the SN expands with velocity $\sim 0.1\,c$.

The above distance is well beyond the light cylinder radius, so it is expected that only the toroidal component of the magnetic field, which decreases as $1/r$ (see

Eqs. 4 and 12), survives (see, e.g., Goldreich & Julian 1969, for details). Therefore, the relevant magnetic field for the synchrotron radiation in the afterglow is the one of the νNS which is stronger (as shown below at that distance is of the order of 10^5 G) that the one possibly produced inside the remnant by dilute plasma currents, unlike the traditional models for the emission of old ($\gtrsim 1$ kyr) SN remnants.

In Ruffini et al. (2018a) and Wang et al. (2019b), we simulate the afterglow by the synchrotron emission of electrons from the optically thin region of the SN ejecta, that expands mildly-relativistic in the νNS magnetic field. The FPA emission at times $t \gtrsim 10^2$ s has two origins: the emission before the plateau phase ($\sim 5\times10^3$ s) is mainly contributed by the remaining kinetic energy of the SN ejecta, and at later times, the continuous energy injection from the νNS takes over the dominance. We extend the same approach in this paper to the GRBs of section 3.

To fully follow the temporal behaviour of radiation spectra, it is necessary to solve the kinetic equation for the electron distribution in the transparent region of the SN ejecta:

$$\frac{\partial N(\gamma,t)}{\partial t} = \frac{\partial}{\partial\gamma}(\dot{\gamma}(\gamma,t)N(\gamma,t)) + Q(\gamma,t)\,, \qquad (1)$$

where $N(\gamma,t)$ is the electron number distribution as a function of electron energy $\gamma = E/m_ec^2$, $\dot{\gamma}(\gamma,t)$ is the electron energy loss rate normalized to the electron rest-mass, $Q(\gamma,t) = Q_0(t)\gamma^{-p}$ is the particle injection rate, assumed to be a the power-law of index p, so the electrons injected are within the energy range of $\gamma_{\rm min}$ and $\gamma_{\rm max}$. The total injection luminosity $L_{\rm inj}(t)$ is provided by the kinetic energy of the SN and the rotational energy of the νNS, here parametrized via the power-law injection power

$$L_{\rm inj}(t) = \int_{\gamma_{\rm min}}^{\gamma_{\rm max}} Q(\gamma,t)d\gamma \simeq L_0\left(1+\frac{t}{\tau_0}\right)^{-k}, \qquad (2)$$

where L_0, k and τ_0 are assessed by fitting of the light curve data. The major energy loss is considered as the adiabatic energy loss and the synchrotron energy loss

$$\dot{\gamma}(\gamma,t) = \frac{\dot{R}(t)}{R(t)}\gamma + \frac{4}{3}\frac{\sigma_T}{m_ec}\frac{B(t)^2}{8\pi}\gamma^2\,, \qquad (3)$$

where $R(t)$ is the size of emitter, σ_T is the Thomson cross section and $B(t)$ is the magnetic field strength expected to have toroidal configuration given by

$$B(t) = B_0\left(\frac{R(t)}{R_0}\right)^{-1}, \qquad (4)$$

here B_0 is the magnetic field strength at the distance R_0. The final bolometric synchrotron luminosity from this system gives

$$L_{\rm syn}(\nu,t) = \int_1^{\gamma_{\rm max}} N(\gamma,t)P_{\rm syn}(\nu,\gamma,B(t))d\gamma\,. \qquad (5)$$

As we have introduced in section 1, the thermal emission during the FPA phase indicates a mildly-relativistic velocity $\sim 0.5-0.9\ c$ at time ~ 100 s (Ruffini et al. 2015, 2018b, 2019c; Wang et al. 2019b). We adopt this value as the initial velocity and radius of the transparent part of SN ejecta.

For later stages at around 10^6 s, when a sizable front shell of SN ejecta becomes transparent, we adopt the velocity of $\sim 0.1\ c$ obtained through observations of Fe II emission lines (see e.g. Xu et al. 2013). We make the simplest assumption of a uniformly decelerating expansion during the time interval $10^2 \lesssim t \lesssim 10^6$ s. The SN ejecta remains in the coasting phase for hundreds of years (see e.g. Sturner et al. 1997), therefore, we adopt a constant velocity from 10^6 s till 10^7 s.

Following the above discussion and our data analysis, we describe the expansion velocity, as

$$\dot{R}(t) = \begin{cases} v_0 - a_0\,t & 10^2 < t < 10^6{\rm s} \\ v_f & 10^7 > t > 10^6{\rm s} \end{cases} \qquad (6)$$

with typical value $v_0 = 2.4\times10^{10}$ cm s^{-1}, $a_0 = 2.1\times10^4$ cm s^{-2} and $v_f = 3\times10^9$ cm s^{-1}.

It is appropriate to clarify how the model parameters presented in this table are obtained: R_0 and τ_0 are fixed by the observed thermal component at around 10^2 s, from which we obtain the radius and expansion velocity of the SN front. The minimum and maximum energy of the injected electrons, $\gamma_{\rm min}$ and $\gamma_{\rm max}$, are fixed once B is given. L_0 is fixed by a normalization of the observed source luminosity. The power-law index of the energy injection rate, p, is fixed to the value $p = 3/2$. The parameter k is fixed to produce the power-law decay of the late time X-ray data. Therefore, the "free parameter" to be obtained is B_0.

In Ruffini et al. (2018a), we have given detailed fitting parameters and figures of GRB 130427A. In this article, we additionally fit GRB 160625B and confirm that the mildly relativistic model is capable of producing GRBs afteglow. As it is shown in Table 2 and Fig. 3, our model fits very well the optical and the X-ray spectrum but not the GeV data. This is in agreement with the BdHN paradigm since the GeV emission is expected to be explained from the newborn BH activity and not from the νNS one (Ruffini et al. 2019c). On the other hand,

Table 2. Parameters used for simulation of GRB 160625B.

Parameter	Value
B_0	1.0×10^6 G
R_0	1.2×10^{11} cm
L_0	8.44×10^{52} erg/s
k	1.42
τ_0	5.0×10^0 s
p	1.5
$\gamma_{\rm min}$	4.0×10^3
$\gamma_{\rm max}$	1.0×10^6

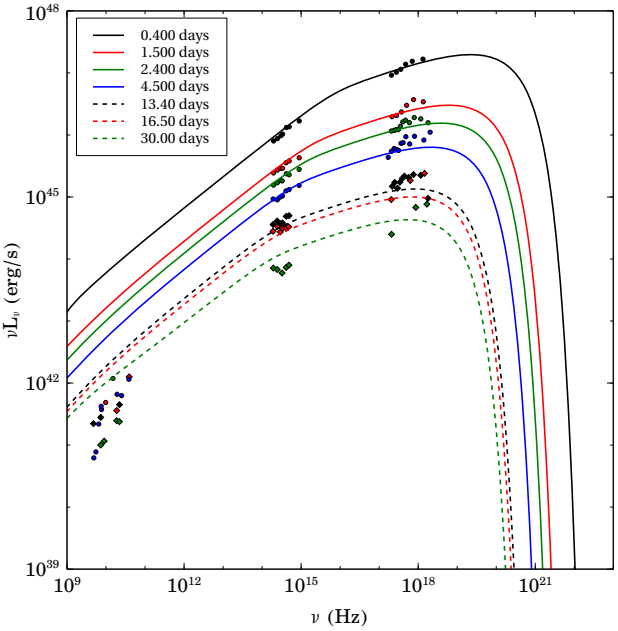

Figure 3. Model evolution of synchrotron spectral luminosity at various times compared with measurements in various spectral bands for GRB 160625B.

radio data show lack of expected flux which comes from synchrotron self-absorption processes which are rather complicated to model in current numerical framework but can be thoroughly neglected at frequencies above 10^{14} Hz.

Comparing the fitting parameters, GRB 130427A and GRB 160625B are similar except the constant of injection power L_0 (see Eq. 2). Such similarities can be extented to other ones. It can be seen from Fig. 4, that taking everything else as similar, from magnetic field strength and structure to expansion evolution, the GRB 190114C simulated light curve at the relevant times, can be obtained from the one of GRB 130427A, by scaling L_0 a factor of 1/5.

The injection power index $k \sim 1.5$ from the fitting suggests that the quadruple emission from a pulsar dominates the late-time afterglow. As we will see below, the complementary analysis allows to infer the initial rotation period of the νNS as well as an independent estimate of its magnetic field structure.

Being just born, the νNS must be rapidly rotating and as such it contains abundant rotational energy:

$$E = \frac{1}{2} I \Omega^2, \tag{7}$$

where I is the moment of inertia, and $\Omega = 2\pi/P_{\nu\rm NS}$ is the angular velocity. For a millisecond νNS and $I \sim 10^{45}$ g cm^2, the total rotational energy $E \sim 2 \times 10^{52}$ erg. Assuming that the rotational energy loss is driven by magnetic dipole and quadruple radiation we have:

$$L_{\rm NS}(t) = \frac{dE}{dt} = -I\Omega\dot{\Omega}$$
$$= -\frac{2}{3c^3}\Omega^4 B_{\rm dip}^2 R_{\nu\rm NS}^6 \sin^2\chi_1 \left(1 + \eta^2 \frac{16}{45}\frac{R_{\nu\rm NS}^2\Omega^2}{c^2}\right), \tag{8}$$

where

$$\eta^2 = (\cos^2\chi_2 + 10\sin^2\chi_2)\frac{B_{\rm quad}^2}{B_{\rm dip}^2}, \tag{9}$$

with χ_1 and χ_2 the inclination angles of the magnetic moment, $B_{\rm dip}$ and $B_{\rm quad}$ are the dipole and quadruple magnetic field, respectively. The parameter η measures the quadruple to dipole magnetic field strength ratio.

Figure 5 shows the bolometric light curves ($\sim$ 5 times brighter than the Swift-XRT light curves inferred from the fitting) of GRB 160625B, 160509A, 130427A, 190114C and 180728A, respectively. We show the νNS luminosities $L_{\rm NS}(t)$ fit the light curves. We report the fitting νNS parameters: dipole ($B_{\rm dip}$) and quadrupole ($B_{\rm quad}$) magnetic field component, initial rotation period ($P_{\nu\rm NS}$) and assuming a νNS of mass and radius, respectively, $1.4M_\odot$ and 10^6 cm. The results are also summarized in Table 3. It becomes also clear from this analysis that the solely νNS emission is not able to explain the emission of the FPA phase at early times 10^2–10^3 s. As we have shown, that emission is mainly powered by the mildly-relativistic SN kinetic energy.

5. A SELF-CONSISTENCY CHECK

Having estimated the magnetic field structure and the rotation period of the νNS from the fit of the data of the FPA phase at times 10^2–10^7 s, we can now assess their self-consistency with expected values within the BdHN scenario.

First, let us adopt the binary as tidally locked, i.e. the rotation period of the binary components is synchronized with the orbital period. This implies that the

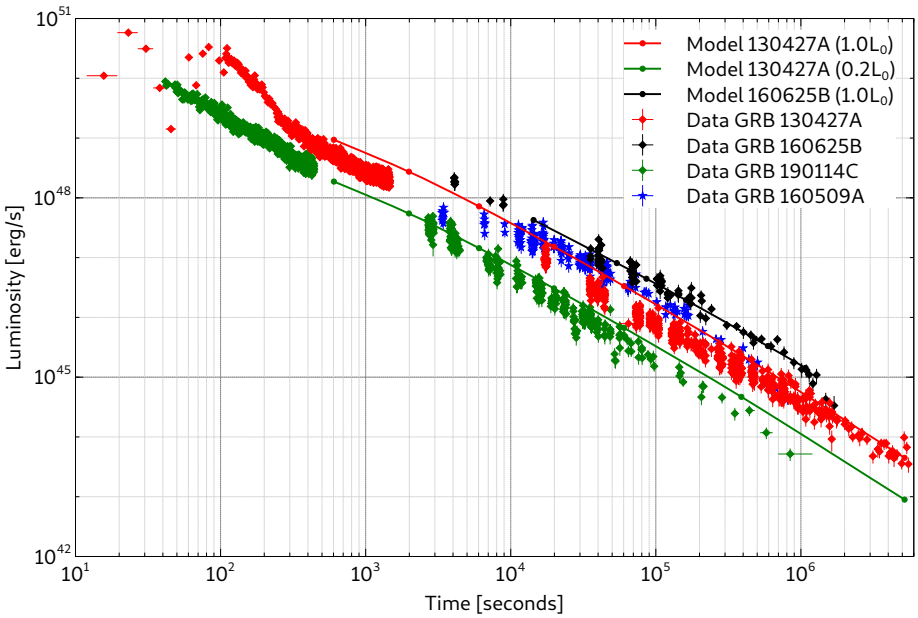

Figure 4. X-ray light-curve of GRB 160625B, GRB 130427A, GRB 190114C and GRB 160509A (black, red and green diamonds and blue stars with error bars respectively). Simulated synchrotron light curves in Swift X-ray band are shown for GRB 160625B (black line) and GRB 130427A (red line). It is also shown how, by scaling the injection power by a factor 1/5, the light curve of GRB 130427A scales down (from the red line to the green one) fitting the data of GRB 190114C

.

Table 3. Observational properties of the GRB and inferred physical quantities of the νNS of the corresponding BdHN model that fits the GRB data. Column 1: GRB name; column 2: identified BdHN type; column 3: the isotropic energy released ($E_{\rm iso}$) in gamma-rays; column 4: cosmological redshift (z); column 5: νNS rotation period ($P_{\nu\rm NS}$), column 6: νNS rotational energy ($E_{\rm rot}$); columns 7 and 8: strength of the dipole ($B_{\rm dip}$) and quadrupole ($B_{\rm quad}$) magnetic field components of the νNS. The quadruple magnetic field component is given in a range that the upper limit is three times than the lower limit, this is brought by the freedom of inclination angles of the magnetic moment. During the fitting, we consistently assume the NS mass of $1.4M_\odot$ and the NS radius of 10^6 cm for all these three cases. The fitted light-curves are shown in Fig. 5, the parameters of GRB 1340427A and 180728A are taken from Wang et al. (2019b).

GRB	Type	Redshift	$E_{\rm iso}$ (erg)	$P_{\nu\rm NS}$ (ms)	$E_{\rm rot}$ (erg)	$B_{\rm dip}$ (G)	$B_{\rm quad}$ (G)
130427A	BdHN I	0.34	1.40×10^{54}	0.95	3.50×10^{52}	6.0×10^{12}	$2.0\times10^{13}\sim6.0\times10^{14}$
160509A	BdHN I	1.17	1.06×10^{54}	0.75	5.61×10^{52}	4.0×10^{12}	$1.3\times10^{14}\sim4.0\times10^{14}$
160625B	BdHN I	1.406	3.00×10^{54}	0.5	1.26×10^{53}	1.5×10^{12}	$5.0\times10^{13}\sim1.6\times10^{14}$
190114C	BdHN I	0.42	2.47×10^{53}	2.1	7.16×10^{51}	5.0×10^{12}	$1.5\times10^{15}\sim5.0\times10^{15}$
180728A	BdHN II	0.117	2.73×10^{51}	3.5	2.58×10^{51}	1.0×10^{13}	$3.5\times10^{15}\sim1.1\times10^{16}$

rotation period of the $\rm CO_{core}$ is $P_{\rm CO}=P$, where P denotes the orbital period. From the Kepler law the value of P is connected to the orbital separation $a_{\rm orb}$ and with the binary mass as:

$$P_{\rm CO}=P=2\pi\sqrt{\frac{a_{\rm orb}^3}{GM_{\rm tot}}}, \tag{10}$$

where G is the gravitational constant and $M_{\rm tot}=M_{\rm CO}+M_{\rm NS}$ is the total mass of the binary, where $M_{\rm CO}$ and $M_{\rm NS}$ are the masses of the $\rm CO_{core}$ and the NS companion, respectively. Thus, $M_{\rm CO}=M_{\rm Fe}+M_{\rm ej}$ with $M_{\rm Fe}$ and $M_{\rm ej}$ the masses of the iron core (which collapses and forms the νNS) and the ejected mass in the SN event, respectively.

The mass of the νNS is $M_{\nu\rm NS}\approx M_{\rm Fe}$. The rotation period, $P_{\nu\rm NS}$, is estimated from the one of the iron core, $P_{\rm Fe}$, by applying the angular momentum conservation in the collapse process, i.e.:

$$P_{\nu\rm NS}=\left(\frac{R_{\nu\rm NS}}{R_{\rm Fe}}\right)^2 P, \tag{11}$$

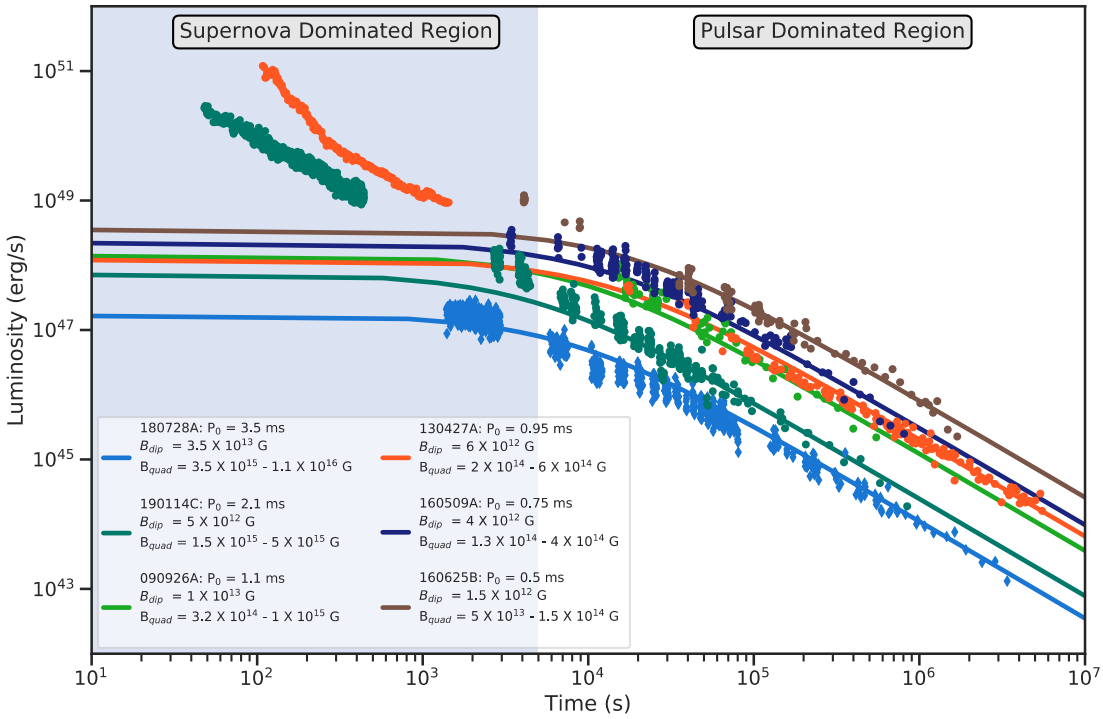

Figure 5. The brown, deep blue, orange, green and bright blue points correspond to the bolometric (about ~ 5 times brighter than the soft X-ray observed by Swift-XRT inferred from the fitted sychrotron spectrum) light curves of GRB 160625B, 160509A, 130427A, 190114C and 180728A, respectively. The lines are the fitting of the energy injection from the rotational energy of the pulsar. The pulsar powers the late afterglow ($t \gtrsim 5 \times 10^3$ s, white background), while in the earlier time ($t \lesssim 5 \times 10^3$ s, dusty blue background), the remaining kinectic energy of the SN ejecta plays the leading role.

The fitted parameters are shown in the legend and in Table 3, the quadruple field are given in a range, its upper value is 3 times the lower value, this is due to the oscillation angle χ_2, which is a free parameter. The fittings of GRB 1340427A and 180728A are reproduced from Wang et al. (2019b).

where $R_{\nu\rm NS}$ and $R_{\rm Fe}$ are the radius of the νNS and of the iron core, respectively, and we have assumed that the pre-SN star has uniform rotation; so $P_{\rm Fe} = P_{\rm CO} = P$.

Without loss of generality, in our estimates we can adopt a νNS order-of-magnitude radius of 10^6 cm. As we shall see below, a more careful estimate is the one of the $\rm CO_{core}$ progenitor (which tell us the radius of the iron core) and the orbital period/binary separation which affect additional observables of a BdHN.

It is instructive to appreciate the above statement with specific examples; for which we use the results of Wang et al. (2019b) for two BdHN archetypes: GRB 130427A for BdHN I and GRB 180827A for BdHN II. Table 3 shows, for the above GRBs, as well as for GRB 190114C, GRB 160625B and GRB 160509A, some observational quantities (the isotropic energy released $E_{\rm iso}$ and the cosmological redshift), the inferred BdHN type and the properties of the νNS (rotation period $P_{\nu\rm NS}$, rotational energy and the strength of the dipole and quadrupole magnetic field components).

By examining the BdHN models simulated in Becerra et al. (2019) (see e.g. Table 2 there), we have shown in Wang et al. (2019b) that the Model '25m1p08e' fits the observational requirements of GRB 130427A, and the Model '25m3p1e' the ones of GRB 180827A. These models have the same binary progenitor components: the $\approx 6.8\ M_\odot$ $\rm CO_{core}$ ($R_{\rm Fe} \sim 2 \times 10^8$ cm) developed by a $25 M_\odot$ ZAMS star (see Table 1 in Becerra et al. 2019) and a $2\ M_\odot$ NS companion. For GRB 130427A the orbital period is $P = 4.8$ min (binary separation $a_{\rm orb} \approx 1.3 \times 10^{10}$ cm), resulting in $P_{\nu\rm NS} \approx 1.0$ ms while, for GRB 180827A, the orbital period is $P = 11.8$ min ($a_{\rm orb} \approx 2.6 \times 10^{10}$ cm) so a less compact binary, which leads to $P_{\nu\rm NS} \approx 2.5$ ms.

We turn now to perform a further self-consistency check of our picture. Namely, we make a cross-check of the estimated νNS parameters obtained first from the early afterglow via synchrotron emission, and then from the late X-ray afterglow via the pulsar luminosity, with respect to expectations from NS theory.

Up to factors of order unity, the surface dipole B_s and the toroidal component B_t at a distance r from the surface are approximately related as (see, e.g., Goldreich & Julian 1969))

$$B_t \approx \left(\frac{2\pi R_{\nu\rm NS}}{cP_{\nu\rm NS}}\right)^2 \left(\frac{R_{\nu\rm NS}}{r}\right) B_s. \quad (12)$$

Let us analyze the case of GRB 130427A. By equating Eqs. (4) and (12), and using the values of $B_0 = 5 \times 10^5$ Gauss and $R_0 = 2.4 \times 10^{12}$ cm from Ruffini et al. (2018a) obtained from the synchrotron analysis, and $P_{\nu\rm NS} = P_0 \approx 1$ ms from the pulsar activity in the late afterglow analysis, we obtain $B_s \approx 2 \times 10^{13}$ G. This value has to be compared with the one obtained from the request that the pulsar luminosity powers the late afterglow, $B_{\rm dip} = 6 \times 10^{12}$ G (see Table 3). If we use the parameters $B_0 = 1.0 \times 10^6$ Gauss and $R_0 = 1.2 \times 10^{11}$ cm from Table 2 for GRB 160625B, and the corresponding $P_{\nu\rm NS} = P_0 \approx 0.5$ ms, we obtain $B_s \approx 6.8 \times 10^{11}$ G, to be compared with $B_{\rm dip} \approx 10^{12}$ G (see Table 3). An even better agreement can be obtained by using a more accurate value of the νNS radius which is surely bigger than the fiducial value $R_{\nu\rm NS} = 10^6$ cm we have used in these estimates.

6. NATURE OF THE DIPOLE+QUADRUPOLE MAGNETIC FIELD STRUCTURE OF THE νNS

We attribute the spin-down energy of the νNS to the energy injection of the late-time afterglow. By fitting the observed emission through the synchrotron model, the spin period and the magnetic field of the νNS can be inferred. In Wang et al. (2019b), we have applied this approach on GRB 130427A and GRB 180728A, here we apply the same method on the recent GRB 190114C and other two, GRB 160509A and GRB 160625B, for comparison. As shown in Fig. 5, we plot the energy injection from the dipole and quadruple emission of νNS, the fitting results indicate 190114C leaves a νNS of spin period 2.1 ms, with dipole magnetic field $B_{dip} = 5 \times 10^{12}$ G, and a quadruple magnetic field $> 10^{15}$ G, the fitting parameters of all the GRBs are listed in table 3. Generally, the NS in the BdHN I system spins faster, of period $\lesssim 2$ ms, and contains more rotational energy $\gtrsim 10^{52}$ erg. We notice that GRB 160625B has the shortest initial spin period of $P = 0.5$ ms, which is exactly on the margin of the rotational period of a NS at the Keplerian sequence. For a NS of mass 1.4 $M_\odot$ and radius 12 km, its Keplerian frequence $f_{\rm K} \simeq 1900$ (Lattimer & Prakash 2004; Riahi et al. 2019), corresponding to the spin period of $P \simeq 0.5$ ms.

From Eq. (10) and (11), the orbital separation of binary system relates to the spin of νNS, $a_{\rm orb} \propto P_{\nu\rm NS}^{2/3}$. Therefore, with the knowledge of the binary separation of GRB 130427A $\sim 1.35 \times 10^{10}$ cm, the spin period of ~ 1 ms, and the newly inferred spin of GRB 190114C ~ 1.2 ms, assuming these two systems have the same mass and radius of the $\rm CO_{core}$ and the νNS, we obtain the orbital separation of GRB 190114C as $\sim 1.52 \times 10^{10}$ cm.

The self-consistent value obtained for the orbital period/separation give a strong support to our basic assumptions: 1) owing to the system compactness the binary components are tidally locked, and 2) angular momentum is conserved in the core-collapse SN process.

We would like to recall that it has been shown that purely poloidal field configurations are unstable against adiabatic perturbations; for non-rotating stars it has been first demonstrated by Wright (1973); Markey & Tayler (1973); see also Flowers & Ruderman (1977). For rotating stars similar results have been obtained, e.g., by Pitts & Tayler (1985). In addition, Tayler (1973) has shown that purely toroidal configurations are also unstable. We refer the reader to Spruit (1999) for a review on the different possible instabilities that may be active in magnetic stars. In this line, the dipole-quadrupole magnetic field configuration found in our analyses with a quadrupole component dominating in the early life of the the νNS are particularly relevant. They also give support to theoretical expectations pointing to the possible stability of poloidal-toroidal magnetic field configurations on timescales longer than the collapsing time of the pre-SN star; see e.g. for details Tayler (1980); Mestel (1984).

It remains the question of how, during the process of gravitational collapse, the magnetic field increase its strength to the NS observed values. This is still one of the most relevant open questions in astrophysics which is at this stage out of the scope of the present work. We shall mention here only one important case which is the traditional explanation of the NS magnetic field strength based on the amplification of the field by magnetic flux conservation. The flux conservation implies $\Phi_i = \pi B_i R_i^2 = \Phi_f = \pi B_f R_f^2$, where i and f stand for initial and final configurations and $R_{i,f}$ the corresponding radii. The radius of the collapsing iron core is of the order of 10^8–10^9 cm while the radius of the νNS is of the order of 10^6 cm; therefore, the magnetic flux conservation implies an amplification of 10^4–10^6 times the initial field during the νNS formation. Therefore, a seed magnetic field of 10^7–10^9 G is necessary to be present in the iron core of the pre-SN star to explain a νNS magnetic field of 10^{13} G. The highest magnetic fields observed in main-sequence stars leading to the pre-SN stars of interest are of the order of 10^4 G (Spruit 2009). If the

magnetic field is uniform inside the star, then the value of the magnetic field observed in these stars poses a serious issue to the magnetic flux conservation hypothesis for the NS magnetic field genesis. A summary of the theoretical efforts to understand the possible sources of the magnetic field of a NS can be found in Spruit (2009).

7. NATURE OF THE MAGNETIC FIELD AROUND THE NEWBORN BH

The BH in a BdHN I is formed from the gravitational collapse of the NS companion of the CO_{core}, which reaches the critical mass by the hypercritical accretion of the ejecta of the SN explosion of the CO_{core}. Hence, the magnetic field surrounding the BH derived in the previous section for the explanation of the GeV emission should originate from the collapsed NS. In fact, the magnetic field of the νNS evaluated at the BH position is too low to be relevant in this discussion. As we shall see, the magnetic field inherited from the collapsed NS can easily reach values of the order of 10^{14} G. Instead, the magnetic field of the νNS at the BH site is $B_{\rm dip}\,(R_{\nu\rm NS}/a_{\rm orb})^3 = 10$ G, adopting fiducial parameters according to the results of Table 3: a dipole magnetic field at the νNS surface $B_{\rm dip} = 10^{13}$ G, a binary separation of $a_{\rm orb} = 10^{10}$ cm and a νNS radius of $R_{\nu\rm NS} = 10^6$ cm.

Having clarified this issue, we proceed now to discuss the nature of the field. Both the νNS and the NS follow an analogous formation channel, namely they are born from core-collapse SNe. In fact, to reach the BdHN stage the massive binary has to survive two SN events: the first SN which forms the NS and the second one which forms the νNS (core-collapse of the CO_{core}). Figure 1 shows the evolutionary path of a massive binary leading to a BdHN I. It is then clear that the NS companion of the CO_{core} will have magnetic field properties analogous to the ones of the νNS, and discussed in the previous section. Therefore, we can conclude that the BH forms from the collapse of a magnetized and fast rotating NS.

In this scenario, the magnetic field of the collapsing NS companion should then be responsible of the magnetic field surrounding the BH. It is needed only a modest amplification of the initial field from the NS, which is $\sim 10^{13}$ G, to reach the value of 10^{14} G around the newborn BH. Then, even the single action of magnetic flux conservation can suffice to explain the magnetic field amplification. The BH horizon is $r_+ \sim GM/c^2$, where M can be assumed to be equal to the NS critical mass, say 3 $M_\odot$, so $r_+ \approx 4.4$ km. The NS at the collapse point, owing to high rotation, will have a radius in excess of the typically adopted 10 km (Cipolletta et al. 2015); let us assume a conservative range 12–15 km. These conditions suggest that magnetic flux conservation magnifies the magnetic field in the BH formation by a factor 7–12. Therefore, a seed field of 10^{13} G present in the collapsing NS is enough to explain the magnetic field of 10^{14} G near the newborn BH.

It is worthy to clarify a crucial point: the magnetic field has to remain anchored to some NS material which guarantee its existence. It is therefore expected that some part of the NS does not take part of the BH formation. Assuming that magnetic flux is conserved during the collapse, then the magnetic energy is a constant fraction of the gravitational energy during the entire process, so only high rotation (see, e.g., Becerra et al. 2016) and some degree of differential rotation (see, e.g., Shibata et al. 2006) of the NS at the critical mass point can be the responsible of avoiding some fraction of NS matter to remain outside with sufficient angular momentum to orbit the newborn BH (see, e.g., Fig. 6).

The three-dimensional simulations of BdHNe presented in Becerra et al. (2019) show that the part of the SN ejecta surrounding the BH forms a torus-like structure around it. The aforementioned matter from the NS with high angular momentum will add to this orbiting matter around the BH. In the off-equatorial directions the density is much smaller (Ruffini et al. 2018a; Becerra et al. 2019; Ruffini et al. 2019b, see also). This implies that on the equatorial plane the field is compressed while in the axial direction the matter accretion flows in along the field lines.

Our *inner engine*, the BH+magnetic field configuration powering the high-energy emission in a BdHN I finds additional support in numerical simulations of magnetic and rotating collapse into a BH. The first numerical computer treatment of the gravitational collapse to a BH in presence of magnetic fields, starts with the pioneering two-dimensional simulations by Wilson (1975) (see Fig. 6 (a) reproduced from Wilson 1978). These works already showed the amplification of the magnetic field in the gravitational collapse process. Rotating magnetized gravitational collapse into a BH has been more recently treated with greater detail by three-dimensional simulations which have confirmed this picture and the crucial role of the combined presence of magnetic field and rotation (Dionysopoulou et al. 2013; Nathanail et al. 2017; Most et al. 2018).

Additional support can be also found in the context of the binary NS mergers. Numerical simulations have indeed shown that the collapse of the unstable massive NS formed in the merger into a BH leads to a configuration composed of a BH surrounded by a nearly collimated magnetic field and an accretion disk (see Duez et al. 2006a; Shibata et al. 2006; Duez et al. 2006b; Stephens

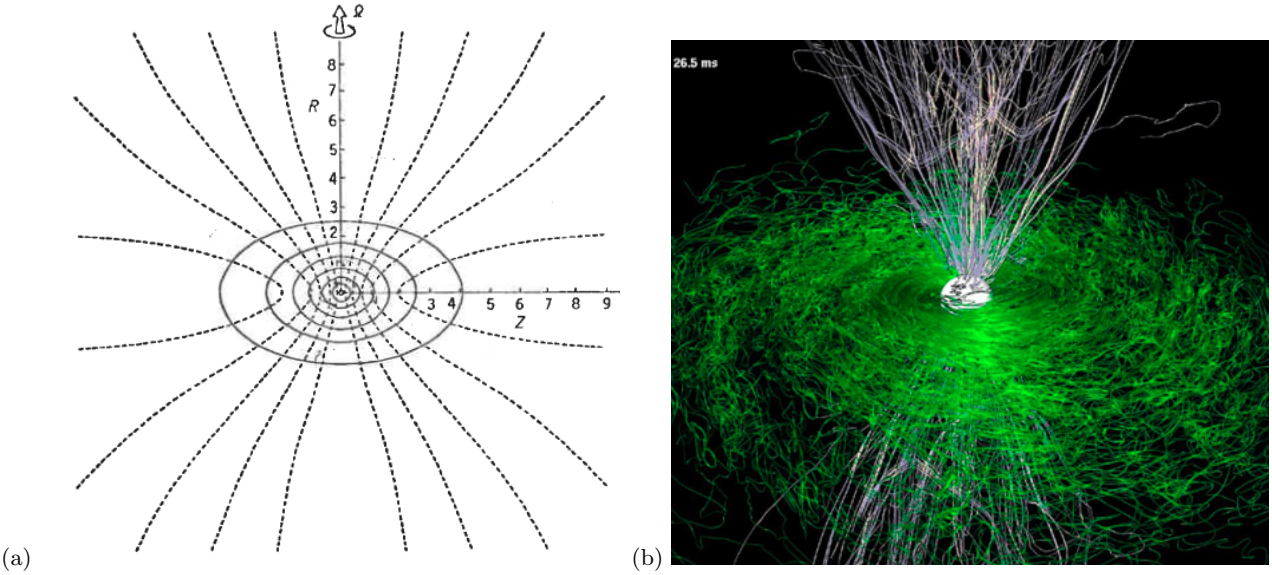

(a) (b)

Figure 6. (a) Figure reproduced from Wilson (1978): numerical simulation of the gravitational collapse of a star accounting for the magnetic field presence. Isodensity surfaces are indicated by the solid lines and poloidal field lines are indicated by the dashed lines. The time is the end of the numerical simulation. (b) Figure taken from Rezzolla et al. (2011) by author's permission. Magnetic-field structure after the collapse to BH. Green refers to magnetic-field lines inside the torus and on the equatorial plane, while white refers to magnetic-field lines outside the torus and near the axis.

et al. 2007, 2008, for details). Three-dimensional numerical simulation have been also performed and confirm this scenario (Rezzolla et al. 2011). In particular, it is appropriate to underline the strong analogy between Fig. 6 (a) taken from Wilson (1978) with Fig. 6 (b) reproduced in this paper from Rezzolla et al. (2011). It is also interesting the value of the magnetic field close to the BH estimated in Rezzolla et al. (2011), along the BH spin axis, 8×10^{14} G , similar to the value of 3×10^{14} G needed for the operation of the "*inner engine*" of GRB 130427A (Ruffini et al. 2018e). What is also conceptually important is that the uniform magnetic field assumed by the Wald solution should be expected to reach a poloidal configuration already relatively close to the BH. This occurs already in the original Wilson (1978) solution confirmed by the recent and most detailed calculation by Rezzolla et al. (2011), see Fig. 6 (a) and (b).

Although the above simulations refer to the remnant configuration of a binary NS merger, the post-merger configuration is analogous to the one developed in BdHNe I related to the newborn BH, which we have applied in our recent works (see e.g. Ruffini et al. 2018a,e, 2019c,b; Wang et al. 2019b, and references therein), and which is supported by the recently presented three-dimensional simulations of BdHNe (see Becerra et al. 2019, for details).

Before closing, let us indicate the difference between the NS merger and the BdHN. In the case of BdHN the gravitational collapse leading to the BH with the formation of an horizon creates a very-low-density cavity of 10^{-14} g cm^{-3} with a radius $\sim 10^{11}$ cm in the SN ejecta, see Fig. 1 and Fig. 7, reproduced from Ruffini et al. (2019a). The presence of such low-density environment is indeed essential for the successful operation of the "*inner engine*".

Both the reaching of a poloidal configuration already close to the BH in the Wald solution, as well as the existing of the cavity are crucial factors in the analysis of the propagation of the photons produced by synchrotron radiation and the fulfilment of reaching the transparency condition by the "*inner engine*" of the BdHNe (Ruffini et al. 2019c).

8. CONCLUSIONS

Our general conclusions have been reached based on the comparison and contrast of the observations of GRB 130427A, GRB 160509A, GRB 160625B, GRB 180728A and GRB 190114C:

1. From the analysis of GRB 130427A (Ruffini et al. 2018c) and GRB 190114C presented here (see Figs. 4 and 5), we conclude that the early ($t \sim 10^2$–10^4 s) X-ray emission of the FPA phase is explained by the injection of ultra-relativistic electrons from the νNS into the magnetized expanding ejecta, producing synchrotron radiation. The magnetic field inferred in this part of the analysis is found to be consistent with the

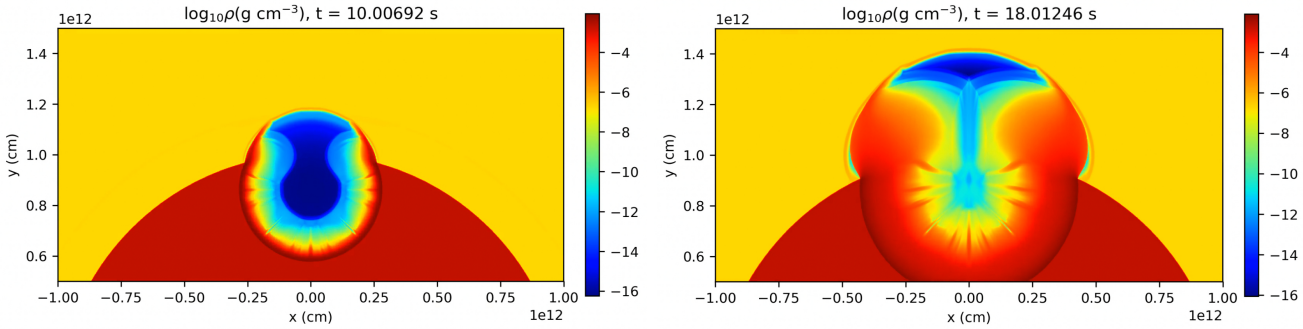

Figure 7. Spatial distribution of matter density at different time of impact of the e^+ e^- γ plasma onto the cavity walls at $t_{\rm imp} = 10$ s (left) and $t_{\rm imp} = 18$ s (right) for GRB 190114C; more information in Ruffini et al. (2019a) .

toroidal/longitudinal magnetic field component of the νNS. The dominance of this component is expected at distances much larger ($\sim 10^{12}$ cm) than the light cylinder radius in which this synchrotron emission occurs. No data of the other GRBs considered in this paper are available in this time interval.

2. Using the data of all the present GRBs, we concluded that at times $t \gtrsim 10^3$–10^4 s of the FPA phase, the power-law decaying luminosity is dominated via the pulsar magnetic-braking radiation. We have inferred a dipole+quadrupole structure of the νNS magnetic field, being the quadrupole component initially dominant. The strength of the dipole component is about 10^{12}–10^{13} G while the one of the quadrupole can be of order 10^{15} G (see Fig. 4 and Table 3). As clearly shown in Figs. 4 and 5, the solely νNS with the dipole+quadrupole magnetic field structure can not explain the emission of the early FPA phase which is dominated by the SN emission.

3. We have checked that the magnetic field of the νNS, inferred independently in the two above regimes of the FPA phase, give values in very good agreement. The νNS magnetic field obtained from the explanation of the FPA phase, at times 10^2–10^3 s by synchrotron radiation, and at times $t \gtrsim 10^4$ s by pulsar magnetic-braking, are in close agreement (see Sec. 4, Table 3 and Fig. 5).

4. In section 5, we have shown the consistency of the inferred νNS parameters with the expectations in the BdHN scenario. In particular, we have used the rotation period of the νNS inferred from the FPA phase at times $t \gtrsim 10^3$–10^4 s, we have inferred the orbital period/separation assuming tidal synchronization of the binary and angular momentum conservation in the gravitational collapse of the iron core leading to the νNS. This inferred binary separation is shown to be in excellent agreement with the numerical simulations of the binary progenitor in Wang et al. (2019b).

Before concluding, in view of the recent understanding gained on the "*inner engine*" of the high-energy emission of the GRB (Ruffini et al. 2019c), we can also conclude:

5. The magnetic field along the rotational axis of the BH is rooted in the magnetosphere left by the binary companion NS prior to the collapse.

6. While in the equatorial plane the field is magnified by magnetic flux conservation, in the axial direction the matter accretion flows in along the field lines; see Fig. 2 and Becerra et al. (2019). Indeed, three-dimensional numerical simulations of the gravitational collapse into a BH in presence of rotation and magnetic field confirm our picture; see Fig. 6 and Rezzolla et al. (2011); Dionysopoulou et al. (2013); Nathanail et al. (2017); Most et al. (2018).

7. The clarification reached in the role of the SN accretion both on the NS and on the νNS, the stringent limits imposed on the Lorentz factor of the FPA phase, the energetic requirement of the "*inner engine*" inferred from the recent publications, clearly points to an electrodynamical nature of the "*inner engine*" of the GRB, occurring close to the BH horizon, as opposed to the traditional, gravitational massive blastwave model.

We acknowledge the public data from Swift and Fermi satellites. We appreciate the discussion with Prof. Shesheng Xue, and the suggestions from the referee.

REFERENCES

Ackermann, M., Ajello, M., Asano, K., et al. 2014, Science, 343, 42, doi: 10.1126/science.1242353

Alexander, K. D., Laskar, T., Berger, E., et al. 2017, ApJ, 848, 69, doi: 10.3847/1538-4357/aa8a76

Becerra, L., Bianco, C. L., Fryer, C. L., Rueda, J. A., & Ruffini, R. 2016, ApJ, 833, 107, doi: 10.3847/1538-4357/833/1/107

Becerra, L., Cipolletta, F., Fryer, C. L., Rueda, J. A., & Ruffini, R. 2015, ApJ, 812, 100, doi: 10.1088/0004-637X/812/2/100

Becerra, L., Ellinger, C. L., Fryer, C. L., Rueda, J. A., & Ruffini, R. 2019, ApJ, 871, 14, doi: 10.3847/1538-4357/aaf6b3

Becerra, L., Guzzo, M. M., Rossi-Torres, F., et al. 2018, ApJ, 852, 120, doi: 10.3847/1538-4357/aaa296

Bianco, C. L., Ruffini, R., & Xue, S.-S. 2001, A&A, 368, 377, doi: 10.1051/0004-6361:20000556

Blandford, R. D., & McKee, C. F. 1976, Physics of Fluids, 19, 1130, doi: 10.1063/1.861619

Blandford, R. D., & Znajek, R. L. 1977, MNRAS, 179, 433, doi: 10.1093/mnras/179.3.433

Cipolletta, F., Cherubini, C., Filippi, S., Rueda, J. A., & Ruffini, R. 2015, PhRvD, 92, 023007, doi: 10.1103/PhysRevD.92.023007

Costa, E., Frontera, F., Heise, J., et al. 1997, Nature, 387, 783, doi: 10.1038/42885

Dai, Z. G., & Lu, T. 1998a, A&A, 333, L87

—. 1998b, Physical Review Letters, 81, 4301, doi: 10.1103/PhysRevLett.81.4301

Damour, T., & Ruffini, R. 1975, Physical Review Letters, 35, 463, doi: 10.1103/PhysRevLett.35.463

de Pasquale, M., Oates, S. R., Page, M. J., et al. 2007, MNRAS, 377, 1638, doi: 10.1111/j.1365-2966.2007.11724.x

Dionysopoulou, K., Alic, D., Palenzuela, C., Rezzolla, L., & Giacomazzo, B. 2013, PhRvD, 88, 044020, doi: 10.1103/PhysRevD.88.044020

Duez, M. D., Liu, Y. T., Shapiro, S. L., Shibata, M., & Stephens, B. C. 2006a, Physical Review Letters, 96, 031101, doi: 10.1103/PhysRevLett.96.031101

—. 2006b, PhRvD, 73, 104015, doi: 10.1103/PhysRevD.73.104015

Fan, Y.-Z., & Xu, D. 2006, MNRAS, 372, L19, doi: 10.1111/j.1745-3933.2006.00217.x

Fan, Y.-Z., Yu, Y.-W., Xu, D., et al. 2013, ApJL, 779, L25, doi: 10.1088/2041-8205/779/2/L25

Filippenko, A. V., Barth, A. J., Matheson, T., et al. 1995, ApJL, 450, L11, doi: 10.1086/309659

Flowers, E., & Ruderman, M. A. 1977, ApJ, 215, 302, doi: 10.1086/155359

Fryer, C. L., Oliveira, F. G., Rueda, J. A., & Ruffini, R. 2015, Physical Review Letters, 115, 231102, doi: 10.1103/PhysRevLett.115.231102

Fryer, C. L., Rueda, J. A., & Ruffini, R. 2014, ApJL, 793, L36, doi: 10.1088/2041-8205/793/2/L36

Fryer, C. L., Woosley, S. E., & Hartmann, D. H. 1999, The Astrophysical Journal, 526, 152

Galama, T. J., Vreeswijk, P. M., van Paradijs, J., et al. 1998, Nature, 395, 670, doi: 10.1038/27150

Goldreich, P., & Julian, W. H. 1969, ApJ, 157, 869, doi: 10.1086/150119

Heger, A., Fryer, C. L., Woosley, S. E., Langer, N., & Hartmann, D. H. 2003, ApJ, 591, 288, doi: 10.1086/375341

Iwamoto, K., Nakamura, T., Nomoto, K., et al. 2000, ApJ, 534, 660, doi: 10.1086/308761

Izzo, L., de Ugarte Postigo, A., Maeda, K., et al. 2019, Nature, 565, 324, doi: 10.1038/s41586-018-0826-3

Kouveliotou, C., Granot, J., Racusin, J. L., et al. 2013, ApJL, 779, L1, doi: 10.1088/2041-8205/779/1/L1

Laskar, T., Alexander, K. D., Berger, E., et al. 2016, ApJ, 833, 88, doi: 10.3847/1538-4357/833/1/88

Lattimer, J. M., & Prakash, M. 2004, Science, 304, 536, doi: 10.1126/science.1090720

Levan, A. J., Cenko, S. B., Perley, D. A., & Tanvir, N. R. 2013, GCN Circ., 14455

Li, L. 2019, ApJS, 242, 16, doi: 10.3847/1538-4365/ab1b78

Li, L., Wang, Y., Shao, L., et al. 2018a, ApJS, 234, 26, doi: 10.3847/1538-4365/aaa02a

Li, L., Wu, X.-F., Lei, W.-H., et al. 2018b, ApJS, 236, 26, doi: 10.3847/1538-4365/aabaf3

Li, L., Wu, X.-F., Huang, Y.-F., et al. 2015, ApJ, 805, 13, doi: 10.1088/0004-637X/805/1/13

Lü, H.-J., & Zhang, B. 2014, ApJ, 785, 74, doi: 10.1088/0004-637X/785/1/74

Lü, H.-J., Zhang, B., Lei, W.-H., Li, Y., & Lasky, P. D. 2015, ApJ, 805, 89, doi: 10.1088/0004-637X/805/2/89

Lü, H.-J., Lü, J., Zhong, S.-Q., et al. 2017, ApJ, 849, 71, doi: 10.3847/1538-4357/aa8f99

MAGIC Collaboration, Acciari, V. A., Ansoldi, S., et al. 2019, Nature, 575, 455, doi: 10.1038/s41586-019-1750-x

Markey, P., & Tayler, R. J. 1973, MNRAS, 163, 77, doi: 10.1093/mnras/163.1.77

Maselli, A., Melandri, A., Nava, L., et al. 2014, Science, 343, 48, doi: 10.1126/science.1242279

Melandri, A., Izzo, L., D'Avanzo, P., et al. 2019, GRB Coordinates Network, 23983

Mestel, L. 1984, Astronomische Nachrichten, 305, 301, doi: 10.1002/asna.2113050606
Mészáros, P., & Rees, M. J. 1997, The Astrophysical Journal Letters, 482, L29
Metzger, M. R., Djorgovski, S. G., Kulkarni, S. R., et al. 1997, Nature, 387, 878, doi: 10.1038/43132
Mirzoyan, R., Noda, K., Moretti, E., et al. 2019, GRB Coordinates Network, 23701
Most, E. R., Nathanail, A., & Rezzolla, L. 2018, ApJ, 864, 117, doi: 10.3847/1538-4357/aad6ef
Narayan, R., Paczynski, B., & Piran, T. 1992, ApJL, 395, L83, doi: 10.1086/186493
Nathanail, A., Most, E. R., & Rezzolla, L. 2017, MNRAS, 469, L31, doi: 10.1093/mnrasl/slx035
Nomoto, K., Yamaoka, H., Pols, O. R., et al. 1994, Nature, 371, 227, doi: 10.1038/371227a0
Paczynski, B. 1991, AcA, 41, 257
—. 1992, Gamma-ray bursts from colliding neutron stars., ed. C. Ho, R. I. Epstein, & E. E. Fenimore, 67–74
Pian, E., Mazzali, P. A., Masetti, N., et al. 2006, Nature, 442, 1011, doi: 10.1038/nature05082
Pitts, E., & Tayler, R. J. 1985, MNRAS, 216, 139, doi: 10.1093/mnras/216.2.139
Price, D. J. 2011, SPLASH: An Interactive Visualization Tool for Smoothed Particle Hydrodynamics Simulations, Astrophysics Source Code Library. http://ascl.net/1103.004
Rees, M. J., & Meszaros, P. 1992, MNRAS, 258, 41P, doi: 10.1093/mnras/258.1.41P
Rezzolla, L., Giacomazzo, B., Baiotti, L., et al. 2011, ApJL, 732, L6, doi: 10.1088/2041-8205/732/1/L6
Riahi, R., Kalantari, S. Z., & Rueda, J. A. 2019, PhRvD, 99, 043004, doi: 10.1103/PhysRevD.99.043004
Rowlinson, A., O'Brien, P. T., Metzger, B. D., Tanvir, N. R., & Levan, A. J. 2013, MNRAS, 430, 1061, doi: 10.1093/mnras/sts683
Rowlinson, A., O'Brien, P. T., Tanvir, N. R., et al. 2010, MNRAS, 409, 531, doi: 10.1111/j.1365-2966.2010.17354.x
Rueda, J. A., & Ruffini, R. 2012, ApJL, 758, L7, doi: 10.1088/2041-8205/758/1/L7
Rueda, J. A., Ruffini, R., & Wang, Y. 2019, Universe, 5, 110, doi: 10.3390/universe5050110
Ruffini, R., Karlica, M., Sahakyan, N., et al. 2018a, ApJ, 869, 101, doi: 10.3847/1538-4357/aaeac8
Ruffini, R., Melon Fuksman, J. D., & Vereshchagin, G. V. 2019a, ApJ, 883, 191, doi: 10.3847/1538-4357/ab3c51
Ruffini, R., & Wilson, J. R. 1975, Phys. Rev., D12, 2959, doi: 10.1103/PhysRevD.12.2959
Ruffini, R., Bianco, C. L., Enderli, M., et al. 2013, GCN Circ., 14526
Ruffini, R., Wang, Y., Enderli, M., et al. 2015, ApJ, 798, 10, doi: 10.1088/0004-637X/798/1/10
Ruffini, R., Rueda, J. A., Muccino, M., et al. 2016, ApJ, 832, 136, doi: 10.3847/0004-637X/832/2/136
Ruffini, R., Wang, Y., Aimuratov, Y., et al. 2018b, ApJ, 852, 53, doi: 10.3847/1538-4357/aa9e8b
Ruffini, R., Becerra, L., Bianco, C. L., et al. 2018c, ApJ, 869, 151, doi: 10.3847/1538-4357/aaee68
Ruffini, R., Rodriguez, J., Muccino, M., et al. 2018d, ApJ, 859, 30, doi: 10.3847/1538-4357/aabee4
Ruffini, R., Rueda, J. A., Moradi, R., et al. 2018e, arXiv e-prints. https://arxiv.org/abs/1811.01839
Ruffini, R., Li, L., Moradi, R., et al. 2019b, arXiv e-prints. https://arxiv.org/abs/1904.04162
Ruffini, R., Moradi, R., Rueda, J. A., et al. 2019c, ApJ, 886, 82, doi: 10.3847/1538-4357/ab4ce6
Ruffini, R., Moradi, R., Aimuratov, Y., et al. 2019d, GRB Coordinates Network, 23715
Sari, R. 1997, ApJL, 489, L37, doi: 10.1086/310957
Sari, R., & Piran, T. 1995, ApJL, 455, L143, doi: 10.1086/309835
Sari, R., Piran, T., & Narayan, R. 1998, ApJL, 497, L17, doi: 10.1086/311269
Selsing, J., Fynbo, J. P. U., Heintz, K. E., Watson, D., & Dyrbye, N. 2019, GRB Coordinates Network, 23695
Shibata, M., Duez, M. D., Liu, Y. T., Shapiro, S. L., & Stephens, B. C. 2006, Physical Review Letters, 96, 031102, doi: 10.1103/PhysRevLett.96.031102
Skilling, J. 2004, AIP Conference Proceedings, 735, 395, doi: 10.1063/1.1835238
Spruit, H. C. 1999, A&A, 349, 189
Spruit, H. C. 2009, in IAU Symposium, Vol. 259, Cosmic Magnetic Fields: From Planets, to Stars and Galaxies, ed. K. G. Strassmeier, A. G. Kosovichev, & J. E. Beckman, 61–74, doi: 10.1017/S1743921309030075
Stephens, B. C., Duez, M. D., Liu, Y. T., Shapiro, S. L., & Shibata, M. 2007, Classical and Quantum Gravity, 24, S207, doi: 10.1088/0264-9381/24/12/S14
Stephens, B. C., Shapiro, S. L., & Liu, Y. T. 2008, PhRvD, 77, 044001, doi: 10.1103/PhysRevD.77.044001
Sturner, S. J., Skibo, J. G., Dermer, C. D., & Mattox, J. R. 1997, ApJ, 490, 619, doi: 10.1086/304894
Tam, P.-H. T., He, X.-B., Tang, Q.-W., & Wang, X.-Y. 2017, ApJL, 844, L7, doi: 10.3847/2041-8213/aa7ca5
Tanvir, N. R., Levan, A. J., Cenko, S. B., et al. 2016, GRB Coordinates Network, Circular Service, No. 19419, #1 (2016), 19419
Tayler, R. J. 1973, MNRAS, 161, 365, doi: 10.1093/mnras/161.4.365
—. 1980, MNRAS, 191, 151, doi: 10.1093/mnras/191.1.151

Troja, E., Cusumano, G., O'Brien, P. T., et al. 2007, ApJ, 665, 599, doi: 10.1086/519450

Vianello, G., Lauer, R. J., Burgess, J. M., et al. 2017, in Proceedings of the 7th International Fermi Symposium, 130

Wald, R. M. 1974, PhRvD, 10, 1680, doi: 10.1103/PhysRevD.10.1680

Wang, Y., Li, L., Moradi, R., & Ruffini, R. 2019a, arXiv e-prints. https://arxiv.org/abs/1901.07505

Wang, Y., Rueda, J. A., Ruffini, R., et al. 2019b, ApJ, 874, 39, doi: 10.3847/1538-4357/ab04f8

Waxman, E., & Piran, T. 1994, ApJL, 433, L85, doi: 10.1086/187554

Wijers, R. A. M. J., Rees, M. J., & Meszaros, P. 1997, MNRAS, 288, L51, doi: 10.1093/mnras/288.4.L51

Wilson, J. R. 1975, in Annals of the New York Academy of Sciences, Vol. 262, Seventh Texas Symposium on Relativistic Astrophysics, ed. P. G. Bergman, E. J. Fenyves, & L. Motz, 123–132, doi: 10.1111/j.1749-6632.1975.tb31425.x

Wilson, J. R. 1978, in Physics and Astrophysics of Neutron Stars and Black Holes, ed. R. Giacconi & R. Ruffini, 644–675

Woosley, S. E. 1993, ApJ, 405, 273, doi: 10.1086/172359

Woosley, S. E., & Bloom, J. S. 2006, ARA&A, 44, 507, doi: 10.1146/annurev.astro.43.072103.150558

Wright, G. A. E. 1973, MNRAS, 162, 339, doi: 10.1093/mnras/162.4.339

Xu, D., Malesani, D., Fynbo, J. P. U., et al. 2016, GRB Coordinates Network, Circular Service, No. 19600, #1 (2016), 19600

Xu, D., de Ugarte Postigo, A., Leloudas, G., et al. 2013, ApJ, 776, 98, doi: 10.1088/0004-637X/776/2/98

Yoshida, T., & Umeda, H. 2011, MNRAS, 412, L78, doi: 10.1111/j.1745-3933.2011.01008.x

Zhang, B. 2018, The Physics of Gamma-Ray Bursts, doi: 10.1017/9781139226530

Zhang, B., & Mészáros, P. 2001, ApJL, 552, L35, doi: 10.1086/320255

Zhang, B.-B., Zhang, B., Castro-Tirado, A. J., et al. 2018, Nature Astronomy, 2, 69, doi: 10.1038/s41550-017-0309-8

Eur. Phys. J. C (2020) 80:300
https://doi.org/10.1140/epjc/s10052-020-7868-z

THE EUROPEAN PHYSICAL JOURNAL C

Letter

The blackholic quantum

J. A. Rueda[1,2,3,4,5,a], **R. Ruffini**[1,2,6,b]

[1] ICRANet, Piazza della Repubblica 10, 65122 Pescara, Italy
[2] ICRA, Dipartimento di Fisica, Sapienza Università di Roma, P.le Aldo Moro 5, 00185 Rome, Italy
[3] ICRANet-Ferrara, Dipartimento di Fisica e Scienze della Terra, Università degli Studi di Ferrara, Via Saragat 1, 44122 Ferrara, Italy
[4] Dipartimento di Fisica e Scienze della Terra, Università degli Studi di Ferrara, Via Saragat 1, 44122 Ferrara, Italy
[5] INAF, Istituto de Astrofisica e Planetologia Spaziali, Via Fosso del Cavaliere 100, 00133 Rome, Italy
[6] INAF, Viale del Parco Mellini 84, 00136 Rome, Italy

Received: 12 July 2019 / Accepted: 3 March 2020 / Published online: 3 April 2020

Abstract We show that the high-energy emission of GRBs originates in the *inner engine*: a Kerr black hole (BH) surrounded by matter and a magnetic field B_0. It radiates a sequence of discrete events of particle acceleration, each of energy $\mathscr{E} = \hbar\,\Omega_{\rm eff}$, the *blackholic quantum*, where $\Omega_{\rm eff} = 4(m_{\rm Pl}/m_n)^8(c\,a/G\,M)(B_0^2/\rho_{\rm Pl})\Omega_+$. Here M, $a = J/M$, $\Omega_+ = c^2\partial M/\partial J = (c^2/G)\,a/(2Mr_+)$ and r_+ are the BH mass, angular momentum per unit mass, angular velocity and horizon; m_n is the neutron mass, $m_{\rm Pl}$, $\lambda_{\rm Pl} = \hbar/(m_{\rm Pl}c)$ and $\rho_{\rm Pl} = m_{\rm Pl}c^2/\lambda_{\rm Pl}^3$, are the Planck mass, length and energy density. Here and in the following use CGS-Gaussian units. The timescale of each process is $\tau_{\rm el} \sim \Omega_+^{-1}$, along the rotation axis, while it is much shorter off-axis owing to energy losses such as synchrotron radiation. We show an analogy with the Zeeman and Stark effects, properly scaled from microphysics to macrophysics, that allows us to define the *BH magneton*, $\mu_{\rm BH} = (m_{\rm Pl}/m_n)^4(c\,a/G\,M)e\,\hbar/(Mc)$. We give quantitative estimates for GRB 130427A adopting $M = 2.3\ M_\odot$, $c\,a/(G\,M) = 0.47$ and $B_0 = 3.5\times10^{10}$ G. Each emitted *quantum*, $\mathscr{E} \sim 10^{37}$ erg, extracts only 10^{-16} times the BH rotational energy, guaranteeing that the process can be repeated for thousands of years. The *inner engine* can also work in AGN as we here exemplified for the supermassive BH at the center of M87.

1 Introduction

The GeV radiation in long GRBs is observed as a continuous, *macroscopic* emission with a luminosity that, in the source rest-frame, follows a specific power-law behavior: for instance the 0.1–100 GeV rest-frame luminosity of GRB 130427A observed by Fermi-LAT is well fitted by $L = A\,t^{-\alpha}$, $A = (2.05\pm0.23)\times10^{52}$ erg s^{-1} and $\alpha = 1.2\pm0.04$ [1]. We have there shown that the rotational energy of a Kerr BH is indeed sufficient to power the GeV emission. From the global energetics we have determined the BH parameters, namely its mass M and angular momentum per unit mass $a = J/M$ and, from the change of the luminosity with time, we have obtained the slowing-down rate of the Kerr BH. We have applied this procedure to the GeV-emission data of 21 sources. For GRB 130427A, we obtained that the BH initial parameters are $M \approx 2.3\ M_\odot$ and $c\,a/(G\,M) \approx 0.47$ [2].

One of the most extended multi-messenger campaign of observation in the field of science, ranging from ultra high-energy photons GeV/TeV (MAGIC) and MeV radiation (Swift, Fermi, Integral, Konus/WIND and UHXRT satellites) and to fifty optical observatories including the VLT, has given unprecedented details data on GRB 190114C. An in-depth time-resolved spectral analysis of its prompt emission, obtaining the best fit of the spectrum, and repeating it in successive time iterations with increasingly shorter time bins has been presented in [3]. It turns out that the spectra are self-similar and that the gamma-ray luminosity, expressed in the rest-frame, follows a power-law dependence with an index -1.20 ± 0.26, similar to the one of the GeV luminosity.

These data have offered us the first observational evidence of the moment of BH formation and, indeed, it clearly appears that the high-energy radiation is emitted in a sequence of elementary events, each of 10^{37} erg, and with an ever increasing repetition time from 10^{-14} to 10^{-12} s [2].

We have shown that this emission can be powered by what we have called the *inner engine* [2–4]: a Kerr BH immersed in a magnetic field B_0 and surrounded by matter. This *inner engine* naturally forms in the binary-driven hypernova (BdHN) scenario of GRBs [5–8]. The BdHN starts with

[a] e-mail: jorge.rueda@icra.it (corresponding author)
[b] e-mail: ruffini@icra.it

the supernova explosion of a carbon-oxygen star that forms a tight binary system with a neutron star companion. The supernova ejecta produces a hypercritical accretion process onto the neutron star bringing it to the critical mass point for gravitational collapse, hence forming a rotating BH. The Kerr BH, in presence of the magnetic field inherited from the neutron star, induces an electromagnetic field that is described by the Wald solution [9]. The BH is surrounded by matter from the supernova ejecta that supply ionized matter that is accelerated to ultrarelativistic energies at expenses of the BH rotational energy. This model has been applied to specific GRB sources in [2,3,10].

We here show that the GRB high-energy (GeV/TeV) radiation is indeed better understood within this scenario and that in particular: (1) it originates near the BH and (2) it is extracted from the BH rotational energy by *packets*, *quanta* of energy, in a number of finite discrete processes. We show that it is indeed possible to obtain the *quantum of energy* of this elementary process: $\mathscr{E} = \hbar\Omega_{\rm eff}$, where $\Omega_{\rm eff}$ is proportional to the BH angular velocity, Ω_+, and the proportionality constant depends only on fundamental constants. The timescale of the elementary process is shown to be $\tau_{\rm el} \sim \Omega_+^{-1}$. Quantitatively speaking, initially $\mathscr{E} \approx 10^{37}$ erg and $\tau_{\rm el}$ is shorter than microseconds.

This elementary process is not only finite in energy but it uses in each iteration only a small fraction of the BH rotational energy which can be as large as $E_{\rm rot} \sim 10^{53}$ erg. As we shall see, this implies that the repetitive process, in view of the slowing-down of the BH, can lasts thousands of years. The considerations on the *inner engine* apply as well to the case of AGN and we give a specific example for the case of M87*, the supermassive BH at the center of the M87.

2 The *inner engine* electromagnetic field structure

The axisymmetric Kerr metric for the exterior field of a rotating BH, in Boyer–Lindquist coordinates (t, r, θ, ϕ), can be written as [11]:

$$ds^2 = -\left(1-\frac{2\hat{M}r}{\Sigma}\right)(cdt)^2 - \frac{4\hat{a}\,\hat{M}\,r\sin^2\theta}{\Sigma}cdtd\phi + \frac{\Sigma}{\Delta}dr^2 + \Sigma d\theta^2 + \left[r^2+\hat{a}^2+\frac{2r\hat{M}\hat{a}^2\sin^2\theta}{\Sigma}\right]\sin^2\theta d\phi^2, \tag{1}$$

where $\Sigma = r^2 + \hat{a}^2\cos^2\theta$ and $\Delta = r^2 - 2\hat{M}r + \hat{a}^2$. The (outer) event horizon is located at $r_+ = \hat{M} + \sqrt{\hat{M}^2 - \hat{a}^2}$, where $\hat{M} = G\,M/c^2$ and $\hat{a} = a/c$, being M and $a = J/M$, respectively, the BH mass and the angular momentum per unit mass. Quantities with the hat on top are in geometric units.

Denoting by η_μ and ψ_μ, respectively, the timelike and spacelike Killing vectors, the electromagnetic four-potential of the Wald solution is $A_\mu = \frac{1}{2}B_0\,\psi_\mu + \hat{a}\,B_0\eta_\mu$, where B_0 is the test magnetic field value [9]. The associated electromagnetic field (in the Carter's orthonormal tetrad), for parallel magnetic field and BH spin, is:

$$E_{\hat{r}} = \frac{\hat{a}B_0}{\Sigma}\left[r\sin^2\theta - \frac{\hat{M}\left(\cos^2\theta+1\right)\left(r^2-\hat{a}^2\cos^2\theta\right)}{\Sigma}\right], \tag{2}$$

$$E_{\hat{\theta}} = \frac{\hat{a}B_0}{\Sigma}\sin\theta\cos\theta\sqrt{\Delta}, \tag{3}$$

$$B_{\hat{r}} = -\frac{B_0}{\Sigma}\cos\theta\left(-\frac{2\hat{a}^2\hat{a}r\left(\cos^2\theta+1\right)}{\Sigma}+\hat{a}^2+r^2\right), \tag{4}$$

$$B_{\hat{\theta}} = \frac{B_0 r}{\Sigma}\sin\theta\sqrt{\Delta}. \tag{5}$$

3 Energetics and timescale of the elementary process

The electrostatic energy gained by an electron (or proton for the antiparallel case) when accelerated from the horizon to infinity, along the rotation axis, is

$$\varepsilon_e = -eA_\mu\eta^\mu|_\infty + eA_\mu\eta^\mu|_{\rm r_+} = e\,\hat{a}\,B_0 = \frac{1}{c}e\,a\,B_0, \tag{6}$$

where we have used that $\psi_\mu\eta^\mu = 0$ and $\eta_\mu\eta^\mu \to -1$ along the rotation axis, and $\eta_\mu\eta^\mu = 0$ on the horizon [9].

The electric field for $\theta = 0$, and at the horizon, E_+, is [2]:

$$|E_+| = \frac{1}{2}\frac{\hat{a}}{\hat{M}}B_0 = \frac{1}{2}\frac{cJ}{G\,M^2}B_0 \approx \frac{1}{c}\Omega_+ r_+ B_0, \tag{7}$$

where the last expression is accurate for $\hat{a}/\hat{M} \lesssim 0.5$ [2], and it evidences the *inducting* role of the BH angular velocity

$$\Omega_+ = \frac{\partial Mc^2}{\partial J} = c\frac{1}{2}\frac{\hat{a}/\hat{M}}{r_+}. \tag{8}$$

Using Eq. (7), Eq. (6) can be written as

$$\varepsilon_e \approx e\,|E_+|\,r_+ \approx \frac{1}{c}e\,r_+^2\,\Omega_+\,B_0. \tag{9}$$

It is worth to note that this angular frequency can be related to the energy gained timescale of the elementary process:

$$\tau_{\rm el} = \frac{\varepsilon_e}{e|E_+|c} \approx \frac{r_+}{c} = \frac{\hat{a}/\hat{M}}{2\Omega_+}, \tag{10}$$

that is the characteristic acceleration time of the particle along the BH rotation axis. Thus, this is the longest timescale for the elementary process and it happens on the rotation axis where no (or negligible) radiation losses occur. This is relevant for the emitting power of ultrahigh-energy charged particles leading to ultrahigh-energy cosmic rays. Off-polar axis,

the charged particles emit e.g. synchrotron radiation at GeV energies, in a much shorter timescale of the order of 10^{-14} s (see [2] for details).

The total electric energy available for the *inner engine* elementary process is [2]:

$$\mathscr{E} \approx \frac{1}{2}|E_+|^2 r_+^3 = \frac{1}{4}\frac{\hat{a}}{\hat{M}}\frac{r_+\Omega_+}{c} r_+^3 B_0^2, \tag{11}$$

where in the last equality we have used Eqs. (7) and (8).

4 The quantum of energy for GRBs

We recall that in a BdHN the BH is formed from the collapse of a neutron star when it reaches the critical mass, $M_{\rm crit}$, by accreting the ejected matter in the supernova explosion of a companion carbon-oxygen star [5–8,12–14]. Thus, for the GRB case we can adopt $r_+ \sim 2\,G\,M/c^2$ and $M = M_{\rm crit} \sim m_{\rm Pl}^3/m_n^2$, where $M_{\rm crit}$ is accurate within a factor of order unity; $m_{\rm Pl} = \sqrt{\hbar c/G}$ and m_n are the Planck and neutron mass. With this, the energy per proton (9) can be written in the *quantized* form:

$$\varepsilon_e = \hbar\,\omega_p, \quad \omega_p \equiv \frac{4\,G}{c^4}\left(\frac{m_{\rm Pl}}{m_n}\right)^4 e\,B_0\,\Omega_+. \tag{12}$$

Following the above steps for ε_e, we can also write Eq. (11) in the *quantized* form:

$$\mathscr{E} = \hbar\,\Omega_{\rm eff}, \quad \Omega_{\rm eff} \equiv 4\left(\frac{m_{\rm Pl}}{m_n}\right)^8\left(\frac{\hat{a}}{\hat{M}}\right)\left(\frac{B_0^2}{\rho_{\rm Pl}}\right)\Omega_+, \tag{13}$$

where $\rho_{\rm Pl} \equiv m_{\rm Pl}c^2/\lambda_{\rm Pl}^3$ and $\lambda_{\rm Pl} = \hbar/(m_{\rm Pl}c)$ are the Planck energy-density and length. The quantities in parenthesis are dimensionless; e.g. B_0^2 is an energy density as it is $\rho_{\rm Pl}$. Each discrete process extracts a specific amount of the BH rotational energy set by the *blackholic quantum* (13).

5 Specific quantitative examples

Concerning quantitative estimates, let us compute the main physical quantities of the *inner engine* for the case of GRB 130427A [2]. We have there estimated that, an *inner engine* composed of a newborn BH of $M \approx 2.3\,M_\odot$, $\hat{a}/\hat{M} = 0.47$ and $B_0 = 3.5 \times 10^{10}$ G, can explain the observed GeV emission. We recall that the *inner engine* parameters in [2] were determined at the end of the prompt emission (at 37 s rest-frame time). At that time, the observed GeV luminosity is $L_{\rm GeV} \approx 10^{51}$ erg s^{-1}. The timescale of synchrotron radiation expected to power this emission was found to be $t_c \sim 10^{-14}$ s (to not be confused with $\tau_{\rm el}$), which implies an energy $\mathscr{E} \sim L_{\rm GeV} \times t_c = 10^{37}$ erg, consistent with the blackholic quantum estimated here for the above *inner engine* parameters (see Table 1).

Table 1 *Inner engine* astrophysical quantities for GRBs and AGN. The power reported in the last row is the one to accelerate ultrahigh-energy particles, i.e. $\dot{\mathscr{E}} = \mathscr{E}/\tau_{\rm el}$. In both cases the parameters (mass, spin and magnetic field) have been fixed to explain the observed high-energy ($\gtrsim$ GeV) luminosity

	GRB (130427-like)	AGN (M87*-like)
$\tau_{\rm el}$	2.21×10^{-5} s	0.49 day
ε_e (eV)	1.68×10^{18}	1.19×10^{19}
$\mathscr{E}$ (erg)	4.73×10^{36}	5.19×10^{47}
$\dot{\mathscr{E}}$ (erg/s)	2.21×10^{41}	1.22×10^{43}

The elementary, discrete process introduced here can also be at work in AGN where the time variability of the high-energy GeV–TeV radiation appears to be emitted on sub-horizon scales (see [15] for the case of M87*). Thus, we also show in Table 1 the physical quantities for an AGN, which can be obtained from the expressions in Sect. 3. We adopt as a proxy M87*, so $M \approx 6 \times 10^9\,M_\odot$ (e.g. [16]), and we assume respectively for the BH spin and the external magnetic field, $\hat{a}/\hat{M} = 0.9$ and $B_0 = 50$ G. The magnetic field has been fixed to explain the observed high-energy luminosity which is few $\times\,10^{42}$ erg s^{-1} (e.g. [17,18]).

This shows that the energy of the *blackholic quantum* is finite and is a very small fraction of the BH rotational energy: for GRBs we have $E_{\rm rot} \sim 10^{53}$ erg and $\mathscr{E}/E_{\rm rot} \approx 10^{-16}$ and for AGN $\mathscr{E}/E_{\rm rot} \approx 10^{-13}$. This guarantees that the emission process has to occur following a sequence of the elementary processes. Under these conditions, the duration of the repetitive sequence, $\Delta t \sim (E_{\rm rot}/\mathscr{E})\tau_{\rm el}$, can be of thousands of years, in view of the slowing-down of the BH leading to an ever increasing value of $\tau_{\rm el}$ [2] (while $\mathscr{E}$ holds nearly constant).

6 The black hole magneton

It is interesting to show the analogy of the above result with the case of an atom placed in an external electric or magnetic field for which its energy levels suffer a shift, respectively, from the Stark or Zeeman effect (see e.g. [19]).

In the case of the Zeeman effect, the energy shift is:

$$\Delta\varepsilon_Z = \mu_B B_0, \quad \mu_B \equiv e\frac{\hbar}{2m_e c}, \tag{14}$$

where μ_B is the Bohr magneton. Indeed, by using $\Omega_+ \approx c(\hat{a}/\hat{M})/(4GM/c^2)$, and introducing $\mu_{\rm BH}$, the *BH magneton*,

$$\mu_{\rm BH} \equiv \left(\frac{m_{\rm Pl}}{m_n}\right)^4\left(\frac{\hat{a}}{\hat{M}}\right) e\frac{\hbar}{Mc}, \tag{15}$$

the particle energy (12) can be written as

$$\varepsilon_e = \mu_{\rm BH} B_0, \tag{16}$$

which adds an unexpected deeper meaning to ε_e.

In the Stark effect, the energy shift is given by

$$\Delta\varepsilon_S = e\,|E_+|\,r_B, \tag{17}$$

where $r_B = \hbar^2/(m_e e^2)$ is the Bohr radius. This expression can be directly compared with the first equality in Eq. (9).

7 A direct application to the electron

The use of the Wald solution overcomes the conceptual difficulty of explaining the origin of the charge in BH electrodynamics. Indeed, an effective charge of the system can be expressed as [2,9]

$$Q_{\rm eff} = \frac{G}{c^3} 2\,J\,B_0, \tag{18}$$

which is not an independent parameter but, instead, it is a derived quantity from the BH angular momentum and the magnetic field B_0. These quantities become the free parameters of the electrodynamical process and therefore the concept of the BH charge is not anymore a primary concept.

The effective charge (18) can be also expressed in terms of M, J and the magnetic moment μ as:

$$Q_{\rm eff} = \frac{Mc}{J}\mu, \tag{19}$$

where we have used the computation of the Geroch–Hansen multipole moments [20,21] performed in [9]. Assuming the electron spin $J_e = \hbar/2$ and $Q_{\rm eff} = e$, the magnetic moment becomes the Bohr magneton. But more interestingly, if we adopt the angular momentum and magnetic moment of the electron, then we obtain that the derived effective charge (19) becomes indeed the electron charge:

$$Q_{\rm eff} = \frac{m_e\,c}{J_e}\mu_B = \frac{2m_e\,c}{\hbar}\frac{\hbar}{2m_e\,c}\,e = e. \tag{20}$$

8 Conclusions

We recall:

1. That in addition of being exact mathematical solutions of the Einstein equations, BHs are objects relevant for theoretical physics and astrophysics as it was clearly indicated in "Introducing the BH" [22].
2. That the mass-energy of a Kerr–Newman BH, established over a few months period ranging from September 17, 1970, to March 11, 1971 in [23–25], can be simply expressed by

$$M^2 = \frac{c^2 J^2}{4G^2 M_{\rm irr}^2} + \left(\frac{Q^2}{4G\,M_{\rm irr}} + M_{\rm irr}\right)^2, \tag{21}$$

$$S = 16\pi G^2\,M_{\rm irr}^2/c^4,$$

$$\delta S = 32\pi G^2\,M_{\rm irr}\delta M_{\rm irr}/c^4 \geq 0, \tag{22}$$

where Q, J and M are the three independent parameters of the Kerr–Newman geometry: charge, angular momentum and mass. $M_{\rm irr}$ and S are, respectively, the derived quantities representing the irreducible mass and the horizon surface area.

3. That for extracting the Kerr BH rotational energy the existence of the Wald solution [9] was essential [2,3,10].

From the observational point of view, the time-resolved spectral analysis of GRB 130427A [1,2] and GRB 190114C [3] clearly points to the existence of self-similarities in the Fermi-GBM spectra, to the power-law in the GeV luminosity of the Fermi-LAT and to a discrete emission of elementary impulsive events of 10^{37} erg. The timescale of the emission is, on the rotation axis $\sim 10^{-6}$ s, leading to ultrahigh-energy particles contributing to cosmic rays, and off-axis of $\sim 10^{-14}$ s, leading to GeV–TeV radiation [2].

Extrapolating these considerations from a BH to an electron, we showed that the electron charge turns out to be a derived quantity, a function of the electron's angular momentum and magnetic moment, with the electron's mass and the speed of light considered as fundamental constants.

The definition, the formulation of the equation and the identification of the mechanism of the process of emission of the *blackholic quantum* has become a necessity and it is presented in this article.

Data Availability Statement This manuscript has no associated data or the data will not be deposited. [Authors' comment: This is theoretical work in which no experimental data are generated and/or analyzed.]

Funded by SCOAP[3].

References

1. R. Ruffini, R. Moradi, J.A. Rueda, Y. Wang, Y. Aimuratov, L. Becerra, C.L. Bianco, Y.C. Chen, C. Cherubini, S. Filippi, M. Kar-

lica, G.J. Mathews, M. Muccino, G.B. Pisani, D. Primorac, S.S. Xue, (2018). arXiv:1803.05476
2. R. Ruffini, R. Moradi, J.A. Rueda, L. Becerra, C.L. Bianco, C. Cherubini, S. Filippi, Y.C. Chen, M. Karlica, N. Sahakyan, Y. Wang, S.S. Xue, Astrophys. J. **886**(2), 82 (2019). https://doi.org/10.3847/1538-4357/ab4ce6
3. R. Ruffini, L. Li, R. Moradi, J.A. Rueda, Y. Wang, S.S. Xue, C.L. Bianco, S. Campion, J.D. Melon Fuksman, C. Cherubini, S. Filippi, M. Karlica, N. Sahakyan, (2019). arXiv:1904.04162
4. J.A. Rueda, R. Ruffini, M. Karlica, R. Moradi, Y. Wang, (2019). arXiv:1905.11339
5. J.A. Rueda, R. Ruffini, Astrophys. J. **758**, L7 (2012). https://doi.org/10.1088/2041-8205/758/1/L7
6. C.L. Fryer, J.A. Rueda, R. Ruffini, Astrophys. J. **793**, L36 (2014). https://doi.org/10.1088/2041-8205/793/2/L36
7. L. Becerra, C.L. Bianco, C.L. Fryer, J.A. Rueda, R. Ruffini, Astrophys. J. **833**, 107 (2016). https://doi.org/10.3847/1538-4357/833/1/107
8. L. Becerra, M.M. Guzzo, F. Rossi-Torres, J.A. Rueda, R. Ruffini, J.D. Uribe, Astrophys. J. **852**, 120 (2018). https://doi.org/10.3847/1538-4357/aaa296
9. R.M. Wald, Phys. Rev. D **10**, 1680 (1974). https://doi.org/10.1103/PhysRevD.10.1680
10. R. Ruffini, J.D. Melon Fuksman, G.V. Vereshchagin, Astrophys. J. **883**(2), 191 (2019). https://doi.org/10.3847/1538-4357/ab3c51
11. B. Carter, Phys. Rev. **174**(5), 1559 (1968). https://doi.org/10.1103/PhysRev.174.1559
12. L. Becerra, F. Cipolletta, C.L. Fryer, J.A. Rueda, R. Ruffini, Astrophys. J. **812**, 100 (2015). https://doi.org/10.1088/0004-637X/812/2/100
13. C.L. Fryer, F.G. Oliveira, J.A. Rueda, R. Ruffini, Phys. Rev. Lett. **115**(23), 231102 (2015). https://doi.org/10.1103/PhysRevLett.115.231102
14. L. Becerra, C.L. Ellinger, C.L. Fryer, J.A. Rueda, R. Ruffini, Astrophys. J. **871**, 14 (2019). https://doi.org/10.3847/1538-4357/aaf6b3
15. J. Aleksić, S. Ansoldi, L.A. Antonelli, P. Antoranz, A. Babic, P. Bangale, J.A. Barrio, J.B. González, W. Bednarek, E. Bernardini, Science **346**(6213), 1080 (2014). https://doi.org/10.1126/science.1256183
16. J.L. Walsh, A.J. Barth, L.C. Ho, M. Sarzi, Astrophys. J. **770**, 86 (2013). https://doi.org/10.1088/0004-637X/770/2/86
17. A.A. Abdo, M. Ackermann, M. Ajello, W.B. Atwood, M. Axelsson, L. Baldini, J. Ballet, G. Barbiellini, D. Bastieri, K. Bechtol, Astrophys. J. **707**(1), 55 (2009). https://doi.org/10.1088/0004-637X/707/1/55
18. S. de Jong, V. Beckmann, S. Soldi, A. Tramacere, A. Gros, Mon. Not. R. Astron. Soc. **450**, 4333 (2015). https://doi.org/10.1093/mnras/stv927
19. L.D. Landau, E.M. Lifshitz, *Quantum Mechanics* (Pergamon Press, Oxford, 1965)
20. R. Geroch, J. Math. Phys. **11**(8), 2580 (1970). https://doi.org/10.1063/1.1665427
21. R.O. Hansen, J. Math. Phys. **15**(1), 46 (1974). https://doi.org/10.1063/1.1666501
22. R. Ruffini, J.A. Wheeler, Phys. Today **24**(1), 30 (1971). https://doi.org/10.1063/1.3022513
23. D. Christodoulou, Phys. Rev. Lett. **25**, 1596 (1970). https://doi.org/10.1103/PhysRevLett.25.1596
24. D. Christodoulou, R. Ruffini, Phys. Rev. D **4**, 3552 (1971). https://doi.org/10.1103/PhysRevD.4.3552
25. S.W. Hawking, Phys. Rev. Lett. **26**, 1344 (1971). https://doi.org/10.1103/PhysRevLett.26.1344

Hierarchical structure in the ultra relativistic prompt emission (UPE) phase of GRB 190114C, GRB 180720, GRB 160509A, and GRB 160625B and their theoretical interpretation

A novel time-resolved spectral analysis in a sequence of ever decreasing time interval, allowed by the sensitivity of Fermi–GBM, performed on ultra-relativistic prompt emission (UPE) phase of GRB 190114C (Ruffini et al. 2019a), GRB 180720, GRB 160509A, and GRB 160625B, has allowed to find the hierarchical structure in their UPE phase

GRB 190114C

On January 15, 2019, we indicated that GRB 190114C, discovered by *Fermi*-GBM on January 14, 2019 (Hamburg et al. 2019), with a redshift $z = 0.424$ observed by NOT (Selsing et al. 2019), had to be identified as a BdHN (Ruffini et al. 2019b). As a BdHN, within 18.8 ± 3.7 days, a SN should be expected to appear in the same location of the GRB. After an extended campaign involving tens of observatories worldwide, the expectation of the optical SN signal was confirmed (Melandri et al. 2019; Wang et al. 2019). This success and the detection of TeV radiation by MAGIC (Mirzoyan et al. 2019) make GRB 190114C one of the best example of multi-messenger astronomy.

The spectral analysis of the ultrarelativistic prompt emission (UPE) phase ([1.9s–3.99s]) in gamma-rays observed by Fermi-GBM clearly shows that cutoff power-law plus blackbody spectrum (CPL+BB) is the preferred model with the parameters of: power-law index $\alpha = -0.71^{+0.02}_{-0.02}$, cut-off energy $E_c = 717.6^{+25.4}_{-25.4}$, temperature , $kT = 111.64^{+2.5}_{-2.5}$ keV. The BB component and the total fluxes are, $F_{\rm BB} = 22.49^{+3.21}_{-2.65}$ (10^{-6} erg cm^{-2} s^{-1}) and $F_{\rm tot} = 111.10^{+11.60}_{-10.40}$ (10^{-6} erg cm^{-2} s^{-1}) respectively; see Table. 1. The ratio of BB to the total flux is, $F_{\rm BB}/F_{\rm tot} = 0.2$ and the isotropic energy of this time interval $E_{\rm iso} = 1.5 \times 10^{53}$ erg.

We now turn to the result obtained by a time-resolved analysis of the UPE spectrum.

Therefore, following the spectral analysis performed over the entire time interval of $t_{\rm rf} = 1.9$ s to $t_{\rm rf} = 3.9$ s, we divide the rest frame time interval in half and perform again the same spectral analysis for the two one second intervals, namely [1.9s–2.9s] and [2.9s–3.9s], obtaining the results shown in Fig. 1a.

We then divide each of these half intervals again in half, i.e., $\Delta t_{\rm rf} = 0.5$ s corresponding to [1.9s–2.40s], [2.40s–2.9s], [2.9s–3.4s] and [3.4s–3.9s] and redo the previous spectral analysis obtaining the results in Fig. 1b.

In a fourth iteration we divide the UPE into 8 sub-intervals of $\Delta t_{\rm rf} = 0.25$ s corresponding to the time intervals [1.9s–2.15s],[2.15s–2.40s], [2.40s–2.65s], [2.65s–2.9s], [2.9s–3.15s], [3.15s–3.4s], [3.4s–3.65s] and [3.65s–3.9s], and redo the spectral analysis, see Fig. 1c.

In the fifth and final iteration of this process we divide the UPE into 16 sub-intervals of $\Delta t_{\rm rf} = 0.125$ s corresponding we perform the spectral analysis and find the hierarchical CPL+BB emission in the time intervals [1.896s–2.019s],[2.019s–2.142s],[2.142s–2.265s], [2.265s–2.388s], [2.388s–2.511s], [2.511s–2.633s], [2.633s–2.756s], [2.756s–2.87s], [2.879s–3.002s], [3.002s–3.125s], [3.125s–3.248s], [3.248s–3.371s], [3.371s–3.494s], [3.494s–3.617s], [3.617s–3.739s] and [3.739s–3.862s] and perform the spectral analysis. After dividing into sub-intervals of 0.125 s one extra time interval of [3.862s–3.985s] also reveals the presence of thermal component; see Fig. 1d.

In conclusion, the time-resolved spectra of the UPE phase for each iterative step are obtained by discretizing each time interval in time bins of equal duration, and the iterative process continued until the adequate S/N is fulfilled. No limit appears to be present where the SNR is sufficiently high.

The results of these iterative spectral fittings are shown in Fig. 1 and Table 1. Most remarkably, the spectral fitting of a cut-off power law plus black body (CPL+BB) is confirmed in each time interval and for each iterative step.

GRB 160625B

On 25 June 2016 at 22:40:16.28 UT, GRB 160625B triggered Gamma-ray Burst Monitor (GBM) onboard the NASA *Fermi* Gamma-ray Space Telescope (Burns 2016). *Fermi*-LAT starts the observation 188.54 s after the trigger (Dirirsa et al. 2016), and detected more than 300 photons with energy > 100 MeV, the highest energy photon is about 15 GeV (Lü et al. 2017). *Swfit*-XRT starts the observation at late time ($> 10^4$ s), a power-law behaviour with decaying index ~ -1.25 (Melandri et al. 2016). GRB 160625B is one of the most energetic GRBs with an isotropic energy $\approx 3 \times 10^{54}$ erg (Troja et al. 2017; Zhang et al. 2018). The redshift $z = 1.406$ is reported in Xu et al. (2016). GRB 160625B is a luminous GRB with the clear detected polarisation (Troja 2017). There is no supernova confirmation due to its high redshift; $z > 1$ (Woosley & Bloom 2006).

Based on the temporal and spectral analysis, we confirm that the UPE phase GRB 160625B starts from $t_{\rm rf} = 77.72$ s and ends at $t_{\rm rf} = 87.70$ s.

Similarly to GRB 190114C, we also find a hierarchical structure in the UPE phase for GRB 160625B after carrying out the detailed time-resolved spectral analysis, with a cutoff powerlaw + blackbody (CPL+BB) model, for five successive iteration process on shorter and shorter time scales (expressed in the laboratory and in the rest frame). For the first iteration, Fig. 2 (first layer) shows the best-fit of the spectrum of the UPE entire duration from $t_{\rm rf} = 77.72$ s to $t_{\rm rf} = 87.70$ s.

We then divide the rest-frame time interval in half and perform again the same spectral analysis for the two intervals, each of 4.99s, namely [77.72s-82.71s] and [82.71s-87.70s], obtaining the results shown in Fig. 2 (second layer). In the third iteration, we divide each of these half intervals again in half. We continue this procedure up to five iterations, i.e up to dividing the UPE in 16 time sub-intervals. For each iterative step, we give the duration and the spectral parameters of CPL+BB model, including: the low-energy photon index α, the peak energy $E_{\rm c}$, the BB temperature kT (k is the Stefan-Boltzmann constant), the model comparison parameter (DIC), the BB flux, the total flux, the BB to total flux ratio, and the total energy. The results are summarized in Fig. 2 and Table 2, which confirm the validity, also in GRB 160625B, of the hierarchical structure first discovered in GRB 190114C.

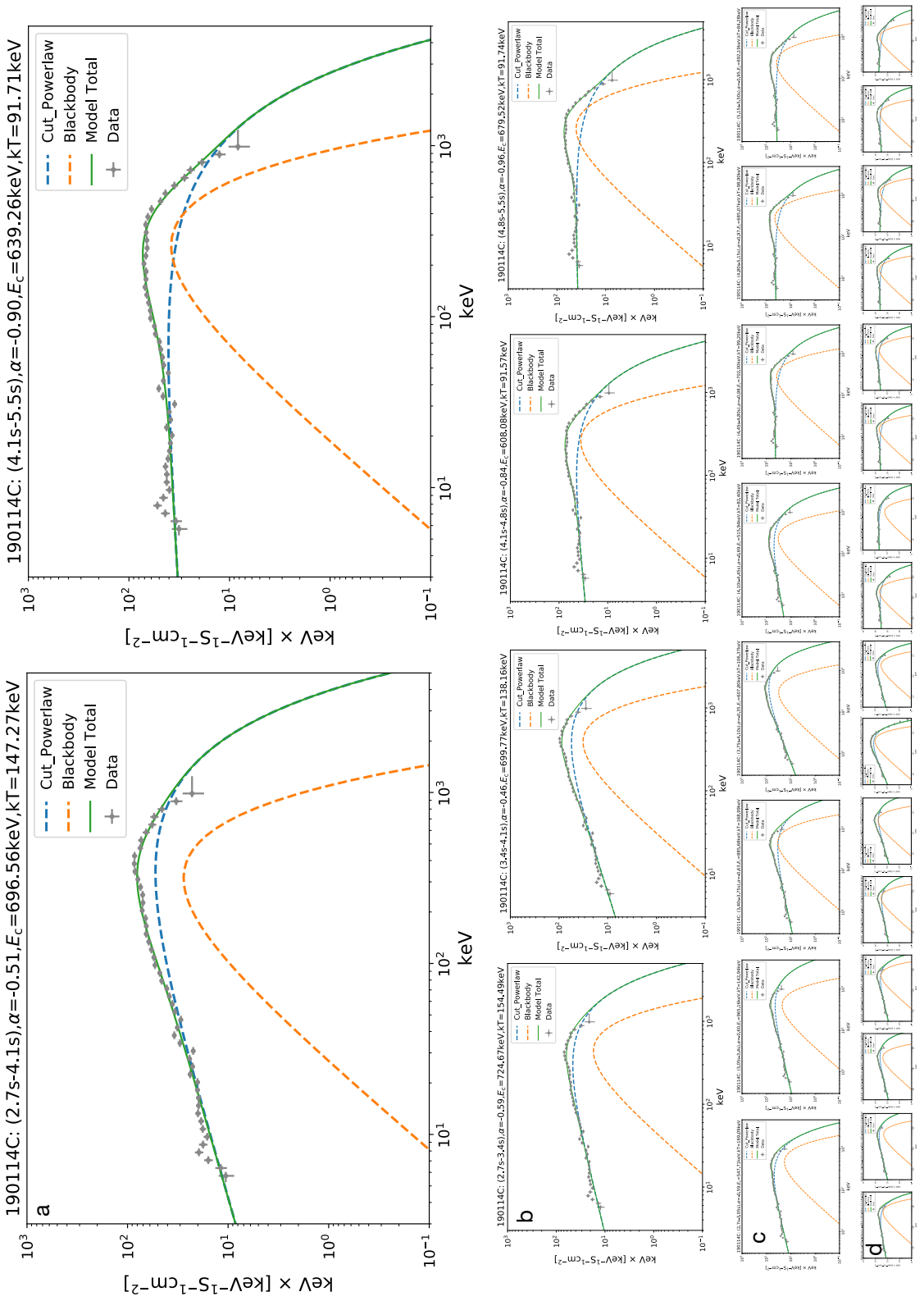

Fig. 1. Time-resolved spectra of GRB 190114C: from t = 2.7 s ($t_{\rm rf}$ = 1.9 s) to t = 5.5 s ($t_{\rm rf}$ = 3.9 s). Here the time interval is divided into two equal parts (first layer; a), four equal parts (second layer; b), eight equal parts (third layer; c), and sixteen equal parts (fourth layer; d), respectively. The results of the spectral analysis including time duration, temperature and cutoff energy in this figure are reported in the observer's frame. Their corresponding source rest-frame values are reported respectively in the columns 2, 5 and 6 of Table 1.

Table 1. Results of the time-resolved spectral fits of GRB 190114C (CPL+BB model) from t = 2.7 s ($t_{\rm rf}$ = 1.9 s) to t = 5.5 s ($t_{\rm rf}$ = 3.99 s). The time intervals both in the rest-frame and observer's frame, the significance (S) for each time interval, the power-law index, rest-frame cut-off energy, rest-frame temperature, AIC/BIC, BB flux, total flux, the ratio of blackbody flux to the total flux, $F_{\rm BB}/F_{\rm tot}$ and finally the isotropic energy are reported in this table. The $F_{\rm BB}/F_{\rm tot}$ remains almost constant in each sample. The Akaike Information Criterion (AIC, Akaike 1974) and the Bayesian Information Criterion (BIC, Schwarz et al. 1978) can be used to select non-nested and nested models, respectively. The AIC and BIC are defined as AIC=-2ln$L(\boldsymbol{\theta})$+2k and BIC=-2ln$L(\boldsymbol{\theta})$+kln(n), respectively. Here L is the maximized value of the likelihood function for the estimated model, k is the number of free parameters to be estimated, n is the number of observations (or the sample size). The prefer model between any two estimated models is the one that provides the minimum AIC and BIC scores. After comparing the AIC and BIC, we find the CPL+BB model is the preferred model than the CPL and other model. The likelihood -log(posterior) and the AIC and BIC scores are reported in column 6.

t_1~t_2	$t_{rf,1}$~$t_{rf,2}$	S	α	$E_{\rm c}$	kT	ΔDIC	$F_{\rm BB}$	$F_{\rm tot}$	$F_{\rm ratio}$	$E_{\rm tot}$
(s)	(s)			(keV)	(keV)		(10^{-6})	(10^{-6})		(erg)
Obs	Rest-frame						(erg cm^{-2} s^{-1})	(erg cm^{-2} s^{-1})		
2.700~5.500	1.896~3.862	418.62	$-0.71^{+0.02}_{-0.02}$	$717.6^{+25.4}_{-25.4}$	$159.0^{+3.6}_{-3.6}$	-3344/6697/6719	$22.49^{+3.21}_{-2.65}$	$111.10^{+11.60}_{-10.40}$	0.20	1.50e+53
2.700~4.100	1.896~2.879	296.60	$-0.51^{+0.02}_{-0.02}$	$696.6^{+31.9}_{-32.4}$	$209.7^{+9.3}_{-9.1}$	-2675/5360/5381	$24.67^{+6.93}_{-5.35}$	$142.50^{+23.90}_{-21.00}$	0.17	9.64e+52
4.100~5.500	2.879~3.862	318.07	$-0.90^{+0.02}_{-0.02}$	$639.3^{+31.9}_{-31.6}$	$130.6^{+2.5}_{-2.5}$	-2529/5069/5090	$25.55^{+2.97}_{-2.75}$	$80.98^{+9.68}_{-8.07}$	0.32	5.48e+52
2.700~3.400	1.896~2.388	204.30	$-0.59^{+0.03}_{-0.03}$	$724.7^{+44.5}_{-45.5}$	$220.0^{+17.1}_{-17.2}$	-1882/3774/3796	$18.55^{+9.42}_{-7.40}$	$123.90^{+29.20}_{-22.30}$	0.15	4.19e+52
3.400~4.100	2.388~2.879	225.88	$-0.46^{+0.04}_{-0.04}$	$699.8^{+47.8}_{-48.3}$	$196.7^{+8.9}_{-8.7}$	-2032/4074/4095	$31.78^{+9.60}_{-7.31}$	$161.40^{+47.10}_{-32.40}$	0.20	5.46e+52
4.100~4.800	2.879~3.371	233.97	$-0.84^{+0.03}_{-0.03}$	$608.1^{+42.1}_{-42.2}$	$130.4^{+3.7}_{-3.9}$	-1880/3770/3792	$23.94^{+4.20}_{-4.22}$	$85.37^{+14.83}_{-12.27}$	0.28	2.89e+52
4.800~5.500	3.371~3.862	227.90	$-0.96^{+0.03}_{-0.03}$	$679.5^{+49.1}_{-48.7}$	$130.6^{+3.1}_{-3.2}$	-1809/3628/3649	$27.18^{+4.01}_{-3.73}$	$78.20^{+11.40}_{-9.66}$	0.35	2.65e+52
2.700~3.050	1.896~2.142	148.59	$-0.59^{+0.03}_{-0.03}$	$547.7^{+44.2}_{-44.9}$	$240.8^{+29.2}_{-29.1}$	-1187/2384/2406	$19.67^{+17.96}_{-8.88}$	$103.20^{+30.60}_{-20.28}$	0.19	1.75e+52
3.050~3.400	2.142~2.388	145.04	$-0.60^{+0.02}_{-0.02}$	$965.2^{+28.5}_{-30.1}$	$203.5^{+14.8}_{-14.8}$	-1320/2650/2671	$22.87^{+8.88}_{-7.23}$	$152.00^{+24.00}_{-21.00}$	0.15	2.57e+52
3.400~3.750	2.388~2.633	134.60	$-0.63^{+0.04}_{-0.04}$	$885.7^{+70.9}_{-70.1}$	$240.6^{+10.5}_{-10.6}$	-1224/2458/2480	$41.02^{+11.09}_{-7.91}$	$129.10^{+32.40}_{-23.40}$	0.32	2.18e+52
3.750~4.100	2.633~2.879	187.77	$-0.35^{+0.06}_{-0.05}$	$607.8^{+57.1}_{-60.1}$	$151.5^{+12.4}_{-14.2}$	-1428/2866/2887	$23.92^{+12.46}_{-10.40}$	$192.00^{+101.70}_{-60.30}$	0.12	3.25e+52
4.100~4.450	2.879~3.125	171.81	$-0.69^{+0.04}_{-0.04}$	$515.9^{+43.6}_{-43.6}$	$117.3^{+5.0}_{-5.0}$	-1271/2552/2573	$19.19^{+4.89}_{-4.40}$	$92.71^{+27.69}_{-22.43}$	0.21	1.57e+52
4.450~4.800	3.125~3.371	230.14	$-0.98^{+0.04}_{-0.04}$	$702.0^{+78.1}_{-78.2}$	$141.3^{+5.8}_{-5.8}$	-1254/2518/2539	$26.76^{+6.41}_{-5.47}$	$80.73^{+17.95}_{-14.95}$	0.33	1.37e+52
4.800~5.150	3.371~3.617	166.30	$-0.97^{+0.04}_{-0.04}$	$685.1^{+69.4}_{-68.6}$	$140.8^{+4.6}_{-4.6}$	-1218/2447/2468	$31.83^{+6.85}_{-4.98}$	$82.51^{+15.62}_{-12.33}$	0.39	1.40e+52
5.150~5.500	3.617~3.862	161.51	$-0.95^{+0.04}_{-0.04}$	$692.2^{+79.1}_{-77.7}$	$120.0^{+4.0}_{-4.0}$	-1203/2416/2438	$23.19^{+5.38}_{-3.81}$	$73.57^{+18.69}_{-12.93}$	0.32	1.24e+52
2.700~2.875	1.896~2.019	117.09	$-0.58^{+0.05}_{-0.05}$	$470.5^{+74.4}_{-83.7}$	$261.5^{+29.0}_{-27.9}$	-640/1291/1311	$33.68^{+20.39}_{-14.33}$	$112.30^{+28.37}_{-25.73}$	0.30	9.50e+51
2.875~3.050	2.019~2.142	94.40	$-0.68^{+0.04}_{-0.05}$	$627.6^{+87.0}_{-91.5}$	$258.0^{+30.1}_{-28.7}$	-664/1337/1359	$28.45^{+20.42}_{-12.51}$	$98.14^{+33.56}_{-26.44}$	0.29	8.30e+51
3.050~3.225	2.142~2.265	106.62	$-0.59^{+0.03}_{-0.03}$	$957.1^{+34.1}_{-34.9}$	$245.3^{+21.5}_{-21.0}$	-768/1547/1568	$25.71^{+13.87}_{-9.03}$	$169.30^{+38.20}_{-31.60}$	0.15	1.43e+52
3.225~3.400	2.265~2.388	100.40	$-0.73^{+0.06}_{-0.06}$	$1275.9^{+208.9}_{-215.4}$	$208.6^{+9.1}_{-9.2}$	-669/1349/1369	$36.78^{+9.54}_{-8.93}$	$144.90^{+33.02}_{-27.63}$	0.25	1.23e+52
3.400~3.575	2.388~2.511	98.23	$-0.59^{+0.05}_{-0.05}$	$804.0^{+86.7}_{-82.3}$	$255.9^{+17.4}_{-17.4}$	-702/1414/1436	$42.19^{+19.41}_{-13.59}$	$139.30^{+48.30}_{-35.60}$	0.30	1.18e+52
3.575~3.750	2.511~2.633	93.84	$-0.65^{+0.04}_{-0.04}$	$916.3^{+64.6}_{-67.7}$	$229.3^{+13.6}_{-13.5}$	-730/1471/1492	$39.25^{+11.97}_{-10.71}$	$119.50^{+32.90}_{-25.45}$	0.33	1.01e+52
3.750~3.925	2.633~2.756	126.63	$-0.51^{+0.02}_{-0.02}$	$960.9^{+30.9}_{-31.4}$	$204.6^{+9.9}_{-10.0}$	-808/1627/1648	$57.70^{+15.81}_{-12.25}$	$221.10^{+35.60}_{-31.50}$	0.26	1.87e+52
3.925~4.100	2.756~2.879	141.61	$-0.27^{+0.06}_{-0.06}$	$412.7^{+12.2}_{-11.9}$	$196.8^{+14.0}_{-16.1}$	-729/1468/1488	$32.20^{+19.05}_{-18.86}$	$176.50^{+12.91}_{-11.21}$	0.18	1.49e+52
4.100~4.275	2.879~3.002	122.91	$-0.54^{+0.06}_{-0.06}$	$474.1^{+45.5}_{-46.2}$	$162.6^{+14.9}_{-14.8}$	-758/1526/1547	$24.26^{+17.09}_{-10.09}$	$116.10^{+52.40}_{-35.12}$	0.21	9.82e+51
4.275~4.450	3.002~3.125	122.62	$-0.64^{+0.08}_{-0.08}$	$365.0^{+44.9}_{-48.5}$	$107.5^{+15.7}_{-12.6}$	-675/1360/1380	$9.04^{+9.47}_{-5.69}$	$72.20^{+19.06}_{-14.95}$	0.13	6.11e+51
4.450~4.625	3.125~3.248	111.94	$-1.04^{+0.05}_{-0.05}$	$640.0^{+108.7}_{-106.1}$	$161.0^{+11.1}_{-10.8}$	-640/1290/1310	$22.34^{+9.36}_{-6.65}$	$68.54^{+11.70}_{-11.21}$	0.33	5.80e+51
4.625~4.800	3.248~3.371	123.33	$-0.95^{+0.05}_{-0.05}$	$694.2^{+96.8}_{-94.2}$	$146.3^{+6.7}_{-6.6}$	-734/1477/1499	$35.59^{+9.47}_{-8.00}$	$89.91^{+27.59}_{-18.82}$	0.40	7.60e+51
4.800~4.975	3.371~3.494	129.65	$-0.85^{+0.05}_{-0.05}$	$564.5^{+68.9}_{-71.9}$	$135.3^{+7.5}_{-7.6}$	-744/1498/1519	$30.78^{+11.12}_{-8.55}$	$96.58^{+31.02}_{-23.68}$	0.32	8.17e+51
4.975~5.150	3.494~3.617	107.36	$-1.10^{+0.04}_{-0.04}$	$820.5^{+115.0}_{-111.2}$	$149.7^{+5.9}_{-5.8}$	-683/1376/1398	$32.76^{+6.98}_{-5.92}$	$71.57^{+16.74}_{-11.99}$	0.46	6.05e+51
5.150~5.325	3.617~3.739	108.96	$-1.04^{+0.05}_{-0.05}$	$765.2^{+119.0}_{-115.8}$	$130.9^{+5.8}_{-5.8}$	-697/1404/1426	$26.14^{+7.02}_{-5.96}$	$66.70^{+20.48}_{-14.17}$	0.39	5.64e+51
5.325~5.500	3.739~3.862	121.57	$-0.88^{+0.06}_{-0.06}$	$635.3^{+88.7}_{-92.0}$	$108.9^{+5.3}_{-5.4}$	-736/1483/1504	$20.90^{+6.51}_{-5.15}$	$79.48^{+28.02}_{-21.03}$	0.26	6.72e+51

GRB 160509A

GRB 160509A was observed by the *Fermi* satellite on May 9, 2016, at 08:59:04.36 UT (Longo et al. 2016). It was a strong source of GeV photons detected by *Fermi*-LAT, including a photon of 52 GeV arrived at 77 s, and another one of 29 GeV, at ~ 70 ks (Laskar et al. 2016). *Swift* has a late-time follow-up, with a total exposure time of 1700 s starting from 7278 s (Kangas et al. 2019). The redshift of 1.17 is measured by Gemini North telescope (Tanvir et al. 2016), inferring a high isotropic energy of 1.06×10^{54} erg (Tam et al. 2017).

We perform the corresponding time-resolved spectral analysis from which we can see that the hierarchical structure first discovered in the UPE phase of GRB 190114C is confirmed in the case of GRB 160509A. For the first iteration, we present the best-fit of the spectrum of the UPE entire duration from $t_{\rm rf}$ = 4.84 s to $t_{\rm rf}$ = 8.53 s (see Fig. 3, first layer).

We then divide the rest-frame time interval in half and perform again the same spectral analysis for the two 1.85 second interval, namely [4.84s-6.68s] and [6.68s-8.53s], obtaining the results shown in Fig. 3. Iteration 3: we then divide each of these half intervals again in half, i.e., $\Delta t_{\rm rf}$= 0.92s corresponding to [4.84s-5.76s], [5.76s-6.68s], [6.68s-7.60s] and [7.60s-8.53s] and redo the previous spectral analysis obtaining the results still in Fig. 3. In a fourth iteration we divide the UPE into 8 sub-intervals of $\Delta t_{\rm rf}$= 0.46s corresponding to the time intervals [4.84s-5.30s], [5.30s-5.76s], [5.76s-6.22s], [6.22s-6.68s], [6.68s-7.14s], [7.14s-7.60s], [7.60s-8.06s] and [8.06s-8.53s], and redo the spectral analysis (see in Fig. 3). In the fifth and final iteration of this process we divide the UPE into 16 sub-intervals of $\Delta t_{\rm rf}$= 0.23s corresponding we perform the spectral analysis and find the hierarchical CPL+BB emission in the time intervals [4.84s-5.07s], [5.07s-5.30s], [5.30s-5.53s], [5.53s-5.76s], [5.76s-5.99s], [5.99s-6.22s], [6.22s-6.45s], [6.45s-6.68s], [6.68s-6.91s], [6.91s-7.14s], [7.14s-7.37s], [7.37s-7.60s], [7.60s-7.83s], [7.83s-8.06s], [8.06s-8.29s] and [8.29s-8.53s], and perform the spectral analysis, see Fig. 3 and Table. 3.

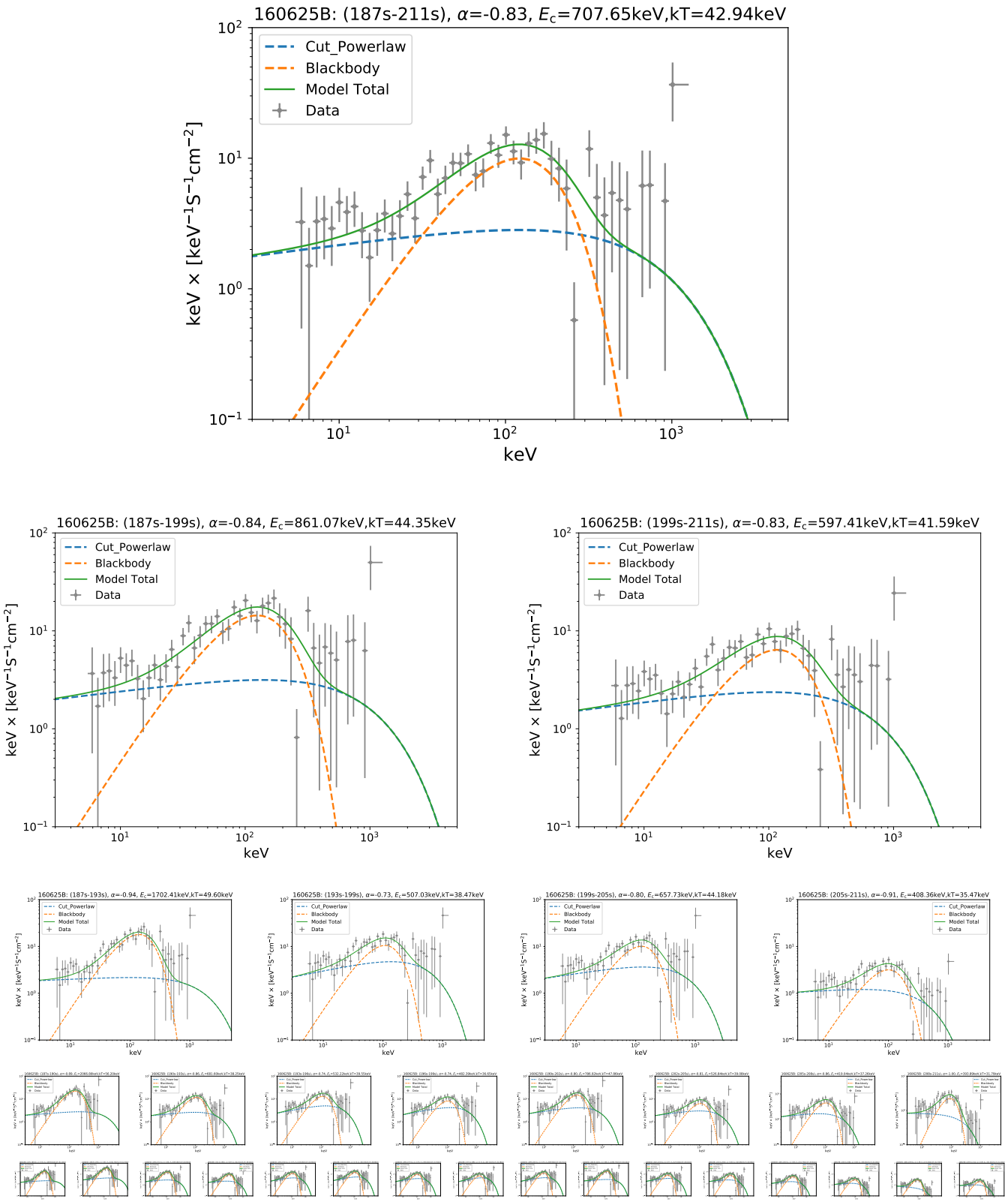

Fig. 2. Time-resolved spectral analysis of GRB 160625B. All the layers have the same time coverage, from ≈ 187 s ($t_{\rm rf}$ = 77.72 s) to ≈ 211 s ($t_{\rm rf}$ = 87.70 s), but with different time divisions: one interval (top layer), two equal parts (second layer), four equal parts (third layer), eight equal parts (fourth layer), and sixteen equal parts (bottom layer), respectively. The results of spectral analysis including time duration, temperature and cutoff energy are obtained in the observed frame, as shown in this figure. We have converted to have their corresponding value in the rest-frame, see Table 2, where rest-frame time in column 2, and rest-frame temperature in column 6.

Table 2. Results of the time-resolved spectral fits of GRB 160625B (CPL+BB model) from the $t_{\rm rf}$ = 77.72 s to $t_{\rm rf}$ = 87.70 s. This table reports: the time intervals both in rest-frame and observer frame, the significance (S) for each time interval, the power-law index, cut-off energy, temperature, ΔDIC, BB flux, total flux, the BB to total flux ratio, $F_{\rm BB}/F_{\rm tot}$ and finally the isotropic energy. To select the best model from two different given models, we adopt the deviance information criterion (DIC), defined as DIC=-2log[p(data$|\ \hat{\theta}$)]+2$p_{\rm DIC}$, where $\hat{\theta}$ is the posterior mean of the parameters, and $p_{\rm DIC}$ is the effective number of parameters. The preferred model is the model with the lowest DIC score. Here we define ΔDIC=(CPL+BB)-CPL, if ΔDIC is negative, indicating the CPL+BB is better. After comparing the DIC, we find the CPL+BB model is the preferred model than the CPL and other model. The ΔDIC scores are reported in column 6.

t_1~t_2	$t_{rf,1}$~$t_{rf,2}$	S	α	$E_{\rm c}$	kT	ΔDIC	$F_{\rm BB}$	$F_{\rm tot}$	$F_{\rm ratio}$	$E_{\rm tot}$
(s)	(s)			(keV)	(keV)		(10^{-6})	(10^{-6})		(erg)
Obs	Rest-frame				Rest-frame		(erg cm^{-2} s^{-1})	(erg cm^{-2} s^{-1})		
187.00~211.00	77.72~87.70	649.12	$-0.83^{+0.01}_{-0.01}$	$707.6^{+13.0}_{-12.9}$	$42.9^{+0.4}_{-0.4}$	-2840.2	$3.13^{+0.16}_{-0.15}$	$35.50^{+0.81}_{-0.87}$	$0.09^{+0.0}_{-0.0}$	4.53e+54
187.00~199.00	77.72~82.71	566.19	$-0.84^{+0.01}_{-0.01}$	$861.1^{+20.8}_{-20.9}$	$44.4^{+0.5}_{-0.5}$	-2789.1	$4.67^{+0.23}_{-0.24}$	$48.44^{+1.41}_{-1.40}$	$0.10^{+0.01}_{-0.01}$	3.09e+54
199.00~211.00	82.71~87.70	421.10	$-0.83^{+0.01}_{-0.01}$	$597.4^{+15.8}_{-15.9}$	$41.6^{+0.8}_{-0.8}$	-716.6	$1.95^{+0.18}_{-0.18}$	$24.53^{+0.83}_{-0.87}$	$0.08^{+0.01}_{-0.01}$	1.57e+54
187.00~193.00	77.72~80.22	426.56	$-0.94^{+0.01}_{-0.01}$	$1702.4^{+42.5}_{-42.7}$	$49.6^{+0.5}_{-0.5}$	-2935.0	$6.51^{+0.35}_{-0.32}$	$69.51^{+1.80}_{-1.92}$	$0.09^{+0.01}_{-0.01}$	2.22e+54
193.00~199.00	80.22~82.71	421.75	$-0.73^{+0.01}_{-0.01}$	$507.0^{+12.2}_{-12.4}$	$38.5^{+0.8}_{-0.8}$	-784.9	$2.95^{+0.30}_{-0.28}$	$37.46^{+1.33}_{-1.31}$	$0.08^{+0.01}_{-0.01}$	1.19e+54
199.00~205.00	82.71~85.20	409.24	$-0.80^{+0.01}_{-0.01}$	$657.7^{+18.1}_{-18.6}$	$44.2^{+0.9}_{-0.9}$	-729.7	$3.25^{+0.35}_{-0.28}$	$40.93^{+1.37}_{-1.59}$	$0.08^{+0.01}_{-0.01}$	1.31e+54
205.00~211.00	85.20~87.70	205.28	$-0.91^{+0.02}_{-0.02}$	$408.4^{+25.3}_{-25.8}$	$35.5^{+1.4}_{-1.4}$	-105.6	$0.82^{+0.17}_{-0.15}$	$9.08^{+0.75}_{-0.68}$	$0.09^{+0.02}_{-0.02}$	2.90e+53
187.00~190.00	77.72~78.97	344.58	$-0.89^{+0.01}_{-0.01}$	$2066.8^{+50.1}_{-50.0}$	$56.2^{+0.7}_{-0.7}$	-2860.2	$9.08^{+0.63}_{-0.55}$	$105.00^{+3.03}_{-3.29}$	$0.09^{+0.01}_{-0.01}$	1.67e+54
190.00~193.00	78.97~80.22	282.28	$-0.86^{+0.01}_{-0.01}$	$681.6^{+31.2}_{-31.7}$	$38.2^{+0.8}_{-0.8}$	-603.9	$3.30^{+0.37}_{-0.35}$	$32.41^{+1.93}_{-1.63}$	$0.10^{+0.01}_{-0.01}$	5.17e+53
193.00~196.00	80.22~81.46	333.07	$-0.74^{+0.01}_{-0.01}$	$532.2^{+17.1}_{-17.0}$	$39.5^{+0.9}_{-1.0}$	-546.1	$3.76^{+0.51}_{-0.42}$	$43.09^{+2.07}_{-1.84}$	$0.09^{+0.01}_{-0.01}$	6.87e+53
196.00~199.00	81.46~82.71	287.45	$-0.74^{+0.01}_{-0.01}$	$482.4^{+16.9}_{-16.5}$	$36.6^{+1.3}_{-1.3}$	-287.5	$2.17^{+0.45}_{-0.34}$	$32.03^{+1.67}_{-1.50}$	$0.07^{+0.01}_{-0.01}$	5.11e+53
199.00~202.00	82.71~83.96	341.22	$-0.80^{+0.01}_{-0.01}$	$786.9^{+29.1}_{-29.2}$	$47.9^{+1.0}_{-1.0}$	-661.0	$5.16^{+0.56}_{-0.50}$	$56.34^{+3.11}_{-2.55}$	$0.09^{+0.01}_{-0.01}$	8.99e+53
202.00~205.00	83.96~85.20	258.65	$-0.81^{+0.02}_{-0.02}$	$526.8^{+21.7}_{-21.7}$	$39.1^{+1.5}_{-1.5}$	-181.9	$1.79^{+0.34}_{-0.31}$	$26.95^{+1.32}_{-1.45}$	$0.07^{+0.01}_{-0.01}$	4.30e+53
205.00~208.00	85.20~86.45	182.22	$-0.86^{+0.03}_{-0.03}$	$419.0^{+28.9}_{-28.9}$	$37.3^{+1.7}_{-1.6}$	-90.1	$1.20^{+0.27}_{-0.27}$	$12.55^{+1.16}_{-1.06}$	$0.10^{+0.02}_{-0.02}$	2.00e+53
208.00~211.00	86.45~87.70	116.10	$-1.00^{+0.04}_{-0.04}$	$393.9^{+46.2}_{-47.4}$	$31.8^{+2.1}_{-2.1}$	-37.9	$0.51^{+0.19}_{-0.15}$	$5.63^{+0.84}_{-0.67}$	$0.09^{+0.04}_{-0.03}$	8.97e+52
187.00~188.50	77.72~78.35	147.15	$-0.91^{+0.01}_{-0.01}$	$2839.8^{+140.7}_{-141.4}$	$61.2^{+1.8}_{-1.8}$	-706.0	$4.47^{+0.74}_{-0.59}$	$63.65^{+3.89}_{-3.71}$	$0.07^{+0.01}_{-0.01}$	5.08e+53
188.50~190.00	78.35~78.97	354.91	$-0.87^{+0.01}_{-0.01}$	$1824.7^{+49.3}_{-49.4}$	$54.7^{+0.8}_{-0.8}$	-2291.1	$13.77^{+1.02}_{-0.93}$	$147.60^{+4.86}_{-5.17}$	$0.09^{+0.01}_{-0.01}$	1.18e+54
190.00~191.50	78.97~79.59	227.35	$-0.86^{+0.02}_{-0.02}$	$849.5^{+52.9}_{-53.5}$	$40.6^{+1.1}_{-1.1}$	-465.8	$4.46^{+0.63}_{-0.58}$	$45.19^{+3.19}_{-3.25}$	$0.10^{+0.02}_{-0.01}$	3.60e+53
191.50~193.00	79.59~80.22	181.28	$-0.87^{+0.03}_{-0.03}$	$522.4^{+37.1}_{-37.6}$	$36.0^{+1.4}_{-1.4}$	-178.9	$2.34^{+0.48}_{-0.42}$	$21.81^{+2.08}_{-1.89}$	$0.11^{+0.02}_{-0.02}$	1.74e+53
193.00~194.50	80.22~80.84	229.41	$-0.75^{+0.02}_{-0.02}$	$525.9^{+25.5}_{-25.2}$	$40.7^{+1.5}_{-1.5}$	-223.5	$3.48^{+0.69}_{-0.62}$	$38.84^{+2.72}_{-2.41}$	$0.09^{+0.02}_{-0.02}$	3.10e+53
194.50~196.00	80.84~81.46	254.52	$-0.73^{+0.02}_{-0.02}$	$540.3^{+23.0}_{-23.0}$	$38.9^{+1.2}_{-1.2}$	-338.7	$4.12^{+0.67}_{-0.58}$	$47.26^{+3.01}_{-2.65}$	$0.09^{+0.02}_{-0.01}$	3.77e+53
196.00~197.50	81.46~82.09	212.08	$-0.76^{+0.02}_{-0.02}$	$495.8^{+24.6}_{-24.4}$	$37.8^{+1.6}_{-1.6}$	-188.9	$2.65^{+0.55}_{-0.49}$	$31.87^{+2.17}_{-2.17}$	$0.08^{+0.02}_{-0.02}$	2.54e+53
197.50~199.00	82.09~82.71	205.41	$-0.71^{+0.02}_{-0.02}$	$467.3^{+22.3}_{-22.4}$	$34.4^{+2.2}_{-2.2}$	-114.0	$1.72^{+0.60}_{-0.51}$	$32.16^{+2.31}_{-2.18}$	$0.05^{+0.02}_{-0.02}$	2.56e+53
199.00~200.50	82.71~83.33	239.62	$-0.75^{+0.02}_{-0.02}$	$670.0^{+31.7}_{-31.3}$	$46.7^{+1.6}_{-1.6}$	-256.6	$4.24^{+0.73}_{-0.65}$	$50.78^{+3.52}_{-3.33}$	$0.08^{+0.02}_{-0.01}$	4.05e+53
200.50~202.00	83.33~83.96	256.45	$-0.88^{+0.02}_{-0.02}$	$1090.8^{+73.8}_{-74.6}$	$50.4^{+1.3}_{-1.2}$	-458.5	$6.88^{+0.91}_{-0.81}$	$66.21^{+5.27}_{-4.91}$	$0.10^{+0.02}_{-0.01}$	5.28e+53
202.00~203.50	83.96~84.58	215.38	$-0.77^{+0.02}_{-0.02}$	$527.0^{+25.3}_{-25.2}$	$38.3^{+1.8}_{-1.8}$	-132.1	$2.18^{+0.54}_{-0.44}$	$34.45^{+2.53}_{-2.25}$	$0.06^{+0.02}_{-0.01}$	2.75e+53
203.50~205.00	84.58~85.20	157.84	$-0.86^{+0.03}_{-0.03}$	$525.7^{+39.3}_{-39.2}$	$40.1^{+2.4}_{-2.4}$	-63.6	$1.43^{+0.46}_{-0.37}$	$19.61^{+2.12}_{-1.73}$	$0.07^{+0.02}_{-0.02}$	1.56e+53
205.00~206.50	85.20~85.83	150.18	$-0.83^{+0.03}_{-0.03}$	$454.8^{+37.1}_{-37.9}$	$39.6^{+2.0}_{-2.0}$	-71.7	$1.63^{+0.47}_{-0.39}$	$16.59^{+1.96}_{-1.59}$	$0.10^{+0.03}_{-0.03}$	1.32e+53
206.50~208.00	85.83~86.45	112.49	$-0.86^{+0.05}_{-0.05}$	$338.3^{+41.3}_{-40.5}$	$32.5^{+2.9}_{-2.9}$	-29.1	$0.70^{+0.39}_{-0.27}$	$8.59^{+1.40}_{-1.15}$	$0.08^{+0.05}_{-0.03}$	6.85e+52
208.00~209.50	86.45~87.07	84.98	$-1.09^{+0.06}_{-0.06}$	$474.3^{+88.9}_{-88.7}$	$32.7^{+2.2}_{-2.2}$	-34.0	$0.70^{+0.28}_{-0.21}$	$5.46^{+1.27}_{-0.84}$	$0.13^{+0.06}_{-0.04}$	4.35e+52
209.50~211.00	87.07~87.70	82.67	$-0.89^{+0.06}_{-0.06}$	$323.5^{+52.4}_{-51.0}$	$31.3^{+3.4}_{-8.4}$	-58.7	$0.26^{+0.56}_{-0.19}$	$6.03^{+1.91}_{-1.15}$	$0.04^{+0.09}_{-0.03}$	4.81e+52

GRB 180720B

On 20 July 2018 at 14:21:39.65 universal time (UT) the Fermi Gamma-Ray Burst Monitor (GBM) triggered and located GRB 180720B (trigger 553789304 / 180720598). The GBM light curve comprises of a very bright pulse, with numerous overlapping pulses with a duration of T_{90}=49 s in the observer frame (50-300 keV) (Roberts & Meegan 2018), categorizing this burst as a long GRB.

The high S/N of the data of prompt emission has allowed us to perform a refined spectral analysis of GRB 180720B in the [9.07-10.89] time interval in 5 iterations on decreasing time bins keeping still the reliable statistical significance: in each time bin a CPL+BB spectrum is found as the best fit. The time intervals both in rest-frame and observer frame, the significance (S) for each time interval, the power-law index, cut-off energy, temperature, ΔDIC, BB flux, total flux, the BB to total flux ratio, $F_{\rm BB}/F_{\rm tot}$ and finally the isotropic energy of entire this time bin and its sub-intervals are shown in Table. 4. The evolution of the temperature and the luminosity of UPE phase, as obtained by the time-resolved spectral analysis are shown in Fig. 4.

The presence of such thermal components indicates presence of an overcritical electric field around the BH in the GRB 180720B, GRB 190114C, GRB 160625B and GRB 160509A. The overcritical electric field produce an optically thick *fireshell* of e^+e^- plasma endowed with baryon load. Its expansion and self-acceleration due to internal pressure has been described in Ruffini et al. (1999). The fireshell expands due to its self-acceleration up to ultra-relativistic velocities ($\Gamma \sim 100$ in the case of long GRBs; Aksenov et al. 2007. When the fireshell becomes transparent, a thermal radiation, what has been called the Proper-GRB (P-GRB), is emitted (Ruffini et al. 1999, 2000).

References

Akaike, H. 1974, IEEE Transactions on Automatic Control, 19, 716
Aksenov, A. G., Ruffini, R., & Vereshchagin, G. V. 2007, Physical Review Letters, 99, 125003

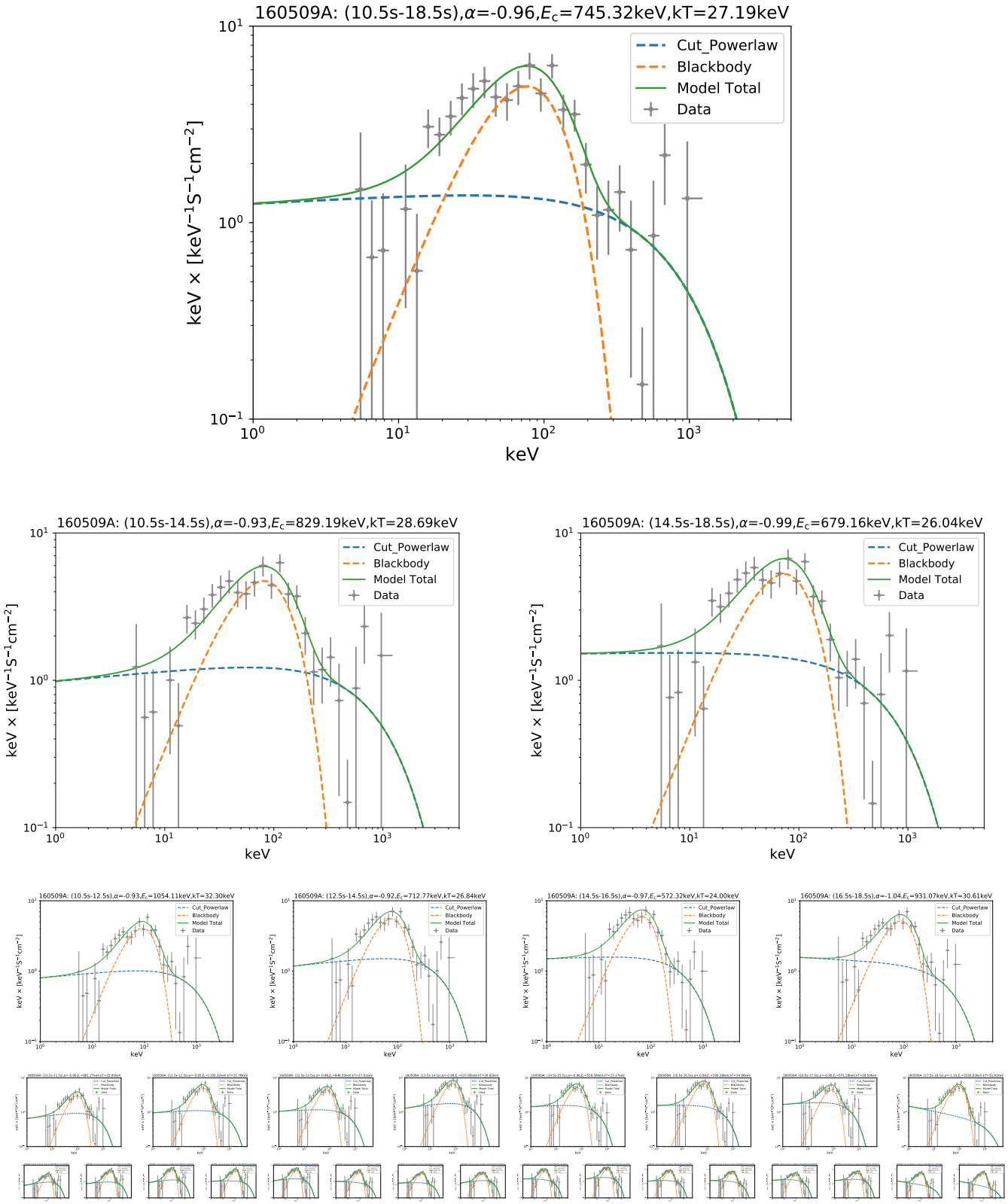

Fig. 3. Time-resolved spectral analysis of GRB 160509A. All the layers have the same time coverage, from 10.5 s ($t_{\rm rf}$ = 4.84 s) to 18.5 s ($t_{\rm rf}$ = 8.53 s), but with different time divisions: one part (top layer), two equal parts (second layer), four equal parts (third layer), eight equal parts (fourth layer), and sixteen equal parts (bottom layer), respectively. Two dash lines represent CPL (blue) and BB (orange) components, while the solid line represents total model (green). The results of spectral analysis including time duration, temperature and cutoff energy are obtained in the observed frame, as shown in this figure. We have converted to have their corresponding value in the rest-frame, see Table 3, where rest-frame time in column 2, rest-frame cutoff energy in column 5 and rest-frame temperature in column 6.

Table 3. Results of the time-resolved spectral fits of GRB 160509A (CPL+BB model) from the $t_{\rm rf}$ = 4.84 s to $t_{\rm rf}$ = 8.53 s. The definitions of parameters are the same as in table 2.

t_1~t_2 (s) Obs	$t_{rf,1}$~$t_{rf,2}$ (s) Rest-frame	S	α	$E_{\rm c}$ (keV)	kT (keV)	ΔDIC	$F_{\rm BB}$ (10^{-6}) (erg cm^{-2} s^{-1})	$F_{\rm tot}$ (10^{-6}) (erg cm^{-2} s^{-1})	$F_{\rm ratio}$	$E_{\rm tot}$ (erg)
10.50~18.50	4.84~8.53	292.18	$-0.96^{+0.01}_{-0.01}$	$745.3^{+27.6}_{-26.9}$	$27.2^{+0.6}_{-0.6}$	-633.8	$0.98^{+0.13}_{-0.11}$	$18.01^{+1.10}_{-1.00}$	$0.05^{+0.01}_{-0.01}$	5.40e+53
10.50~14.50	4.84~6.68	199.13	$-0.93^{+0.02}_{-0.02}$	$829.2^{+47.6}_{-47.0}$	$28.7^{+0.9}_{-0.9}$	-335.4	$1.00^{+0.19}_{-0.15}$	$18.50^{+1.70}_{-1.57}$	$0.05^{+0.01}_{-0.01}$	2.77e+53
14.50~18.50	6.68~8.53	232.97	$-0.99^{+0.01}_{-0.01}$	$679.2^{+31.9}_{-32.3}$	$26.0^{+0.8}_{-0.8}$	-324.2	$0.99^{+0.19}_{-0.15}$	$18.00^{+1.28}_{-1.27}$	$0.05^{+0.01}_{-0.01}$	2.70e+53
10.50~12.50	4.84~5.76	127.55	$-0.93^{+0.02}_{-0.02}$	$1054.1^{+97.5}_{-97.1}$	$32.3^{+1.7}_{-1.7}$	-145.5	$0.94^{+0.30}_{-0.22}$	$18.83^{+2.62}_{-2.40}$	$0.05^{+0.02}_{-0.01}$	1.41e+53
12.50~14.50	5.76~6.68	161.51	$-0.92^{+0.02}_{-0.02}$	$712.8^{+47.1}_{-47.4}$	$26.8^{+1.1}_{-1.1}$	-205.1	$1.08^{+0.26}_{-0.20}$	$18.81^{+1.96}_{-1.82}$	$0.06^{+0.01}_{-0.01}$	1.41e+53
14.50~16.50	6.68~7.60	169.80	$-0.97^{+0.02}_{-0.02}$	$572.3^{+32.9}_{-33.2}$	$24.0^{+1.0}_{-1.0}$	-203.4	$1.02^{+0.27}_{-0.20}$	$16.14^{+1.53}_{-1.39}$	$0.06^{+0.02}_{-0.01}$	1.21e+53
16.50~18.50	7.60~8.53	169.78	$-1.04^{+0.02}_{-0.02}$	$931.1^{+87.8}_{-86.6}$	$30.6^{+1.6}_{-1.6}$	-147.6	$1.15^{+0.31}_{-0.27}$	$20.87^{+2.83}_{-2.24}$	$0.06^{+0.02}_{-0.01}$	1.56e+53
10.50~11.50	4.84~5.30	77.67	$-0.90^{+0.04}_{-0.04}$	$881.3^{+135.4}_{-141.4}$	$33.0^{+3.3}_{-3.3}$	-43.8	$0.69^{+0.45}_{-0.27}$	$14.27^{+3.75}_{-2.93}$	$0.05^{+0.03}_{-0.02}$	5.35e+52
11.50~12.50	5.30~5.76	104.90	$-0.95^{+0.02}_{-0.02}$	$1195.3^{+126.1}_{-124.3}$	$31.8^{+1.9}_{-1.9}$	-117.1	$1.21^{+0.45}_{-0.33}$	$23.14^{+3.53}_{-3.11}$	$0.05^{+0.02}_{-0.02}$	8.67e+52
12.50~13.50	5.76~6.22	102.77	$-0.96^{+0.03}_{-0.03}$	$848.5^{+91.0}_{-89.5}$	$27.0^{+1.8}_{-1.8}$	-81.4	$0.86^{+0.37}_{-0.25}$	$17.63^{+2.89}_{-2.59}$	$0.05^{+0.02}_{-0.02}$	6.61e+52
13.50~14.50	6.22~6.68	129.10	$-0.90^{+0.03}_{-0.03}$	$638.0^{+53.1}_{-52.7}$	$26.8^{+1.4}_{-1.4}$	-128.1	$1.30^{+0.38}_{-0.31}$	$20.50^{+3.12}_{-2.65}$	$0.06^{+0.02}_{-0.02}$	7.68e+52
14.50~15.50	6.68~7.14	117.25	$-0.96^{+0.03}_{-0.03}$	$550.6^{+44.3}_{-44.5}$	$23.2^{+1.5}_{-1.5}$	-85.7	$0.86^{+0.32}_{-0.26}$	$15.20^{+2.37}_{-1.68}$	$0.06^{+0.02}_{-0.02}$	5.69e+52
15.50~16.50	7.14~7.60	127.21	$-0.99^{+0.03}_{-0.03}$	$599.2^{+52.7}_{-52.5}$	$24.7^{+1.3}_{-1.3}$	-124.5	$1.17^{+0.40}_{-0.28}$	$17.14^{+2.23}_{-2.19}$	$0.07^{+0.03}_{-0.02}$	6.42e+52
16.50~17.50	7.60~8.06	131.95	$-0.95^{+0.03}_{-0.03}$	$571.3^{+47.4}_{-46.6}$	$28.5^{+2.3}_{-2.4}$	-49.8	$0.90^{+0.46}_{-0.34}$	$19.51^{+2.69}_{-2.19}$	$0.05^{+0.02}_{-0.02}$	7.31e+52
17.50~18.50	8.06~8.53	112.19	$-1.15^{+0.02}_{-0.02}$	$2226.8^{+325.2}_{-326.2}$	$32.9^{+1.9}_{-1.9}$	-133.0	$1.33^{+0.47}_{-0.34}$	$27.25^{+4.66}_{-3.82}$	$0.05^{+0.02}_{-0.01}$	1.02e+53
10.50~11.00	4.84~5.07	48.87	$-0.87^{+0.06}_{-0.06}$	$804.0^{+189.6}_{-191.8}$	$33.4^{+8.6}_{-8.3}$	-23.1	$0.33^{+0.86}_{-0.24}$	$12.55^{+5.59}_{-3.97}$	$0.03^{+0.07}_{-0.02}$	2.35e+52
11.00~11.50	5.07~5.30	61.64	$-0.93^{+0.05}_{-0.05}$	$1004.5^{+202.6}_{-211.2}$	$33.3^{+3.5}_{-3.5}$	-40.8	$1.00^{+0.67}_{-0.42}$	$16.82^{+6.06}_{-4.34}$	$0.06^{+0.05}_{-0.03}$	3.15e+52
11.50~12.00	5.30~5.53	74.34	$-0.89^{+0.05}_{-0.05}$	$875.2^{+145.3}_{-147.8}$	$28.6^{+2.4}_{-2.4}$	-64.6	$1.13^{+0.55}_{-0.37}$	$19.22^{+5.94}_{-4.13}$	$0.06^{+0.03}_{-0.02}$	3.60e+52
12.00~12.50	5.53~5.76	75.45	$-0.98^{+0.03}_{-0.03}$	$1487.0^{+208.8}_{-205.9}$	$35.1^{+3.4}_{-3.4}$	-57.0	$1.16^{+0.74}_{-0.44}$	$27.26^{+6.00}_{-4.46}$	$0.04^{+0.03}_{-0.02}$	5.11e+52
12.50~13.00	5.76~5.99	81.26	$-0.91^{+0.03}_{-0.03}$	$786.1^{+96.3}_{-96.7}$	$26.9^{+2.3}_{-2.3}$	-49.0	$0.94^{+0.54}_{-0.34}$	$20.82^{+4.08}_{-3.74}$	$0.05^{+0.03}_{-0.02}$	3.90e+52
13.00~13.50	5.99~6.22	65.10	$-1.03^{+0.05}_{-0.05}$	$977.8^{+201.9}_{-199.4}$	$27.8^{+3.1}_{-3.1}$	-39.8	$0.77^{+0.62}_{-0.34}$	$14.55^{+4.63}_{-3.02}$	$0.05^{+0.05}_{-0.03}$	2.73e+52
13.50~14.00	6.22~6.45	90.78	$-0.97^{+0.04}_{-0.04}$	$937.5^{+151.2}_{-151.4}$	$31.4^{+2.1}_{-2.1}$	-77.7	$1.62^{+0.68}_{-0.42}$	$23.85^{+6.01}_{-4.95}$	$0.07^{+0.03}_{-0.02}$	4.47e+52
14.00~14.50	6.45~6.68	93.73	$-0.86^{+0.04}_{-0.04}$	$525.0^{+50.2}_{-49.4}$	$23.6^{+1.9}_{-1.9}$	-65.2	$1.13^{+0.61}_{-0.37}$	$18.94^{+3.46}_{-3.06}$	$0.06^{+0.03}_{-0.02}$	3.55e+52
14.50~15.00	6.68~6.91	80.00	$-1.01^{+0.04}_{-0.04}$	$648.6^{+79.1}_{-80.5}$	$22.8^{+2.2}_{-2.2}$	-41.5	$0.75^{+0.51}_{-0.30}$	$15.08^{+3.14}_{-2.32}$	$0.05^{+0.04}_{-0.02}$	2.82e+52
15.00~15.50	6.91~7.14	87.43	$-0.92^{+0.04}_{-0.04}$	$494.1^{+51.9}_{-50.7}$	$23.7^{+1.9}_{-1.9}$	-50.0	$0.96^{+0.54}_{-0.33}$	$15.80^{+3.08}_{-2.56}$	$0.06^{+0.04}_{-0.02}$	2.96e+52
15.50~16.00	7.14~7.37	91.73	$-0.95^{+0.04}_{-0.04}$	$582.5^{+63.7}_{-65.1}$	$24.0^{+1.6}_{-1.6}$	-80.8	$1.30^{+0.56}_{-0.39}$	$17.48^{+3.38}_{-2.64}$	$0.07^{+0.03}_{-0.02}$	3.27e+52
16.00~16.50	7.37~7.60	90.06	$-1.02^{+0.04}_{-0.04}$	$640.4^{+91.4}_{-92.2}$	$25.6^{+2.2}_{-2.2}$	-51.2	$1.10^{+0.58}_{-0.41}$	$16.62^{+3.91}_{-2.84}$	$0.07^{+0.04}_{-0.03}$	3.11e+52
16.50~17.00	7.60~7.83	90.67	$-0.96^{+0.04}_{-0.04}$	$576.5^{+78.4}_{-77.9}$	$30.3^{+5.5}_{-5.2}$	-25.1	$0.71^{+0.87}_{-0.48}$	$18.83^{+4.75}_{-3.42}$	$0.04^{+0.05}_{-0.03}$	3.53e+52
17.00~17.50	7.83~8.06	97.88	$-0.92^{+0.04}_{-0.04}$	$561.8^{+62.8}_{-63.6}$	$26.8^{+2.8}_{-2.8}$	-40.2	$1.03^{+0.72}_{-0.42}$	$20.40^{+3.97}_{-3.30}$	$0.05^{+0.04}_{-0.02}$	3.82e+52
17.50~18.00	8.06~8.29	82.94	$-1.13^{+0.03}_{-0.03}$	$2375.2^{+440.5}_{-440.1}$	$33.8^{+3.1}_{-3.2}$	-68.8	$1.35^{+0.83}_{-0.55}$	$31.18^{+7.03}_{-5.27}$	$0.04^{+0.03}_{-0.02}$	5.84e+52
18.00~18.50	8.29~8.53	77.25	$-1.17^{+0.04}_{-0.04}$	$2143.3^{+521.4}_{-532.9}$	$32.5^{+2.5}_{-2.5}$	-65.0	$1.37^{+0.74}_{-0.45}$	$23.06^{+6.84}_{-4.79}$	$0.06^{+0.04}_{-0.02}$	4.32e+52

Burns, E. 2016, GRB Coordinates Network, Circular Service, No. 19581, #1 (2016), 19581
Dirirsa, F., Vianello, G., Racusin, J., & Axelsson, M. 2016, GRB Coordinates Network, Circular Service, No. 19586, #1 (2016), 19586
Hamburg, R., Veres, P., Meegan, C., et al. 2019, GRB Coordinates Network, Circular Service, No. 23707, #1 (2019), 23707
Kangas, T., Fruchter, A. S., Cenko, S. B., et al. 2019, arXiv e-prints, arXiv:1906.03493
Laskar, T., Alexander, K. D., Berger, E., et al. 2016, ApJ, 833, 88
Longo, F., Bissaldi, E., Bregeon, J., et al. 2016, GRB Coordinates Network, 19403, 1

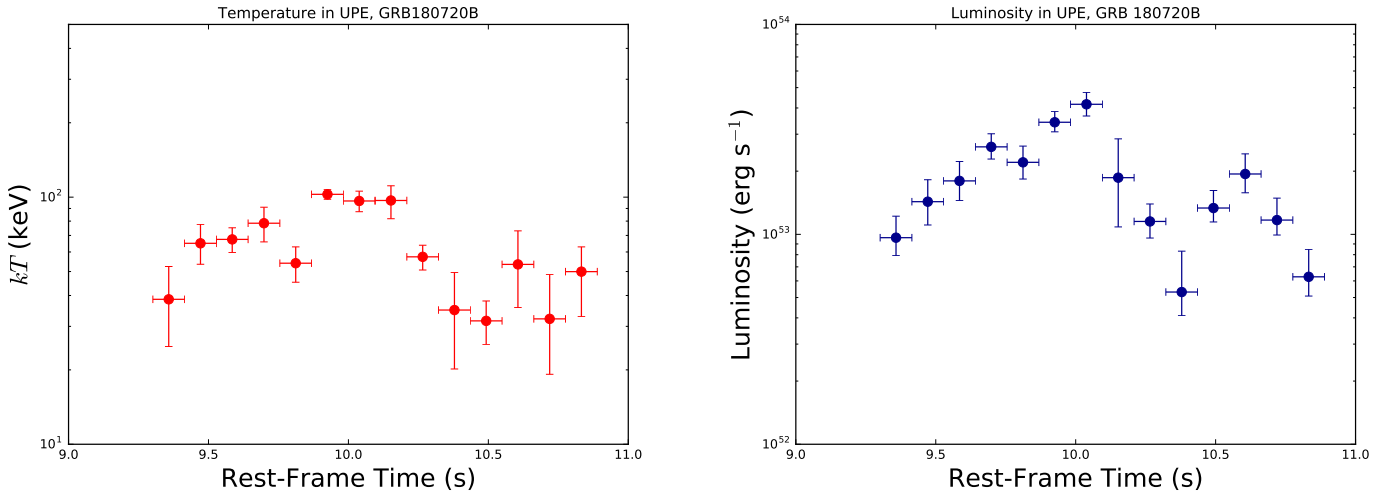

Fig. 4. The temperature (kT) and the luminosity evolution during the UPE phase of GRB 1807820B obtained from time-resolved spectral analysis of the Fermi-GBM data.

Table 4. Results of the time-resolved spectral fits of GRB 180720B (CPL+BB model) from the $t_{\rm rf}$ = 9.07 s to $t_{\rm rf}$ = 10.89 s. This table reports: the time intervals both in rest-frame and observer frame, the significance (S) for each time interval, the power-law index, cut-off energy, temperature, ΔDIC, BB flux, total flux, the BB to total flux ratio, $F_{\rm BB}/F_{\rm tot}$ and finally the isotropic energy. To select the best model from two different given models, we adopt the deviance information criterion (DIC), defined as DIC=-2log[p(data$|\ \hat{\theta}$)]+2$p_{\rm DIC}$, where $\hat{\theta}$ is the posterior mean of the parameters, and $p_{\rm DIC}$ is the effective number of parameters. The preferred model is the model with the lowest DIC score. Here we define ΔDIC=(CPL+BB)-CPL, if ΔDIC is negative, indicating the CPL+BB is better. After comparing the DIC, we find the CPL+BB model is the preferred model than the CPL and other model. The ΔDIC scores are reported in column 6. The redshift z=0.653

t_1~t_2	$t_{rf,1}$~$t_{rf,2}$	S	α	$E_{\rm c}$	kT	ΔDIC	$F_{\rm BB}$	$F_{\rm tot}$	$F_{\rm ratio}$	$E_{\rm tot}$
(s)	(s)			(keV)	(keV)		(10^{-6})	(10^{-6})		(erg)
Obs	Rest-frame				Rest-frame		(erg cm^{-2} s^{-1})	(erg cm^{-2} s^{-1})		
$15.00\sim18.00$	$9.07\sim10.89$	274.60	$-1.06^{+0.01}_{-0.01}$	$1502.5^{+88.6}_{-87.5}$	$39.8^{+1.6}_{-1.6}$	-226.4	$1.99^{+0.43}_{-0.34}$	$45.55^{+3.11}_{-2.70}$	$0.04^{+0.01}_{-0.01}$	$16.0^{+1.1}_{-0.952}$
$15.00\sim16.50$	$9.07\sim9.98$	190.63	$-1.04^{+0.01}_{-0.01}$	$1750.5^{+112.7}_{-111.1}$	$40.5^{+2.0}_{-2.0}$	-176.6	$2.08^{+0.58}_{-0.46}$	$48.03^{+3.28}_{-3.09}$	$0.04^{+0.01}_{-0.01}$	$8.46^{+0.577}_{-0.543}$
$16.50\sim18.00$	$9.98\sim10.89$	215.76	$-1.05^{+0.02}_{-0.02}$	$1151.3^{+117.3}_{-119.6}$	$37.1^{+2.8}_{-2.8}$	-78.7	$1.63^{+0.69}_{-0.54}$	$41.83^{+4.61}_{-4.04}$	$0.04^{+0.02}_{-0.01}$	$7.37^{+0.812}_{-0.712}$
$15.00\sim15.75$	$9.07\sim9.53$	105.93	$-1.07^{+0.03}_{-0.03}$	$1198.0^{+211.1}_{-217.8}$	$31.4^{+3.3}_{-3.3}$	-41.5	$0.94^{+0.70}_{-0.42}$	$23.84^{+4.65}_{-3.86}$	$0.04^{+0.03}_{-0.02}$	$2.1^{+0.41}_{-0.34}$
$15.75\sim16.50$	$9.53\sim9.98$	168.59	$-0.92^{+0.02}_{-0.02}$	$1028.0^{+74.9}_{-73.9}$	$74.8^{+20.8}_{-25.7}$	-15.4	$0.14^{+0.37}_{-0.13}$	$58.57^{+5.42}_{-4.80}$	$0.0^{+0.01}_{-0.0}$	$5.16^{+0.478}_{-0.423}$
$16.50\sim17.25$	$9.98\sim10.44$	155.67	$-1.15^{+0.02}_{-0.02}$	$2382.3^{+217.5}_{-221.3}$	$45.3^{+2.7}_{-2.7}$	-125.6	$2.85^{+1.00}_{-0.76}$	$53.96^{+4.55}_{-4.28}$	$0.05^{+0.02}_{-0.01}$	$4.75^{+0.401}_{-0.377}$
$17.25\sim18.00$	$10.44\sim10.89$	159.05	$-0.93^{+0.02}_{-0.02}$	$684.7^{+49.7}_{-49.2}$	$23.9^{+3.8}_{-4.0}$	-30.8	$0.63^{+0.93}_{-0.37}$	$35.74^{+3.28}_{-3.21}$	$0.02^{+0.03}_{-0.01}$	$3.15^{+0.289}_{-0.283}$
$15.00\sim15.38$	$9.07\sim9.30$	69.11	$-1.06^{+0.07}_{-0.08}$	$711.2^{+209.5}_{-215.5}$	$28.9^{+5.7}_{-5.6}$	-30.2	$0.78^{+1.14}_{-0.55}$	$14.27^{+6.80}_{-3.54}$	$0.05^{+0.08}_{-0.04}$	$0.628^{+0.299}_{-0.156}$
$15.38\sim15.75$	$9.30\sim9.53$	83.03	$-1.01^{+0.03}_{-0.03}$	$1319.4^{+210.9}_{-208.7}$	$31.0^{+5.2}_{-5.2}$	-28.9	$0.83^{+1.14}_{-0.48}$	$32.18^{+6.45}_{-5.45}$	$0.03^{+0.04}_{-0.02}$	$1.42^{+0.284}_{-0.24}$
$15.75\sim16.12$	$9.53\sim9.75$	109.59	$-1.02^{+0.02}_{-0.02}$	$1967.9^{+193.8}_{-194.9}$	$43.6^{+4.0}_{-4.0}$	-72.6	$2.63^{+1.51}_{-0.96}$	$62.61^{+6.83}_{-6.58}$	$0.04^{+0.02}_{-0.02}$	$2.76^{+0.301}_{-0.29}$
$16.12\sim16.50$	$9.75\sim9.98$	133.10	$-1.01^{+0.02}_{-0.02}$	$1919.4^{+162.1}_{-168.5}$	$47.9^{+3.5}_{-3.5}$	-107.5	$4.31^{+1.60}_{-1.38}$	$82.08^{+8.46}_{-7.17}$	$0.05^{+0.02}_{-0.02}$	$3.61^{+0.372}_{-0.316}$
$16.50\sim16.88$	$9.98\sim10.21$	133.12	$-1.09^{+0.02}_{-0.02}$	$2574.3^{+264.0}_{-267.2}$	$55.7^{+3.8}_{-3.7}$	-117.9	$5.16^{+2.03}_{-1.44}$	$83.97^{+8.79}_{-7.60}$	$0.06^{+0.02}_{-0.02}$	$3.7^{+0.387}_{-0.335}$
$16.88\sim17.25$	$10.21\sim10.44$	89.16	$-1.24^{+0.05}_{-0.05}$	$1537.9^{+522.7}_{-558.0}$	$31.9^{+3.4}_{-3.4}$	-27.8	$1.38^{+0.94}_{-0.57}$	$24.25^{+7.37}_{-6.29}$	$0.06^{+0.04}_{-0.03}$	$1.07^{+0.325}_{-0.277}$
$17.25\sim17.62$	$10.44\sim10.66$	125.76	$-0.86^{+0.03}_{-0.03}$	$696.1^{+59.2}_{-57.7}$	$22.5^{+3.8}_{-3.7}$	-27.3	$0.83^{+1.39}_{-0.48}$	$45.89^{+5.21}_{-4.69}$	$0.02^{+0.03}_{-0.01}$	$2.02^{+0.23}_{-0.206}$
$17.62\sim18.00$	$10.66\sim10.89$	102.97	$-1.02^{+0.04}_{-0.04}$	$622.4^{+77.4}_{-80.6}$	$25.7^{+8.4}_{-9.5}$	-25.5	$0.39^{+1.32}_{-0.34}$	$25.51^{+4.95}_{-3.40}$	$0.02^{+0.05}_{-0.01}$	$1.12^{+0.218}_{-0.15}$
$15.00\sim15.19$	$9.07\sim9.19$	51.57	$-1.01^{+0.14}_{-0.15}$	$805.3^{+449.1}_{-380.0}$	$33.0^{+13.1}_{-18.2}$	-288.8	$0.80^{+5.09}_{-0.77}$	$19.23^{+23.49}_{-7.86}$	$0.04^{+0.27}_{-0.04}$	$0.423^{+0.517}_{-0.173}$
$15.19\sim15.38$	$9.19\sim9.30$	42.03	$-1.19^{+0.09}_{-0.09}$	$1201.3^{+667.6}_{-595.4}$	$27.5^{+4.3}_{-4.2}$	-27.1	$0.97^{+1.06}_{-0.55}$	$12.89^{+8.98}_{-4.04}$	$0.08^{+0.1}_{-0.05}$	$0.284^{+0.198}_{-0.0889}$
$15.38\sim15.56$	$9.30\sim9.41$	53.84	$-1.00^{+0.04}_{-0.04}$	$1158.5^{+201.4}_{-200.2}$	$23.4^{+8.3}_{-8.3}$	-27.1	$0.29^{+1.66}_{-0.26}$	$27.59^{+7.34}_{-4.93}$	$0.01^{+0.06}_{-0.01}$	$0.608^{+0.162}_{-0.109}$
$15.56\sim15.75$	$9.41\sim9.53$	63.61	$-1.06^{+0.05}_{-0.05}$	$1839.8^{+434.0}_{-420.6}$	$39.4^{+7.6}_{-7.0}$	-32.2	$1.74^{+2.60}_{-1.11}$	$40.95^{+11.15}_{-9.24}$	$0.04^{+0.06}_{-0.03}$	$0.902^{+0.246}_{-0.203}$
$15.75\sim15.94$	$9.53\sim9.64$	72.54	$-1.04^{+0.04}_{-0.04}$	$1896.8^{+350.9}_{-351.5}$	$40.8^{+4.7}_{-4.7}$	-30.3	$2.78^{+2.13}_{-1.19}$	$51.44^{+12.23}_{-9.91}$	$0.05^{+0.04}_{-0.03}$	$1.13^{+0.269}_{-0.218}$
$15.94\sim16.12$	$9.64\sim9.75$	83.99	$-0.99^{+0.03}_{-0.03}$	$1950.2^{+231.8}_{-232.1}$	$47.5^{+7.6}_{-7.6}$	-34.3	$2.34^{+3.12}_{-1.29}$	$74.72^{+11.53}_{-9.35}$	$0.03^{+0.04}_{-0.02}$	$1.65^{+0.254}_{-0.206}$
$16.12\sim16.31$	$9.75\sim9.87$	85.09	$-0.95^{+0.04}_{-0.04}$	$1379.2^{+207.4}_{-203.8}$	$32.7^{+5.4}_{-5.3}$	-39.2	$1.84^{+2.29}_{-1.02}$	$63.06^{+12.29}_{-10.56}$	$0.03^{+0.04}_{-0.02}$	$1.39^{+0.271}_{-0.233}$
$16.31\sim16.50$	$9.87\sim9.98$	104.94	$-1.05^{+0.02}_{-0.02}$	$2304.7^{+260.1}_{-261.8}$	$62.1^{+2.8}_{-2.8}$	-85.4	$6.72^{+1.63}_{-1.29}$	$97.87^{+12.08}_{-9.75}$	$0.07^{+0.02}_{-0.01}$	$2.15^{+0.266}_{-0.215}$
$16.50\sim16.69$	$9.98\sim10.10$	107.18	$-1.04^{+0.03}_{-0.03}$	$2737.1^{+346.9}_{-340.9}$	$58.4^{+5.6}_{-5.6}$	-86.1	$6.57^{+3.89}_{-2.56}$	$119.20^{+16.65}_{-14.38}$	$0.06^{+0.03}_{-0.02}$	$2.62^{+0.367}_{-0.317}$
$16.69\sim16.88$	$10.10\sim10.21$	82.58	$-1.13^{+0.13}_{-0.08}$	$1910.0^{+709.1}_{-1074.0}$	$58.6^{+8.6}_{-9.2}$	-86.9	$3.67^{+4.06}_{-3.43}$	$53.29^{+28.29}_{-22.24}$	$0.07^{+0.08}_{-0.07}$	$1.17^{+0.623}_{-0.49}$
$16.88\sim17.06$	$10.21\sim10.32$	64.96	$-1.24^{+0.03}_{-0.03}$	$2412.4^{+580.9}_{-576.0}$	$34.7^{+4.0}_{-4.0}$	-28.1	$1.52^{+1.46}_{-0.72}$	$32.97^{+6.96}_{-5.49}$	$0.05^{+0.05}_{-0.02}$	$0.726^{+0.153}_{-0.121}$
$17.06\sim17.25$	$10.32\sim10.44$	62.39	$-1.06^{+0.08}_{-0.08}$	$480.3^{+112.6}_{-114.6}$	$21.1^{+8.8}_{-8.9}$	-125.2	$0.39^{+3.01}_{-0.35}$	$15.20^{+8.60}_{-3.47}$	$0.03^{+0.2}_{-0.02}$	$0.335^{+0.189}_{-0.0764}$
$17.25\sim17.44$	$10.44\sim10.55$	81.92	$-0.89^{+0.05}_{-0.05}$	$720.6^{+93.9}_{-92.3}$	$19.1^{+3.9}_{-3.8}$	-23.5	$0.82^{+1.62}_{-0.55}$	$38.20^{+8.11}_{-5.42}$	$0.02^{+0.04}_{-0.01}$	$0.841^{+0.179}_{-0.119}$
$17.44\sim17.62$	$10.55\sim10.66$	97.68	$-0.84^{+0.05}_{-0.05}$	$713.4^{+96.8}_{-97.0}$	$32.3^{+11.9}_{-10.7}$	-38.1	$1.05^{+5.66}_{-0.87}$	$55.49^{+13.70}_{-10.34}$	$0.02^{+0.1}_{-0.02}$	$1.22^{+0.302}_{-0.228}$
$17.62\sim17.81$	$10.66\sim10.78$	82.29	$-0.95^{+0.05}_{-0.05}$	$628.7^{+86.6}_{-86.2}$	$19.5^{+9.9}_{-7.8}$	-66.8	$0.33^{+4.15}_{-0.30}$	$33.47^{+9.11}_{-5.06}$	$0.01^{+0.12}_{-0.01}$	$0.737^{+0.201}_{-0.111}$
$17.81\sim18.00$	$10.78\sim10.89$	64.36	$-1.08^{+0.06}_{-0.06}$	$565.9^{+123.9}_{-118.5}$	$30.2^{+7.8}_{-10.3}$	-15.3	$0.36^{+1.63}_{-0.33}$	$17.96^{+6.32}_{-3.42}$	$0.02^{+0.09}_{-0.02}$	$0.395^{+0.139}_{-0.0752}$

Lü, H.-J., Lü, J., Zhong, S.-Q., et al. 2017, ApJ, 849, 71
Melandri, A., D'Avanzo, P., D'Elia, V., et al. 2016, GRB Coordinates Network, Circular Service, No. 19585, #1 (2016), 19585
Melandri, A., Izzo, L., D'Avanzo, P., et al. 2019, GRB Coordinates Network, 23983
Mirzoyan, R., Noda, K., Moretti, E., et al. 2019, GRB Coordinates Network, Circular Service, No. 23701, #1 (2019), 23701
Roberts, O. J. & Meegan, C. 2018, GRB Coordinates Network, 22981, 1
Ruffini, R., Li, L., Moradi, R., et al. 2019a, arXiv:1904.04162 [arXiv:1904.04162]
Ruffini, R., Moradi, R., Aimuratov, Y., et al. 2019b, GRB Coordinates Network, Circular Service, No. 23715, #1 (2019), 23715
Ruffini, R., Salmonson, J. D., Wilson, J. R., & Xue, S. 2000, A&A, 359, 855
Ruffini, R., Salmonson, J. D., Wilson, J. R., & Xue, S.-S. 1999, A&A, 350, 334
Schwarz, G. et al. 1978, The annals of statistics, 6, 461
Selsing, J., Fynbo, J. P. U., Heintz, K. E., Watson, D., & Dyrbye, N. 2019, GRB Coordinates Network, 23695
Tam, P.-H. T., He, X.-B., Tang, Q.-W., & Wang, X.-Y. 2017, ApJ, 844, L7
Tanvir, N. R., Levan, A. J., Cenko, S. B., et al. 2016, GRB Coordinates Network, Circular Service, No. 19419, #1 (2016), 19419
Troja, E. 2017, in AAS/High Energy Astrophysics Division, Vol. 16, AAS/High Energy Astrophysics Division #16, 305.05
Troja, E., Lipunov, V. M., Mundell, C. G., et al. 2017, Nature, 547, 425
Wang, Y., Rueda, J. A., Ruffini, R., et al. 2019, ApJ, 874, 39
Woosley, S. E. & Bloom, J. S. 2006, ARA&A, 44, 507
Xu, D., Malesani, D., Fynbo, J. P. U., et al. 2016, GRB Coordinates Network, Circular Service, No. 19600, #1 (2016), 19600
Zhang, B.-B., Zhang, B., Castro-Tirado, A. J., et al. 2018, Nature Astronomy, 2, 69